Modelling of the in service behaviour of passive insulated structures for deep sea offshore applications

van Trung Phan

THÈSE / UNIVERSITÉ DE BRETAGNE OCCIDENTALE
sous le sceau de l'Université européenne de Bretagne

pour obtenir le titre de
DOCTEUR DE L'UNIVERSITÉ DE BRETAGNE OCCIDENTALE
Mention : Mécanique
École Doctorale SICMA

présentée par
Van Trung PHAN

Préparée au LBMS (EA 4325) Laboratoire Brestois de Mécanique et des Systèmes (ENSTA-Bretagne) et au Services Matériaux et Structures (IFREMER, centre de Brest)

Modélisation du comportement en service de structures d'isolation passive pour l'offshore profond

Modelling of the in service behaviour of passive insulated structures for deep sea offshore applications

Thèse soutenue le 30 novembre 2012
devant le jury composé de :

P. CARTRAUD
Professeur, GeM, Ecole Centrale de Nantes / rapporteur

J.F. FERRERO
Professeur, ICA, Université Paul Sabatier / rapporteur

J.F. CARON
Dir de Recherche, Institut Navier ENPC

L. CANGEMI
Ingénieur, IFPEN

L. SOHIER
Maître de Conférences, LBMS, Université de Brest

J.Y. COGNARD
Professeur, LBMS, ENSTA - Bretagne / *directeur de thèse*

D. CHOQUEUSE
Ingénieur, IFREMER / co-*encadrement*

Table of contents

List of figures

List of tables

Résumé en français

L'étude se situe dans le cadre de la recherche de gains de performance de structures d'isolations passives pour l'offshore profond. Le travail proposé a pour support des analyses expérimentales et numériques de tubes revêtus par des matériaux isolants utilisés en eau profonde pour transporter du fluide chaud. . Le raboutage des tubes en acier, préalablement revêtus en atelier, nécessite un dégagement du revêtement aux extrémités pour réaliser l'opération d'assemblage (généralement par soudure). La partie dégagée est ensuite recouverte par un nouveau matériau pouvant être appliqué sur site. Ainsi l'isolation de cette partie du tube (Field Joint), qui est soumise à des chargements thermomécaniques en service, doit être optimisée pour assurée une durée de vie compatible avec les contraintes de l'exploitation offshore en eau profonde.

Le document comporte cinq parties :

- une étude bibliographique,
- la modélisation du comportement thermique pour analyser l'évolution en temps et en espace de la température du matériau au cours de la fabrication, de la pose et en service sachant que pour les matériaux d'isolation le comportement mécanique est fortement dépendant de la température,
- une partie expérimentale pour l'analyse du comportement des matériaux isolants en fonction de la température et en fonction de la pression hydrostatique qui est le principal chargement mécanique de ces structures en service,
- la modélisation du comportement mécanique des isolants
- et une partie modélisation et simulation du comportement en service d'assemblages multi-matériaux de type industriel, avec prise en compte du comportement non-linéaire des constituants.

Etude bibliographique

La partie bibliographie débute par une présentation du contexte actuel de l'exploitation d'offshore. La découverte des sources de pétrole et de gaz) à des grandes profondeurs en mer induit des conditions d'exploitation sévères : la pression hydrostatique peut atteindre 30 MPa, la température de l'effluent pétrolier est parfois supérieure à 130 °C et la température extérieure peut atteindre 4 °C. Il faut d'autre part mentionner que, pour ces applications, les durées de vie souhaitées sont de l'ordre de la vingtaine d'années. Pour la sécurité et l'efficacité, la conception des pipelines doit être fiable pour éviter plusieurs phénomènes causés par la diminution de la viscosité du pétrole (formation d'hydrates de gaz, dépôt de paraffine...) pouvant conduire à l'obturation de la conduite. La solution la plus utilisée est de protéger les pipelines vis-à-vis de la faible température extérieure par des matériaux d'isolation thermique passive pour maintenir la température du fluide transportée

supérieure à environ 40 °C. La protection thermique doit également résister aux sollicitations mécaniques en présence d'un fort gradient thermique dans l'épaisseur de l'isolant. Il faut d'autre part s'assurer d'un bon comportement vis-à-vis des contraintes environnementales. La solution retenue pour ces applications passe souvent par l'utilisation d'un assemblage multi matériaux aux propriétés spécifiques répondant à l'application souhaitée. Pour assurer la durabilité des revêtements isolants, des procédures de mise en œuvre spécifiques sont utilisées pour assurer une bonne adhérence entre les différents matériaux nécessitant des préparations de surfaces adaptées. En fonction des conditions en service de la structure (profondeur maximale, température maximale, propriétés thermiques recommandées...), les matériaux d'isolation thermique proposés sont différents [Watkins & Hershey, 2001]. La conception des pipelines et du système d'isolation doit prendre en compte les différentes histoires de chargement associées à la phase d'installation et à la phase d'exploitation. Outre le fonctionnement normal de transfert de l'effluent vers le support flottant, les phases d'arrêt de production doivent être aussi prises en compte. La perte de chaleur au cours de l'écoulement du pétrole dans les pipelines doit être limitée et le système d'isolation doit également permette le maintien à une température minimum de l'effluent pétrolier sur une certaine période en cas d'arrêt de production. Ainsi l'analyse du comportement thermo-mécanique des matériaux d'isolation thermique est indispensable pour assurer la fiabilité des installations et leur durabilité. Une présentation générale des principaux matériaux d'isolation est proposée ainsi que les stratégies utilisées pour la réalisation de l'isolation des zones de raccordement (Field joint). Des structures multicouches sont principalement utilisées : le polypropylène ainsi que les mousses syntactiques sont souvent utilisés pour ces applications. A titre d'exemple, le système proposé par Socotherm® se compose d'une protection anticorrosion de l'acier et de plusieurs couches de polypropylène (polypropylène massif, mousse syntactique polypropylène pour garantir une faible conductivité thermique, polypropylène adhésif). Compte tenue de sa composition, cette structure d'isolation présente l'avantage d'une forte compatibilité entre les différents matériaux : forte adhésion entre chaque couche, pas de vides significatifs ou de bulles d'air emprisonnées.

La mousse syntactique est un matériau constituée de microsphères en verre noyées dans une résine polymérique. Dépendant de la profondeur d'utilisation des pipelines et des conditions de déploiement, la nature de la résine est différente (polypropylène, polyuréthane ou époxy). Le diamètre des microsphères creuses varie de 10 à 200 microns et l'épaisseur de la coque est de l'ordre de 1 à 2 microns. Son rapport résistance/poids est très intéressant. Ce type de matériau présente une faible conductivité thermique, une résistance à la pression hydrostatique de plusieurs centaines de bars et une bonne résistance aux chocs grâce à une grande déformation anélastique admissible.

La région du Field joint est initialement non revêtue lors que deux pipes sont assemblées par la soudure et est ensuite revêtue par généralement par moulage pour garantir la performance thermique locale. Le matériau utilisé pour la réalisation du Field joint, est choisi en fonction de

différents paramètres. La rapidité de mise en œuvre gouverne généralement le choix du matériau (dans ce cas le polyuréthane est souvent utilisé) mais des contraintes de tenue en température conduisent à l'utilisation d'autre matériau (dans notre cas d'étude : le polypropylène massif est retenu). Le polypropylène est un matériau peu couteux qui possède de bonnes propriétés thermomécaniques et dont le comportement vis-à-vis de l'eau est très satisfaisant par rapport aux d'autres matériaux polymériques.

La procédure générale pour la réalisation d'un Field joint est la suivante :

- Chauffage de la surface de l'acier à la température souhaitée par induction,
- la surface de l'acier est ensuite recouverte par une protection anti corrosion (généralement époxy poudre appliquée par fusion),
- les surfaces latérales de l'isolant principal du pipeline sont chauffés par rayonnement afin d'assurer une bonne liaison lors de l'application du matériau de Field joint,
- un moule à double paroi est placé sur la zone de Field joint afin d'assurer le moulage par la zone d'injection de Polypropylène en fusion,
- après injection du polypropylène, une circulation d'eau dans le moule assure le refroidissement du matériau du Field joint. A l'obtention d'une certaine température de surface le moule est ouvert et le refroidissement du Field joint se poursuit en dehors du moule.
- inspection du Field joint.

Compte tenu de la procédure de fabrication, la zone du Field joint est reconnue pour être une zone critique du pipeline. Une analyse thermomécanique du processus de moulage d'un Field joint et une analyse des contraintes induites au cours de l'installation et en service est essentielle pour garantir la durabilité de l'exploitation (20 ans). Il est donc important d'étudier l'influence des contraintes résiduelles, de la pression hydrostatique et du gradient de température dans l'épaisseur de l'isolant sur le comportement à long terme du système d'isolation.

En ce qui concerne les méthodes d'installation des pipelines de type rigide, deux méthodes sont principalement utilisée : la méthode de pose en S et la méthode de pose en J. Pour la méthode de pose en S, le pipeline est soudé en position horizontale et se déplacent vers l'arrière de la barge de pose avant d'atteindre le fond de l'océan, le pipeline prend la forme d'un «S» dans l'eau. Le pipeline doit être soutenu par une structure en treillis de type circulaire équipé de rouleaux (stinger). Cette méthode est communément utilisée pour des applications en eau relativement peu profonde, car il nécessite un "stinger" long (pouvant mesurer jusqu'à 100 mètres de long) pour guider le pipeline et éviter le flambage. La méthode de pose en S peut être utilisée jusqu'à des profondeurs d'environ 2000 mètres [Boyun Guo et al, 2005]. Lorsque la profondeur d'exploitation augmente, la pose du pipeline en J est préférée. Les pipelines sont soudés en position verticale et sont immergés en

position verticale ou presque verticale. Il y a donc moins de contraintes générées dans le pipeline ; ainsi cette technique de pose est bien adaptée aux applications en eau plus profondes. La technique de pose en J entraîne une meilleure résistance du pipeline aux courants que la technique de pose en S.

Modélisation thermique

Cette partie présente une approche simplifiée pour estimer l'évolution de la température pendant le processus de refroidissement d'un moulage de Field joint ainsi que la distribution de température dans l'épaisseur de pipeline en service. Comme les principaux paramètres thermo-mécaniques dépendent de la température, une analyse fine du comportement demande une étude expérimentale relativement complexe. Ainsi, nous proposons une étude simplifiée, en particulier pour la partie refroidissement du Field joint. La modélisation du transfert thermique dans les solides (conduction et convection) est rappelée. L'étude prend principalement en compte l'influence de la température sur le comportement mécanique à long terme du polymère massif et aussi de la mousse syntactique. Pendant la phase de solidification, pour tenir compte de façon simplifié de l'effet chimique (exotherme de solidification), une source de chaleur est associée à la polymérisation et une loi de mélange est utilisée pour estimer la conductivité thermique du matériau. Pour les isolants, hors de la zone de changement de phase, une hypothèse d'évolution linéaire des paramètres thermiques en fonction de la température est utilisée.

Pour le problème étudié, la convection est associée à un flux sur la surface intérieure et extérieure du pipeline. La couche limite (ou de transfert de chaleur par convection) provient de la différence de température entre le fluide et la surface. Dans une étude simplifiée, le phénomène de convection est représenté par un coefficient de transfert thermique. Cette approche est très utile dans de nombreux cas, surtout quand on ne se concentre pas sur le comportement du flux, mais plutôt sur sa puissance de refroidissement. La valeur du coefficient de transfert thermique dépend de plusieurs paramètres comme la température de surface du solide, la température de surface loin de la couche limite, la nature du fluide (propriétés du matériau, le débit du fluide) et la géométrie de l'interface. Un refroidissement par convection peut être divisé en quatre catégories principales en fonction du type des conditions de convection (naturelle ou forcée) et du type de géométrie (interne ou externe flux de convection) [Frank P, 2006; Lienhard IV and V, 2001; Bejan & Kraus, 2003; Bai. Y & Bai. Q, 2005]. L'autre approche pour simuler le refroidissement d'un Field joint est de construire un modèle de couplage avec le champ de vitesse convective autour des pipelines (flux non isotherme, laminaire ou turbulent). Avant la simulation, il faut estimer le nombre de Grashof (convection naturelle) ou le nombre de Reynolds (convection forcée) pour définir les propriétés du modèle (laminaire ou turbulent). La convection naturelle est ajoutée à l'écoulement du fluide par l'approximation de Boussinesq. Cette approximation ignore les variations de densité avec la température, à l'exception des variations créent par la force de flottabilité du fluide. Cette force

entre ensuite dans la force volumique dans l'équation de Navier-Stokes. Pour mieux comprendre l'évolution thermique au cours de moulage d'un Field joint et pour faire le bon choix des conditions aux limites thermiques, nous avons proposé deux modèles de résolution thermique. Le premier utilise le coefficient de transfert thermique et l'autre utilise un écoulement de l'air générée par la force de flottabilité volumique créé par le gradient de la température. La différence entre deux modèles qui n'est pas importante nous permet d'utiliser le coefficient de transfert thermique pour la suite de l'étude. Le temps de refroidissement d'un Field joint est un point important pour optimiser le processus de fabrication du pipeline. La connaissance du gradient de température au sein du matériau nous permet d'estimer l'évolution au cours du temps de la rigidité de la structure. Pour valider cette approche, des essais du moulage de type structural sur des pipelines réels ont été développés en collaboration avec la société EUPEC. Lors de la réalisation du Field joint, le matériau fondu est stocké à 200 °C dans un réservoir afin de remplir rapidement le moule par injection en une seule opération. Ce processus limite les risques de fissures dans le Field joint. Un moule en acier à double paroi, est utilisé pour faciliter le refroidissement rapide du matériau injecté par une convection forcée en utilisant une circulation d'eau froide. Enfin, après démoulage le matériau injecté est refroidi par un système d'arrosage. Grâce à des thermocouples et à une caméra infrarouge, il est possible d'analyser l'évolution de la température au sein du matériau ainsi que de la partie extérieure du moule.

Une étude supplémentaire sur l'effet thermique de la présence d'une fissure au niveau de Field joint est aussi présentée. La profondeur et l'ouverture de la fissure est paramétrée. Une modélisation thermique simple est initialement développée. Les coefficients de transfert thermique sont utilisés pour les surfaces intérieures et extérieures du pipeline. Pour cette étude, les conditions utilisées sont : un fluide chaud à 100 °C à l'intérieur du pipeline (écoulement à faible vitesse 0,1 m/s) et une convection naturelle dans l'eau à l'extérieur du pipeline créée par la différence de température. Pour l'étude thermique en présence d'une fissure (de taille assez importante) le modèle est complexifié par l'ajout de deux flux laminaires. Ce modèle reste simple car il ne tient pas compte de la zone de turbulence autour de la fissure. Toutefois, les résultats obtenus sont encourageants. Ils montrent que la détérioration du Field joint (modélisé par une fissure de taille assez importante) peut entrainer une forte réduction de la température locale à l'intérieur du pipe (environ 20 °C). Ceci peut entraîner la formation d'hydrates dans des pipelines et ainsi entraîner des pertes d'efficacité du pipeline.

Comportement mécanique

Dans la partie de caractérisation du comportement mécanique des matériaux, comme le chargement mécanique principal de la structure est la pression hydrostatique, des essais spécifiques de compression hydrostatique à différentes températures (de 20 °C à 80 °C) et selon différents profils de charges ont été réalisés au centre d'IFREMER de Brest. Les essais ont été réalisés en utilisant un

caisson hyperbare en mesurant l'évolution de la flottabilité des échantillons avec la pression. La prise en compte la variation de la densité de l'eau (en fonction de la pression et la température) permet de mesurer l'évolution de déformation volumique du matériau en fonction de la pression hydrostatique. Le matériau utilisé est une mousse syntactique polypropylène (matrice de polypropylène, microsphères de type 3M Glass type S38 HS [Lefebvre et al, 2009]). A partir des essais, le comportement sous chargements monotones a été analysé et peut être divisé en quatre phases comme suit :

- Phase 1 : phase initiale caractérisée par un faible module de compressibilité (déformation volumique de 0 à 2%). Ce comportement peut être lié à la porosité initiale du matériau associé au processus de fabrication. En raison de la rigidité de la matrice PP, les porosités sont comprimées à basse pression. Dans cette phase, le module diminue presque linéairement avec la température. Les limites de la phase 1 (pression et déformation volumique maximale) diminuent aussi avec la température.
- Phase 2 : phase associée à un module de compressibilité élevé (pression maximale inférieure à 40 à 50 MPa). Dans cette phase, le comportement est principalement gouverné par une déformation élastique linéaire du matériau avant l'endommagement des microsphères. Il est important de noter que la limite de pression de cette phase diminue lorsque la température augmente. D'autre part, la rigidité augmente progressivement avec la température. La consolidation du matériau peut être associée à une diminution de la porosité initiale. Pendant cette phase, le comportement mécanique est également contrôlé par le comportement des microsphères. En raison de la morphologie du matériau et en considérant que les microsphères n'ont pas tous les mêmes dimensions ; il y a des zones locales dans le matériau, où les contraintes de cisaillement peuvent être élevées. Donc, à haute température, la matrice polymère étant moins rigide, les microsphères peuvent se déplacer plus facilement à une position stable dans la matrice polymère. Ce phénomène conduit à une augmentation de la consolidation avec une augmentation de la température.
- Phase 3 : Plateau de densification avec une augmentation significative de la déformation volumique. Le plateau de densification correspond à l'endommagement du matériau associé à la rupture de microsphères. La pression obtenue est généralement identifiée comme la pression de collapse du matériau. Cette pression, qui caractérise le plateau, dépend de la température. Une augmentation de la température conduit à une diminution de la rigidité de la matrice et donc une augmentation du chargement des microsphères. Par conséquent, la pression de collapse diminue avec la température. En outre, à basse température, les microsphères sont plus rigides, mais plus fragile et, par conséquent, le taux de rupture des microsphères peut diminuer avec la température. Cette phase fait intervenir des phénomènes de stockage d'énergie, les microsphères travaillent comme un système de ressorts pendant le chargement. La raideur des ressorts diminue avec la température à un même niveau de

chargement, ainsi l'énergie stockée diminue avec l'augmentation de la température. Ceci explique l'effondrement des microsphères à des niveaux de chargement plus faible à basse température.

- Phase 4 : la déformation volumique supérieure à 15 %. Cette phase correspond à la deuxième phase de la consolidation du matériau. La rupture de la plus part des microsphères conduit à un comportement similaire à celui de la matrice (polypropylène solide) pour une augmentation de la pression hydrostatique. Cette propriété se révèle lors du déchargement du matériau. On peut noter que l'augmentation de la déformation volumique est presque indépendante de la température. Ainsi, pour ce matériau, après la rupture de microsphères, la déformation volumique en fluage peut être expliquée par la porosité induite par la rupture de microsphères. Normalement, pour les polymères solides de la déformation volumique en fluage est très faible [Bardenhagen et al, 1997].

Le comportement du matériau sous des chargements hydrostatiques est assez complexe et inclut des phénomènes de viscosité et d'endommagement. Pour étudier les effets visqueux, des tests ont été effectués à 60 °C, à différentes vitesses de chargement (0.1, 1 et 5 MPa/min), en utilisant la même durée pour la phase de fluage (une heure) à une pression de 60 MPa. Les résultats expérimentaux sont similaires pour les vitesses de 1 et 5 MPa/min. Cependant, pour les essais à vitesse plus faible (0.1 MPa / min) les limites de pression de la phase 1 et phase 2 sont plus faibles. Ce phénomène peut être expliqué en considérant que la redistribution des contraintes se produit entre la matrice polymère et les microsphères. A faible vitesse de chargement, la matrice a le temps de se déformer ce qui augmente le transfert de charges aux microsphères.

Afin de continuer à étudier le comportement du matériau, des tests sous chargements cycliques (vitesse de chargement et de déchargement de 1 MPa/min) ont également été réalisés. Sous chargements cycliques, pour une faible pression hydrostatique, une partie irréversible de la déformation volumique est identifiée dans la phase 1. La déformation par fluage volumique reste faible jusqu'à 30 MPa.

Pour compléter la caractérisation du comportement à long terme du GSPP (glass syntactique polypropylène), des essais de fluage sous des pressions hydrostatiques différentes à 60°C ont également été effectuées. Si nous considérons que le comportement du matériau est viscoélastique linéaire, la déformation volumique totale peut être séparé en trois parties : une déformation élastique, une déformation inélastique et un retard de déformation visqueuse [Ward & Hadley, 1993]. Après un chargement de fluage sous une faible pression hydrostatique, lorsque la pression est relâchée, la partie de déformation de recouvrance est presque égale à la déformation élastique. Mais à un niveau de charge plus élevée, la partie de déformation de recouvrance est plus petite que la déformation élastique. L'évolution de la déformation volumique peut conduire à la rupture des certains microsphères qui contribuent à la partie résiduelle de la déformation volumique.

Associée au comportement dépendant du temps et de la température du polymère et au collapse des microsphères, le comportement de la mousse syntactique est complexe. Pour compléter les essais réalisés dans le caisson hyperbare, la mesure du volume et de la densité de la mousse syntactique et des microsphères a été réalisée en utilisant un Pycnomètre. Ce dispositif nous permet d'identifier la densité et le volume de matière solide en mesurant la variation de la pression de l'hélium dans des volumes calibrés. Son avantage est que le processus de test est simple, rapide et donne d'excellents résultats. Ces essais permettent non seulement de mesurer la densité des matériaux mais aussi de quantifier le pourcentage de vide. Ces essais ont également permis d'estimer après chargement et calcination de la résine le pourcentage de microsphères cassées dans ces matériaux.

Modélisation du comportement mécanique du matériau

A partir des résultats expérimentaux, le développement d'une loi de comportement thermomécanique des matériaux est proposé. De nombreuses études sur le comportement viscoélastique sont proposées dans la littérature pour les matériaux polymères. Selon la façon dont la température affecte la réponse mécanique, on peut considérer qu'un polymère a un comportement thermo-rhéologique simple ou thermo-rhéologique complexe. Dans le cas de matériaux thermo-rhéologique simples, l'influence de la température est prise en compte par l'utilisation d'un facteur de décalage dans le temps de relaxation. Ce facteur est basé sur le principe de superposition temps-température où le temps et la température peuvent être interchangés. Dans le cas de comportement thermo-rhéologique complexes des polymères, la température induit un changement de la forme du spectre de temps de relaxation [Muliana & Khan, 2008]. Avant de développer le modèle, nous avons effectué quelques analyses DMA (Dynamic Mechanical Analysis) de la mousse syntactique, du polyuréthane et du polypropylène afin de vérifier le comportement thermo-rhéologique du matériau (en traction, plage de déformation de 10^{-3}, de -70°C à 150°C par pas de 10°C, une plage de fréquences de 100 Hz). Ainsi, le module de stockage est tracé en fonction du module de perte. On peut noter que pour le polyuréthane solide, une bonne corrélation est observée, alors que dans le cas de la mousse syntactique, aucune corrélation claire entre le module de stockage et le module de perte n'est observée, de sorte que le GSPP doit être considéré comme un matériau thermo-rhéologique complexe [Gueguen, 2005]. Un modèle thermomécanique de la mousse syntactique est proposé pour modéliser la déformation volumique en fluage sous pression hydrostatique en prenant en compte la propriété thermo-rhéologique complexe du matériau. Ce modèle est aussi applicable pour d'autres mousses syntactiques (époxy, polyuréthane, phénolique) qui ont le même type de comportement. En assumant que le comportement est viscoélastique linéaire, un spectre de temps de relaxation dépendant de la température est utilisé en se basant sur le modèle initialement développé par [D. Perreux et al]. Afin de modéliser l'influence des vides et du comportement du matériau sous chargements cycliques de pression hydrostatique, une déformation volumique irréversible est proposée et une dépendance entre module d'Young et l'évolution de déformation volumique est introduite.

Un processus d'optimisation a été utilisé pour identifier les paramètres matériaux en utilisant les différents résultats expérimentaux disponibles.

Pour le matériau GSPP les paramètres du modèle ont été identifiés à partir des essais de fluage en traction sous une charge faible (0,5 MPa) et à différentes températures (de 25 °C à 100 °C). A ce niveau de chargement nous considérons qu'aucun dommage n'est généré dans le matériau. Le modèle donne des bons résultats pour des températures comprises entre 25 et 100 °C. Une évolution plus complexe des paramètres en ce qui concerne la température permettrait d'améliorer la qualité de la réponse pour une plus large gamme de températures. Compte tenu de l'effet de la consolidation par la pression hydrostatique pour la mousse syntactique, son modèle viscoélastique est amélioré par l'ajout de la déformation limite de la phase 1 et également du changement de module d'Young en fonction de la température et de la déformation volumique. Le même procédé d'optimisation, utilisant la fonction Fminsearch de Matlab® est utilisé pour déterminer les paramètres du modèle. Le résultat final de cette optimisation donne une bonne corrélation entre les données expérimentales et les résultats numériques avant le collapse des microsphères.

En ce qui concerne le matériau injecté (polypropylène massif), il est supposé que la partie visqueuse de déformation volumique est incompressible, c'est à dire que le changement volumique est purement élastique. Un modèle viscoélastique de type Maxwell généralisé est utilisé. La même méthode d'identification inverse que celle utilisée pour la mousse syntactique a été utilisée. Les essais de traction en fluage à différentes températures (de 25 °C à 120 °C) ont été effectués pour identifier les paramètres de ce modèle. Comme un des objectifs principaux est d'estimer l'évolution de l'état mécanique des matériaux après l'opération de moulage, une stratégie est proposée pour modéliser de façon simplifiée le changement de phase liquide-solide en utilisant une fonction spéciale dans [COMSOL] pour éviter des instabilités numériques.

Modélisation du comportement de la structure

La dernière partie concerne la modélisation d'un pipeline. Un élément de pipe isolé (5LPP à base de mousse syntactique polypropylène) incluant un Field joint en polypropylène injecté est ici modélisé. Par mesure de simplification la méthode de pose en J pour l'application ultra profonde est considérée. La séquence de réalisation et d'installation correspondant aux différentes étapes de la modélisation est décrite ci après :

- La surface de l'acier et du chanfrein des matériaux isolation thermique sont initialement chauffés par flux de chaleur en 2 minutes. Les températures atteintes au niveau des surfaces sont d'environ 150 °C.
- L'injection du polypropylène est ensuite réalisée. La température initiale de la matière est de 200 °C.

- Refroidissement du Field Joint par convection forcée externe dans le moule en acier pendant 10 minutes.
- Refroidissement du Field Joint avec convection naturelle dans l'air sans le moule en acier
- Immersion du pipeline à la vitesse de 1m/min
- Après atteinte de la profondeur maintien dans l'eau avant mise en service pendant 5 jours
- Mise en service du pipeline avec une température interne de 100 °C

La longueur du pipeline modélisée de 2 m est suffisante pour représenter les effets thermiques liés au processus de moulage. Comme la géométrie et le chargement thermomécanique sont supposés être symétriques par rapport à l'axe vertical, un modèle 2D axisymétrique est utilisé. Afin d'analyser correctement les différentes concentrations de contraintes possibles des maillages raffinés doivent être utilisés à différents endroits de la structure. Les différentes conditions aux limites mises en œuvre sont les suivantes :

Pour la première étape, deux flux de chaleur sont appliquées sur les interfaces du Field Joint; la convection naturelle dans l'air (à coefficient de transfert thermique constant) est utilisée pour les autres surfaces du pipeline interne et externe. On suppose que la longueur du pipeline est importante. Ainsi, les conditions de symétrie peuvent être utilisées pour les surfaces supérieure et inférieure dans les problèmes thermique et mécanique.

Les deuxième et troisième étapes sont calculées en prenant en compte les conditions initiales (température, contrainte, déformation) obtenues à la fin de l'étape précédente. Au cours de la mise en place du pipeline, le pipeline est supposé être ouvert. Ainsi, la pression et la température à l'intérieur et à l'extérieur sont identiques.

Lors du fonctionnement en service, la température associée au fluide atteint 100 °C.

Au niveau du comportement des matériaux l'évolution en température des coefficients de dilatation reste à définir. Dans le cas de PP solide, deux coefficients de dilation distincts et constants sont utilisés pour la phase solide et pour la phase liquide (analyse simplifiée). Au cours du changement de phase, sa valeur peut être estimée grâce à une fonction de Heaviside lissée (fonction "flc2hs" dans COMSOL). Dans le cas du GSPP, une relation linéaire entre le coefficient de dilatation thermique et la température est utilisé [Bouchoneau, 2007].

Ce modèle simule donc au plus proches le processus de fabrication et les conditions de service d'un pipeline. Pour chaque étape de modélisation, l'évolution de l'état thermomécanique est analysée. L'état de sollicitation des matériaux est analysé en traçant l'état de contrainte dans le plan contrainte de Von Mises – pression hydrostatique. L'analyse de ces résultats permet d'avoir les états de sollicitations les plus critiques pour les matériaux et dans les zones de liaison (interfaces) entre les différents matériaux. Ces résultats permettent de proposer les essais complémentaires

pouvant être intéressant à réaliser pour compléter l'analyse du comportement des matériaux et des interfaces en service. Du fait de l'opération de moulage du Field joint d'une part et de l'influence de la pression hydrostatique et du gradient de température en service, il est important d'analyser les sollicitations des interfaces (polymère-polymère et polymère-acier) et en particulier le signe de la contrainte normal (traction ou compression).

Pour étudier le comportement des interfaces entre deux matériaux (polymère-polymère et polymère-acier), le dispositif expérimental de type d'Arcan modifiée est utilisé. Ce dispositif nous permet de combiner compression ou traction avec des chargements de cisaillement. En outre, les dimensions de l'échantillon doivent être représentatives de la structure réelle. Notre ambition est de pouvoir analyser le comportement de ces interfaces et en particulier de construire l'enveloppe de rupture pour assurer un dimensionnement fiable des systèmes étudiés. Une adaptation de la technique développée au LBMS pour analyser le comportement de colles dans un assemblage a été proposée. Des modélisations numériques ont été utilisées pour définir la géométrie des éprouvettes afin de limiter les concentrations de contraintes proche des interfaces. Des contraintes de fixation des éprouvettes a conduit à la réalisation d'un montage Arcan modifié adapté à ce type d'assemblages. Pour une étude de faisabilité de la démarche expérimentale proposée et pour faciliter la réalisation des éprouvettes des matériaux ont été choisis spécifiquement pour cette étude en fonction des contraintes de réalisation. La liaison entre un PVC (chlorure de polyvinyle) et un PU injecté a été analysé. Les résultats expérimentaux obtenus sont prometteurs et montrent la faisabilité de la démarche proposée pour analyser expérimentalement le comportement mécanique des différentes interfaces (ou liaisons entre différents matériaux) pour les applications de type Field joints.

Conclusion et perspectives

L'exploitation offshore pétrolière en eau profonde nécessite des systèmes d'isolation thermique efficaces. Le comportement mécanique des matériaux d'isolation thermique est complexe et nécessite l'utilisation de modèles dépendant du temps en raison de la nature de la matrice polymérique. Afin d'analyser le comportement à long terme des matériaux, l'influence de la pression hydrostatique et de la température a été analysée. Le type des chargements correspond aux conditions d'installation et de service de ces structures.

Pour caractériser le comportement thermomécanique des matériaux d'isolation différentes études expérimentales ont été proposées. Comme le chargement mécanique principal de la structure est la pression hydrostatique, des essais spécifiques de compression hydrostatique à différentes températures et selon différents profils de charges ont été réalisés en utilisant un caisson hyperbare en mesurant l'évolution de la flottabilité des échantillons avec la pression. De plus, le comportement mécanique des matériaux de fluage en traction a été examiné à l'aide des tests sur DMA. En utilisant ces résultats expérimentaux des modèles de comportements ont été développés.

Pour analyser le comportement en service d'un pipe, un modèle numérique a été développé (élément de pipe incluant un Field joint). Le modèle thermomécanique prend en compte l'influence du processus de fabrication, du processus d'installation et des conditions de service. Ainsi, il est possible d'analyser l'influence de différents paramètres sur la répartition des contraintes dans les isolants en fonction du temps. Pour compléter les critères possibles de ruines de la structure dans la zone du Field joint, qui est la plus critique, une analyse de l'enveloppe de rupture des interfaces entre les isolants (revêtement principal et revêtement du Field joint) d'une part, et entre les isolants et le pipe en acier d'autre part doit être déterminée. Dans ce but, une adaptation de la démarche développée au LBMS pour caractériser le comportement d'assemblage collé a été proposée. Les premiers résultats sont prometteurs.

Différentes perspectives au travail réalisé peuvent être proposées.

Pour l'aspect modélisation, le comportement thermomécanique des matériaux pourrait être amélioré en prenant en compte des différents phénomènes. En ce qui concerne la GSPP, l'introduction d'une variable d'endommagement est envisagée. Une idée est de considérer la variable d'endommagement comme une fonction intégrale de la distribution de microsphères. La fonction d'évolution de la variable est généralement composée de deux termes, une contribution de von Mises et une composante de la pression [Perreux et al, 2008]. L'introduction de la nouvelle variable transforme le modèle de petites transformations en un modèle de grandes déformations où le gradient de la transformation doit être pris en compte dans le calcul de la contrainte. La variable d'endommagement pourrait jouer un rôle important dans le changement de la porosité (pourcentage de vide intégré par des microsphères), les paramètres visqueux et la rigidité (module d'Young et coefficient de Poisson). Dans ce cas, l'idée basée sur les théories de matériaux poreux [Moris & Tanaka, 1973; Martin, 2007] paraît convenable. De toute façon, COMSOL Multiphysics s'adapte à cette simulation en utilisant d'autres modules PDE pour les variables d'endommagement et de transformation de contraintes Piola-Kirchhoff (hypothèse des petites transformations) aux contraintes de Cauchy (grandes déformations).

En ce qui concerne le matériau PP injecté, l'influence du degré de polymérisation [Le Goff et al, 2005 ; 2011] peut être prise en compte. Ce paramètre sera gouverné par la vitesse de refroidissement du matériau et va influencer les propriétés thermomécaniques du matériau.

Une difficulté associée à l'amélioration du modèle est de prendre en compte le comportement de l'interface entre le matériau de revêtement principal et le PP injecté. Injection de PP fondu affecte le comportement GSPP par fusion locale à l'interface entre deux matériaux. Avec la connaissance du comportement d'interface, un modèle d'interface 1D peut être utilisé en se couplant avec le modèle 3D global de la structure. Cependant, actuellement, le couplage entre les modèles 1D et 3D n'est pas disponible dans COMSOL Multiphysics.

D'un point de vue expérimental, deux actions peuvent être proposées.

Le développement de l'essai de type Arcan modifié pour l'étude du comportement des interfaces dans les assemblages polymère-polymère et polymère-acier doit être poursuivi. Cela permettra de construire une enveloppe de rupture qui pourrait être utilisée en liaison avec le modèle d'interface 1D proposé. Pour valider la démarche des essais à l'échelle structurale doivent être développés. Par exemple, pour analyser l'influence de la phase de pose des pipelines un essai de flexion sur pipeline est intéressant. Pour analyser l'influence du fonctionnement en service, il semble intéressant de développer un essai prenant en compte le chargement thermique et l'influence de la pression hydrostatique ; un essai en caisson hyperbare sur une portion de pipe peut être envisagé. Ce type de tests est indispensable pour nous donner une information globale du comportement du pipeline.

Enfin, de nouveaux matériaux sont en cours de développement pour la réalisation des Field joints, principalement dans le but de réduire le temps d'installation et d'augmenter la température d'utilisation. Ainsi, pour faciliter ces développements, la démarche de modélisation proposée dans cette étude peut être adaptée pour évaluer l'impact du nouveau matériau sur la réponse du système et limiter les essais coûteux.

Chapter 1. Presentation of the problem

Offshore oil exploitation is developing very fast because new oil and gas reserves are being found in deep water. At 3000m depth, the offshore exploitation conditions are very severe; the hydrostatic pressure can reach 30 MPa and the sea water temperature drops to 4°C. For safety and efficiency purposes, design of subsea flowlines and risers has to be optimized in order to avoid many phenomena caused by the decrease of oil viscosity, induced by low temperature environment (gas hydrate, wax deposition…). The most used solution is the protection of metal pipelines from the cold water by passive thermal insulations to maintain the temperature of the fluid flow above 40°C. Thermal leaks during the oil transport, under service conditions, have to be limited and thus the understanding of the thermo-mechanical behaviour of the thermal insulation material around the pipes is of great interest.

In this chapter, an overview of the main insulation coatings of pipelines is presented together with the coating materials used in field joints. A field joint region is the initially uncoated area that results when two pipes with coating cutbacks are assembled by welding and then coated, usually in situ, during the installation process. This coating zone aims to guarantee local thermal performance. The field joint area is known to be the most critical zone in a pipe. To guarantee the durability of exploitation (about 20 years), the understanding of the field joint moulding process and the main constraints induced during the installation and the service life of pipelines (influence of residual constraints, thermal expansion, hydrostatic pressure, thermal response of the system) is essential.

1.1 Overview

Offshore oil exploitation began at the end of the 19th century. In 1896, the fist oil wells were drilled in Summerland, California. At that time, the depth of the wells was limited (from 100 to 150m) and offshore pipelines became the efficient way to transport the petroleum products. Today the increasing need for oil requires more and more new production, especially deep-sea oil exploitations. Until 2010 there were about 6000 subsea wells in the world. "Global Offshore Drilling Expenditure is Expected to Grow to More Than $490 Billion in the Period from 2009 to 2015" is an estimation of Global Business Intelligence (GBI) in 2010 [GBI, 2010] and the principal interesting regions are US Gulf of Mexico (USGOM), West Africa, Brazil and Asia Pacific. The most important challenge in offshore oil exploitation is the depth of subsea wells. There are many types of oil platform depending on each situation, the oil platform may be fixed to the ocean floor, may consist of an artificial island, or may float (Fig. 1.1.).

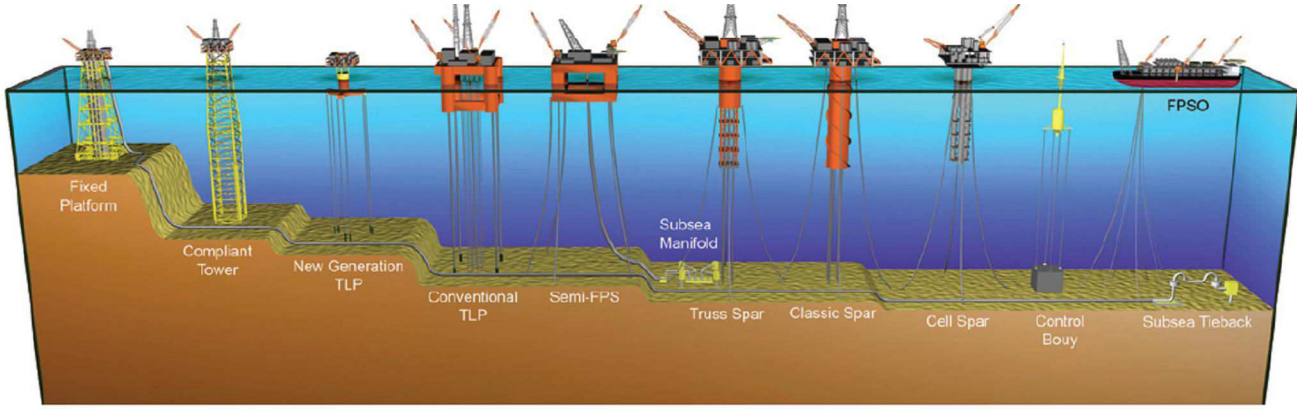

Fig. 1.1. Types of oil platform [Kyriakides & Corona, 2007]

The exploitation of petroleum reservoirs in deep water requires the use of materials to resist both the high hydrostatic pressure and the important temperature gradient in the marine environment. Considering inner temperature of the pipe (oil temperature) and external temperature (sea water) the coating material is exposed to important thermal gradients which may affect its long term behaviour. A key point is to guarantee the fluid flow speed during the service life (over 20 years) and to ensure the thermal properties of the pipe during this period. One aim of the flow assurance is to maintain a minimum temperature while the product is being transported, i.e. to conserve the heat of the fluid and prevent the cooling under the high pressure. Considering the costs and difficulties of access to offshore equipment, everything must be done to minimize the breakdowns and the interventions. The pipeline must be designed to account for other operational events, such as pipeline shutdowns, when the product is stationary.

The subsea production of hydrocarbons can be blocked by many effects. There are two common phenomena in the flow assurance challenge: Gas hydrate and wax depositions (Fig.1.2). Hydrates

were known to cause plugging and flow stoppage in pipelines in 1934 as described in the work of Hammerschmidt [Hammerschmidt, 1934]

Gas hydrates are snow-like crystals that can be formed when small gas molecules are in contact with water at high pressure and low temperature. Hydrates are formed when the gas molecules are trapped inside cages of the hydrogen-bonded water molecules. The physical properties of hydrates are similar to those of ice. The hydrates can form on the wall or in the bulk of pipelines. As a consequence, the growth of the deposit and formation of plugs can occur.

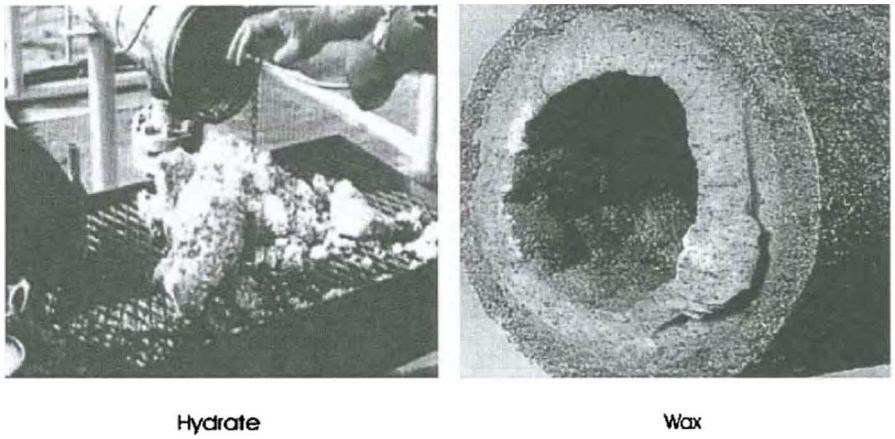

Fig. 1.2. Solid depositions formed in hydrocarbons flowlines [Bai. Y & Bai. Q, 2005]

In figure 1.3, a typical curve presents the influence of the pressure and the temperature on the forming of the gas hydrate. So, in order to avoid risk of hydrate formation, in a high pressure condition, the control of heat loss in pipelines must be more rigorous.

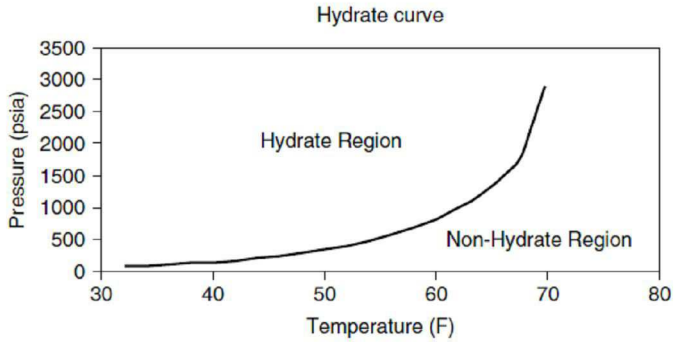

Fig. 1.3. A typical gas hydrate curve [Guo et al, 2005]

Moreover, a crude oil is a complex mixture of hydrocarbons which consists of aromatics, paraffins, naphthenics, resins, asphaltences, diamondoids, mercaptans, ... When the temperature of crude oil is reduced, the heavy components of oil, like paraffin/wax, will precipitate and deposit on the pipe wall. The pipe internal diameter will be reduced with wax deposition, resulting in higher pressure drop. Wax deposition problems can become so severe that the whole pipeline can be completely blocked.

To reduce the heat loss in the fluid, one of the most common techniques is protection of the metal pipe from cold seawater by passive thermal insulations. Depending upon the service condition of the structure (maximum service depth, maximum temperature, thermal properties recommendations...) the proposed insulation materials are different [Watkins & Hershey, 2001]. Thermo-mechanical protection requires several combined properties that are not easy to satisfy with a single material. The best way is through a variety of combined materials, all of which should be compatible with each other. In this study, we are interested in the thermo-mechanical behaviour of multilayer structures which consist of several types of polymeric materials deposited on a metallic pipe. The main materials used are solid polymers and syntactic foams which consist of polymeric matrix and hollow glass microspheres (Fig 1.4). The more critical parts of the pipelines are the thermal protections of the junctions between the pipes which are called field joints (Fig 1.5). A field joint region is the uncoated area that results when two pipes with coating cutbacks are assembled by welding. After welding, this area has to be coated in order to guarantee local thermal performance to limit thermal leaks. This coating is generally performed in situ (on the barge or in the spool base) and manufacturing constraints impose short manufacturing time and thus adapted coating materials. Field joints are considered as a weak point of a pipeline because of the discontinuous materials and the manufacturing conditions.

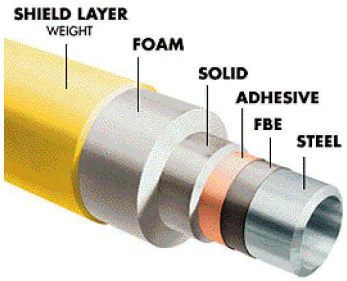

Fig. 1.4. Thermal insulation based on foamed polypropylene of Thermotite®

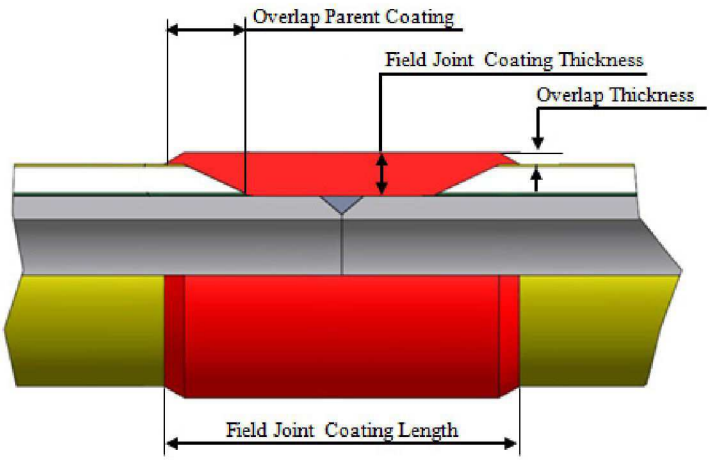

Fig. 1.5. 5-layer Field Joint Coating Design of Thermotite®

1.2 Insulation material for offshore applications

1.2.1 Mainline coating

1.2.1.1 Overview

The pipeline coating represents about 5% of the total cost of offshore exploitation. The choice of material plays in important role in pipeline economics. The combination of multilayer materials is used to obtain the required mechanical, thermal properties and long term behaviour in ultra deep sea. A variety of pipeline-coating technologies are available: 3 layer polyethylene (3-layer PE), single Fusion bonded epoxy (FBE) and dual-layer FBE (or Dual Powder System, DPS), multi-layer polypropylene (MLPP) coatings... [Tailor et al, 2003]. Recently, new technology (Bredero Shaw's High Performance Composite Coating, HPCC) has been developed to adapt to challenging environments [Singh et al, 2005]. HPCC is produced by melt fusing all components in powder form. Currently coatings based on use of polypropylene are the most frequently used in deep sea environment.

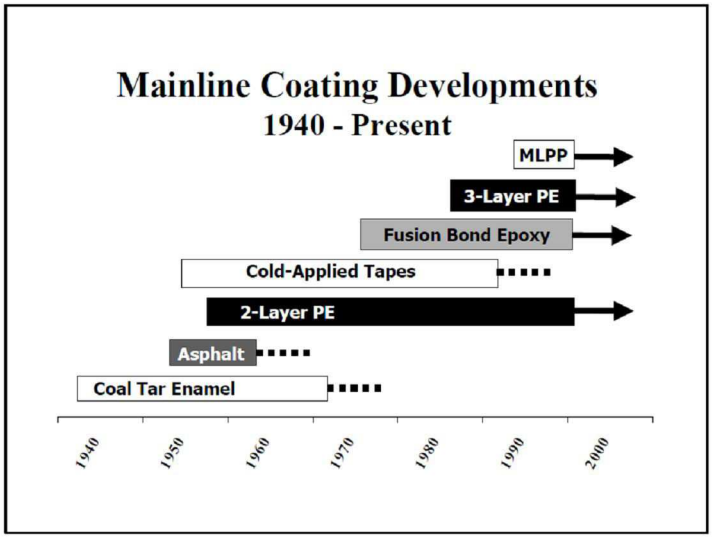

Fig. 1.6. Mainline Coating Developments of the Past 60 Years [Tailor et al, 2003]

Polypropylene is known to be an excellent material which has good thermo-mechanical properties and also less water penetration with respect to other materials (Tab. 1.1). So, we are interested here in the multi-layer polypropylene coating for its application in ultra deep offshore oil exploitation. The system of MLPP proposed by Socotherm® is called "Multypass" [Berti, 2004]. It consists of an anti-corrosion protection and of several polypropylene layers (solid polypropylene, glass syntactic polypropylene, adhesive polypropylene. The glass syntactic polypropylene (see 1.2.12), which is the main thermal insulation material in this system, is characterized by good thermal insulation properties and high resistance to hydrostatic pressure [Socotherm®]. The other layers of solid polypropylene are used to protect the metal pipe from corrosion and mechanical impacts.

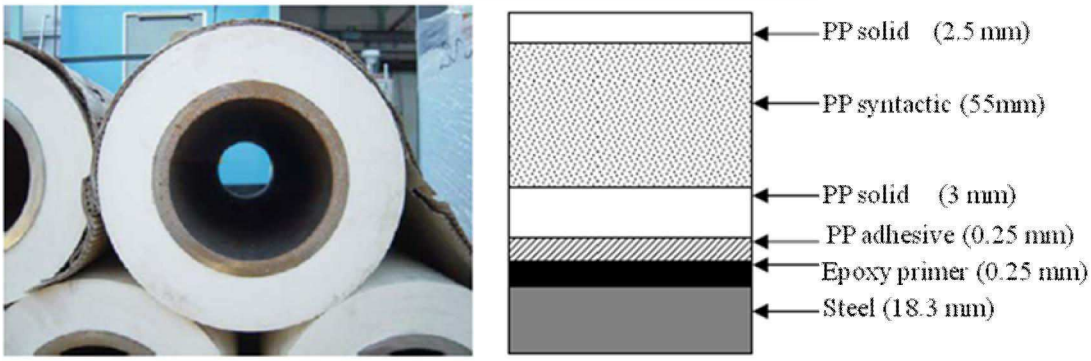

Fig. 1.7. Thermal insulated five layer system of Socotherm [Bouchonneau, 2007]

	PP	PE	FBE	Bitumen
Impact strength	5	4	3	2
Weathering resistance	4	4	4	3
Abrasion resistance	4	4	5	2
Damage resistance	5	3	3	2
Environmentally friendly	5	5	4	2
Legend: 1 = very poor... 5 = excellent				

Tab. 1.1. Comparison among anticorrosion coatings: transport, handling and laying [Guidetti et al, 1996]

The so-called "Multypass" is known to have important advantages like: strong adhesion between each of the layers, no significant voids or air entrapment in materials and perfect concentricity of the pipeline. In general, the pipeline fabrication follows the sequence detailed on the Figure 1.8. During the extrusion coating of syntactic foam (or foam), the rollers apply a constant pressure at the contact of material to ensure a good homogeneity of the thickness and eleminate air entrapment. Each pass provides about 1cm thickness of insulated material. The use of different polypropylene layers to coat the pipeline insures a good compatibility between the different layers. It must be mentioned that for syntactic foam layers a small percentage of microsphere breakage may occur during the extrusion process.

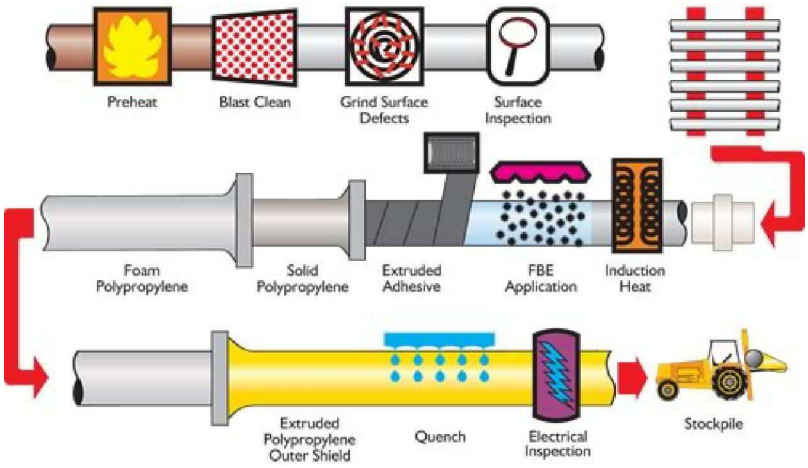

Fig. 1.8. Product application process [Bredero Shaw]

1.2.1.2 Syntactic foam

Syntactic foam, the main component of MLPP coating, is a lightweight, engineered foam consisting of manufactured hollow glass spheres (called microspheres) embedded in a polypropylene matrix. These hollow spheres typically range from 10 to 200 microns in diameter and are available in several materials, including glass, ceramic, and polymers but currently the use of glass microspheres is generalized. The thickness of microspheres varies between 1 and 2 microns (Fig 1.9). This type of system has a very high compressive strength-to-weight ratio. In our study, the matrix materials used are polymer; the hollow particles are called microspheres.

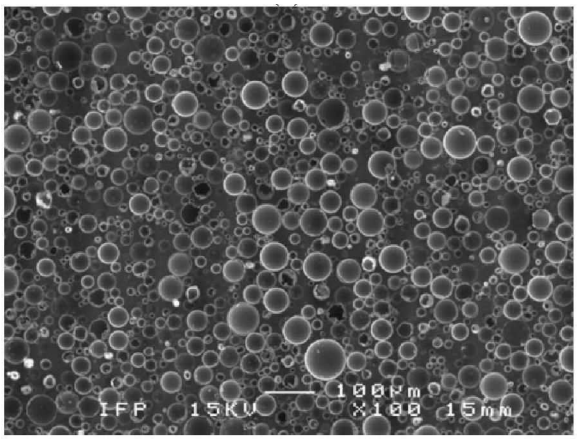

Fig. 1.9. Glass Syntactic Polypropylene [Bouchonneau, 2007]

Major advantages of syntactic foams are:

- lightweight: by increasing or decreasing the proportion of microspheres, density approaching 600 kg/m^3 can be reached,
- resistance to hydrostatic pressure of several hundred bars,
- good thermal insulation comparing to the solid polymer,
- good resistance to impact loads thanks to high plastic deformation.

Depending on the water depth, different types of syntactic material can be used in order to adapt to the different compressive behaviours recommendation [Watkins and Hershey, 2001]. They have a similar type of glass microspheres distribution but different matrix nature (Tab 1.2). Glass Syntactic Polypropylene can be obtained by mixing in the melt state polypropylene and microspheres. For Glass Syntactic polyurethane and Glass Syntactic Epoxy, the nature of matrix is respectively cross-linked elastomer and glassy thermoset. So mixing of binder resin and microspheres before polymerization is needed [Adrien et al, 2007].

Reference material	Matrix	Density $\left(kg.m^{-3}\right)$	Thermal conductivity (W/m.K)	Compressive Strength (MPa)
Glass Syntactic Polypropylene	Polypropylene	640	0.16	>10
Glass Syntactic polyurethane	Polyurethane	790	0.16	10
Glass Syntactic Epoxy	Epoxy/anhydride	720	0.14	80

Tab. 1.2. Industrial syntactic foam

The behaviour of insulation materials has been studied in various experimental programs and adapted characterization methods have been developed [Bardenhagen et al, 1997, 2005; Wouterson et al, 2005; Adrien et al, 2007; Wysocki et al, 2005; Choqueuse et al, 2010]. These studies showed that the mechanical behaviour of syntactic foams depends on the nature of material and loading types, e.g. Fig. 1.10.

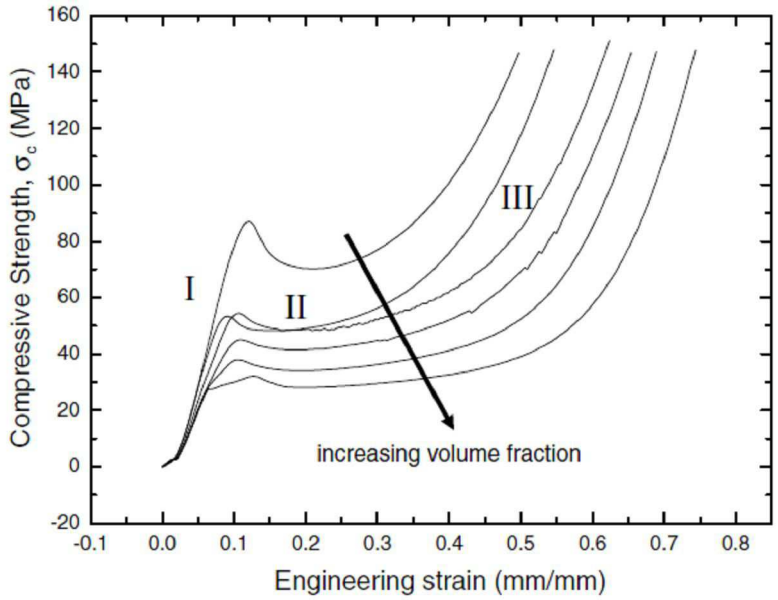

Fig. 1.10. Compression stress-strain curve of syntactic foam with various amounts of K15 (= 0.15g.cm^{-3}) microspheres content [Wouterson et al, 2005]

The mechanical failure modes of syntactic foam under uni axial compression have been studied: one was characterised by longitudinal splitting; and another by layered crushing [Kim and Plubrai, 2004, Islam and Kim, 2011]. The different mechanisms depend on the density of the syntactic foam. The longitudinal splitting is the main failure mode of material with lower density and the layered crushing causes the rupture of material of higher density. The sequence of microspheres collapse can be observed by scanning electron microscopy (Fig 1.11).

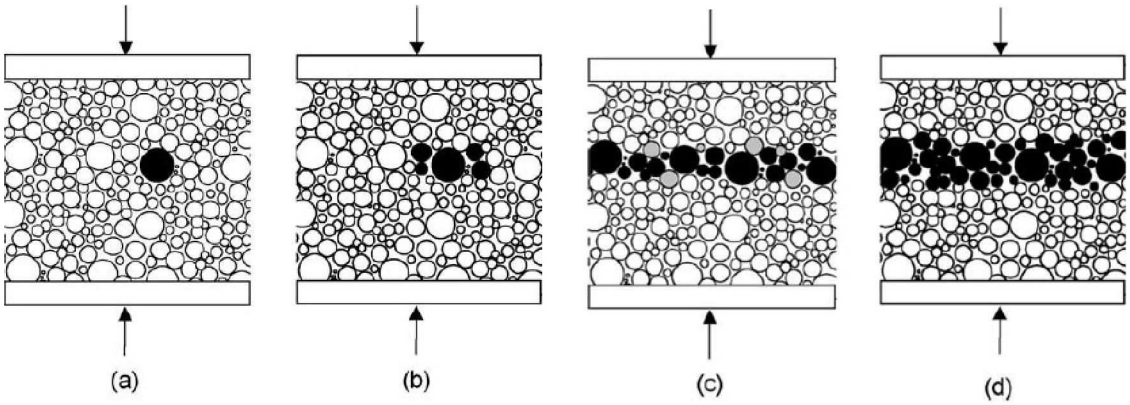

Fig. 1.11. Suggested sequence of microspheres crushing [Kim and Plubrai, 2004]

Hydrostatic pressure is one of the main components of mechanical loading of submarine structures. So it is important to analyse the mechanical behaviour of the materials under such loadings. By the use of a confinement ring [Adrien et al, 2007] the loading is not purely hydrostatic but coupled with uni axial compression loading (Fig 1.12); the notations MS1, MS2 and MS3 correspond to Glass Syntactic Polypropylene, Glass Syntactic Polyurethane and Glass Syntactic Epoxy respectively.

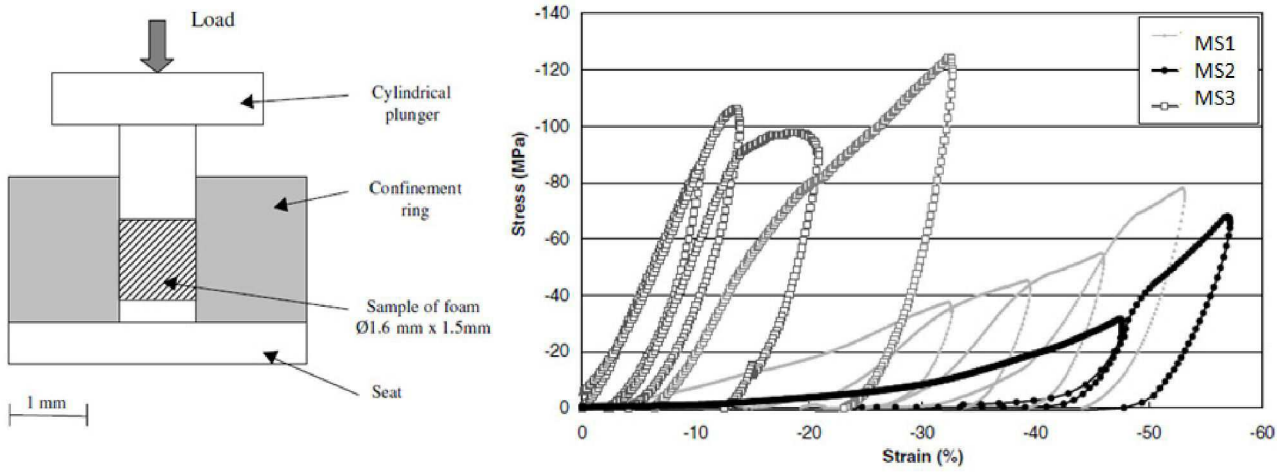

Fig. 1.12. Stress-strain responses for the three foams during stepwise confined compression [Adrien et al, 2007]

To improve the hydrostatic pressure tests, another method based on the direct measurement of the buoyancy evolution of a sample in water has been proposed [Choqueuse et al, 2010]. A comparison of two materials (Fig 1.13) shows that having the same grade of microspheres, the crush pressure of material with rigid matrix (epoxy) is significantly higher than the one with soft matrix (polyurethane). Even in the case of thermosetting matrix (epoxy), the temperature plays an important role.

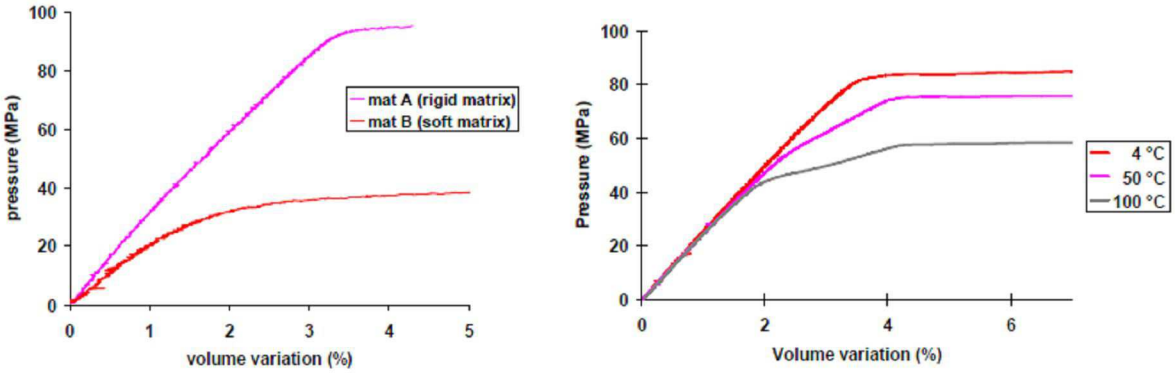

a- Effect of matrix rigidity b- Effect of temperature

Fig. 1.13. Hydrostatic compression behaviour [Choqueuse et al, 2010]

According to [Bouchonneau, 2007], the behaviour of syntactic foam (Glass syntactic polypropylene) subjected to cyclic hydrostatic loading can be divided into three phases (Fig 1.14):

- Phase of damage to the material with the progressive failure of the microspheres under the effect of loading during the first cycle.
- Brutal crushing of the structure probably related to the collapse of the structure on its own after breaking all spheres.
- Increased pressure: behaviour can be likened to that of a solid material.

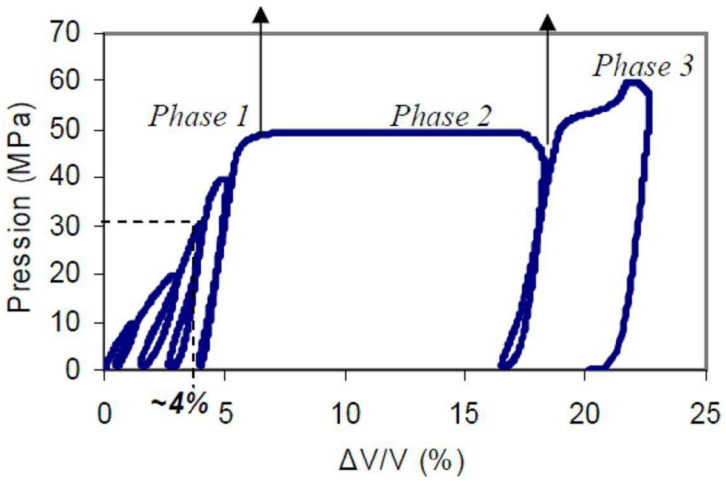

Fig. 1.14. Hydrostatic pressure-volumetric strain diagram of Glass syntactic PP at 20°C [Bouchonneau, 2007]

The collapse of microspheres leads to the increase of thermal conductivity and density of material. Because of the considerable thermal conductivity of glass microspheres, the mean thermal conductivity of syntactic foam after the collapse may be higher than that of solid polymer.

Consequently, collapse of microspheres reduces the efficiency of thermal insulated systems. In order to reduce the damaged kinetics stiffer matrix material is required.

The effects of microspheres radius ratio and specimen aspect ratio on the material behaviour under compression were presented by [Gupta et al, 2004; Sanders and Gibson, 2003]. An increase of microspheres density and changes in the thickness to radius ratio can lead to a modification of the mechanical behaviour of syntactic foam [Wouterson et al, 2005]. In order to precisely observe the microstructure response of the material, tomography [Roux et al, 2008; Kim and Plubrai, 2004] or ultrasonic imaging technique [Gupta and Woldesenbet, 2003] can be used. Using X-ray microtomography (Fig. 1. 15), syntactic foam composition (volume fraction) and also the microspheres distribution can be determined (Tab 1.3). Another methodology which is useful to calculate the particle densities of syntactic foam is the air pycnometer [Kim and Plubrai, 2004]. By mass conservation, the syntactic foam composition is also estimated.

	Matrix (% vol)	Glass (% vol)	Gas (% vol)	Microsphere (% vol)
Glass Syntactic Polypropylene	47	16	37	53
Glass Syntactic polyurethane	54	12	34	46
Glass Syntactic Epoxy	38	16	46	62

Tab. 1.3. Syntactic foams composition determined by X-ray microtomography [Sauvant-Moynot et al, 2006]

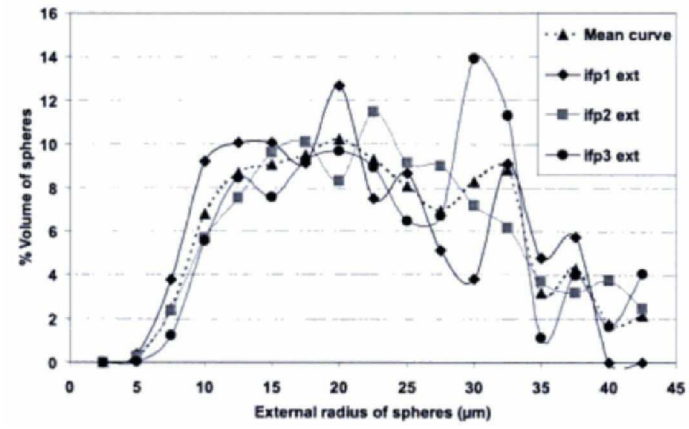

Fig. 1.15. Comparaison of initial microsphere granulometry in syntactic foams measured by X-ray microtomography [Sauvant-Moynot et al, 2006]

One of the challenges of oil offshore exploitation is heat loss during the service of pipelines in ultra-deep water that is able to cause the formation of hydrates and paraffin plugs inside of pipelines.

Experimental testing and modelling were realised on industrial prototypes to better understand the thermal properties of the structure [Bouchonneau et al, 2010]. The thermal properties of syntactic polypropylene in the transient state with respect to hydrostatic pressure were presented:

Test sequence	Pressure	Heating mat power	Water temperature	Mean external convection coefficient	Apparent thermal conductivity of syntactic PP	Apparent heat capacity of syntactic PP
	(bar)	(W)	(°C)	($Wm^{-2}K^{-1}$)	($Wm^{-1}K^{-1}$)	($Jkg^{-1}K^{-1}$)
Test A step 2	1	120	15.3	125	0.150	1501
Test B step 3	300	120	16.7	170	0.154	1500

Tab. 1.4. Thermal properties of syntactic polypropylene by the transient state analysis [Bouchonneau et al, 2010]

For the long term service life, the extreme conditions (high pressure, important thermal gradient, and sea water) accelerate the aging process of thermal insulated material by the water uptake phenomenon. A significant loss of thermo-mechanical properties makes the material much less effective. A methodology of ageing test is presented by [Choqueuse et al, 2004] to predict the evolution of thermal properties and water absorption's phenomena of syntactic foam. Moreover, the main coating materials have a tendency to deform slowly even under the constant stress. This phenomenon is known as creep of material. The higher the temperature and the stress, the higher the creep effect. In the case of solid polymer, the volume change can be considered to be elastic, i.e. the viscous part of the volumetric deformation can be neglected. However, in the case of glass syntactic foam, because of the presence of microspheres and of voids, the viscous part of volumetric deformation which comes from the creep hydrostatic pressure can be important. The high volumetric deformation in creep must lead to a reduction in volume, a collapse of microspheres, and an increase of thermal conductivity. Thus, the efficiency of the insulation material will be reduced. In addition important creep deformation can lead to the loss of the structural stability by buckling.

In terms of modelling, different approaches have been used to model the mechanical behaviour of syntactic foams, based on Drucker-Prager elastoplastic type models taking into account the different responses under tension and compression and taking into account different damage effects [Rizzi et al, 2000]. The long term behaviour of the material can be modelled by considering the collapse of microspheres under different loadings using a damage variable in a viscoelastic model [Perreux and Robinet, 2008]. The homogenisation method can also be used to characterise the thermo-mechanical behaviour [Perreux and Robinet, 2008; Marur, 2005, 2009; Antunes et al, 2011; Bardella and Genna, 2001]. Regarding the densification effect, the foam behaviour can be modelled as a chain of elastic springs in order to model the progressive collapse [Pampolini and Del Piero, 2008].

1.2.2 Field joint coating

The field joint coating (FJC) system must not be the weak link in the pipeline chain. As a minimum, it must provide protections that is equal to or better than the mainline coating and to that end it must be fully compatible with and similar in behaviour to the parent coating [Tailor et al, 2003]. Fig. 1.16 shows field joint coating development.

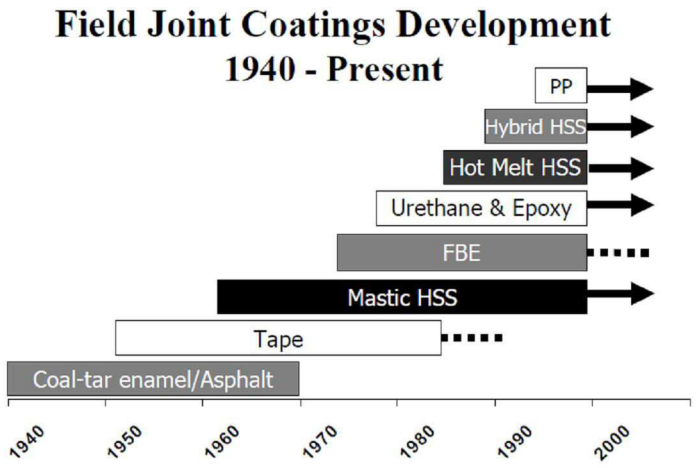

Fig. 1.16. Field Joint Coating Developments [Tailor et al, 2003]

The solid polypropylene proposed by [Bredero Shaw] presents good compatibility with the MLPP coating materials. The thermal mechanical properties of solid polypropylene are:

Density: 900 kg/m^3

Thermal Conductivity : 0.22 W/m.K

Specific Heat Capacity (40^{o}C): 2000 J/kg.K

Tensile strength @ yield: >18 MPa

Elongation at break: >400%

Young's modulus: >600-1400 MPa

The solid polypropylene is known as a good insulation material with a low thermal efficiency. Considered as an incompressible material, with an important elongation at break and a high corrosion protection coating, it could be used in ultra deepwater application, particularly in the field joint coating. It has only one disadvantage during the field joint moulding (the process needs to use the liquid material in forming): cooling time for the solid polypropylene is longer than the other thermosetting materials like polyurethane because its melting temperature is important (about 140°C) and its thermal conductivity is low.

Another field joint coating material used is polyurethane. It is compatible with other existing parent coatings, such as solid, syntactic, glass syntactic and foam polyurethane coatings. The thermal mechanical properties of solid polyurethane are provided hereafter [Bredero Shaw®]:

Density: 1150 kg/m^3

Thermal Conductivity : 0.195 W/m.K

1.3 Pipeline installation

Particular attention is focused on the installation of pipelines. Each installation mode has different advantages and disadvantages. There are many methods for installation of pipelines including S-lay, J-lay, O-lay, reeling, and towing methods. The solution is generally chosen as a function of the installation depth. The imposed short manufacturing time of the field joints can have an influence on the long term behaviour of the pipeline (residual stresses, stress concentrations ...).

1.3.1 S-Lay method

One of the first methods for installing offshore pipelines was S-lay method (Fig 1.17). The pipeline is welded in the line and moved across the stern of the lay barge before it reaches the ocean floor; the pipeline forms the shape of an "S" in the water. The pipeline must be supported by a truss-like circular structure equipped with rollers and known as a stinger. This method is commonly used in relatively shallow water because it needs a long stinger (measuring up to 300 feet long) to guide the pipelines and keep them from buckling. In extremely deep water, that will require the stinger to be longer and/or more curved to accommodate the greater arc of reverse curvature in the overbend region. So, a bigger stinger, buoyancy and/or structural strength will be necessary to support the increased weight of the suspended pipe span [globalsecurity.org]. The S-lay method can be used to about 2000m depth [Boyun Guo et al, 2005].

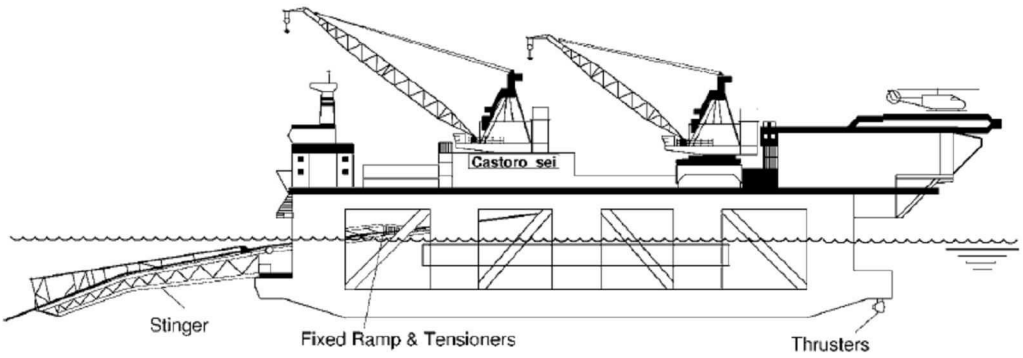

Fig. 1.17. Saipem's Castoro Sei semi-submersible S-lay vessel [Kyriakides & Corona, 2007]

The understanding of stress concentrations during the S-lay installation has been studied [Dixon & Jackson, 2003]. It was shown that the stress concentration can occur in the field joint area. If the

stress concentration leads to the creation of cracks, the pipeline loses its thermal insulation capacity and also may be attacked by seawater and buckle.

The pipes are welded together in the near horizontal position which causes a great bending of the pipe in the stinger (Fig. 1.20). A stinger which is not long enough can buckle the pipelines. In general, the stress distribution during the installations is represented in the figure below [Kyriakides and Corona, 2007].

To improve the offshore installation time, the combination of S-lay and a spiralled pipe is proposed [Buijvoets, 2011]. The new method is called O-lay (Fig. 1.18). The pipelines are welded together onshore and then transported into the water by using the buoyancy systems. A pipeline spiral will be formed with a diameter that is sufficiently large (bigger than 500 times the pipeline diameter). When the pipeline spiral arrives on site, the laying is done by a traditional S-lay method. This mixed method gives a considerable reduction of cost and also the field joint moulding quality is guaranteed. However, it cannot solve the important bending forces that come from the S-lay method.

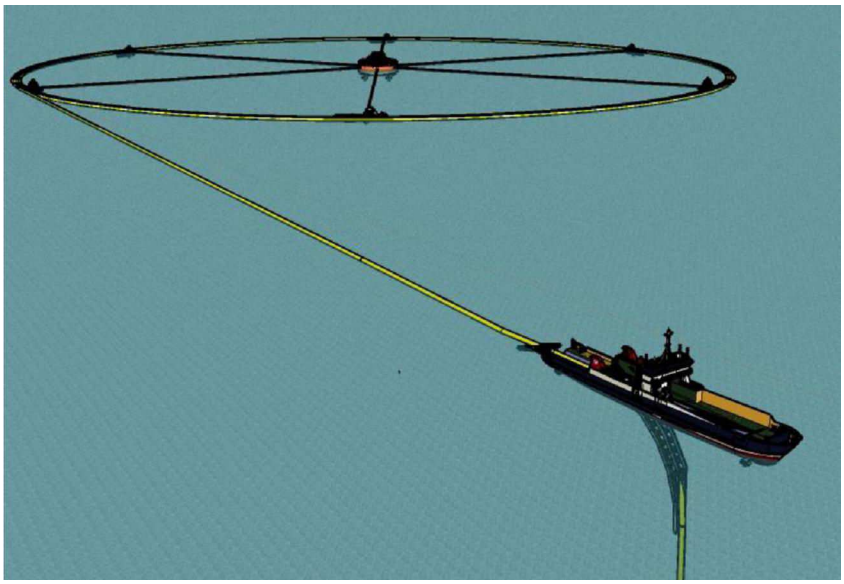

Fig. 1.18. O-lay method

1.3.2 J-Lay method

When the water depth increases, J-lay pipeline installation is preferred (Fig. 1.19). This method allows the pipelines to leave the barge from a vertical or nearly vertical position. So, there is less stress on the pipelines. As the stress due to the installation and the shape of pipelines decreases, the pipelines can be used in deeper water depths. Moreover, the pipelines from the J-lay installation withstand the motion and underwater currents better than the pipelines from S-lay installation.

Fig. 1.19. The Saipem 7000 semi-submersible crane vessel with a J-lay tower at its stern [Kyriakides & Corona, 2007]

To change the orientation of pipelines at the top, a stinger will be used. In J-lay installation, there is usually only one welding and one inspection station. So, one of the important impacts of J-lay installation is its slower realisation rate and it is therefore more costly. Additionally, the J-lay installation is not used in shallow water depths because of limited pipe angle and the important bending stress imposed on the pipelines. J-lay method has another inconvenient: the pipelines must be clamped on an installation tower. So the longer the pipelines, the heavier, and the recommended pinning force used to hold the pipelines is more important. It may lead to the collapse of thermal insulated material around the pipelines.

For J-lay the tension is the principal loading because of the weight of the pipe string suspended during laying (Fig. 1.21).

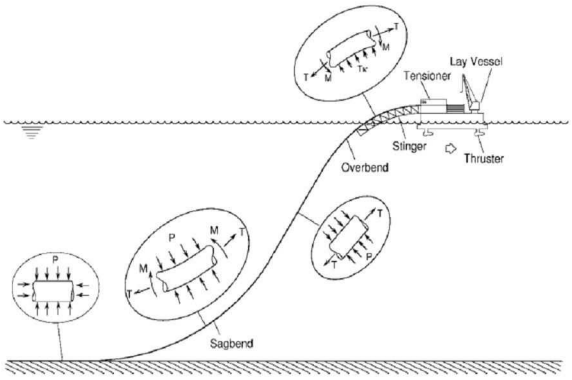

Fig. 1.20. Schematic representation of S-lay pipeline installation and associated pipeline loading [Kyriakides & Corona, 2007]

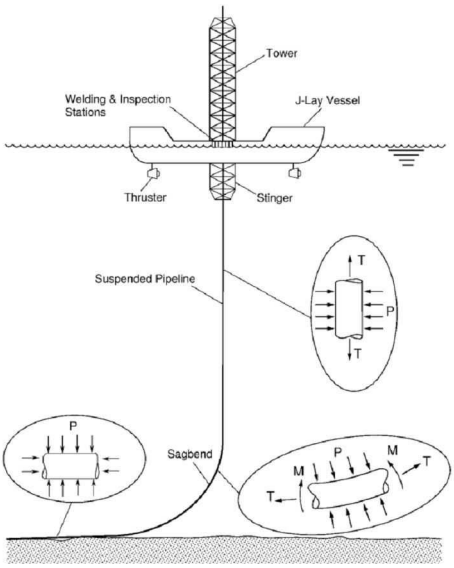

Fig. 1.21. Schematic representation of J-lay pipeline installation and associated pipeline loading [Kyriakides & Corona, 2007].

1.3.3 Moulding of Field Joint

There are two common solutions to mould a Field Joint depending on the injected material: Injected moulded polypropylene (IMPP) and injected moulded polyurethane (IMPU). The preparation for IMPP (Fig 1.22) requires that the anti-corrosion layer is in good condition and the faces of the parent coating (usually PP) are cleaned, abraded and then pre-heated to build bond strength between the PP and IMPP. Once this preparation is completed a mould is placed over the area to be treated and Solid Polypropylene is injected into the annulus.

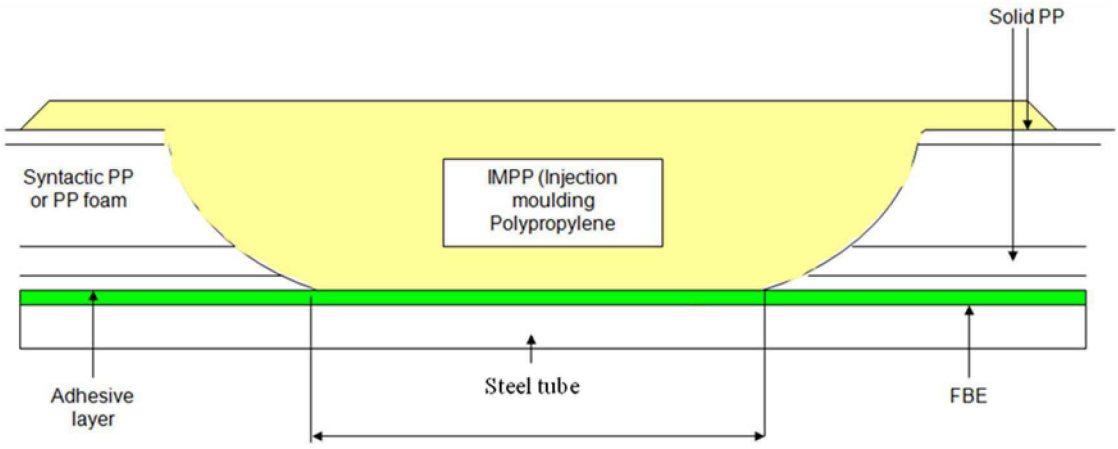

Fig. 1.22. Injection moulding Polypropylene

The following Field Joint coating process was proposed by Thermotite® (Fig. 1.23):

- The residual dust from the blasting operation is removed. The temperature of the steel is raised to coating temperature by use of an induction heating coil.
- Using specially developed applicators the bare steel is then coated with Fusion Bonded Epoxy Powder and a sintered layer of adhesive. The adhesive is applied as a powder onto the gelling FBE and forms an interlinking bond to the FBE and the subsequent injected PP.
- The chamfer areas of the parent coating are heated to the softening point of the material by use of radiant heaters.
- The joint area is then enclosed within a mould, and the mould locked in position. The annulus is then injected with molten PP.
- Upon the initial cooling of the surface of the PP, the mould is opened and the joint is quenched with cold water.
- The field joints are then visually inspected for defects or disbonding.

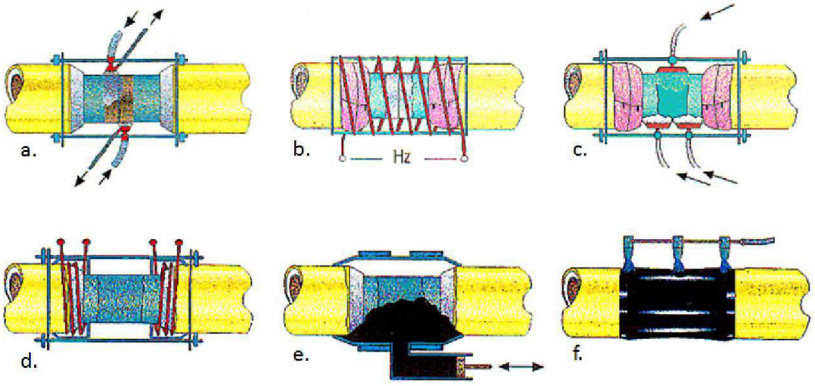

Fig. 1.23. Field Joint Coating Process Polypropylene [Thermotite®]

The preparation for IMPU (Fig. 1.24) requires the same preparation. Once this preparation is completed a mould is placed over the area to be treated and Solid Polyurethane is injected into the annulus, often overlapping the parent coating bevel faces and onto the OD surface of the PP.

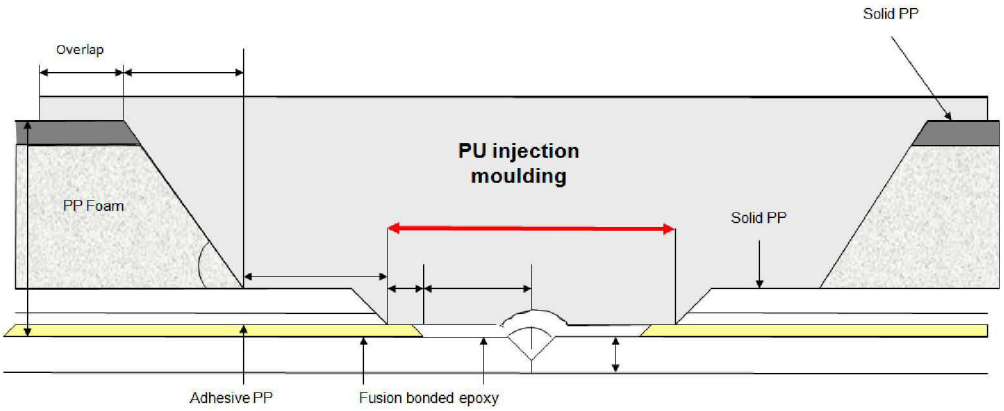

Fig. 1.24. Polyurethane injection moulding

1.4 Constraints during installation of Field Joint

A residual constraint phenomenon is one of the important problems in the field joint installation. Upon the cooling of the field joint material, because of different coefficients of thermal expansion of the materials and the heterogeneity of thermal distribution of this structure, residual constraints may lead to the appearance of a critical zone (with high stress concentrations, even with cracks). Moreover, depending on the installation's operation, unexpected stress could be introduced when the Field Joint is set up.

1.4.1 Thermal expansion

Thermal expansion is the tendency of matter to change in volume in response to a change in temperature. The degree of expansion divided by the change in temperature is called the material's coefficient of thermal expansion and generally varies with temperature:

$$\alpha = \frac{dl}{l \times dT}$$

where:

dl = the change in length of material in the direction being measured
l = overall length of material in the direction being measured
dT = the change in temperature over which dl is measured

The coefficient of thermal expansion can be measured as a function of temperature with an inductive dilatometer [Schwarz, 1986] or by Thermo-mechanical analysis (TMA-ASTM E 831-86) [Bouchonneau, 2007]. TMA is used to measure the change of a dimension of the sample while it is subjected to a temperature ramp. The samples (5mm length and 2mm thickness size) were tested with temperature ranges from 0°C to 100°C (Tab 1.5). In the case of solid polymer, the coefficient of thermal expansion tends to increase with temperature. However, the coefficients of Glass

syntactic PP and Glass syntactic PU decrease with temperature. Their value is very large, compared to that of steel (12.5×10^{-6} $°C^{-1}$). The difference in thermal response of materials in multilayer-structures like pipelines causes large constraints because of high temperature gradients during the installation and the service of pipeline.

Material	Coefficient of thermal expansion from 5 to 20°C ($°C^{-1}$)	Coefficient of thermal expansion from 20 to 60°C ($°C^{-1}$)	Coefficient of thermal expansion from 60 to 100°C ($°C^{-1}$)
Polypropylene (PP)	8.2×10^{-5}	12.4×10^{-5}	21.6×10^{-5}
Polyurethane (PU)	15.7×10^{-5}	23.2×10^{-5}	19.2×10^{-5}
Epoxy	3.7×10^{-5}	5.3×10^{-5}	6.0×10^{-5}
Glass syntactic PP	6.2×10^{-5}	5.1×10^{-5}	3.7×10^{-5}
Glass syntactic PU	13.4×10^{-5}	6.3×10^{-5}	1.6×10^{-5}
Glass syntactic EP	1.9×10^{-5}	2.5×10^{-5}	2.8×10^{-5}

Tab. 1.5. Coefficient of thermal expansion of offshore material coating [Bouchonneau, 2007]

1.4.2 Phase change of field joint material

A polymer is composed of long molecules which contain chains of atoms held together by covalent bonds. It is produced through a process known as polymerisation whereby monomer molecules react together chemically to form either linear chains or a three-dimensional network of polymer chains. The main characteristic of the chain is that the chemical bonding is strong and directional along the chains, but they are only bonded sideways by weak secondary van der Waals bonding or occasionally by hydrogen-bonding [Young, 1981]. In offshore exploitation, the most used Field joint's materials are polypropylene (semi-crystalline) and polyurethane (thermosets or elastomer). The thermal response of their thermo-mechanical properties is different, particularly during the phase change. So, to estimate the residual constraints, the stress state and temperature evolution in the field joint area it is primordial to known the thermal behaviour of the different materials. Depending on the material, the behaviour is different: during the cooling of polypropylene, a crystallization phenomenon that takes place; but in the case of polyurethane, it is a chemical reaction that happens. In addition, for each polymer type, its properties evolve differently at its transition temperature (Fig. 1.25). In the case of a semi-crystalline polymer, there is a transition zone which starts from the glass transition temperature up to the melting temperature, the thermal mechanical properties change less suddenly than those of 100% crystalline polymer.

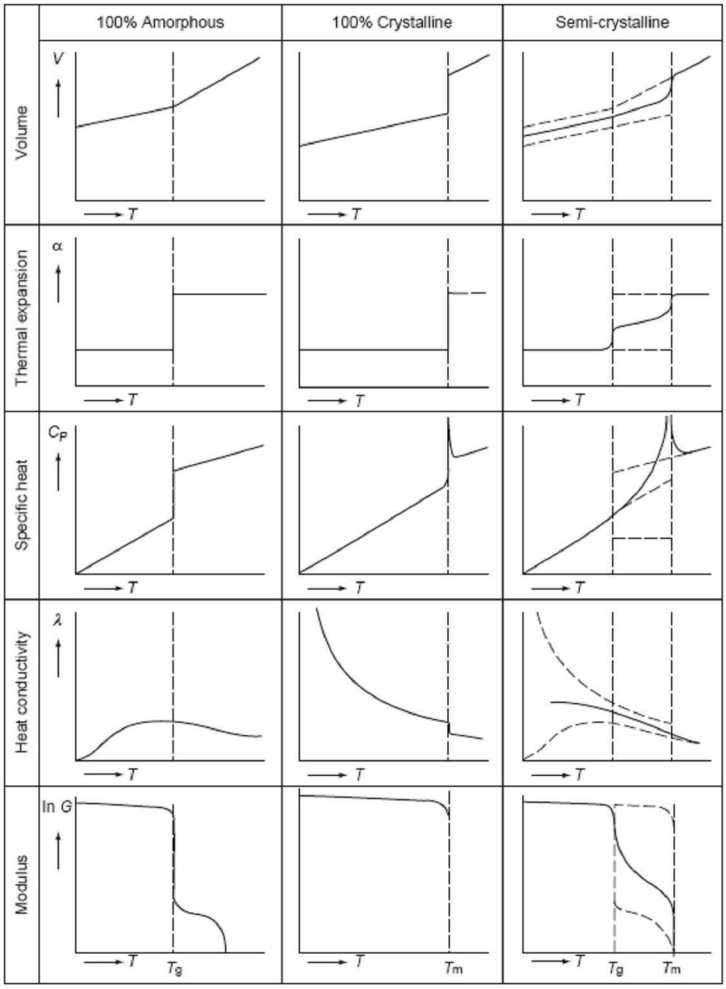

Fig. 1.25. Behaviour of some polymer properties at transition temperature [Krevelen and Nijenhuis, 2009].

Concerning the crystallization and melting of semi-crystalline polymers like a solid polypropylene, the degree of crystallinity and the size and arrangement of the crystallites have a profound effect upon the physical and mechanical properties. There are many factors which can affect the rate and extent to which crystallisation occurs for a particular polymer: rate of cooling, the presence of orientation in the melt and the melt temperature... The degree of crystallinity is estimated by different analytical methods and it typically ranges between 10 and 80%, thus crystallized polymers are often called "semi-crystalline". The properties of semi-crystalline polymers are related not only to chemical nature of polymer, but also to degree of crystallinity, distribution of polymer chain lengths and nature of additives [Seymour & Carraher, 2003]. The use of a temperature modulated differential scanning calorimetry (TMDSC) can be useful to study the transitions in semi-crystalline polymers [Genovese & Shanks, 2004; Privalko et al, 2005]. The enthalpy of melting can be calculated depending on the cooling rate of material. The degree of crystallinity of the material can be estimated by the ratio between the measured enthalpy (ΔH_m) and the enthalpy in case of 100%

crystallinity (ΔH_0). There are two main TMDSC cooling profiles: linear and modulated cooling. A series of temperature profiles obtained by changing the period of modulation (per), modulation temperature amplitude (T_a), cooling rate ($_0$) gave the different specific heat during the change in phase (Fig. 1.26). It is interesting to note that the different cooling profiles result in different released enthalpy and melting point.

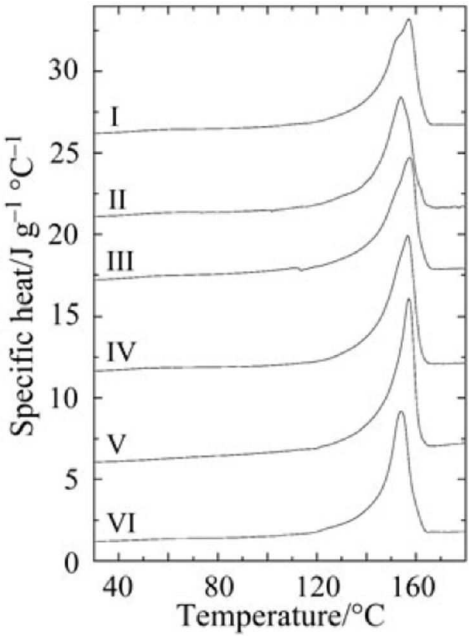

Fig. 1.26. Specific heating melting curves obtained at 10°C min^{-1} for isotactic PP crystallized under modulated and linear cooling. The crystallization conditions are: curves I-III; per = 60s, T_a = 2.0, 1.5 and 1.0 and $_0$ = 2.0°C min^{-1}, curves IV and V; per = 120, 60s, T_a = 1.0, 0.75, respectively and $_0$ = 1.0°C min^{-1}. Reference curve VI has linear cooling at a rate of 2°C min^{-1}. The curves have been displaced 5 units consecutively [Genovese & Shanks, 2004]

To study the thermal evolution during crystallization of a semi-crystalline polymer, the combination of Nakamura equation and the mixing rule between the solid state and the liquid state weighted by the relative crystallinity [Boutaous et al, 2010] gave a good result. In the field joint moulding process, the realization time must be as short as possible. This leads to increasing cooling rate at the outer extremity of the Field Joint. So, it results in the heterogeneity of thermal-mechanical properties of field joint coating material.

As regards to thermosetting polymers or elastomer like solid polyurethane, the material is a polymer composed of a chain of organic units joined by carbamate (urethane) links. A urethane linkage is produced by reacting an isocyanate group, -N=C=O with a hydroxyl (alcohol) group, -OH. Polyurethane polymers are formed through step-growth polymerisation, by reacting a monomer (with at least two isocyanate functional groups) with another monomer (with at least two hydroxyl or alcohol groups) in the presence of a catalyst. When the covalent linkages are formed, the enthalpy is released as an exotherm (Fig. 1.27). This heat source can have a considerable influence

on the cooling rate of material. The shaping of polyurethane must be realized before the forming of macromolecular links. In the injection moulded polyurethane process, the casting systems consist of two liquid components which come from basic products (polyether polyols, polyester polyols, diphenylmethane diisocyanate and toluene diisocyanate. To obtain a good conversion rate, the preferred reactive temperature is about 80°C. It is possible to characterize the kinetics with time or temperature. Once again, DSC is well adapted to observe thermal evolution during the chemical reaction of polyurethane [Dimier, 2003].

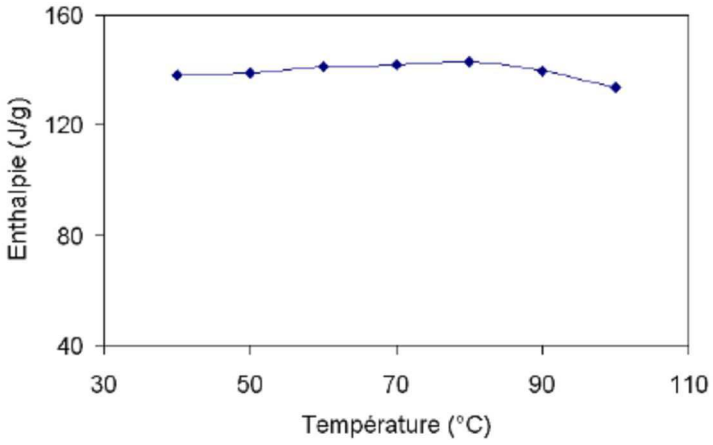

Fig. 1.27. Released enthalpy during the isothermal reaction at different temperatures [Dimier, 2003]

1.4.3 Constraints due to installation process

Depending on the installation operation, the critical zones are different. In S-lay, during the field joint moulding, because the pipelines are assembled in a horizontal position, the inhomogeneous cooling rate in field joint material causes inhomogeneous mechanical properties and also creation of air bubbles in the material at the top of field joint.. Another disadvantage of the S-lay method is that the field joint area must be lifted onto the roller system of the stinger (Fig. 1.28). At a short time after moulding, its stiffness may not be enough to support the complex load created by pipeline weight. So a longer cooling time is recommended.

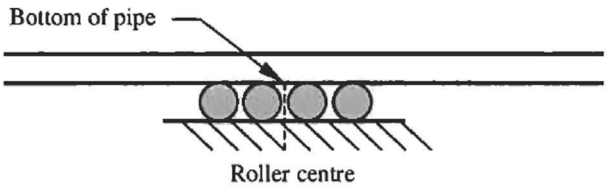

Fig. 1.28. Typical roller/support for pipeline [Bai. Y, 2001]

The field joints are always the most critical zones in the structure [Dixon & Jackson, 2003]. During J-lay, the stress concentration occurs in the flowline at the toe of the fillet weld due to the rotation caused through application of tension to the carrier which is transferred to the flowline at the field joint via the swaged section. During S-lay, the stress concentrations are seen to occur in the carrier

pipe at locations where the external sleeve for the field joint ends (Fig 1.29). This is due to the significant discontinuity in bending stiffness between the main body of the system and the field joint with external sleeve. A secondary concentration can also be found at the toe of the fillet weld connecting the carrier and flowline but this is significantly less than those at the end of the external sleeve. Because of discontinuity of material geometry and the residual stress during the Field Joint moulding, the interfacial area between the main coating material and field joint material is a high area for damage.

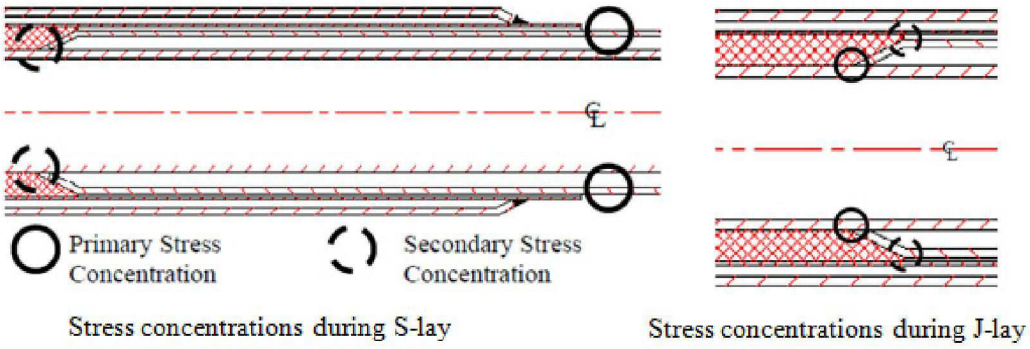

Fig. 1.29. Stress concentrations during pipeline laying [Dixon & Jackson, 2003]

1.5 Interface between main coating material and field joint material

The field joint coating material used must be compatible with the existing multilayer thermal insulation parent coating systems. To prepare the field joint moulding, the interfaces of parent coating material are heated to the softening point of the material by use of radiant heaters. So the polymer materials are intended to become continuous and not be susceptible to cracking or delamination during installation and operation. In fact, during the field joint material injection, because of the pressure in the mould, then in the material, the microspheres at the interface are brought close together. Thus, an interphase is formed. The higher the pressure and the temperature the easier it is for this interphase to appear. The high concentration of microspheres can lead to a weak link between materials.

1.6 Study position

As we have seen in the bibliographic study above, the behaviour of isolated multi-layer materials under the installation and service conditions is complex.

- the strong influence of temperature during the injection moulding of the polymer the evolution in temperature and in time of the thermo mechanical parameters, especially close to the changing liquid-solid phase of the material.

- As the GSPP is a composite material with glass hollow microspheres embedded in a resin matrix it could lead to a specific behaviour under hydrostatic pressures.

Our aim is to propose a representative model of such material allowing the behaviour of industrial application under service conditions to be numerically analysed. This model has to be able to take into account the development of residual stress during the Field Joint moulding and the influence of the installation process.

The issue of this work is thus oriented around four main axes corresponding to the next four chapters.

First, the thermal analysis is studied. It focuses on the temperature evolution of thermal parameter of main coating material and injection material. For such thermal analysis a correct model of the thermal boundary conditions, especially for convection (heat transfer coefficient, temperature or a fluid created by buoyancy force...) is required. In order to propose a validation of this approach, an instrumented experimental test on a representative application has been developed in collaboration with EUPEC. The aim is to propose a simplified approach in order to numerically analyse the influence of the main parameters of the moulding process of a field joint.

Secondly, specific tests, using a hyperbaric chamber, developed at Ifremer have been used to characterize the mechanical behaviour of GSPP under hydrostatic pressure at various temperatures. The different loading types (monotonic, cyclic and creep) give a global response of material. The tests are completed using experimental analyses with a pycnometer, in order to analyse the evolution of the failure of microspheres with respect to the applied hydrostatic pressure.

Thirdly, a thermo-mechanical model of GSPP allowing hydrostatic creep deformation is developed and implemented in COMSOL Multiphysic® software. For the IMPP material a viscoelastic model based on the generalised Maxwell model is considered to be suitable for a simplified analysis. Creep tests in tension on GSPP and solid PP have been performed on DMA (Dynamic Mechanical Analysis) with respect to temperature to determine the parameters of the model. We focus on the validation of the implemented model and on the identification of its parameters with respect to the experimental tests using an inverse identification type procedure.

The final stage of this study is to build a complete numerical model of the Field Joint, in order to allow an optimisation of industrial pipelines. As an example, a Five Layer Syntactic Polypropylene system using the injection moulding of the Polypropylene is analysed. This model follows the simplified process of an industrial Field Joint coating used with a J-lay installation type method for deep water applications (Fig 1.30). The model takes into account the influence of the manufacturing process and the influence of the service conditions (difference of external temperature and pressure). For each stage of the model, the evolutions of the thermo mechanical state are analysed. The von Mises stress - hydrostatic pressure envelopes allow us to analyse the stress state. The stress at the GSPP - Field Joint coating material and also steel-Field Joint coating material interfaces,

which are known as the weakness parts of pipelines, are presented. The encouraging results enable us to define the critical zones. The proposed numerical tool allows an optimisation of the geometrical parameters of the Field Joint to be developed in order to reduce the stress state in the critical zones. Moreover a complementary experimental analysis has been proposed in order to identify the behaviour and the strength of the interfaces.

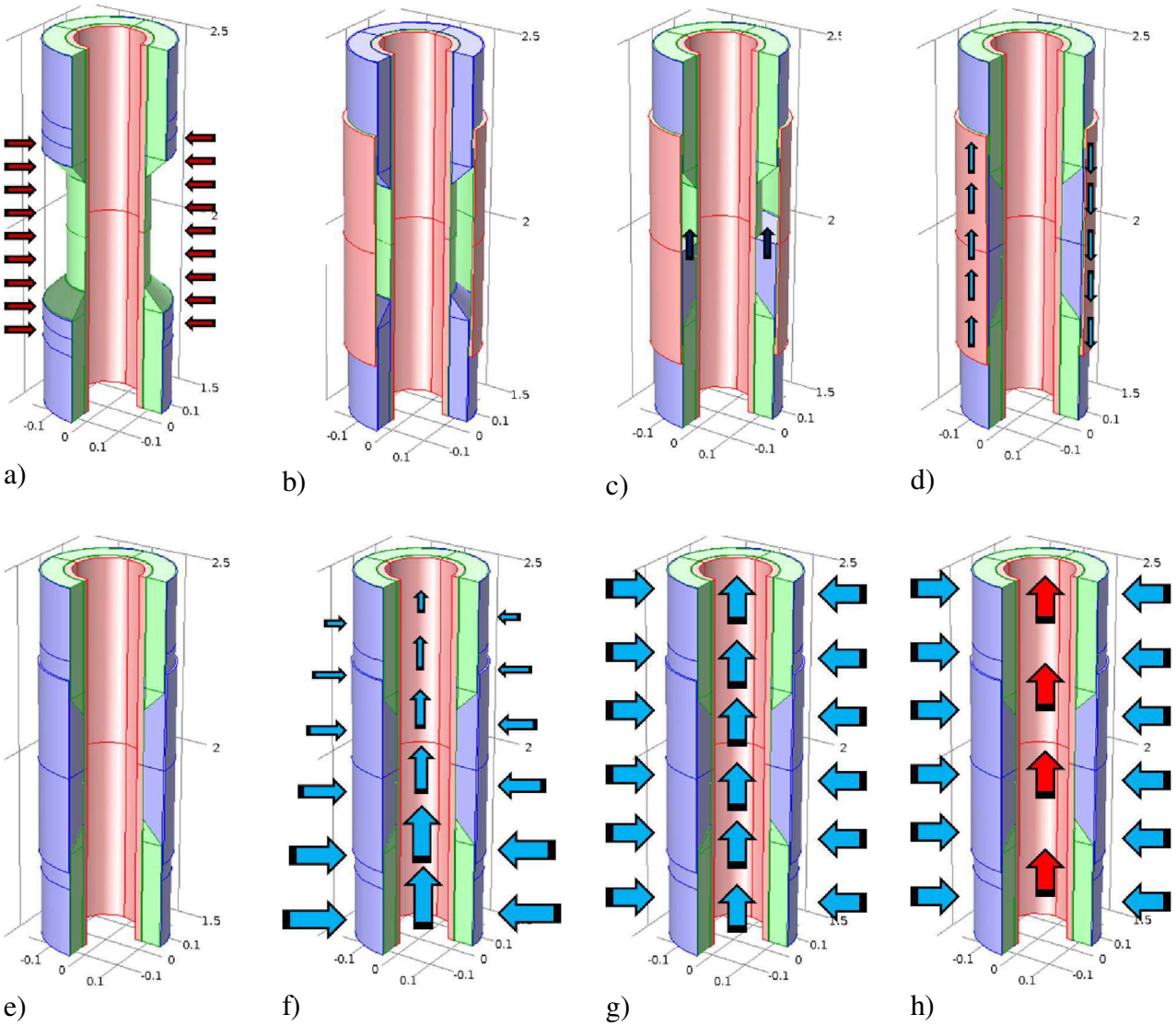

Fig. 1.30. Schematic representation of J-lay pipeline including Field joint moulding. a) Heating the chamfer areas; b) Enclosure of Field Joint area within a mould; c) Injection of molten PP; d) Cooling by forced convection in the mould; e) Cooling by natural convection; f) Laying down of pipeline (thermal mechanical boundaries conditions depend on the pipeline's depth); g) pipeline's state before in service stage; h) pipeline's state in service

Chapter 2. Thermal modelling

This chapter presents a simplified approach to estimate the temperature evolution during the cooling process of field joint moulding and the temperature distribution through the thickness of thermal insulated pipeline in service. Because of the large temperature dependence of the mechanical properties of polymeric materials, the analysis of the time evolution of the mechanical strength of the materials in the field joint region is required in order to optimise the moulding process. The heat transfer in solid material (conduction and convection) and the basic equations of thermal phenomena are recalled. Concerning the thermal behaviour, we focus on the thermal effect on the mechanical characteristics of the field joint and of the main coating materials. During the solidification process, a simplified approach is proposed to model the complex material behaviour, including chemical effects. Regarding the convection effects, both the heat transfer coefficient, associated with the cooling of the mould and the fluid flow inside created by the gradient of temperature (so called thermal buoyancy force) will be used to model the cooling process of a field joint. The main mechanical parameters have been obtained using literature results. Some numerical examples are presented using the finite element software COMSOL Multiphysics®. In order to propose a validation of this approach, an instrumented experimental test has been developed in collaboration with EUPEC. The aim of this study is to propose a simplified approach in order to numerically analyse the influence of the main parameters of the moulding process of a field joint.

2.1 Heat transfer fundamentals

Heat transfer is defined as the movement of energy due to a difference in temperature. It is characterized by: conduction, convection and radiation.

The first law of thermodynamics governs all heat transfers. On the assumption of small perturbations, we have the complete heat equation [Lemaitre & Chaboche, 2006]:

$$\lambda \Delta T = \rho C \dot{T} - \underline{\underline{\sigma}} : \dot{\underline{\underline{\varepsilon}}}^{p} + A_k \dot{V}_k - r - T\left(\frac{\partial \underline{\underline{\sigma}}}{\partial T} : \dot{\underline{\underline{\varepsilon}}} + \frac{\partial A_k}{\partial T} \dot{V}_k \right)$$

The heat equation corresponds to a classical process:

- No change in inelastic deformation: $\underline{\underline{\sigma}} : \dot{\underline{\underline{\varepsilon}}}^{p} = 0$
- No change in variables: $A_k \dot{V}_k = 0$
- No internal production of heat generated by external sources: $r = 0$
- Without thermomechanical coupling: $\frac{\partial \underline{\underline{\sigma}}}{\partial T} : \dot{\underline{\underline{\varepsilon}}} = 0$ and $\frac{\partial A_k}{\partial T} \dot{V}_k = 0$

$$\lambda \Delta T = \rho C_p \frac{\partial T}{\partial t}$$

λ, thermal conductivity ($W.m^{-2}.K^{-1}$)

C_p, thermal capacity ($J.kg^{-1}.K^{-1}$)

T, temperature (K)

- Conduction

Conduction is the phenomenon where heat is transferred to a material environment (solid or fluid) by molecular vibration. Conduction may be understood as a transfer of energy from the more energetic to the less energetic particles of a substance due to interactions between the particles [Incropera et al, 2006]. So there is no movement of material.

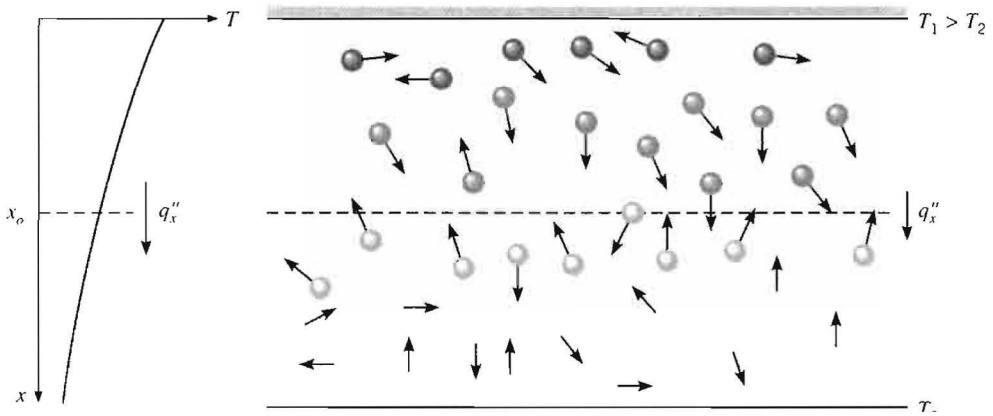

Fig. 2.1. Association of conduction heat transfer with diffusion of energy due to molecular activity [Incropera et al, 2006]

- Convection

Convection is heat transfer in a material environment with movement of material. We talk about natural convection when the movement of material is only caused by temperature difference. When the movement of material is caused by a mechanical action, we have a forced convection. In the case of this study, three convection phenomena can be cited:

- Heat transfer by forced convection between the metal wall of the pipe and oil outflow.

- Heat transfer by forced convection between the outer wall of the pipe and the mould of field joint during cooling.

- Heat transfer by natural convection between the outer wall of the pipe and seawater.

- Radiation

Radiation is heat transfer between two bodies through electromagnetic waves. It is an exchange of energy between bodies without contact. We consider that the radiation effect is negligible as long as the temperature of the solid is below 200°C.

- Heat transfer of composite cylindrical wall

In the case of a hollow composite cylinder with the cylindrical coordinate system (r, ϕ, z), the heat equation has a form:

$$\frac{1}{r}\frac{\partial}{\partial r}\left(\lambda r\frac{\partial T}{\partial T}\right)+\frac{1}{r^2}\frac{\partial}{\partial \phi}\left(\lambda\frac{\partial T}{\partial \phi}\right)+\frac{\partial}{\partial z}\left(\lambda\frac{\partial T}{\partial z}\right)+\phi = \rho C_p\frac{\partial T}{\partial t}$$

For the thermal analyses of pipelines, we ignore the heat transfer along the axial (z axis) and circumferential directions. So, the heat equation without heat source can be simplified:

$$\frac{1}{r}\frac{\partial}{\partial r}\left(\lambda r\frac{\partial T}{\partial T}\right)=\rho C_p\frac{\partial T}{\partial t}$$

2.2 Heat transfer coefficient

In this part, we focus on boundary conditions during the convective problems. For a flow over a surface, there is a velocity boundary layer. In the case of thermal problems, the boundary layer (or convection heat transfer) comes from the difference of temperature between the fluid and the surface. The boundary's type the most used is convective cooling or heating represented by a heat transfer coefficient, h:

$$-n.(\lambda \nabla T) = h(T_{\inf} - T)$$

This approach is very useful in many cases, especially when we don't focus on the flow's behaviour but rather on its cooling power. The heat transfer coefficient depends on the solid's surface temperature T, surface temperature far from the boundary $T_{\inf}$, the fluid's nature (material properties, fluid flow rate) and the geometry of the interface. A convection cooling can be divided into four main categories depending on the type of convection conditions (natural or forced) and on the type of geometry (internal or external convection flow)

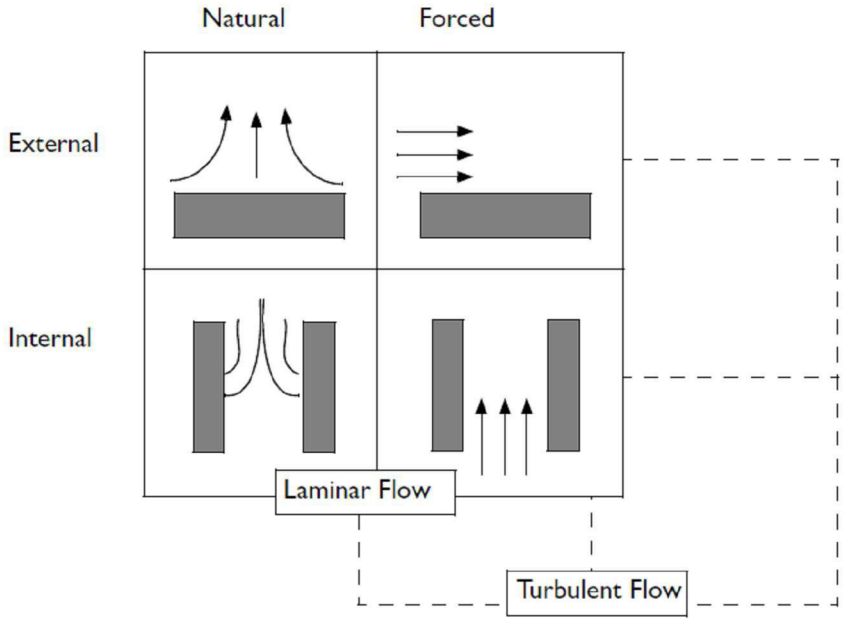

Fig. 2.2. Possible categories of convective cooling [COMSOL]

[Frank P, 2006] presented an empirical method to calculate the average heat transfer coefficients h. With a studied geometry (flat plate in parallel flow, for example) heated by electricity to maintain $T_s > T_\infty$, convection heat transfer occurs from the surface to the fluid. By measuring the T_s, T_∞, and electrical power, E.I, which is equal to the total heat transfer rate, h is calculated.

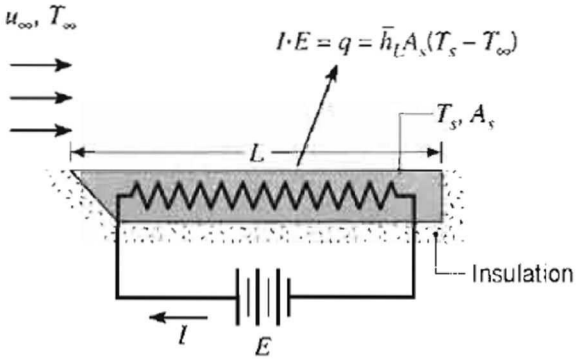

Fig 2.3. Experiment for measuring the average convection heat transfer coefficient [Incropera et al, 2006]

An application of this principle was used to measure and model an industrial insulated pipeline under the high hydrostatic pressure in the stationary case [Bouchonneau et al, 2010]. But in a time dependent case like a field joint moulding process, the use of invese indentification can be useful, i.e. the experimetal results will be used as the input in optimisation problems using the finite element method.

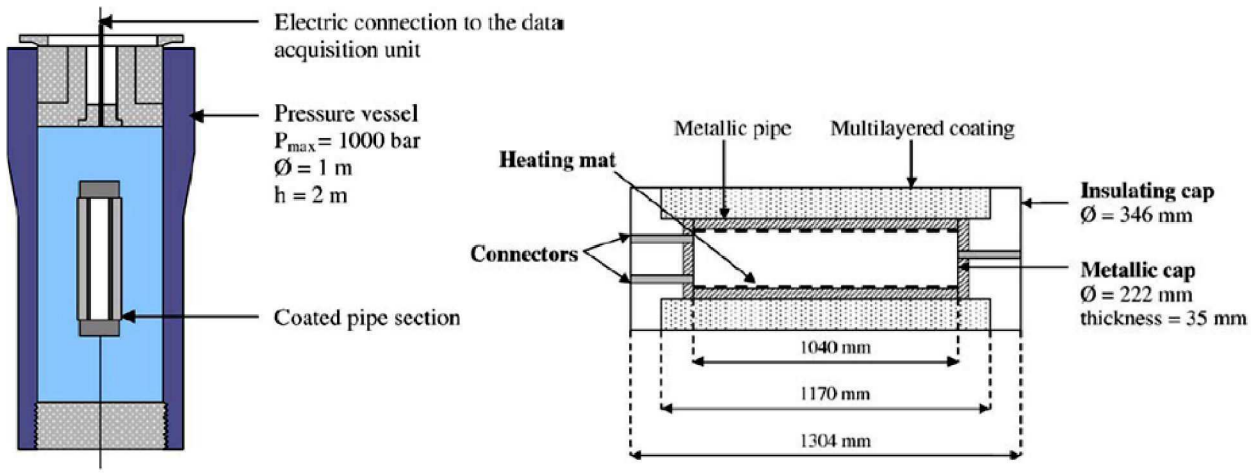

Fig 2.4. Experimental test of an industrial insulated pipeline [Bouchonneau et al, 2010]

2.2.1.1 Calculation of h for natural convection

The external surfaces of pipelines are in contact with seawater. We consider that the natural convection phenomenon occurs. In the case of natural convection, the buoyancy forces due to the temperature gradients lift the fluid near the solid-fluid interface. If the flow of cool fluid crosses over a warm surface, there is a thermal boundary layer thickness, δ_t [Lienhard IV and V, 2001]

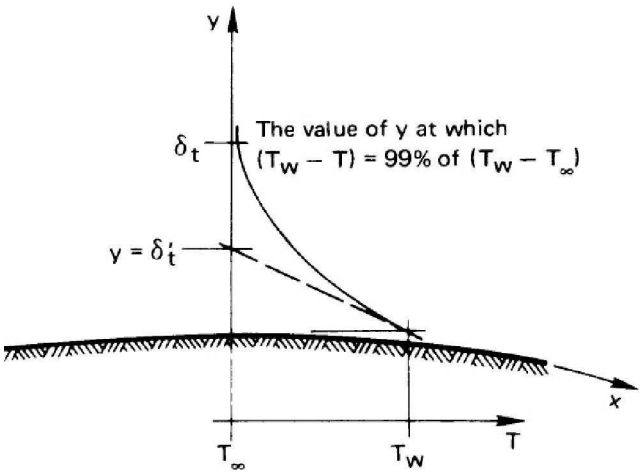

Fig 2.5. The thermal boundary layer during the flow of cooling fluid over a warm plate [Lienhard IV and V, 2001]

The heat flux exchanged between a fluid and a solid is governed by Newton's law:

$$q_y = hA\left(T_p - T_f\right)$$

The heat transfer at the surface of solid is governed by conduction:

$$q_y = -\lambda S \frac{\partial}{\partial y}\left(T - T_p\right)\Big|_{y=0}$$

We have:

$$-\lambda S \frac{\partial}{\partial y}\left(T - T_p\right)\Big|_{y=0} = hS\left(T_p - T_f\right)$$

$$\frac{hL}{\lambda} = \frac{-\frac{\partial}{\partial y}\left(T_p - T\right)\Big|_{y=0}}{\left(T_p - T_f\right)/L} = \mathrm{Nu}_L \text{, the Nusselt number}$$

Where L is a length scale (the length of a plate, the diameter of a cylinder, or at a point of interest along a flat surface). The Nusselt number expresses the relationship between the quantity of heat exchanged by convection and the quantity of heat exchanged by conduction. We can imagine that the physical significance of Nusselt number is inversely proportional to the thickness of the thermal boundary layer:

$$\mathrm{Nu}_L = \frac{L}{\delta_t}$$

The empirical formula of Nusselt number has generally a form:

$$\mathrm{Nu} = C\left(\mathrm{Gr}.\mathrm{Pr}\right)^n$$

The Prandtl number, $\mathrm{Pr} = \mu C_p / \lambda$, ratio of the momentum and thermal diffusivities. The Grashof number, $\mathrm{Gr}_L = \dfrac{\rho^2 g \beta L^3 \Delta T}{\mu^2}$, ratio of internal driving force (buoyancy force) to a viscous force acting on the fluid. β is the fluid's coefficient of volumetric thermal expansion, μ is the fluid's dynamic viscosity and ρ is the density. C depends on the geometry. n is equal to 0.25 for laminar flow and equal to 0.33 for turbulent flow. Note that all properties are evaluated at $\left(T_p + T_f\right)/2$.

In natural convection, the convection boundary layer is not always a laminar flow because of hydrodynamic instabilities. By use of Rayleigh number, which represents the relative magnitude of the buoyancy and viscous forces in the fluid, we can define this change.

The Rayleigh number, $\mathrm{Ra} = \mathrm{Gr}.\mathrm{Pr} = \rho^2 g C_p \Delta T L^3 / (\mu\lambda)$

In the case of vertical flat surfaces [Bejan & Kraus, 2003]:

$$\overline{Nu} = \begin{cases} 0.59\,\mathrm{Ra}^{1/4} & for\, 10^4 < \mathrm{Ra} < 10^9 \,(\mathrm{laminar}) \\ 0.10\,\mathrm{Ra}^{1/3} & for\, 10^9 < \mathrm{Ra} < 10^{13} \,(\mathrm{turbulent}) \end{cases}$$

In our study, we focus on the thermal behaviour of pipelines with cylindrical form. Assuming that the velocity and thermal layer thickness are equal, Merk and Prins [Bejan & Kraus, 2003] proposed the mean value of the Nusselt number for a horizontal isothermal cylinder as:

$$\overline{Nu} = \frac{\bar{h}D}{\lambda} = C(\mathrm{Pr}).(\mathrm{Gr}.\mathrm{Pr})^{1/4}$$

Where $\overline{Nu}$ and Gr are calculated for the diameter D. The constant $C(\mathrm{Pr})$ is 0.436, 0.456, 0.520, 0.523, and 0.523 for Pr values of 0.7, 1.0, 10.0, 100.0, and ∞, respectively.

Another formula of mean value of the Nusselt number was proposed by Churchill and Chu [Bejan & Kraus, 2003]:

$$\overline{Nu} = \left(0.60 + 0.387 \left\{ \frac{\mathrm{Ra}}{\left[1 + (0.559/\mathrm{Pr})^{9/16}\right]^{16/9}} \right\}^{1/6} \right)^2 \quad \text{in the case of } 10^{-5} \le \mathrm{Ra} \le 10^{12}$$

McAdams [Bejan & Kraus, 2003] gave a correlation for an isothermal cylinder as:

$$\overline{Nu} = \begin{cases} 0.53\,\mathrm{Ra}^{1/4} & for\, 10^4 < \mathrm{Ra} < 10^9 \,(\mathrm{laminar}) \\ 0.13\,\mathrm{Ra}^{1/3} & for\, 10^9 < \mathrm{Ra} < 10^{13} \,(\mathrm{turbulent}) \end{cases}$$

In the case of a vertical cylinder, if D/L is large enough (the boundary layer thickness is much less than the cylinder diameter), the heat transfer coefficient can be calculated in the same way in the

case of flat plate, where D is the diameter of the cylinder and L its height. This condition is known to be satisfied when:

$$\frac{D}{L} \geq \frac{35}{Gr_L^{1/4}}$$

The average Nusselt number can be calculated by:

$$\overline{Nu} = \frac{4}{3}\Phi(\mathrm{Pr})\,\mathrm{Gr}^{1/4}$$

where

$$\Phi(\mathrm{Pr}) = \left(\frac{0.316\,\mathrm{Pr}^{5/4}}{2.44 + 4.88\,\mathrm{Pr}^{1/2} + 4.95\,\mathrm{Pr}}\right)^{1/4}$$

Or with an empirical formula by Churchill and Chu [Bejan & Kraus, 2003]:

$$\overline{Nu} = \left(0.825 + 0.387\frac{0.387\,\mathrm{Ra}^{1/6}}{\left[1+(0.492/\mathrm{Pr})^{9/16}\right]^{8/27}}\right)^2 \quad \text{in case of } 10^{-1} \leq \mathrm{Ra} \leq 10^{12}$$

2.2.1.2 Calculation of h for forced convection

In manufacturing process of field joint, a special mould with internal fluid flow is used to cool the field joint material. To model the cooling process, we consider that the cooling of material is due to the external forced convection. In the case of forced convection from a surface in external flow, the average Nusselt number depends on the geometry, flow rate and thermal properties of the flow. The fluid's data may be represented by a form:

$$\mathrm{Nu}_L = f(\mathrm{Re}_L, \mathrm{Pr}) = C\,\mathrm{Re}_L^{\,m}\,\mathrm{Pr}^n$$

With the Reynolds number, $\mathrm{Re}_L = \rho UL/\mu$, ratio of the inertia and viscous forces,

For a laminar flow over an isothermal plate, the local Nusselt number can be obtained from a single formula of Churchill and Ozoe:

$$\mathrm{Nu}_x = 1/2\,\mathrm{Nu}_L = \frac{0.3387\,\mathrm{Re}_x^{\,1/2}\,\mathrm{Pr}^{1/3}}{\left[1+(0.0468/\mathrm{Pr})^{2/3}\right]^{1/4}}$$

For a turbulent flow over an isothermal plate, we can use the following form:

$$\mathrm{Nu}_L = \left(0.037\,\mathrm{Re}_L^{\,4/5} - A\right)\mathrm{Pr}^{1/3}$$

For a transition Reynolds number of 5.10^5 and A = 871 [Incropera et al, 2006].

On the other hand, to model the thermal problem of a field joint in service, the internal forced convection occurs between internal oil flow and the pipe internal surface [Bai. Y & Bai. Q, 2005]. For the internal convection of pipelines, following the Dittus and Boelter (1930) proposal [Bai. Y & Bai. Q, 2005], we have:

$$\mathrm{Nu}_L = 0.0255\,\mathrm{Re}_L^{0.8}\,\mathrm{Pr}^n$$

With n = 0.4 if the fluid is being heated, and n = 0.3 if the fluid is being cooled.

Typical internal convection coefficients for turbulent flow were proposed by Gregory in 1991 (Tab.2.1). Regarding the pipelines with multiphase flow, the value of coefficients could be approximated by the basic values in the table.

Fluid	Internal convection coefficient
	W/(m^2.K)
Water	1700-11350
Gases	17-285
Oils	55-680

Tab. 2.1. Typical internal convection coefficients for turbulent flow (Gregory, 1991) [Bai. Y & Bai. Q, 2005]

2.3 Convective modelling by internal or external flow

The other approach to simulate the field joint's cooling is to build a coupled model with the convective velocity field around the pipelines (nonisothermal laminar or turbulent buoyancy flow). Before proceeding with a simulation, it is a good idea to estimate the Grashof number (in case of natural convection) or Reynolds number (in case of forced convection) to choose the laminar flow or the turbulent flow.

The use of compressible Navier-Stokes equations working together with a heat transfer equation is presented below:

$$\rho\frac{\partial \mathrm{u}}{\partial t} + \rho\mathrm{u}.\nabla\mathrm{u} = \nabla.\left[-p\mathrm{I} + \eta\left(\nabla\mathrm{u} + (\nabla\mathrm{u})^T\right) - (2\eta/3 - \kappa)(\nabla\mathrm{u})\mathrm{I}\right] + \mathrm{F}$$

$$\frac{\partial p}{\partial t} + \nabla.(\rho\mathrm{u}) = 0$$

Where u is the velocity (m/s), p is the pressure (Pa), denotes the dilatational viscosity (characterizes the non equilibrium response of the fluid to volume changes).

The buoyancy forces are included by using an internal volumetric force, in the case of convection in air:

$$\mathrm{F} = \left(\rho - \rho_{ref}\right)\mathrm{g}$$

$$\mathrm{g}\left(r, z\right) = \left(0, -9.81\right)\ \mathrm{m/s^2}$$

The density is given by the ideal gas law:

$$\rho = \frac{pM}{RT}$$

Where M is the average molecular weight of air, and R is the gas constant.

The heat equation says that the change in energy is equal to the heat source minus the divergence of the diffusive heat flux:

$$\rho C_p \left(\frac{\partial T}{\partial t} + \mathrm{u}.\nabla T \right) + \nabla.\left(-\lambda \nabla T\right) = Q$$

The velocity field comes from the compressible Navier-Stokes equation.

In the case of convection in water, the use of an incompressible Navier-Stokes equation is required.

$$\rho \frac{\partial \mathrm{u}}{\partial t} + \rho \mathrm{u}.\nabla \mathrm{u} = -\nabla p + \eta \nabla^2 \mathrm{u} + \mathrm{F}$$

$$\nabla.\mathrm{u} = 0$$

The free convection is added to the fluid flow with the Boussinesq approximation. This approximation ignores variations in density with temperature, except that the variations give rise to a buoyancy force lifting the fluid. This force enters the volume force in the incompressible Navier-Stokes equations.

$$\mathrm{F} = \mathrm{g}\rho_{ref}\alpha\left(T - T_{ref}\right)$$

Another approximation of buoyancy force uses nondimensional Raleigh and Prandtl numbers:

$$\mathrm{F} = \frac{\mathrm{Ra}_L}{\mathrm{Pr}_L}\left(T - T_{ref}\right)$$

2.4 Thermal modelling of Field joint

2.4.1 Thermal modelling during the phase change of field joint material

In this study, we focus only on the thermal effect applying to the mechanical characteristics of field joint material. This means that the evolution of thermal mechanical characteristics depends on temperature. The thermal mechanical coupling has been not yet been studied.

- Crystallization and melting of polypropylene

During the crystallization of polypropylene, the latent heat released slows down the cooling rate of the material. The thermal properties like degree of crystallinity and melting point depend on the cooling rate. To simplify the coupling problem, we suppose that the thermal properties (and also the mechanical properties for the next chapter) only depend on the temperature (the influence of degree of crystallinity is not taken into account).

2.4.1.1 .Thermal properties of solid PP

The specific heat C_p of solid polypropylene was identified by using DSC measurement [Le Goff, 2005].

$$C_{p_{liquid}} = 3.10T + 2124$$
$$C_{p_{solid}} = 10.68T + 1451$$

The thermal conductivity was presented by the same author.

$$\lambda_{liquid} = -6.25\times10^{-5}T + 0.189$$
$$\lambda_{solid} = -4.96\times10^{-4}T + 0.31$$

With T in °C, C_p in J/(kg.K) and λ in W/(m.K)

The melting point of polypropylene T_m is 140°C and the transition temperature span ($2.\Delta T$) is 30K.

The heat released ΔH is supposed constant and equal to 50 kJ/kg.

To account for the latent heat related to the phase transition, the specific heat is simply replaced by $\left(C_p + \delta\Delta H\right)$ [COMSOL, Continuous Casting] assuming that the latent heat released depends on temperature by a Gaussian law:

$$\delta = \frac{\exp(-(T - T_m)^2/(\Delta T)^2)}{\Delta T\sqrt{\pi}}$$

The thermal conductivity during the changing phase ($\left(T_m - \Delta T\right) \le T \le \left(T_m + \Delta T\right)$) is modelled by using the Specifying Discontinuous Function called "flc2hs". This function in COMSOL

Multiphysics is a smoothed Heaviside function with continuous second derivative without overshoot which allows us to avoid the singular points. The function gives the value of zero in case of liquid state and it is equal to 1 in case of solid state. So the thermal conductivity of polypropylene is given by the following form:

$$\lambda^{pp} = \lambda^{pp}_{solid} + \left(\lambda^{pp}_{liquid} - \lambda^{pp}_{solid}\right) \mathrm{flc2hs}\left[\left(T - T_m\right), \Delta T\right]$$

2.4.1.2 Thermal properties of GSPP

Given the temperature range of (10°C to 100°C), the thermal properties of GSPP are assumed to be linear with temperature [Bouchonneau, 2007]:

$$C_p^{gspp} = 6.26T + 1506.6 \left(\mathrm{J}/\left(\mathrm{kg}.\mathrm{K}\right)\right)$$
$$\lambda^{gspp} = 10^{-4}T + 0.165 \left(W/\left(m.\mathrm{K}\right)\right)$$

2.4.2 Cooling of field joint in moulding

To better understand the thermal evolution of field joint during its moulding and to make the right choice of thermal boundaries conditions, we propose two axisymmetric thermal models with the same geometry. The field joint position is vertical (corresponding to the J-lay process). The first one (Model 1) uses the natural convection in the interior of the pipeline; the second one (Model 2) uses the internal flow created by the buoyancy force. The boundaries conditions in the outer part of pipelines are similar: the natural convection applies to the surface of the main coating material and the forced convection is used to model the thermal effect of the double steel mould. The first model guarantees the symmetry condition through the middle of the field joint (following the horizontal axis). However, in the second model, because the hot fluid of air tends to lift up the flow, the symmetric condition is not applied.

To follow the changing phase of solid polypropylene, the "liquid coefficient" B is introduced. B is equal to 1 for the liquid state, to zero for solid state and to an intermediate value during the changing phase.

$$B = \begin{cases} 1 & if\ \left(T > T_m + \Delta T\right) \\ \left(T - T_m + \Delta T\right)/\left(2\Delta T\right) & if\ \left(\left(T_m - \Delta T\right) \le T \le \left(T_m + \Delta T\right)\right) \\ 0 & if\ \left(T < T_m - \Delta T\right) \end{cases}$$

The two problems are solved in time dependent mode. The cooling process is modeled for 24 hours. The figures 2.6-2.9 present the thermal properties during the field joint moulding.

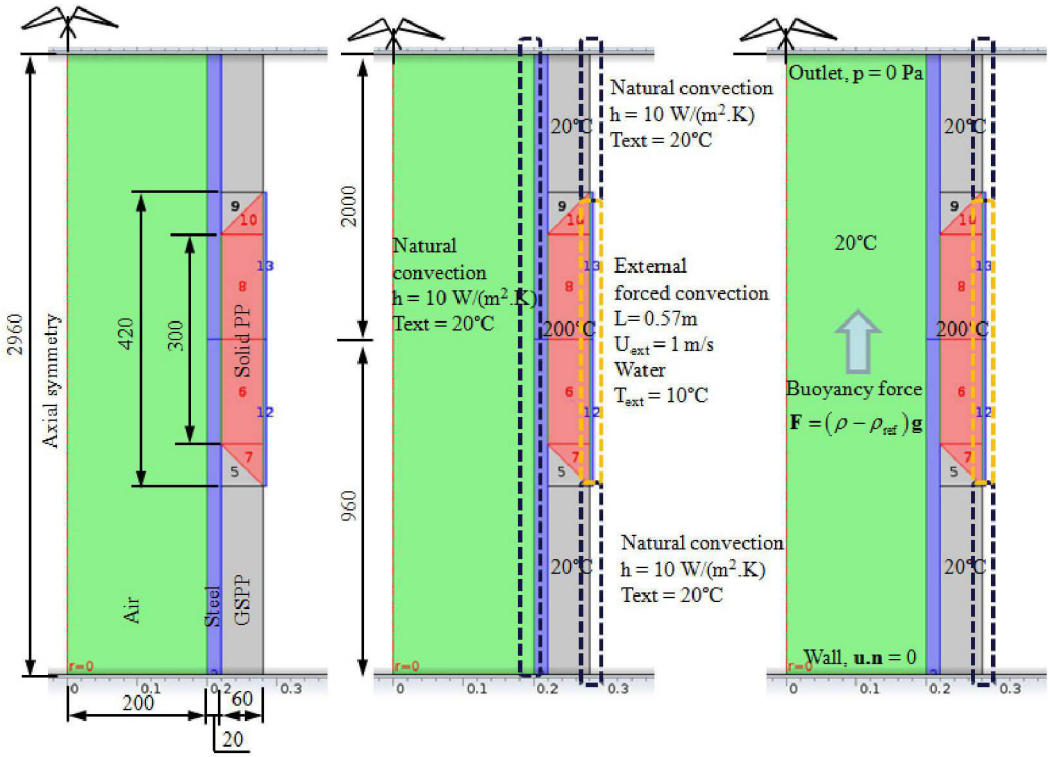

2.6.a. Dimensions 2.6.b. Model 1 2.6.c. Model 2

Fig 2.6. Geometry and boundary conditions of two thermal models

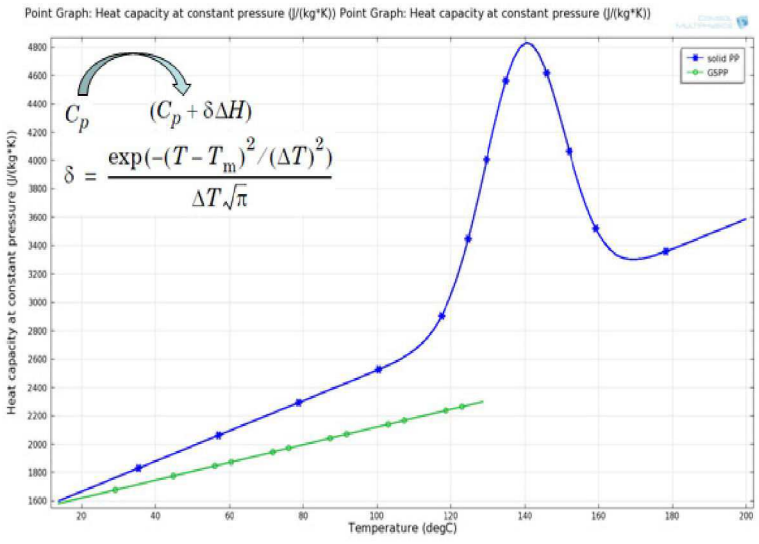

Fig. 2.7. Heat capacity evolution with time

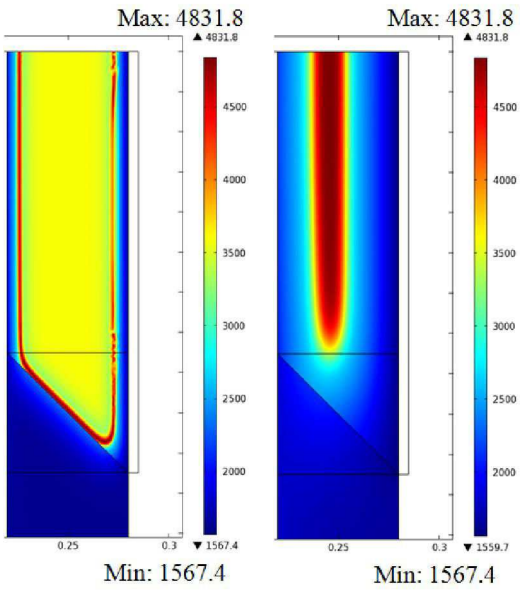

Fig. 2.8. Heat capacity distribution at 300s and 3600s

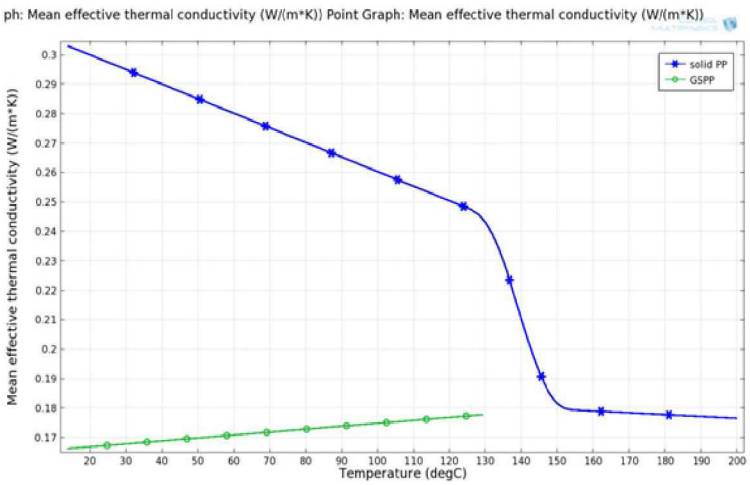

Fig 2.9. Thermal conductivity's evolution with time

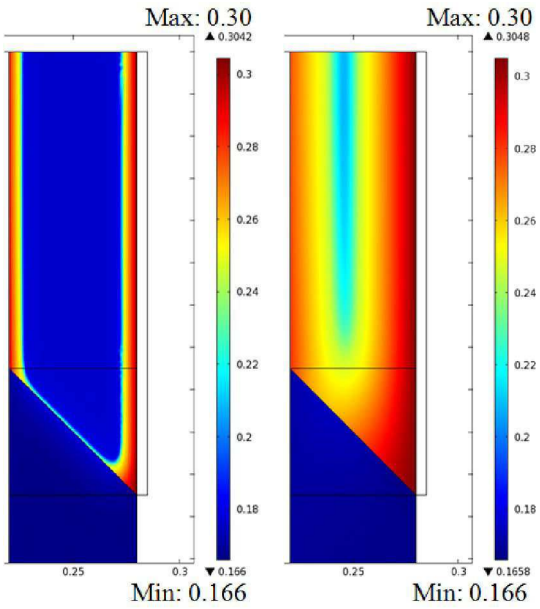

Fig 2.10. Thermal conductivity's distribution at 300s and 3600s

The figure 2.11 and 2.12 allow us to analyse the differences between the two models. In the first hour of cooling, the difference is quite small but after two hours, the difference in maximum temperature is significant (6°). If we make a zoom on the local field joint (Fig. 2.12), the large difference in temperature distribution in the steel part can be noted.

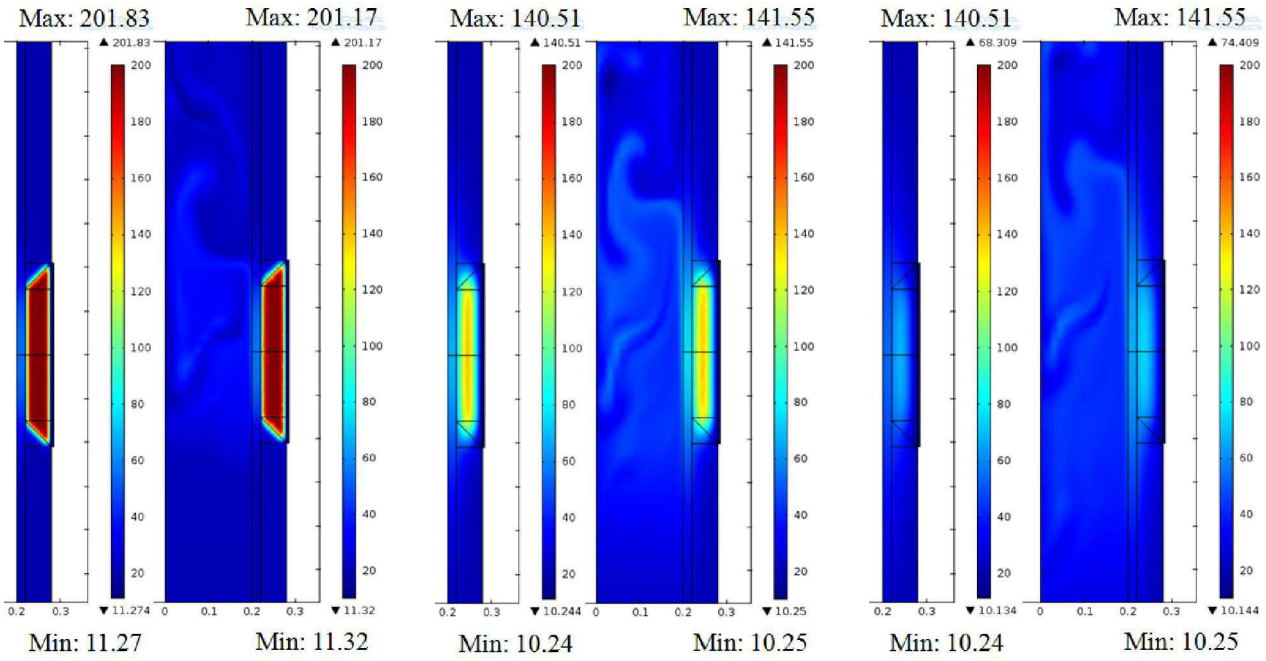

t=300s t=3600s t=7200s

Fig 2.11. Temperature evolution

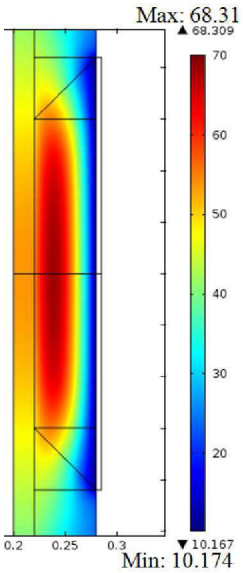

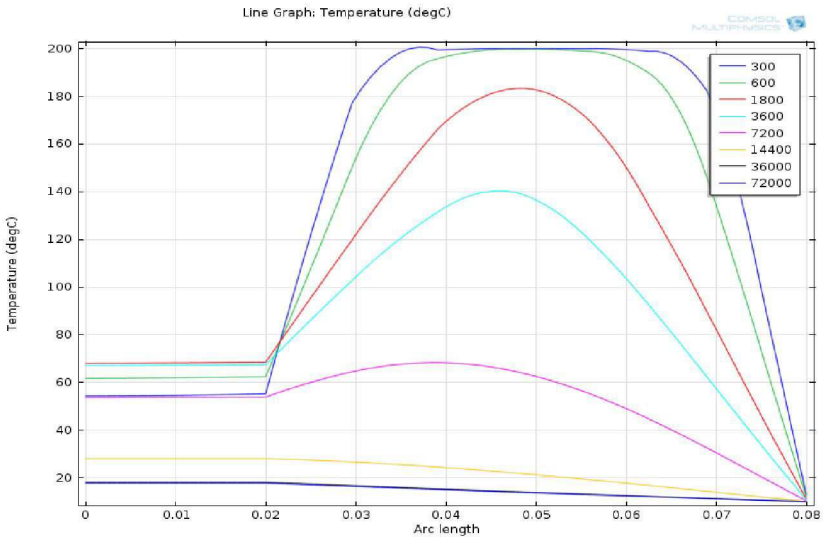

Fig. 2.12.a. Model 1

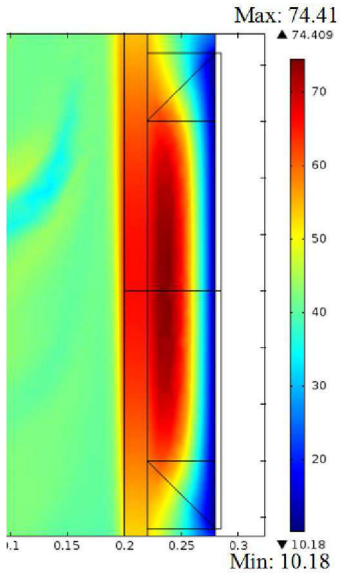

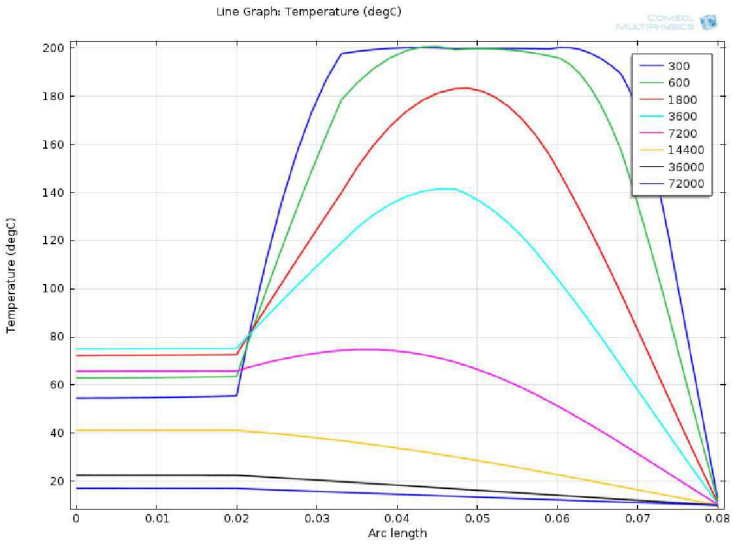

Fig. 2.12.a. Model 2

Fig 2.12. Temperature evolution in the middle of field joint

For the S-lay process, the field joint position is horizontal. So the heat inside the pipeline tends to be stocked in the top of the pipe (Fig. 2.13). Moreover, the thermal exchange between the inner pipeline and the ambiant temperature is more turbulent (Fig. 2.14). This phenomenon doesn't allow us to use the axisymmetric model, 3D modelling is the only solution. It needs considerable calculation time and computer memory.

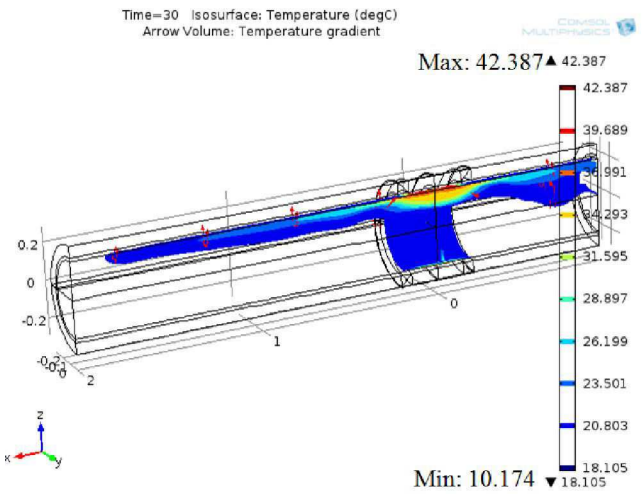

Fig 2.13. Temperature inside pipeline in case of horizontal moulding

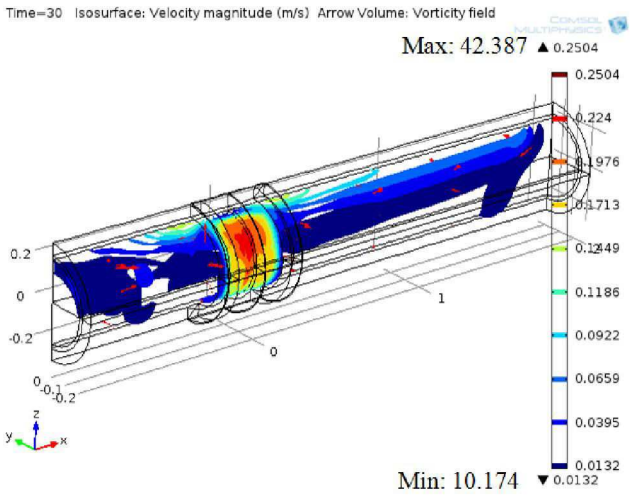

Fig 2.14. Velocity magnitude of fluid inside pipeline in case of horizontal moulding

So, the thermal fluid coupling model enables us to obtain better temperature distribution during the Field Joint moulding. However, it is time-consuming to perform. Because our study focuses on themo-mecanical behaviour of coating and field joint materials, the fluid behaviour (temperature distribution and the velocity of fluid) do not seem to be priority. To simplify the model, the thermal boundary conditions using the heat transfer coefficient are sufficient for subsequent modelling which is more complex.

2.5 Influence of crack on thermal distribution of Field joint

We know that the interface between the field joint coating material and main coating material is one weakness of the pipeline. The cracks could come from the high residual stress during the material cooling or the installation (an over bending of pipeline on the stinger during S-lay). If a crack appears, the high hydrostatic pressure and the important temperature gradient accelerate the water ingress (Fig. 2.15). In this paragraph, the thermal modelling is studied considering that the length of crack is a parameter. By changing this parameter we could obtain the influence of a crack on thermal distribution in a Field Joint.

Once again, the use of the thermal fluid coupling model with the Boussinesq approximation allows us not only to better understand the thermal boundary conditions but also to study the thermal problem where the geometry is more complex suck as the appearance of a crack in a Field Joint. There are two examples with cracks in the interface between the main coating material and the injecting material to be studied. The first one uses only the heat transfer coefficients and the second one uses the thermal fluid coupling approximation.

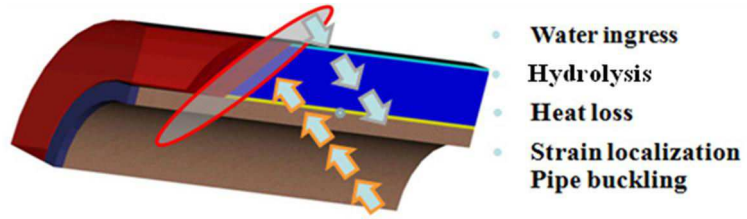

Fig 2.15. Unexpected phenomena created by the cracks in a field joint

We start with a simple thermal model. The heat transfer coefficients in the inner and the outer parts of the pipeline are used. In service, there is a hot oil fluid at 100°C inside the pipeline which heats all material layers. The natural convection in the water outside the pipeline is created by the difference of temperature between the interface of pipeline and the cold water. The constant heat transfer coefficients were used for the thermal boundary condition. The crack between the field joint coating material and main coating material is considered as a parameter. Its value represents the length of crack. On the figure (Fig. 2.16) the temperature distribution at the steel surface is presented. The temperature loses 5°C when the fluid passes through the crack.

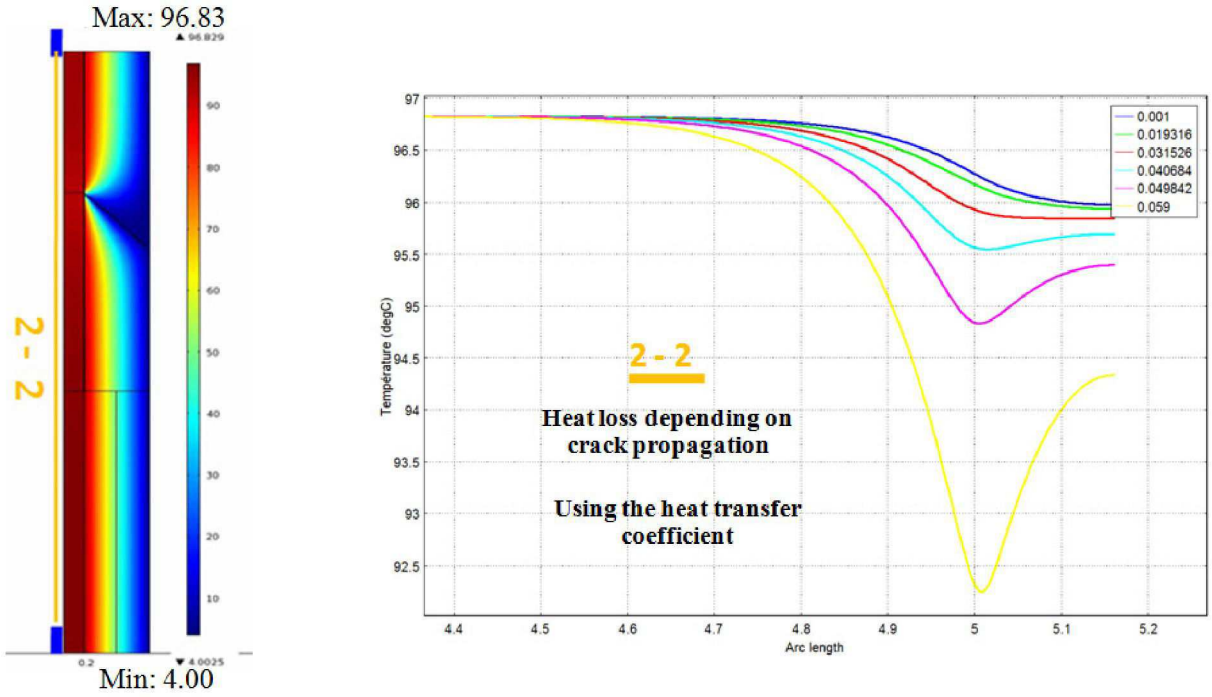

Fig 2.16. Parametric crack thermal modelling using the heat transfer coefficient

The previous model does not represent all heat loss effects because even if there is no crack; the hot oil fluid tends to lose the heat along the pipeline. For the next thermal model, two laminar flows are used. The hot forced oil fluid with a low velocity (0.1 m/s) is inside the pipeline. The second fluid is used to model the natural flow in the water using the buoyancy force (Fig. 2.17). This model remains simple because it does not take account of a turbulent zone around the crack and the hot oil fluid is laminar. However, its results are encouraging (Fig 2.18), the heat loss following the steel interface is important (about 20°C) and the temperature near the crack is low. It could give us the reason for the appearance of a hydrate region inside the pipeline.

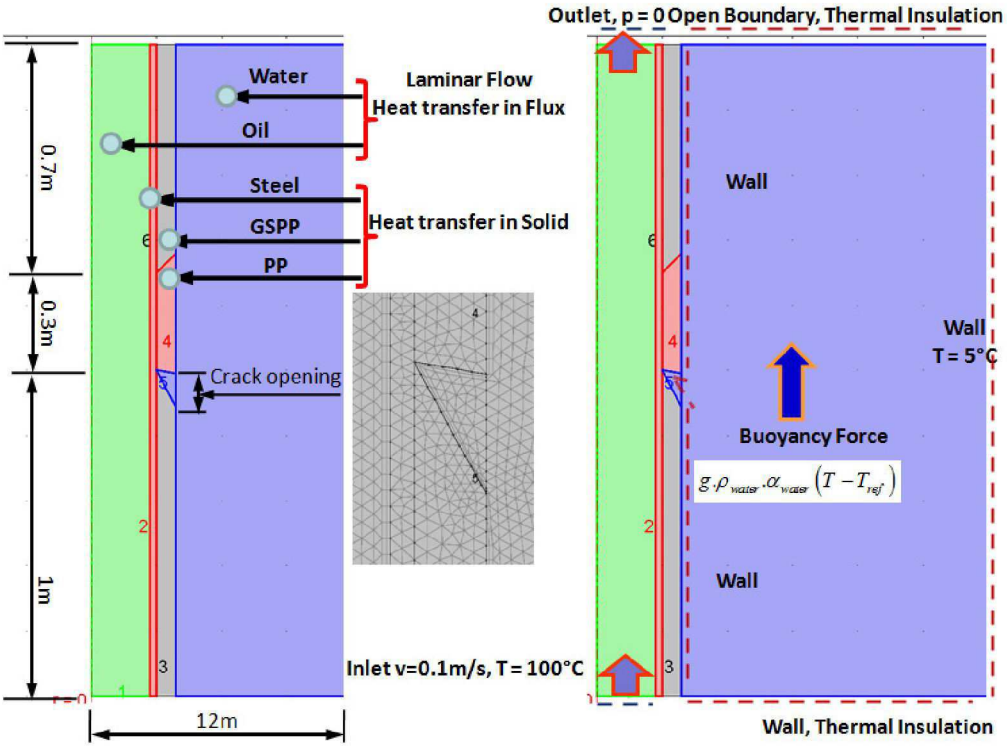

Fig 2.17. Parametric crack thermal modelling using the buoyancy force

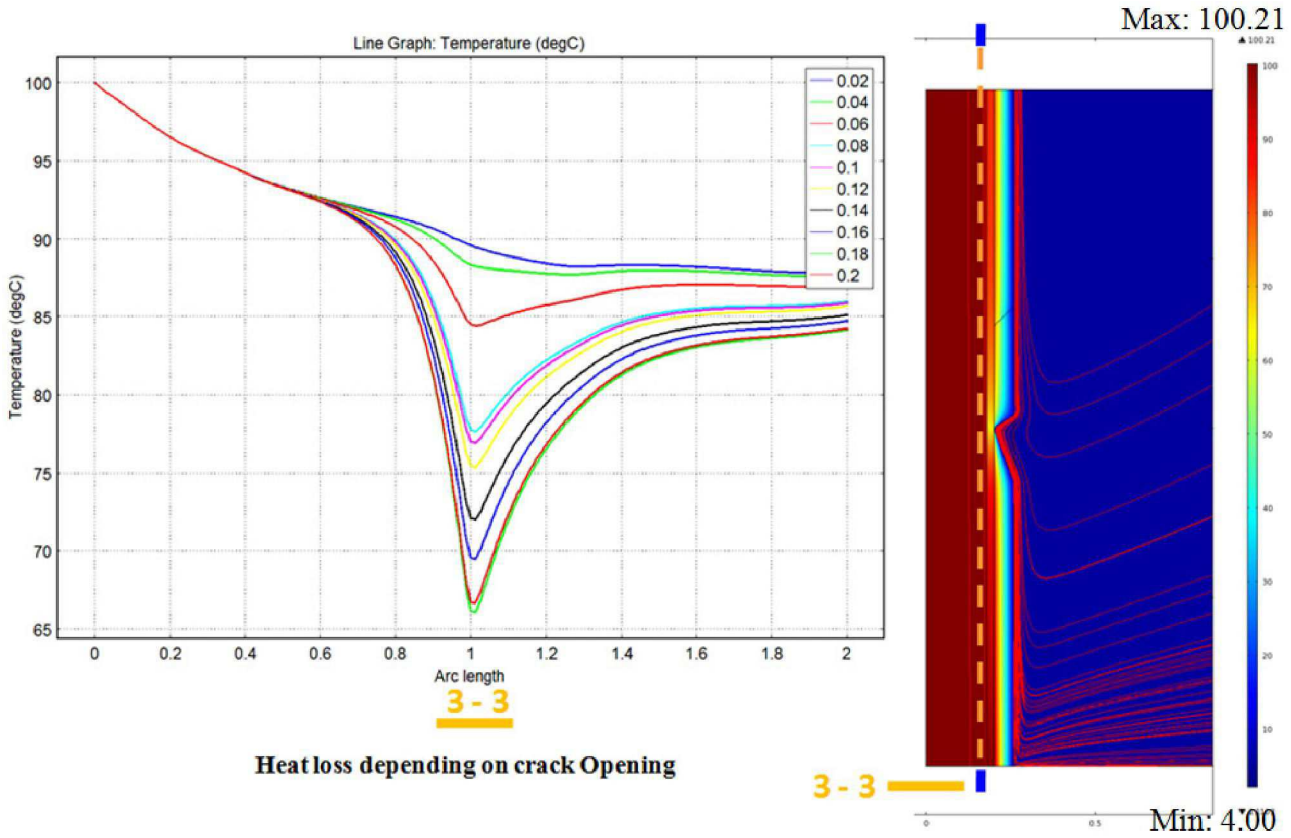

Fig 2.18. Heat loss depending on crack opening in the model using the buoyancy force

2.6 Proposition of validation thermal tests by injection moulded Polypropylene

2.6.1 Objective of tests

The main objective is to measure the temperature's evolution during the field joint moulding in order to provide data to be compared with simulations issued from the model. Tests were performed at the EUPEC Company (Dunkerque, France)

2.6.2 Description of test process

The test was performed during a real injection of moulded polypropylene (IMPP) on a mock up of an offshore subsea structure. Prior to the injection process thermocouples were placed in the mould (fig 2.18) at different positions in order to follow the through thickness temperature gradient. These thermocouples are supported by a Teflon plate. All the thermocouples are connected to a data logger to collect all the data during the injection and cooling process. The steel pipe is preheated in order to reach the temperature required during an in situ injection process. The steel temperature before the injection was 200°C simulating the temperature obtained after applying the Fusion Bound Epoxy system.

At 200°C, polypropylene granules are melted by the elasticising cylinder systems (Reciprocating screw with heaters) [Peacok, 2000]. Then, the liquid material is stocked in an accumulator in order to be transferred in the mould by only one injection (Fig. 2.19). This one shot process avoids possible delamination generated during multi shot operation. A double skin steel mould is used to provide quick cooling of injected material by a forced convection using cold water (Fig. 2.20). In a second step, after the demoulding of the joint the injected material is cooled by a water system (Fig 2.21). Thanks to the thermocouples (Fig. 2.22-2.23) and infrared camera, we can observe the temperature evolution of the mould and in many points in the injected material.

By comparing with a thermal model, we can estimate the thermal parameters and also the efficiency of cooling systems (Fig. 2.24). The thermal boundary conditions are the same as those used for the previous model; the constant heat transfer coefficient for natural convection and the external forced convection for the cooling in the moulding zone. On the Fig. 2.25, the dotted lines come from the thermal modelling. Each dotted line corresponds to the temperature evolution of the thermocouple's position. Because the heat transfer coefficients used are constant for the top and the bottom of the mould, the temperature distribution remains axissymmetric following the central axis of the pipeline.

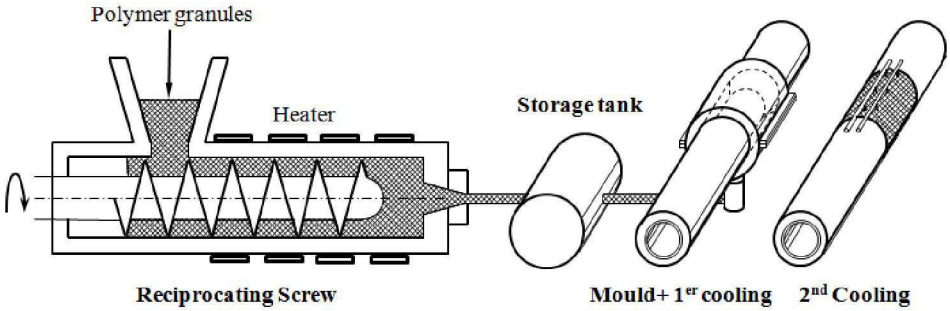

Fig 2.19. Injection moulded polypropylene system

Fig 2.20. Double skin Steel mould

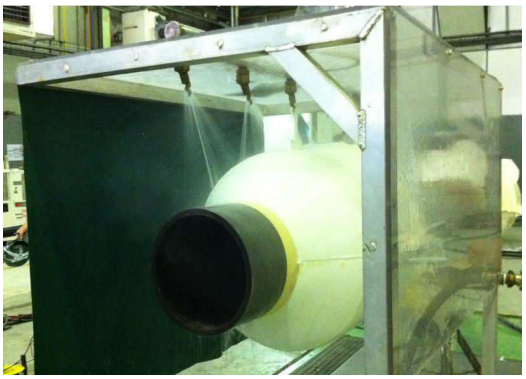

Fig 2.21. Watering system

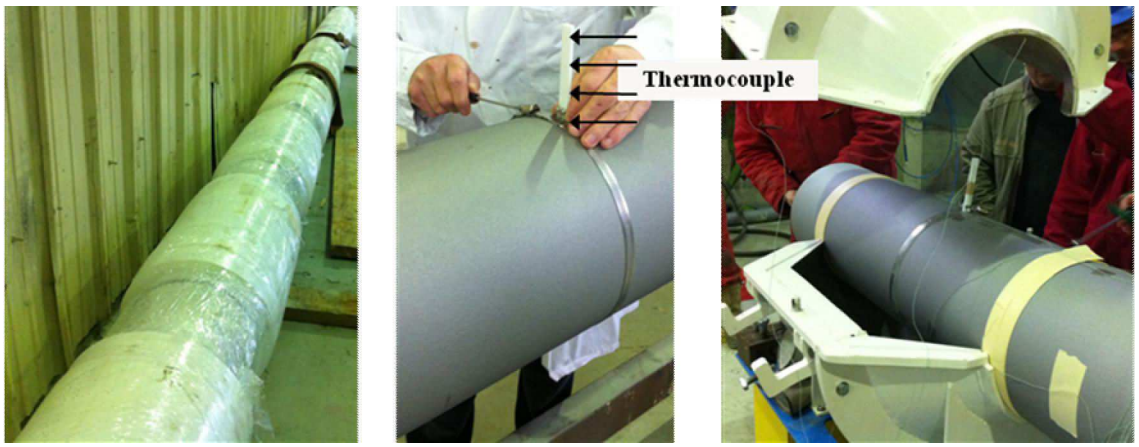

Fig 2.22. Testing installation

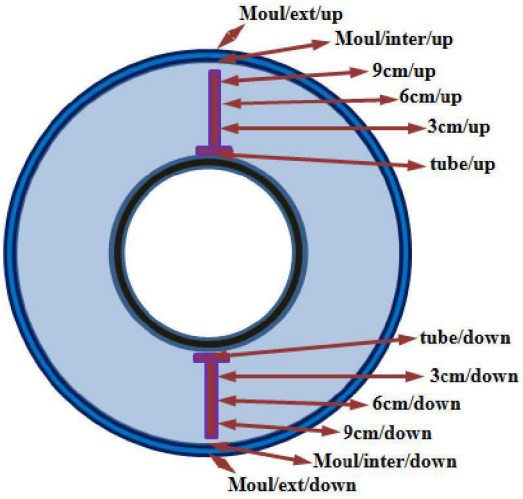

Fig 2.23. Position of thermocouples

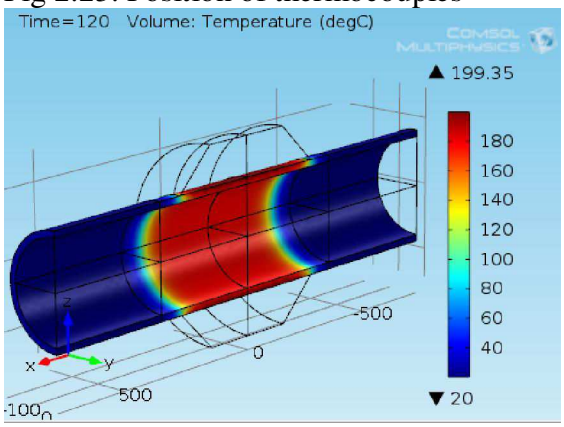

a. Heating the steel surface

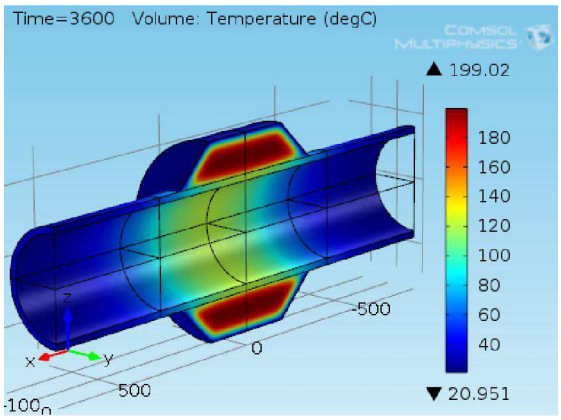

b. Temperature distribution after one hour

Fig 2.24. Modelling of IMPP

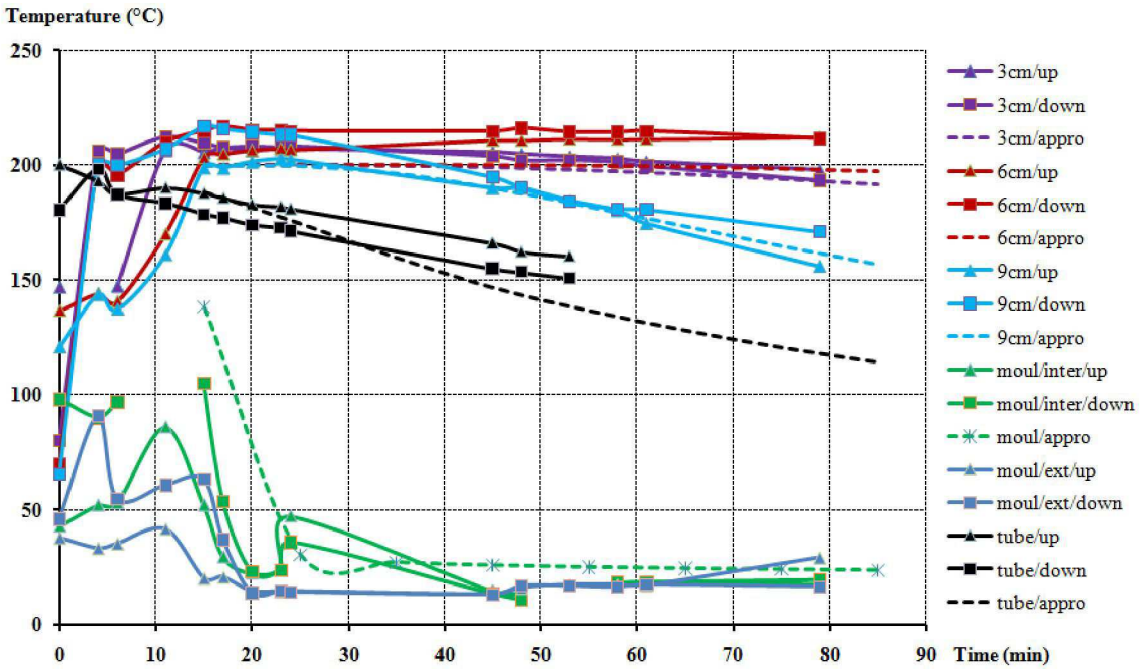

Fig 2.25. Temperature evolution during the cooling of IMP

Chapter 3. Experimental analysis of the thermo mechanical behaviour of GSPP material

During the service life of thermally insulated pipelines in ultra deep water, one of the main mechanical loads is hydrostatic pressure. The mechanical behaviour of the currently mainly used insulation material (Glass syntactic polypropylene) is quite complex, associating the time-dependent behaviour of polymers and the damage behaviour of glass microspheres. In order to allow an optimisation of such systems, while ensuring in-service durability, accurate numerical models of insulation materials are thus required. This study aims to describe the mechanical behaviour of the material under representative conditions of pressure and temperature. Using a hyperbaric chamber, available at IFREMER, the analysis of the evolution of the volumetric strain with time, with respect to the temperature, under different time-evolutions of the applied hydrostatic pressure is presented. The principle of these hydrostatic compression tests is to measure the buoyancy force of materials during hydrostatic loading in water, taking into account the variation of water density. Moreover for a better understanding of the Glass syntactic polypropylene's behaviour, several tests have been performed using a gas pycnometer in order to evaluate the density of the material, to analyse the damage of microspheres and also to detect the existence of voids in the material. Those experimental results allow numerical modelling of some mechanical behaviours of such materials.

3.1 Hydrostatic pressure test

3.1.1 Material

As a passive insulation material, GSPP (Glass/Polypropylene Syntactic), a syntactic foam type material, is currently the most used for this application. Syntactic foams are made from hollow glass microspheres (an outer diameter between 10 and 150 m and a wall thickness between 1 and 1.5 m) embedded in a polymer matrix. The mechanical behaviour of such materials can be quite complex due to the influence of the two components. Table 3.1 and 3.2 present the main nominal properties of the GSPP material used here (polypropylene, PP, matrix with 3M Glass type S38 HS filler [Lefebvre et al, 2009]).

Isostatic crush strength	MPa	38
True density	g/cm^3	0.38
Diameter (average)	µm	44
Effective top size	µm	85
Particle distribution (% volume)	10th (µm)	19
	50th (µm)	44
	90th (µm)	70

Tab. 3.1. Physical properties of microspheres, 3D Glass Bubbles S38HS [3M®]

Property	Typical Value	Test Method
Density (Base Resin)	900 kg/m^3	ISO 1183
Density (Compound)	920 kg/m^3	ISO 1183
Melt Flow Rate (230 °C/2,16 kg)	0.9 g/10min	ISO 1133
Flexural Modulus (2 mm/min)	1200 MPa	ISO 178
Tensile Strain at Yield (50 mm/min)	8 %	ISO 527-2
Tensile Stress at Yield (50 mm/min)	25 MPa	ISO 527-2
Vicat softening temperature (10 N)	145 °C	ISO 306

Tab 3.2. Physical properties of PP matrix [Borealisgroup®]

The samples of glass/polypropylene syntactic were cut from an industrial pipeline (Five Layer Syntactic Polypropylene 5LPP [Socotherm®] (Fig.3.1) which is manufactured by an extrusion process called "Multypass" [Berti, 2004]). On account of the industrial and commercial constraints there is no information available on the interfacial bonding between matrix and fillers.

- Layer 1: FBE Primer
- Layer 2: PP Co-Polymer Adhesive
- Layer 3: Solid PP
- Layer 4: Syntactic Polypropylene
- Layer 5: Solid PP Outer Layer

Fig. 3.1. Five Layer Syntactic Polypropylene 5LPP [Socotherm®]

3.1.2 Test description

The principle of the hydrostatic compression tests used in this study (Fig. 3.2) is to measure the buoyancy force of materials during hydrostatic loading in water, taking into account the variation of water density (as a function of pressure and temperature). A load control system is used in order to reach the prescribed pressure. To extend to the preferred pressure, the pump adds or withdraws water following the loading profile. The tolerance between the measured value and the preferred value is specified. The characteristics of the hyperbaric chamber available at the IFREMER Brest Centre are presented in table 3.3.

Internal radius	300 mm
height	580 mm
maximal pressure	60 MPa
temperature range	20 to150 °C

Tab. 3.3. Characteristics of hyperbaric chamber

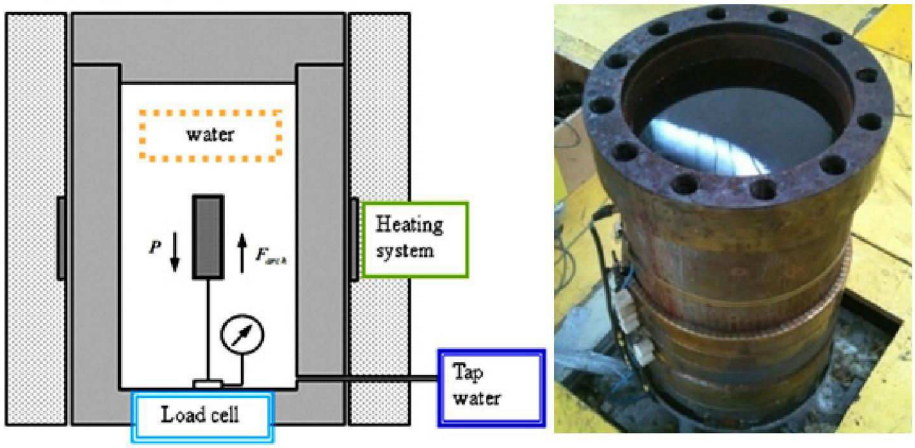

Fig. 3.2. Hyperbaric chamber

The range of force of the weighing device used to measure the buoyancy is –5N to +5N with accuracy better than 1%. The volume of GSPP samples is 0.5 dm^3 (Fig. 3.3). The loading and unloading rates were 10 bars per minute. The tests were performed at different temperatures 20, 40, 60 and 80°C.

Fig. 3.3. Specimens of GSPP

Taking the formula of Archimedes, the volumetric deformation can be calculated:

$$F_{buoyancy} = V_{mat}\rho_{water}g - V_{0mat}\rho_{mat}g$$

$$V_{mat} = \frac{V_{0mat}\rho_{mat}g + F_{buoyancy}}{\rho_{water}g}$$

$$\varepsilon_{vmat} = \frac{V_{0mat} - V_{mat}}{V_{0mat}}$$

$F_{buoyancy}$: Buoyancy force of the sample (N)

V_{0mat} : Initial volume of the sample (m^3)

$\rho_{water} = \rho_{water}(S,T,p)$: Density of water (N/m^3) which depends on the salinity, temperature and pressure. (International Equation of State of sea water, 1980)

$$\rho(S,t,p) = \rho(S,t,0)\Big/\Big[1 - p/K(S,t,p)\Big]$$

$$\begin{aligned}\rho(S,t,0) = {} & 999.842594 + 6.793952\times10^{-2}t - 9.095290\times10^{-3}t^2 + 1.001685\times10^{-4}t^3 - 1.120083\times10^{-6}t^4 \\ & + 6.536332\times10^{-9}t^5 + 8.24493\times10^{-1}S - 4.0899\times10^{-3}tS + 7.6438\times10^{-5}t^2S - 8.2467\times10^{-7}t^3S \\ & + 5.3875\times10^{-9}t^4S - 5.72466\times10^{-3}S^{3/2} + 1.0227\times10^{-4}tS^{3/2} - 1.6546\times10^{-6}t^2S^{3/2} \\ & + 4.8314\times10^{-4}S^2\end{aligned}$$

$$\begin{aligned}K(S,t,p) = {} & 19652.21 + 148.4206t - 2.327105t^2 + 1.360447\times10^{-2}t^3 - 5.155288\times10^{-5}t^4 + 3.239908p \\ & + 1.43713\times10^{-3}tp + 1.16092\times10^{-4}t^2p - 5.77905\times10^{-7}t^3p + 8.50935\times10^{-5}\times p^2 \\ & - 6.12293\times10^{-6}tp^2 + 5.2787\times10^{-8}t^2p^2 + 54.6746S - 0.603459tS + 1.09987\times10^{-2}t^2S \\ & - 6.1670\times10^{-5}t^3S + 7.944\times10^{-2}S^{3/2} + 1.6483\times10^{-2}tS^{3/2} - 5.3009\times10^{-4}t^2S^{3/2} + 2.2838\times10^{-3}pS \\ & - 1.0981\times10^{-5}tpS - 1.6078\times10^{-6}\times t^2pS + 1.91075\times10^{-4}pS^{3/2} - 9.9348\times10^{-7}p^2S \\ & + 2.0816\times10^{-8}tp^2S + 9.1697\times10^{-10}t^2p^2S\end{aligned}$$

The advantages of the test are that the load is purely hydrostatical pressure; the tests can be performed at different temperatures. Moreover, the load control allows us to test the material in its service condition (hydrostatic creep tests). However, the loading rate of the tests remains limited because at high loading rate, the pump cannot follow the loading profile. In certain cases, the water uptake by the sample must be considered.

3.1.3 Behaviour under monotonic loading

For the loading profile shown in (Fig. 3.4.a), monotonic load followed by a creep loading and an unloading phase, the relation between volumetric strain and time is reported in Fig. 3a for different temperatures (20, 40, 60 and 80°C). The relation between hydrostatic pressure and volumetric strain is plotted in Fig. 3.4.b for the different temperatures.

The behaviour under monotonic loadings can be split into four phases which can be described as:

-Phase 1: Void compression (volumetric strain between 0 and 2%).

This behaviour can be related to the porosity generated in the material during the manufacturing process. Due to the rigidity of the PP matrix, the porosities are compressed at low pressure. In this phase, the modulus decreases almost linearly with temperature. The boundaries of phase 1 (pressure and maximum strain) also decrease with pressure (Table 5).

- Phase 2: Microsphere compression (maximum pressure less than 40 - 50 MPa).

In this phase the behaviour is governed by linear elastic behaviour of the material before damage of the microspheres. It may be noted that the pressure limit of this phase is higher at low temperatures than at high temperatures. On the other hand, the stiffness increases slowly with temperature. The consolidation of the material can be associated with a decrease of the initial porosity. During this

phase, the mechanical behaviour is also strongly governed by the behaviour of the microspheres. Due to the morphology of the material and considering that the microspheres do not all have the same dimensions; there are local zones in the material where the shear stress can be high. So, at high temperature, the polymer matrix being softer, the microspheres can move more easily to a stable position in the polymer matrix. This phenomenon leads to more important consolidation at high temperature.

- Phase 3: densification plateau (significant increase of volumetric strain).

The densification plateau corresponds to damage in the material associated with microsphere failures. The pressure obtained is generally identified as the collapse pressure of the material. This pressure, which characterizes the plateau, depends on temperature. An increase of the temperature leads to a decrease of the matrix stiffness and thus to an increase of the microsphere load. Therefore, the collapse pressure decreases with the temperature. In addition, at low temperature, microspheres are more rigid but more brittle; therefore, the breakage rate of the microspheres can decrease with the temperature. This phase involves energy storage phenomena, the microspheres working as a system of springs during loading. The spring stiffness decreasing with temperature at the same loading level, the energy stocked in the rigid springs is larger than the soft ones. This explains why most microspheres collapse earlier at low temperature.

- Phase 4: volumetric strain greater than 15%

This phase corresponds to the second phase of consolidation of the material. The total breakdown of glass microspheres causes the material to behave almost as a one phase solid material (solid polypropylene). This property is revealed during the unloading of the material.

During creep loading (60 MPa for one hour), as the hydrostatic pressure is quite high, most of the microspheres fail. It can be noted that the increase of the volumetric strain is nearly independent of the temperature. Thus for this material, after the microsphere failure, the volumetric strain in creep can be explained by the porosity induced by the microsphere failure; normally, for solid polymers the volumetric strain in creep is very low [Bardenhagen et al, 1997].

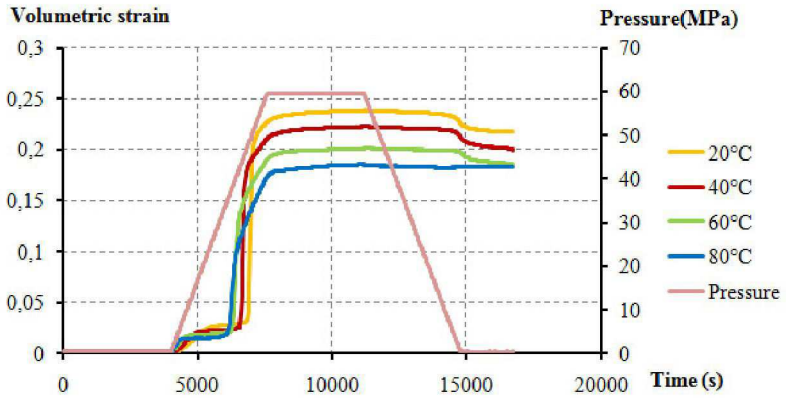

3.4.a. Volumetric strain-time and pressure-time diagrams

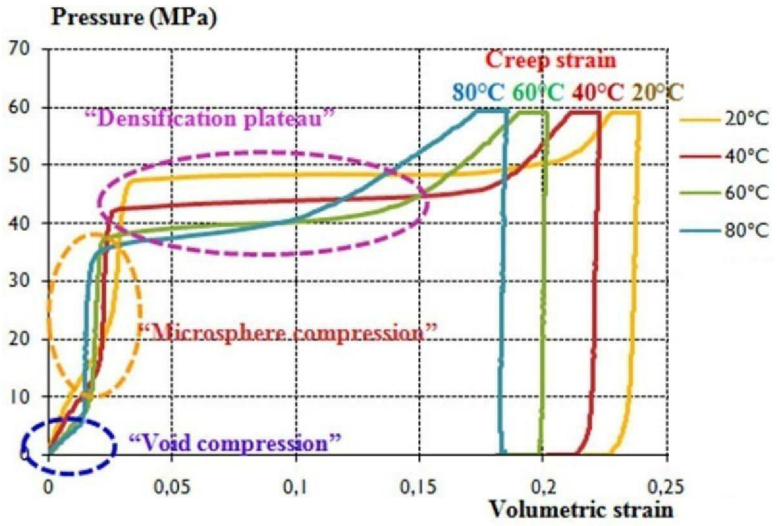

3.4.b. Hydrostatic pressure - volumetric strain diagram

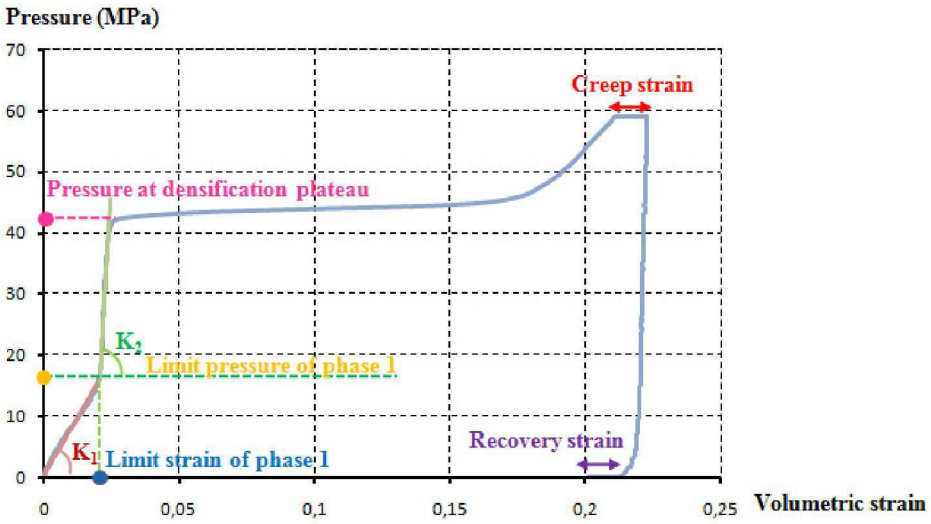

3.4.c. Different parameters of thermo-mechanical behaviour under monotonic hydrostatic pressure

Fig 3.4. Behaviour under hydrostatic pressure at different temperatures with a loading rate of 1 MPa/min

The main results of these experimental results are reported on table 3.4 in order to underline the influence of the temperature on the behaviour of the GSPP material.

Temperature (°C)	22.6	39.6	59.4	80.2
Limit pressure of phase 1 (MPa)	24.4	17.1	9.7	5.7
Limit strain of phase 1	0.026	0.021	0.018	0.013
Bulk modulus of phase 2 (MPa)	4577.6	6350.0	7558.4	8334.7
Bulk modulus of phase 1 (MPa)	910	750	520	380
Pressure at densification plateau (MPa)	48.6	44.2	39.4	37.7

Tab. 3.4. Different parameters of thermo-mechanical behaviour under monotonic hydrostatic pressure

In order to verify the reproducibility of the experimental results, for the hydrostatic crush compression three tests have been performed at 60°C and the reproducibility of the results has been evaluated. The results of the three tests are reported in figure 4 and table 6 and it can be noted that the scatter in the experimental result is quite low.

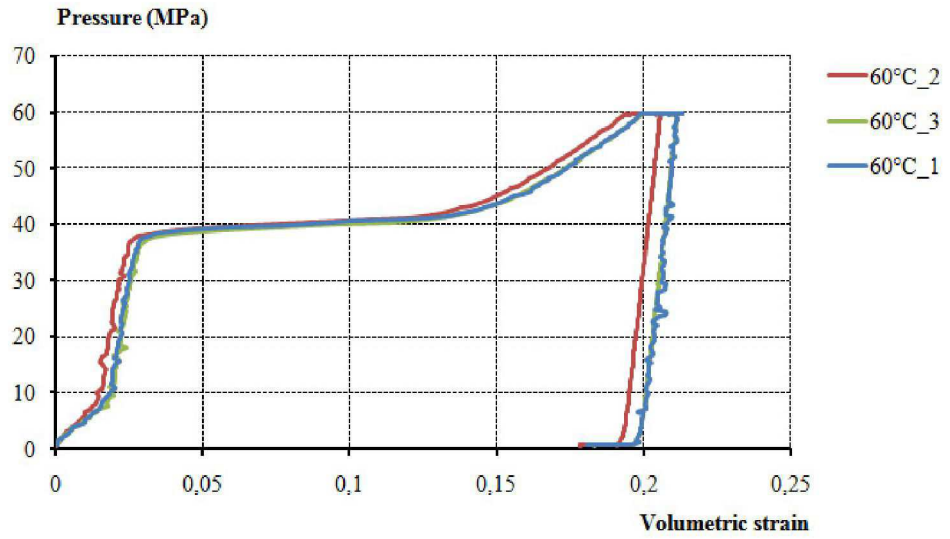

Fig 3.5. Behaviour under hydrostatic pressure at 60°C using a loading rate of 1 MPa/min (mean results of three tests)

The determination of the K_2 parameter (bulk modulus in the microsphere compression phase) is very sensitive to the experimental procedure and at this step a value of 3 GPa is retained for this parameter, which is not very strongly affected by temperature.

Property	60°C_1	60°C_2	60°C_3
Temperature (°C)	59.4	60.5	60.2
Limit pressure of phase 1 (MPa)	9.7	8.8	9.3
Limit strain of phase 1	0.018	0.014	0.018
Bulk modulus of phase 1 (MPa)	520	540	510
Bulk modulus of phase 2 (MPa)	3020	2680	2820
Pressure at densification plateau (MPa)	39.4	39.6	38.7

Tab. 3.5. Different parameters of thermo-mechanical behaviour under monotonic hydrostatic pressure at 60°C (results of three tests)

3.1.4 Influence of loading type

The material behaviour under hydrostatic loadings is quite complex and includes viscoelastic and damage phenomena. To investigate the viscous effects, tests have been performed at 60°C, at different loading rates (0.1, 1 and 5 MPa/min), using the same time duration for the creep phase (one hour) at a pressure of 60 MPa (Fig. 3.6).

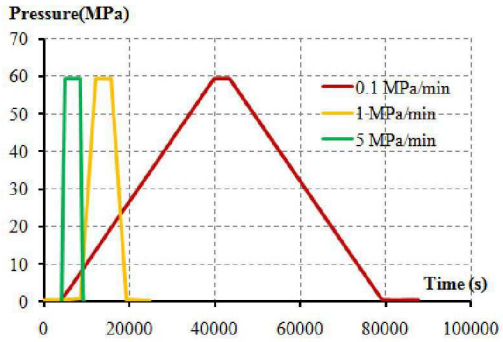

3.6.a. Loading profiles

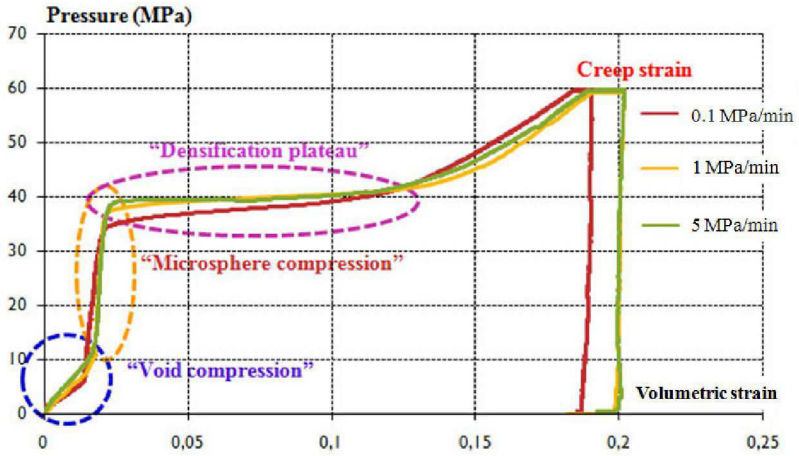

3.6.b. Hydrostatic pressure - volumetric strain diagram

Fig 3.6. Influence of the loading rate on the behaviour under hydrostatic pressure at 60°C

Experimental results in the hydrostatic pressure - volumetric strain diagram are quite similar for loading rates of 1 and 5 MPa/min. However, for the tests with a lower loading rate (0.1 MPa/min) the pressure limits of phase 1 and phase 2 are lower. This phenomenon can be explained by considering that stress redistribution occurs between the polymeric matrix and the microspheres. At low loading rate, the matrix has time to deform and then the load transfer to the microspheres becomes more important.

In addition, in order to further investigate the behaviour of the material, tests under cyclic loads using a loading and unloading rate of 1 MPa/min (Fig. 3.7-3.8) associated with a 1 hour plateau duration, have also been performed.

Under cyclic loading, at low hydrostatic pressure, an irreversible part of volumetric strain is identified (Fig. 3.7.c) in phase 1. The creep volumetric strain remains low until the hydrostatic pressure is above about 30 MPa. Similar behaviour is observed for solid polymers.

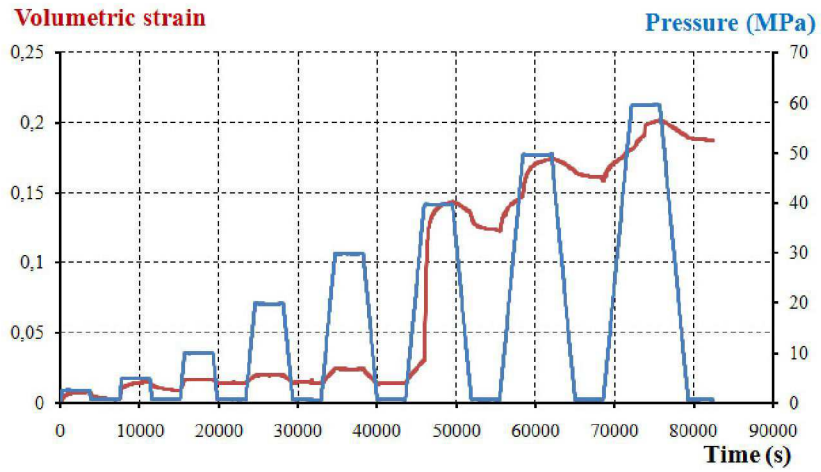

3.7.a. Volumetric strain-time and pressure-time diagrams

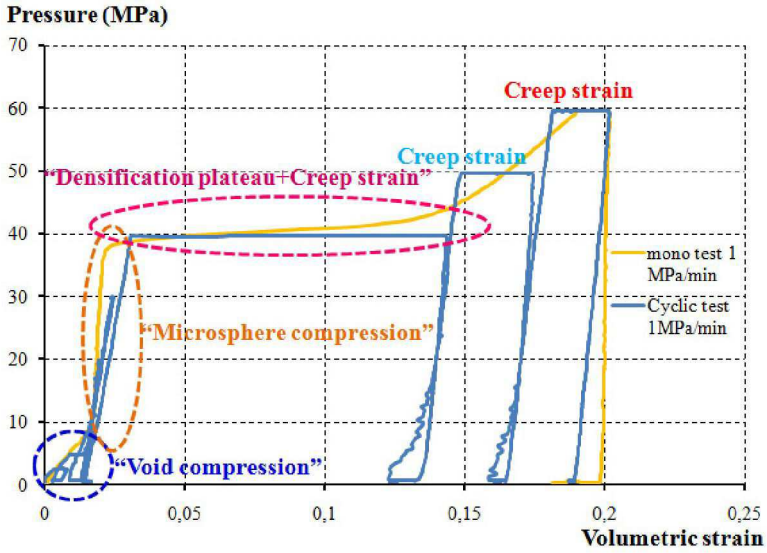

3.7.b. Hydrostatic pressure - volumetric strain diagram

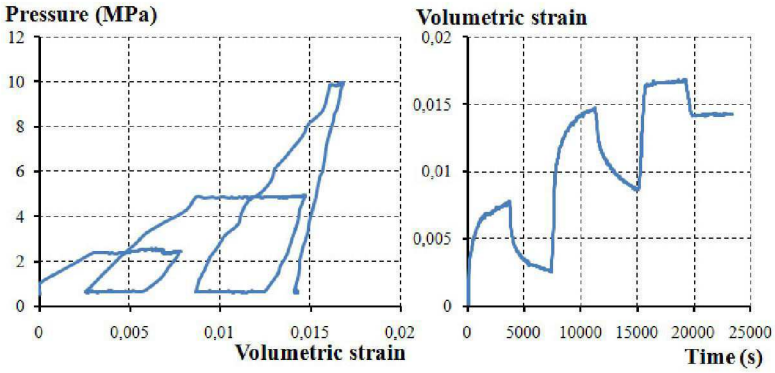

3.7.c. Influence of cycles under low hydrostatic pressure

Fig. 3.7. Behaviour under 1 cyclic hydrostatic pressure at 60°C with a loading rate of 1 MPa/min

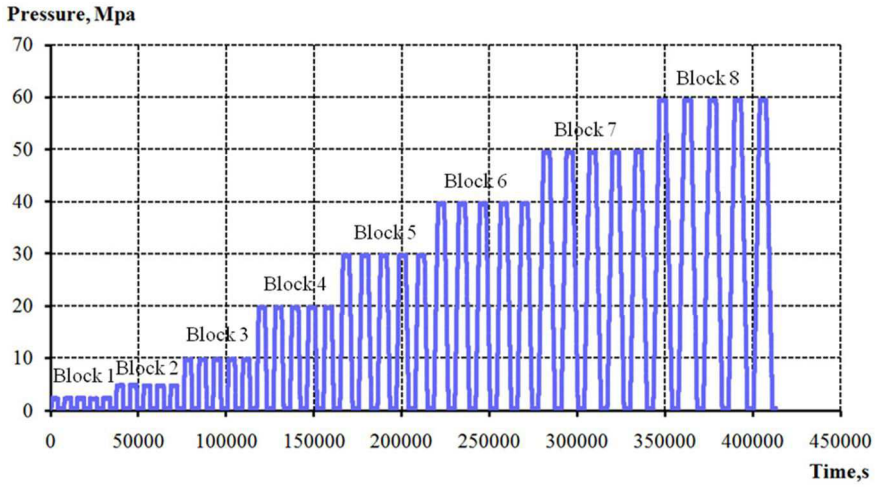

3.8.a. Loading profiles

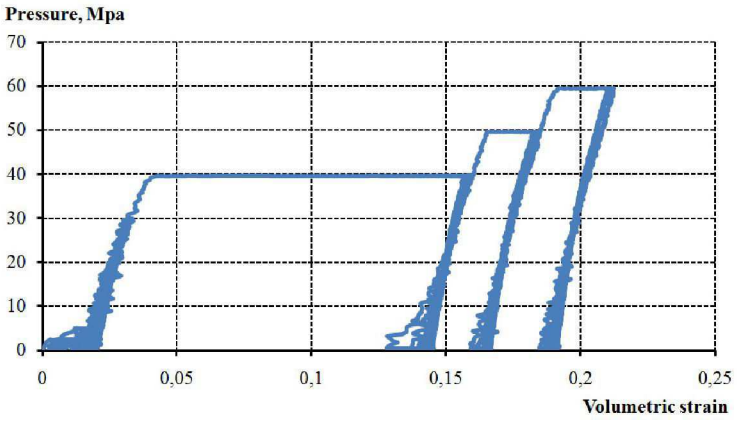

3.8.b. Hydrostatic pressure - volumetric strain diagram

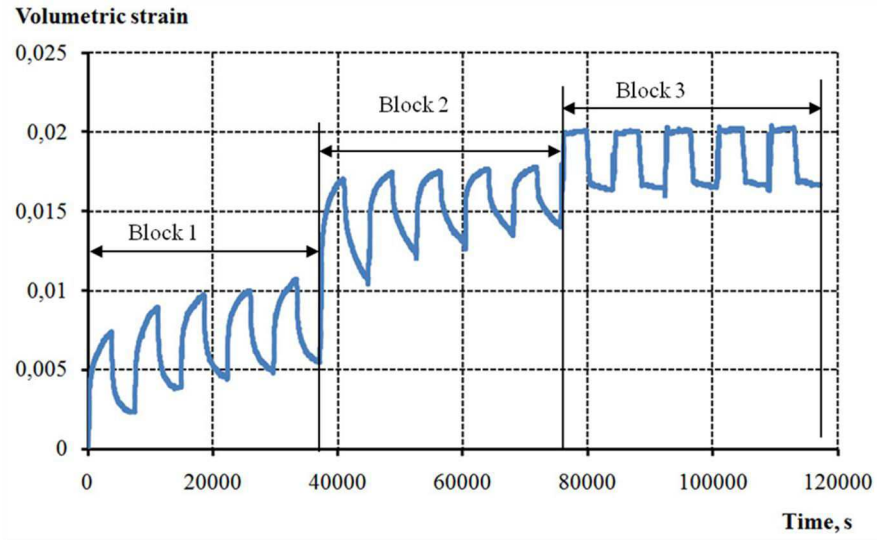

3.8.c. Influence of cycles under low hydrostatic pressur

Fig. 3.8. Behaviour under 5 cyclic hydrostatic pressures at 60°C with a loading rate of 1 MPa/min

A comparison of these experimental results with those presented previously from tests under so-called monotonic load, at the same temperature, reveals that the deformations are quite similar at the beginning of the loading (Fig. 3.7.b). The first loading cycles induce a little more deformation associated with the viscous effects. After each unloading (60 minutes plateau at 0.5 MPa) a quite large recovery can be noted. Moreover, an increase of the maximal hydrostatic pressure leads to a decrease of the recovery strain rate after unloading.

The porosity of the GSPP depends on the level of loading. Under low loadings (first phase), the porosity is the volume of micro-voids developed in the matrix during the manufacturing process. In the third phase, the failure of the microspheres may be associated with an increase in the porosity of the material. This is why after the densification plateau, in the unloading process, there is a large recovered strain. The behaviour of GSPP after collapse of microspheres is similar to that of closed cell foam [Gibson & Ashby, 1999].

To complete the characterization of the long-term behaviour of GSPP, creep tests under different hydrostatic pressures at the same temperatures of 60°C have been also performed. The material is subjected to a constant load at a given temperature. According to the results of creep tests at 60 °C (Fig. 3.9), the initial effective secant bulk modulus is 1.75 GPa and relaxed secant bulk modulus (estimated creep at infinite time) is 0.75 GPa. If we consider that the material behaviour is linear viscoelastic, the total volumetric strain can be separated into three parts: an elastic deformation, a delayed elastic deformation and a viscous deformation [Ward &Hadley, 1993]. After a creep loading under a low hydrostatic pressure (Fig. 3.9), when the pressure is released the recovery part of the strain is nearly equal to the elastic deformation. But for a high loading level such 30 MPa, the recovery part of the strain is considerably smaller compared to the elastic deformation. The evolution of volumetric strain can lead to the failure of some microspheres which contribute to the residual part of the volumetric strain.

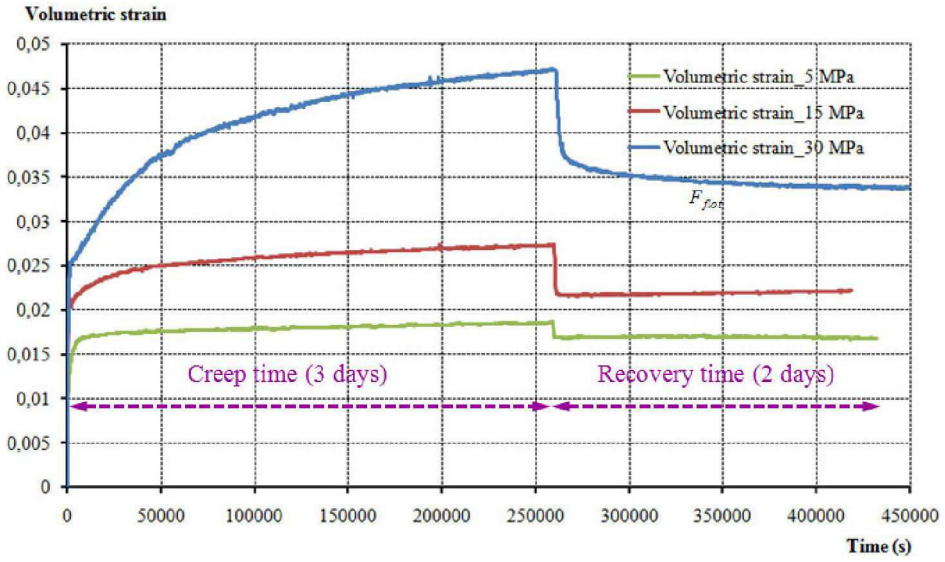

Fig 3.9. Hydrostatic creep test

3.2 Evolution of the failure of microspheres with respect to the applied hydrostatic pressure

3.2.1 Objectives

To evaluate the initial effective density of the material, the real filler density of the sampled specimens and the evolution of the failure of microspheres with respect to the applied hydrostatic pressure, a gas pycnometer [micromeritics®] has been used. To evaluate the real filler density the fillers have been recovered after burning off the resin (12 hours in an oven at 450 °C) and measured. From these data and considering a matrix density of 0.90 g/cm^3 [Borealisgroup®], an initial void volume fraction has been evaluated. Moreover, the measurement of microspheres density after different hydrostatic loading levels allows us to estimate the percentage of damaged microspheres. The results give important information in order to model the evolution of damage of the material.

3.2.2 Descriptions

The AccuPyc 1340 Pycnometer is an easy-to-use, fully automatic gas displacement pycnometer [micromeritics®]. This device allows us to identify the density and the volume of solid material by measuring the pressure change of helium within calibrated volumes (Fig. 3.10). Its advantage is that the test process is simple, fast and gives excellent results. The Pycnometer available at Ifremer Centre has a sample chamber of 10 cm^3.

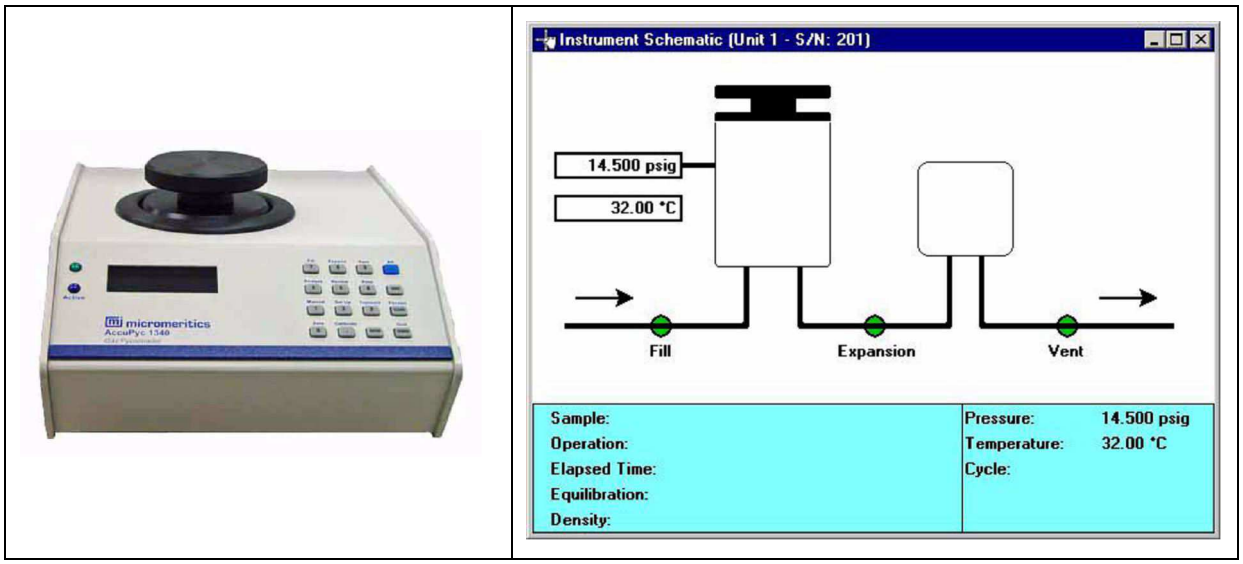

Fig. 3.10. AccuPyc 1340 Pycnometer

Fig. 3.11. Image of GSPP samples

For each test, the measurement is performed 10 times (Fig. 3.12). The process starts with a purge in order to clean the sample and to take air out of the chamber. Then the chamber is filled with helium

under low pressure (about 1.5 bar). The expansion process allows the reference chamber to be compared with the sample chamber.

- Specimen density

The samples must be carefully machined to a form corresponding to the cylindrical form of the sample chamber. The volume of sample is preferred to be at least two-third of $10cm^3$. The samples must also be free of moisture in order to have constant mass and to avoid the distorting effect of water vapor on the volume measurement during the tests (Fig. 3.11).

- Filler density

After measurement of the material density the specimens are placed in an owen for 12 hours at 450°C to fully burn the polymeric matrix. The filler is then recovered and placed in the metallic cap to be measured

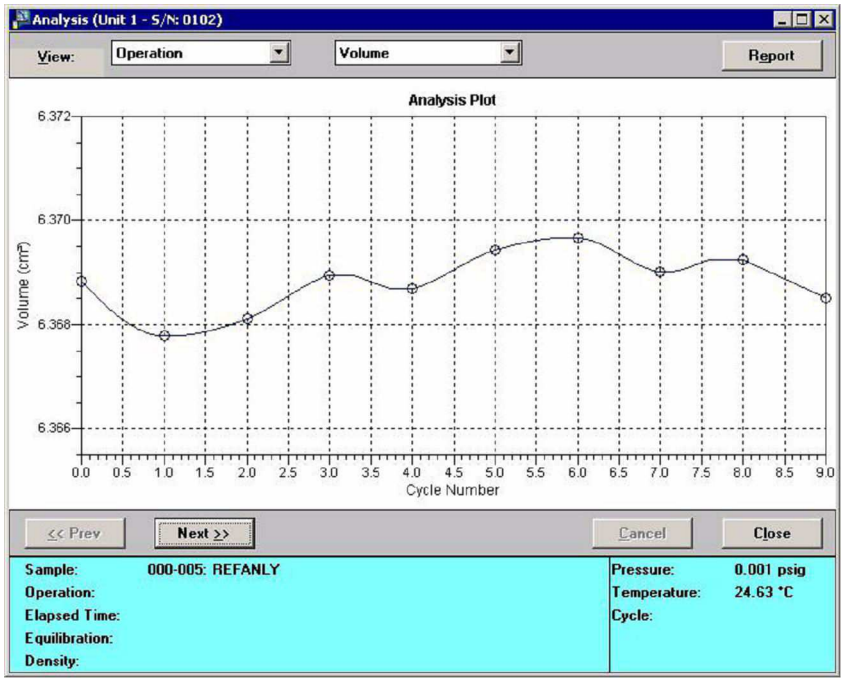

Fig. 3.12. Analysis dialog window during the test with AccuPyc 1340 Pycnometer

3.2.3 Results

The results obtained from 10 samples of GSPP are reported in (Tab. 3.6). Once again, existence of voids is detected. Their volume is estimated to be about 3.5% which corresponds to the values of limit strain of phase 1 (Tab. 3.4). It can be noted that the density of recovered filler (0.408 g/cm^3) after burning is slightly higher than the nominal density of glass microspheres (0.38 g/cm^3). This can be attributed to the mineral fillers, included in the matrix in order to facilitate the manufacturing process.

Property	Mean value	Standard deviation
Density of GSPP (g/cm^3)	0.652	0.001
Density of filler (g/cm^3)	0.408	0.001
Density of matrix (g/cm^3)	0.9	-
Volume fraction of spheres (%)	44.15	0.1
Volume fraction of voids (%)	3.5	0.15

Tab 3.6. Physical properties of GSPP

Evaluation of density of filler after hydrostatic loading

At different step of loading the filler density has been measure (same procedure as previous)

Assuming that the relation between the gas volume in the microspheres which have not yet broken and the damaged microspheres is linear, the measurement of the evolution of microspheres' density after burning off the resin (so called the filler), allows us to estimate the percentage of damaged microspheres after an experimental test under hydrostatic pressure (Fig.3.13).

When we take 1g of microspheres after burning off the resin, in the case of unloaded material, the volume of the filler $V^0_{spheres}$ is composed of the volume of glass V^0_{glass} and the volume of gas enclosed in the microspheres V^0_{gas}. Based on the results in (Tab 3.6), we have the volume of microspheres.

$$V^0_{spheres} = \frac{m_{sphere}}{\rho^0_{sphere}} = \frac{1(g)}{0.408(\mathrm{g/cm^3})} = 2.4495(cm^3)$$

Assuming that the mass of gas is equal to zero, i.e. the mass of filler is nothing more than the mass of glass, the volume of glass is:

$$V^0_{glass} = \frac{m_{sphere}}{\rho_{glass}} \frac{1(g)}{2.7(g/cm^3)} = 0.3703(cm^3)$$

With $V^0_{spheres} = V^0_{glass} + V^0_{gas}$

So the volume of gas: $V^0_{gas} = V^0_{spheres} - V^0_{glass} = 2.4495 - 0.3703 = 2.0792\left(cm^3\right)$

This corresponds to the case where the percentage of damaged microspheres is equal to zero.

In the case of a percentage of damaged microspheres of 100%, the gas volume enclosed in the microspheres is equal to zero. So, the volume of glass is equal to the volume of the filler by assuming a glass density of 2.7 (g/cm^3).

$V^{100}_{spheres} = V^{100}_{glass} = \frac{1}{2.7} = 0.3703\left(cm^3\right)$ and $V^{100}_{gas} = 0$

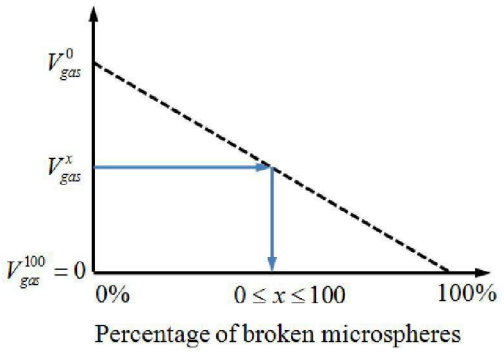

Fig 3.13. Assumption used to estimate the percentage of broken microspheres

After a monotonic hydrostatic pressure until 60 MPa (Fig. 3.4), the percentage of damaged microspheres is presented in (Tab. 3.7).

	22.6°C	39.6 °C	59.4 °C	80.2 °C
Density of filler (g/cm^3)	0.79	0.72	0.67	0.63
Standard deviation	0.0001	0.0005	0.0004	0.0005
% damaged filler	56.11	50.63	45.68	41.00

Tab 3.7. Percentage of damaged microspheres after monotonic hydrostatic pressure until 60 MPa

The same type of results for the GSPP after the creep pressure at different loading levels is also presented in (Tab 4.8). For the low loading case, the volumetric strain due to the creep pressure does not lead to the damage of microspheres in the material. But for higher loads, the volumetric strain may cause the collapse of microspheres. It must be noted that a 30 MPa creep test induced an increase of the apparent density of the filler which indicates initiation of damage.

	5 MPa	15 MPa	30 MPa
Density of filler (g/cm^3)	0.40	0.40	0.42
Standard deviation	0.0002	0.0002	0.0003
% damaged filler	0	0	3.489

Tab 3.8. Percentage of damaged microspheres after hydrostatic creep test at 60 °C

Chapter 4. Thermo-mechanical modelling of offshore polymeric material

From the experimental results presented in the previous chapter, a thermo-mechanical model of GSPP is proposed to model the creep volumetric strain under hydrostatic pressure taking into account the properties of thermo-rheologically complex material. This model is also applicable to other syntactic foam materials (Glass/epoxy, Glass/polyurethane, and Glass/phenolic) which exhibit the same type of behaviour. Assuming the material behaviour is linear viscoelastic, its modelling requires the use of a relaxation time spectrum depending on the temperature. The model initially developed by [D. Perreux et al] is used in this study. In order to accurately model the influence of the initial voids and the behaviour of the material under cyclic hydrostatic pressure, an irreversible volumetric deformation is proposed and an evolution of Young's modulus with respect to the evolution of the volumetric strain is introduced. For the field joint coating material (solid polypropylene) which is nearly a solid polymer, it is assumed that the viscous part of the deformation is incompressible, i.e. the volume change is purely elastic. Thus a generalized Maxwell temperature-dependent model is used for such material. These models are used to analyse the thermo-mechanical behaviour of a field joint during the manufacturing process and under service's conditions. Therefore, an estimation of the stress state in the assembly and a localization of the critical zones close to the different interfaces are obtained.

4.1 Overview of viscoelastic behaviour of polymeric material

Basically, for offshore applications such as studied herein, the time and temperature dependent behaviour of polymeric materials has to be taken into account. The polymeric materials could be classified according to their thermo-mechanical properties [Ward & Hadley, 1993]:

- Thermoplastic, which becomes malleable when heated, eases the implementing. The well-known thermoplastic used in offshore pipeline is solid polypropylene;
- Thermosetting, which hardens by chemical reaction and withstands the high temperature. The solid epoxy can be cited in this group;
- Elastomer, which has an important reversible deformation before its rupture (for example: polyurethane)

A general representation of the total deformation of polymer under tensile loads can be divided into many steps with different material behaviours (Fig. 4.1) for a given temperature and a given strain rate. When the load is small, material behaviour is linear viscoelastic and the deformation can be considered to be fully reversible, i.e. if the load is released, the material comes back to the initial form after some time. The material behaviour can be described by linear differential equations with only derivatives with respect to time [Leblanc, 2003]. With increasing load, the material behaviour becomes nonlinear. The use of the linear differential equations with only upper derivative terms is not enough; new derivatives with respect to stress must be added. The plastic deformation is reached at the yield point and the hardening process is observed due to the reorientation of the material molecules.

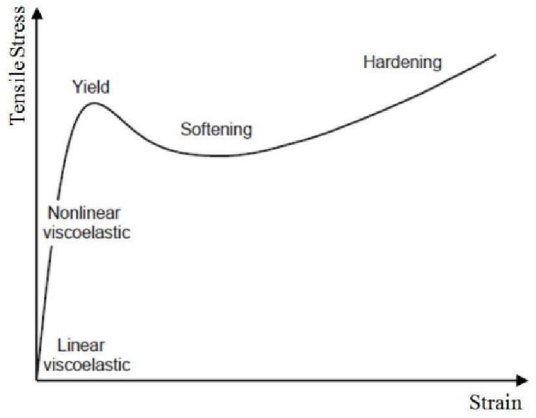

Fig. 4.1. Schematic representation of the total deformation behaviour of a polymer material [Gueguen, 2005]

The linear viscoelastic behaviour of polymer is based on the Bolzmann superposition principle. It is one of the most important theories of polymer physics [Shaw & MacKnight, 2005]. It is assumed that the stress or deformation state of a viscoelastic material is variable depending on the all loads which are applied to the material and each loading effect's contribution is independent. The

expression (Eq.4.1) allows us to understand the significant physics of this principle: the first term is the instant response of material and the second one comes from the previous loading response.

$$\varepsilon(t) = \sigma(t) J(t) - \int_{t_0}^{t} \sigma(\tau) \frac{\partial J(\tau, t)}{\partial \tau} d\tau \quad \text{[Salençon, 2009]} \qquad \text{[Eq. 4.1]}$$

Where

$\varepsilon(t)$, strain tensor; $\sigma(t)$, stress tensor and $J(t)$, delay function all depend on the loading history, i.e. are associated to time.

In the case of the nonlinear viscoelastic material, there are many available solutions which are proposed by a generalization of the classical Boltzmann principle or by using the stress or strain's derivatives [Kola ík & Pegoretti, 2006, 2008].

To study the viscous effect, there are three standard tests: creep test, relaxation test and recovery test. In the case of tensile creep test, the sample is subjected to a tensile stress σ, which is held constant. Because of the delayed response of the material, the strain ε increases during time (Fig. 4.2). Depending on the stress level, the strain response may be different (Fig. 4.3). In case of low stress, the primary creep is a dominant phenomenon: the deformation rate decreases in time. The secondary creep corresponds to the constant deformation rate. When the stress is important, the tertiary creep can occur with the apparition of the rupture of the material. In offshore exploitation of pipeline, the main load which applies on the structure is hydrostatic pressure. So the loading value is considered to do not change during its service life. In fact, the high deformation of pipeline under the constant pressure could lead to reduce the effectiveness of insulation; the microspheres could be collapsed, the average density and thermal conductivity coefficient increase and the mechanical rigidity decreases. For the thermal mechanical modelling in this chapter, it is assumed to be primary creep, i.e. the structure is subjected to the small deformation and the creep does not lead to material damage not to the change of the material structure.

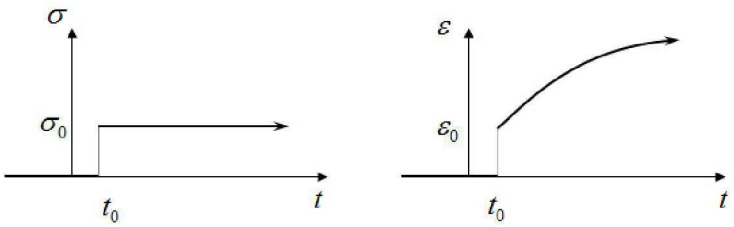

Fig 4.2. Creep test

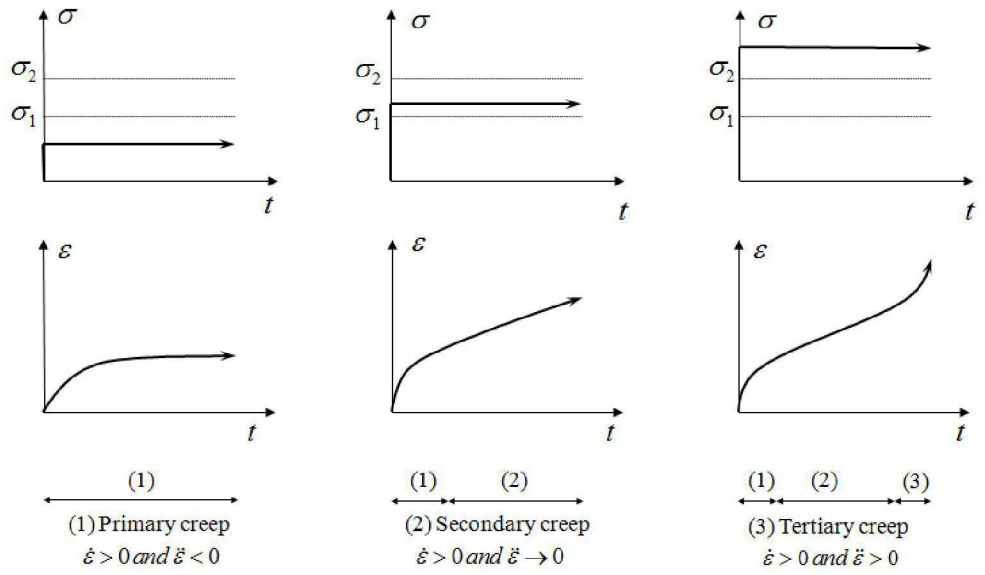

Fig 4.3. Classification of creep responses

In the case of relaxation tests, a constant strain ε is applied to the sample. The material tends to relax; the stress σ decreases (Fig. 4.4). The relaxation stress plays an important role too. During the moulding process of field joints, thanks to this effect, the residual stress in the critical zone decreases, so the damage of material does not appear. The relaxation phenomenon will reduce the local stress and then reduce the risk of crack occurrence. During the service life, the pipeline is subjected to an important deformation (bending, for example), and cracking may be avoided.

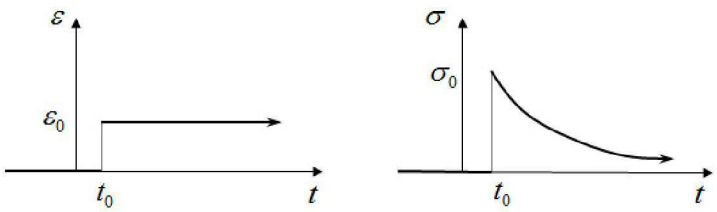

Fig 4.4. Relaxation test

The third case is recovery (Fig. 4.5). The material was loaded by a stress, and then the stress is released. Momentarily, the strain decreases (elastic response); the remaining strain rest tends to go down with time. In the case of a linear viscoelastic model, the strain can reach zero.

The combination of the three phenomena allows us to study the stress redistribution in a structure.

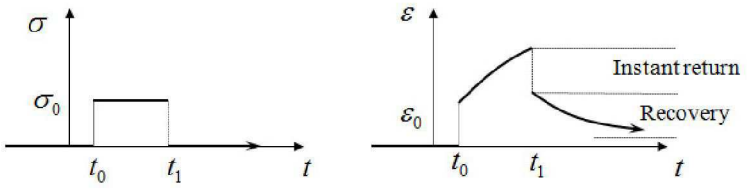

Fig 4.5. Recovery test

Many studies have described the thermal and mechanical behaviour of polymer materials. Depending on how temperature affects the mechanical response, we can consider a polymer to be either a thermo-rheologically simple or a thermo-rheologically complex material. In the case of thermo-rheologically simple materials, the temperature's influence is transformed into a change in the relaxation time by only using a shift factor (a_T), the ratio of the relaxation times at temperature T and reference temperature T_0. This factor is based on the time-temperature superposition principle, i.e. time and temperature can be interchanged. One frequently used shift factor was defined by the Williams-Landel-Ferry (WLF) equation:

$$\log(a_T) = \frac{-C_1(T - T_0)}{C_2 + (T - T_0)} \qquad \text{(Eq. 4.2)}$$

Where the reference temperature T_0 is the glass temperature, the two constants C1 and C2 were originally thought to be universal constants (C1=17.4 and C2=51.6 K) for all polymer materials. The other values of C1 and C2 were proposed in [Shaw & MacKnight, 2005]. The WLF equation provides a good indication of thermal behaviour of polymers in the glassy region and the glass transition region. Above the glass transition temperature (in the rubber region), the results from the WLF equation can diverge considerably [Williams et al 1955]. In this case the Arrhenius equation using the activation energy E_0 and the gas constant R is preferred, in order to predict the behaviour properly:

$$\log(a_T) = \frac{E_0}{R(T - T_0)} \qquad \text{(Eq. 4.3)}$$

In the case of thermo-rheologically complex polymers, the temperature induces a change in the shape of relaxation time spectrum (Fig.4.6) and the initial, long-term mechanical properties of the material [Muliana & Khan, 2008].

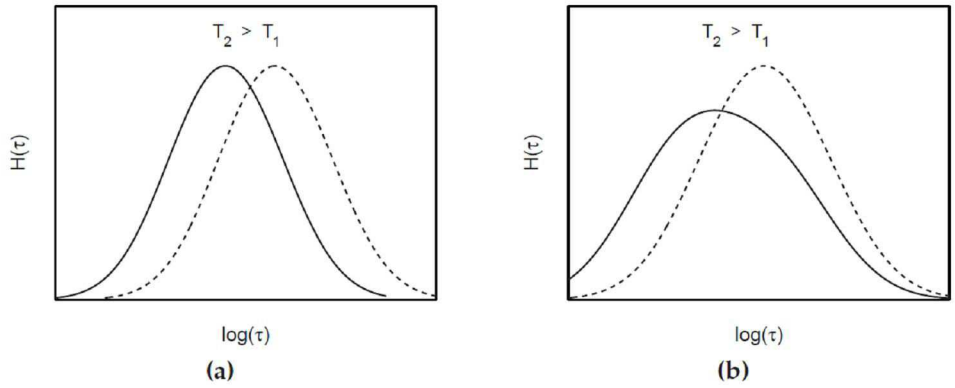

Fig 4.6. Total relaxation time spectrum at a temperature T1 and T2>T1 for a material (a) thermo-rheologically simple, and (b) thermo-rheologically complex [Edwin, 2005]

Before developing the model, we have performed some experimental DMA tests on our materials in order to verify the thermo-rheological behaviour of the GSPP (tension-tension, strain range 10^{-3}, from -70°C to 150°C by step of 10°C, frequency range 1 to 100Hz). Thus, the storage modulus is plotted as a function of loss modulus. It can be noted that for solid polyurethane (Fig. 4.7), under these conditions, the plot is quite smooth, whereas in the case of GSPP (Fig. 4.8), no clear correlation between storage modulus and loss modulus is observed, so GSPP must be considered as a thermo-rheologically complex material. [Gueguen, 2005].

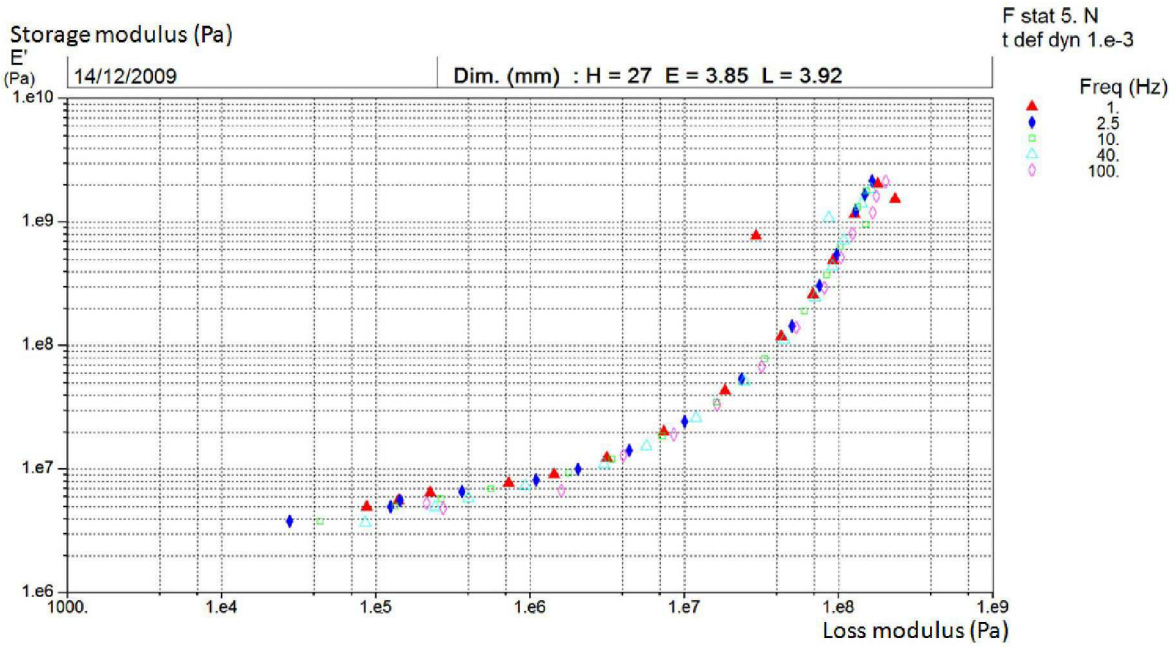

Fig 4.7. Diagram of Storage modulus and Loss modulus of solid polyurethane (thermo-rheologically simple)

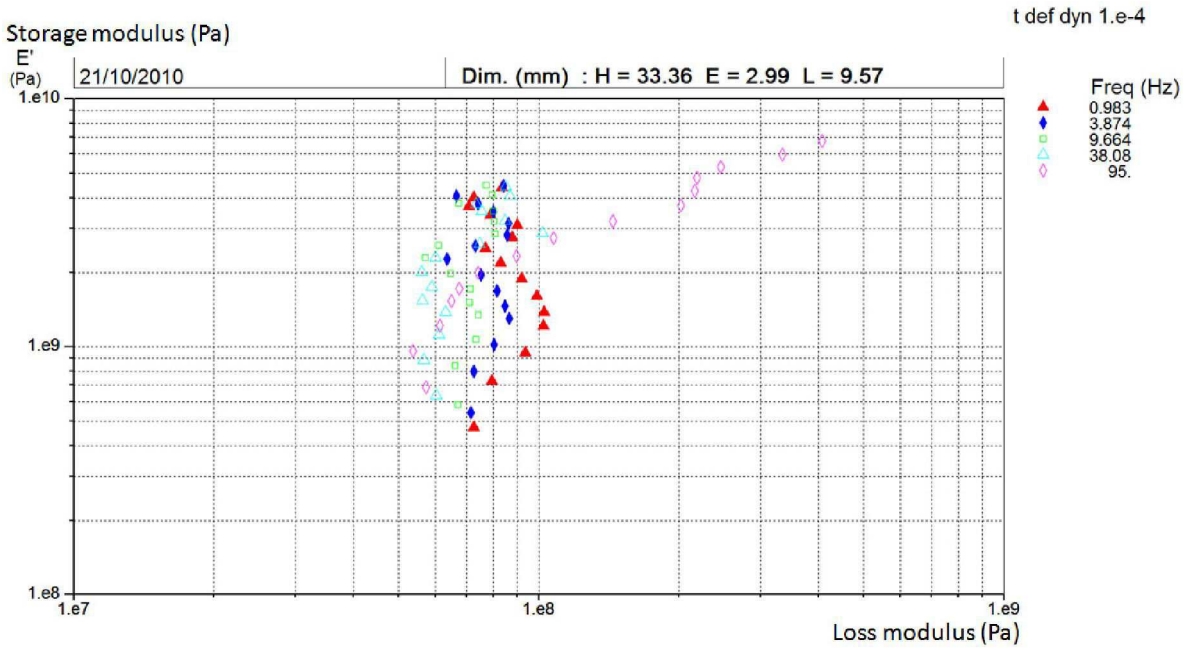

Fig 4.8. Diagram of Storage modulus and Loss modulus of GSPP (thermo-rheologically complex)

4.2 Viscoelastic model of syntactic foam

4.2.1 Rheology model

A thermo-mechanical model of GSPP is proposed to take into account the creep volumetric strain under hydrostatic pressure; the thermo-rheologically complex property of material is solved by introducing the experimental relations between the viscoelastic parameters and the temperature. This model is also applicable to other syntactic foam materials (Glass/epoxy, Glass/polyurethane, and Glass/phenolic) which exhibit the same type of behaviour. It has been implemented in the COMSOL Multiphysics® Software, which was selected as it is well-suited to model coupling between different physical phenomena.

A model of syntactic foam was originally proposed to represent the elastic behaviour of a material combined with a damage process related to the rupture of the microspheres which was associated with a permanent deformation [Choqueuse et al, 2007]. To take into account the viscous behaviour, a relaxation spectrum has been introduced [Perreux & Robinet, 2008; Treasurer, 2010; Edwin, 2005, Phan et al, 2012]. The shape of the spectrum is chosen as triangular and thus defined by two parameters n_c and n_o (Fig.4.9). The total strain rate $\underline{\underline{\dot{\varepsilon}}}$ is the sum of elastic strain rate $\underline{\underline{\dot{\varepsilon}}}$ and viscous strain rate $\underline{\underline{\dot{\varepsilon}}}^{ve}$ (Eq. 4.4). The viscous strain is composed of several (n_b) contributions $\underline{\underline{\xi_n}}$ that form the relaxation spectrum (Eq.4.5-4.7).

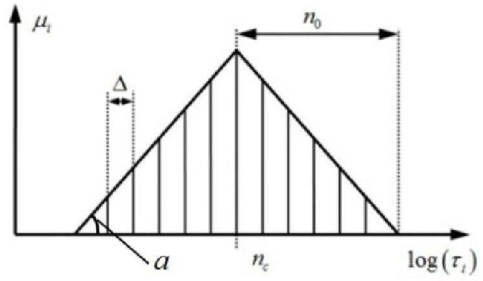

Fig. 4.9. Relaxation time spectrum

Two last parameters n_c and n_0 (logarithm of average relaxation time and width of relaxation spectrum) are defined by creep test at constant damage [Perreux & Robinet, 2008].

$$\underline{\underline{\dot{\varepsilon}}} = \underline{\underline{\dot{\varepsilon}}} + \underline{\underline{\dot{\varepsilon}}}^{ve} \qquad \text{(Eq. 4.4)}$$

$$\underline{\underline{\dot{\varepsilon}}}^{ve} = \sum_{i=1}^{n_b} \underline{\underline{\xi}}_i \text{ and } \underline{\underline{\dot{\varepsilon}}} = \underline{\underline{\underline{\underline{S}}}}_{eff} : \underline{\underline{\dot{\sigma}}} \qquad \text{(Eq. 4.5)}$$

Each viscous branch can be described by a differential equation:

$$\underline{\underline{\dot{\xi}}}_i = -\frac{1}{\tau_i}\left(\underline{\underline{\xi}}_i - \mu_i \underline{\underline{\underline{\underline{S}}}}_{Reff} : \underline{\underline{\sigma}}\right) \qquad \text{(Eq. 4.6)}$$

The form of relaxation time spectrum is normalized by the weighted sum:

$$\sum_{i=1}^{n_b} \mu_i = 1$$

$\underline{\underline{\underline{\underline{S}}}}_{eff}$ and $\underline{\underline{\underline{\underline{S}}}}_{Reff}$ are the initial state and those in the relaxed state in the flexibility matrix successively.

Thank to the characteristics of homogeneous and isotropic material, the flexibility matrix can be expressed in the simplified form: $\underline{\underline{\underline{\underline{S}}}}_{eff} \Leftrightarrow \underline{\underline{S}}^*_{eff}$; $\underline{\underline{\underline{\underline{S}}}}_{Reff} \Leftrightarrow \underline{\underline{S}}^*_{Reff}$

$$\underline{\underline{S^*_{eff}}} = \begin{bmatrix} \frac{1}{E_{eff}} & \frac{-\nu_{eff}}{E_{eff}} & \frac{-\nu_{eff}}{E_{eff}} & 0 & 0 & 0 \\ & \frac{1}{E_{eff}} & \frac{-\nu_{eff}}{E_{eff}} & 0 & 0 & 0 \\ & & \frac{1}{E_{eff}} & 0 & 0 & 0 \\ & & & \frac{1}{G_{eff}} & 0 & 0 \\ & & & & \frac{1}{G_{eff}} & 0 \\ & & & & & \frac{1}{G_{eff}} \end{bmatrix}; \underline{\underline{S^*_{Reff}}} = \begin{bmatrix} \frac{A}{E_{eff}} & \frac{-B\nu_{eff}}{E_{eff}} & \frac{-B\nu_{eff}}{E_{eff}} & 0 & 0 & 0 \\ & \frac{A}{E_{eff}} & \frac{-B\nu_{eff}}{E_{eff}} & 0 & 0 & 0 \\ & & \frac{A}{E_{eff}} & 0 & 0 & 0 \\ & & & \frac{C}{G_{eff}} & 0 & 0 \\ & & & & \frac{C}{G_{eff}} & 0 \\ & & & & & \frac{C}{G_{eff}} \end{bmatrix} \quad \text{(Eq. 4.7)}$$

with $G_{eff} = \frac{E_{eff}}{2\left(1+\nu_{eff}\right)}$

Now, we calculate the relaxation times τ_i which correspond to its correlated weight μ_i.

The viscous branches in relaxation time spectrum are separated by the interval Δ. So, the relaxation times are τ_i calculated by:

$$\tau_i = 10^{n_i} = 10^{(i.\Delta + n_c - n_0)}$$

$$\Delta = \frac{2.n_0}{n_b + 1} \text{ and } n_i = i.\Delta + n_c - n_0 \qquad \text{(Eq. 4.8)}$$

The contributions μ_i are calculated by the slope of relaxation time spectrum a and the position of viscous braches n_i:

$$\mu_i = a\left[n_i - \left(n_c - n_0\right)\right] \text{ with } n_i \in \left[\left(n_c - n_0\right), n_c\right]$$

$$\mu_i = -a\left[n_i - \left(n_c + n_0\right)\right] \text{ with } n_i \in \left[n_c, \left(n_c + n_0\right)\right]$$

The slope of the relaxation time spectrum a is calculated from the normalization of the spectrum:

$$1 = \sum_{i=1}^{n_b} \mu_i = a \sum_{n_i = n_c - n_0}^{n_i = n_c} \left[n_i - \left(n_c - n_0\right)\right] - a \sum_{n_i = n_c}^{n_i = n_c + n_0} \left[n_i - \left(n_c + n_0\right)\right] - a n_0$$

Replacing n_i by its expression in (Eq.4.8), we have:

$$1 = a\sum_{i=1}^{i=(n_b-1)/2}\left[i.\Delta + n_c - n_0 - (n_c - n_0)\right] - a\sum_{(n_b-1)/2}^{i=n_b}\left[i.\Delta + n_c - n_0 - (n_c + n_0)\right] - an_0$$

$$\Leftrightarrow 1 = a\left[\sum_{i=1}^{i=(n_b-1)/2} i\Delta - \sum_{(n_b-1)/2}^{i=n_b}\left[i.\Delta - 2n_0\right] - n_0\right]$$

By characteristic of an arithmetic progression, we have:

$$1 = a\left[\frac{2.n_0}{n_b+1}\frac{(n_b-1)/2+1}{2}.\frac{(n_b+1)}{2} - \frac{2.n_0}{n_b+1}.\frac{n_b+(n_b-1)/2}{2}.\frac{(n_b+1)}{2} + 2n_0.\frac{(n_b+1)}{2} - n_0\right]$$

$$\Leftrightarrow 1 = a\left[\frac{(n_b+1)}{2}.\frac{2.n_0}{n_b+1}.\frac{(-1-n_b)}{2} + 2n_0.\frac{(n_b+1)}{2} - n_0\right]$$

$$\Leftrightarrow a = \frac{2}{n_0(n_b-1)}$$

There are 5 parameters to describe the linear viscoelastic behaviour of the material. A, B, and C (Eq. 6) represent the ratios between stiffness parameters in the initial state and those in the relaxed state in the flexibility matrix $\underline{\underline{S_{eff}}}$ and $\underline{\underline{S_{Reff}}}$. The constant A depends on the temperature and is the ratio between the initial effective Young's modulus, E_{eff}, and the relaxed effective Young's modulus, E_{Reff}. It can be estimated from creep tensile tests results. To calculate the constant B, the hydrostatic creep tests are used and it is estimated from relationships between the bulk modulus, Young's modulus and Poisson's ratio for isotropic material.

From (Eq.4.7) we can deduct: $\frac{-B\nu_{eff}}{E_{eff}} = \frac{-\nu_{Reff}}{E_{Reff}} = \frac{-A.\nu_{Reff}}{E_{eff}} \rightarrow \nu_{Reff} = \frac{B}{A}\nu_{eff}$.

So, if the Poisson's ratio is constant, i.e. $\nu_{Reff} = \nu_{eff}$, then $A = B$

In the initial state, the effective bulk modulus can be calculated by $K_{eff} = \frac{E_{eff}}{3(1-2\nu_{eff})}$

The same relation for the relaxed state: $K_{Reff} = \frac{E_{Reff}}{3(1-2\nu_{Reff})}$ and $K_{Reff} = \frac{K_{eff}}{D} = \frac{1}{D}.\frac{E_{eff}}{3(1-2\nu_{eff})}$.

D is the ratio between initial effective bulk modulus and relaxed effective bulk modulus.

So,

$$\frac{E_{Reff}}{3(1-2v_{Reff})} = \frac{1}{D}.\frac{E_{eff}}{3(1-2v_{eff})}$$
$$\Leftrightarrow A(1-2v_{eff}.B/A) = D(1-2v_{eff})$$
$$\Leftrightarrow B = \frac{A-D(1-2v_{eff})}{2v_{eff}}$$

It can be noted that if the Poisson's ratio is constant, B = A = D.

4.2.2 Application of rheology model in simple loading cases

Our ambition is to estimate the strain and stress state of a field joint area during its moulding and under service conditions. The complex thermo-mechanical loads and the structure do not allow us to find out all analytical solutions, but finite element software like COMSOL Multiphysics® is adapted to solve these coupled problems. However, to calculate the necessary quantity of viscous branches and validate the implementation of the viscoelastic model in COMSOL Multiphysics®, the analytical and modelling solutions for the simple loading cases (creep hydrostatic pressure and uni-axial creep tensile) are essential. An inverse identification method using the optimisation functions in Matlab® is also used to determine the parameters of the viscoelastic model. Taking into account the thermal effects and solidification of GSPP, an improvement of the model is proposed.

4.2.2.1 Analytical solutions of rheology model

- Application in the case of creep hydrostatic pressure

The analytical solutions can be found by solving the differential equations (Eq. 4.4-4.7) with initial and relaxed conditions. Considering the unknowns (viscous strain) and the loading types are tensors of order 2 and depend on time, the Laplace-Carson method is well-suited. This transform is a method to solve the differential physical equations [Lemaitre & Chaboche, 2006]. It allows us to transform a function of time $g(t)$ to a function of Laplace variable $g^*(s)$ using the exponential factor $e^{(-st)}$:

$$g^*(s) = s\int_{-\infty}^{\infty} g(t)e^{-st}dt$$

In Laplace-Carson's space, the convolution product is transformed to ordinary product. The transformation allows us to solve the differential equations easily. The ordinary solutions of differential equations were already established. The most useful Laplace-Carson transformations are presented in [Lemaitre & Chaboche, 2006]. Some examples of results obtained by using this transformation on a classical rheological model are presented below:

Rheological model	Constitution	Creep function	Relaxation function
Maxwell model	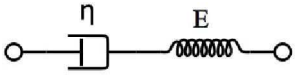	$f(t)=\left(\frac{1}{E}+\frac{t}{\eta}\right)$	$r(t)=\left(Ee^{-\frac{E}{\eta}t}\right)$
Voigt-Kelvin model	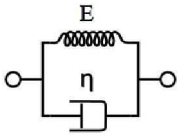	$f(t)=\frac{1}{E}\left(1-e^{-\frac{E}{\eta}t}\right)$	$r=\eta\delta+EY$

For the case of creep under hydrostatic pressure on syntactic foam, a hydrostatic pressure p held constant leads to an evolution of the volumetric deformation.

From the main equations

$\underline{\underline{\dot{\varepsilon}}}=\underline{\underline{\dot{\varepsilon}}}+\underline{\underline{\dot{\varepsilon}}}^{e}$ (Eq. 4.4)

$\underline{\underline{\dot{\xi}_i}}=-\frac{1}{\tau_i}\left(\underline{\underline{\xi_i}}-\mu_i\underline{\underline{\underline{\underline{S}}}}_{Reff}:\underline{\underline{\sigma}}\right)$ (Eq. 4.6)

$\rightarrow \text{trace}\left(\underline{\underline{\dot{\xi}_i}}\right)+\frac{1}{\tau_i}\text{trace}\left(\underline{\underline{\xi_i}}\right)=\frac{\mu_i}{\tau_i}\frac{p}{K_{Reff}}$

With initial condition:

$\left(\frac{\Delta V}{V}\right)_{t=0}=\text{trace}\left(\underline{\underline{\varepsilon}}^{t}\right)_{t=0}=\frac{p}{K_{eff}}$

And the relaxed condition:

$\left(\frac{\Delta V}{V}\right)_{t=\infty}=\text{trace}\left(\underline{\underline{\varepsilon}}^{t}\right)_{t=\infty}=\frac{p}{K_{Reff}}$

Using the Laplace-Carson transform and the relation between the bulk modulus, Young's modulus and Poisson's ratio, the final form of volumetric deformation is obtained:

$$\text{trace}\left(\underline{\underline{\varepsilon}}^{t}\right)=3\sum_{i=1}^{n_b}\left[\mu_i p\left(\frac{1}{E_{eff}}-\frac{A}{E_{eff}}-\frac{2v_{eff}}{E_{eff}}+\frac{2Bv_{eff}}{E_{eff}}\right)\exp\left(-\frac{t}{\tau_i}\right)\right]+3p\left(\frac{A}{E_{eff}}-\frac{2Bv_{eff}}{E_{eff}}\right)$$

For uni-axial creep tensile, we use the same calculation process as for the previous case, an axial tensile stress σ_x in the direction x, held constant, leads to an evolution of the axial deformation (longitudinal direction) and transversal deformation.

$$\varepsilon_x^t = \sum_i \left[\mu_i \sigma_x \left(\frac{1}{E_{eff}} - \frac{A}{E_{eff}} \right) \exp\left(-\frac{t}{\tau_i} \right) \right] + \frac{A.\sigma_x}{E_{eff}}$$

$$\varepsilon_y^t = \varepsilon_z^t = \sum_i \left[\mu_i \sigma_x \left(-\frac{v_{eff}}{E_{eff}} + \frac{Bv_{eff}}{E_{eff}} \right) \exp\left(-\frac{t}{\tau_i} \right) \right] - \frac{Bv_{eff}}{E_{eff}} \sigma_x$$

4.2.2.2 Model implementation in a finite element analysis

- Implementation of model in COMSOL Multiphysics

The numerical implementation of the model in COMSOL Multiphysics is carried out according to the diagram shown in (Fig.4.10). The solid mechanics model is composed of one elastic mechanics module and n_b general form partial differential equations used to model the viscous part of the material.

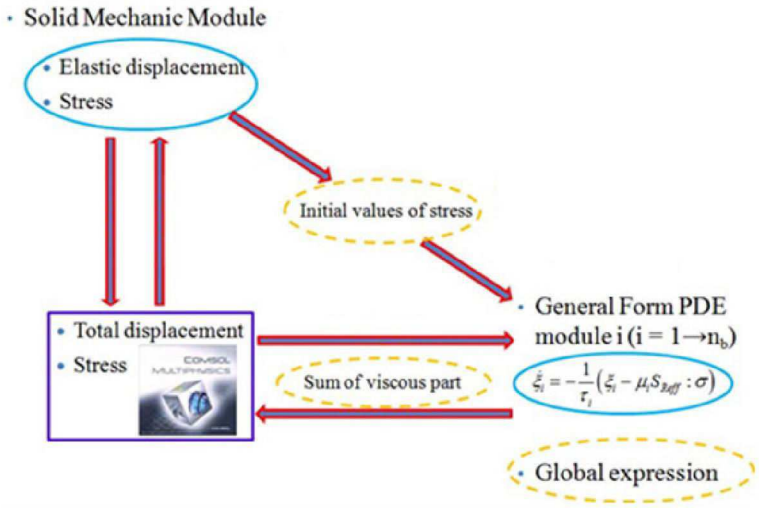

Fig 4.10. Implementation of the model

With:

- One structural mechanics module. The governing equation is: $\rho \frac{\partial^2 \underline{u}}{\partial t^2} - \nabla \underline{\underline{\sigma}} = \underline{F_v}$

Where $\underline{u}$ is the displacement, $\underline{\underline{\sigma}}$ is the stress tensor, $\underline{F_v}$ is volumetric force and ρ is the density of material

- (n_b) general form of Partial Differential Equations. The variable $_i$ can be calculated from the equation : $\underline{\underline{e_a}} : \frac{\partial^2 \underline{\underline{\xi_i}}}{\partial t^2} + \underline{\underline{d_a}} : \frac{\partial \underline{\underline{\xi_i}}}{\partial t} + \nabla . \underline{\Gamma} = \underline{F}$

Where,

$\nabla = \left[\frac{\partial}{\partial x}, \frac{\partial}{\partial y}, \frac{\partial}{\partial z}\right]$ in case of 3D and $\nabla = \left[\frac{\partial}{\partial r}, \frac{\partial}{\partial z}\right]$ in case of 2D axisymmetric

$\underline{\underline{e_a}}$, the mass coefficient, is a null tensor of order 2; $\underline{\underline{d_a}}$, damping coefficient, is a unit tensor of order 2 (Kronecker delta); $\underline{\Gamma}$, conservative flux vector, is null; and $\underline{F}$, source term, is a vector which depends on the stress.

$$\underline{F} = \begin{bmatrix} -\frac{1}{\tau_i}\xi_x^i + \frac{\mu_i}{\tau_i}\frac{1}{E_{eff}}\left[A.\sigma_x - Bv_{eff}\left(\sigma_y + \sigma_z\right)\right] \\ -\frac{1}{\tau_i}\xi_y^i + \frac{\mu_i}{\tau_i}\frac{1}{E_{eff}}\left[A.\sigma_y - Bv_{eff}\left(\sigma_x + \sigma_z\right)\right] \\ -\frac{1}{\tau_i}\xi_z^i + \frac{\mu_i}{\tau_i}\frac{1}{E_{eff}}\left[A.\sigma_z - Bv_{eff}\left(\sigma_y + \sigma_x\right)\right] \\ -\frac{1}{\tau_i}\xi_{xy}^i + \frac{\mu_i}{\tau_i}\frac{C}{2G_{eff}}\sigma_{xy} \\ -\frac{1}{\tau_i}\xi_{xz}^i + \frac{\mu_i}{\tau_i}\frac{C}{2G_{eff}}\sigma_{xz} \\ -\frac{1}{\tau_i}\xi_{yz}^i + \frac{\mu_i}{\tau_i}\frac{C}{2G_{eff}}\sigma_{yz} \end{bmatrix}$$

n_b general form FDE modules will be used. Depending on the geometry, the quantity of viscous variable $\underline{\underline{\xi_i}}$ is different. In a 3D problem the six components of the viscous strain have to be computed for each branch i. So, $_i = \left[\xi_x^i \quad \xi_y^i \quad \xi_z^i \quad \xi_{xy}^i \quad \xi_{xz}^i \quad \xi_{yz}^i\right]^T$ corresponding to six components in the 3D Cartesian coordinate system. For 2D axisymmetrical geometry, we have only 4 components of the strain. So, $_i = \left[\xi_r^i \quad \xi_\varphi^i \quad \xi_z^i \quad \xi_{rz}^i\right]^T$ corresponding to four components in the 2D axisymmetrical coordinate system.

The global expression allows us to calculate the total stress:

$$\underline{\underline{\sigma}} = \underline{\underline{\underline{\underline{C}}}}\left(E_{eff}, v_{eff}\right) : \left(\underline{\underline{\varepsilon^t}} - \sum_{i=1}^{n_b} \underline{\underline{\xi_i}}\right) \qquad \text{(Eq. 4.9)}$$

$$\underline{\underline{\dot{\xi}_i}} = -\frac{1}{\tau_i}\left(\underline{\underline{\xi_i}} - \mu_i \underline{\underline{\underline{\underline{S}}}}_{Reff} : \underline{\underline{\sigma}}\right);\ i = 1 \to n_b \qquad \text{(Eq. 4.10)}$$

The equation (Eq.4.9) means the total stress is calculated by the elastic part of deformation. The equation (Eq.4.10) allows a redistribution of stress during the evolution of deformation due to the viscous effect.

$$\underline{\underline{\underline{\underline{C}}}}\left(E_{eff}, v_{eff}\right) \Leftrightarrow \underline{\underline{\underline{\underline{C}}}}^{*} = \begin{bmatrix} \frac{\left(1-v_{eff}\right)E_{eff}}{\left(1+v_{eff}\right)\left(1-2v_{eff}\right)} & \frac{v_{eff}E_{eff}}{\left(1+v_{eff}\right)\left(1-2v_{eff}\right)} & \frac{v_{eff}E_{eff}}{\left(1+v_{eff}\right)\left(1-2v_{eff}\right)} & 0 & 0 & 0 \\ & \frac{\left(1-v_{eff}\right)E_{eff}}{\left(1+v_{eff}\right)\left(1-2v_{eff}\right)} & \frac{v_{eff}E_{eff}}{\left(1+v_{eff}\right)\left(1-2v_{eff}\right)} & 0 & 0 & 0 \\ & & \frac{\left(1-v_{eff}\right)E_{eff}}{\left(1+v_{eff}\right)\left(1-2v_{eff}\right)} & 0 & 0 & 0 \\ & & & \frac{E_{eff}}{2\left(1+v_{eff}\right)} & 0 & 0 \\ & & & & \frac{E_{eff}}{2\left(1+v_{eff}\right)} & 0 \\ & & & & & \frac{E_{eff}}{2\left(1+v_{eff}\right)} \end{bmatrix}$$

- Inverse identification of the parameters of the viscoelastic model

Two identification methods could be used (Fig. 4.11). The first one comes from the analytical solutions which give the continuous functions with variables depending on the time (or stress). By using a least squares method function developed by the Levenberg-Marquardt algorithm [Moré, 1977] in Matlab® [lsqucurvefit], the parameters x can be determined by fitting the analytical solutions data $F\left(xdata_i\right)$ with the tested values $ydata_i$. The identification process finishes when the following function is minimized:

$$\min_x \frac{1}{2}\sum_i \left(F\left(x, xdata_i\right) - ydata_i\right)^2$$

This solution allows us to use a large number of branches of the viscous model (i.e. the number n_b is high). This method requires a user-defined function and this function must be continuous. But in the case of complexity of load and geometry, the analytical solutions are difficult or even impossible to determine.

The second one is an inverse identification type method using the Nelder-Mead simplex algorithm [Lagarias et al, 1997] without any derivative information. The numerical modelling software uses the finite element method; the unknown parameters are considered to be the parameters input (with initial values). So a direct search method function will be used [Fminsearch]. The algorithm is known as unconstrained nonlinear optimisation. This shows indispensable advantages which could compensate the first one but the calculated time is higher and the viscous branches are limited. Because the two methods may only give local solutions, the choice of initial parameters is very important.

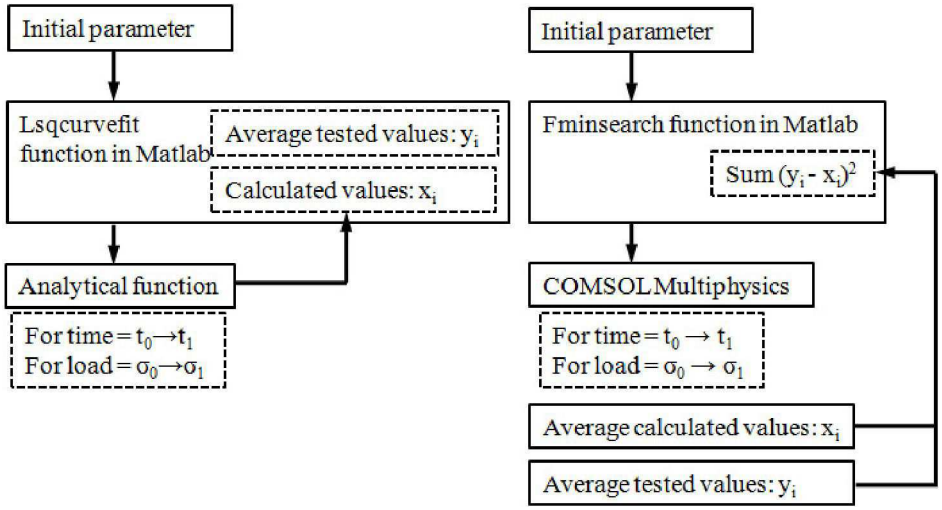

Fig. 4.11. How to identify the parameter of viscoelastic model

The analytical methods and modelling method have been used in the same loading condition for hydrostatic creep loading (60°C) of syntactic foam. In the two cases, the bulk modulus, the parameters A, B, C, n_c and n_0 do not change. The only difference is the number of viscous branches: $n_b = 31$ in the analytical solution and $n_b = 5$ in the case of modelling (Fig.4.12).

In fig 4.13, the red curve corresponds to the test values, the blue solid curve is obtained by modelling in COMSOL Multiphysic® and the green dotted line represents the result in Matlab® with analytical solution. The results are good (Fig.4.13). For the next modelling, the number of viscous branches used is 5.

$K_{eff} = 1750\,\text{MPa}$

$A = B = C = 2,35$

$n_c = 5,083$

$n_0 = 1,264$

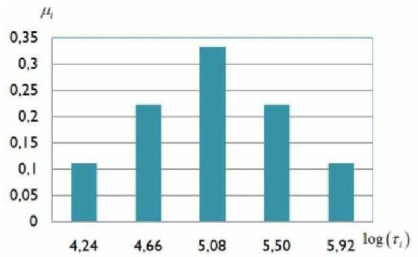

Fig. 4.12. Relaxation time spectrum at 60°C

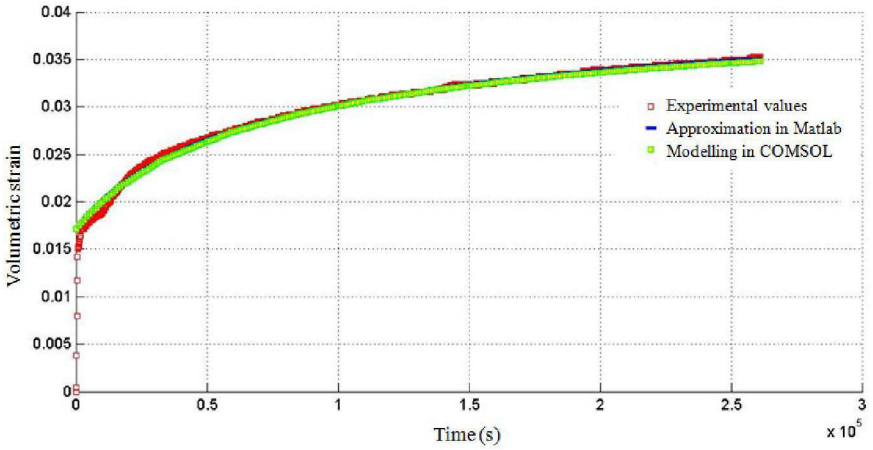

Fig. 4.13. Comparison between the analytical, modelling solution and test values

- Thermal effects

The calculation process starts to model the temperature evolution in the structure with time. Even in case of only thermal modelling, the main thermal parameters (C_p, k) depend on the temperature. Then the mechanical parameters (Young's modulus, Poisson's ratio, and viscous parameters) are calculated from the temperature evolution. The weak coupling between the heat transfer model (conduction, convection) and the solid mechanics model will be used (Fig.4.14). One heat transfer in solid is added in our modelling. The fundamental law of heat transfer is:

$$\rho C_p \frac{\partial T}{\partial t} = \nabla.(\lambda \nabla T) + Q$$

Where C_p is the specific heat capacity at constant pressure, T is absolute temperature, k is thermal conductivity and Q is the heat source

A thermal expansion strain is added to the equation (Eq.4.9)

$$\underline{\underline{\sigma}} = \underline{\underline{\underline{\underline{C}}}}(E,\nu) : \left(\underline{\underline{\varepsilon}} - \sum_{i=1}^{n_b} \underline{\underline{\xi_i}} - \alpha(T - T_{ref})\underline{\underline{\delta}} \right) \qquad \text{(Eq.4.11)}$$

Where, $\underline{\underline{\delta}}$ is a unity tensor of order 2 (Kronecker delta)

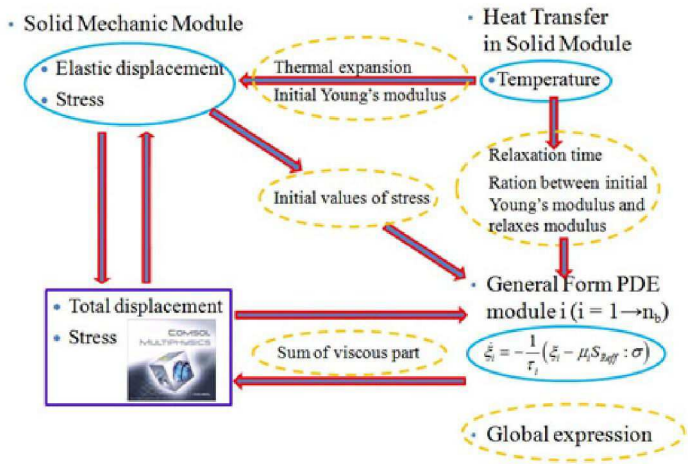

Fig. 4.14. Improving the model considering the thermal effect

Because GSPP is a thermo-rheologically complex material, the experimental relation between the thermo-mechanical parameters and the temperature will be used. The model parameters have been identified from tensile creep tests under low load (0.5 MPa) performed at different temperatures (Fig. 4.15). At this loading level we consider that no damage is generated in the material

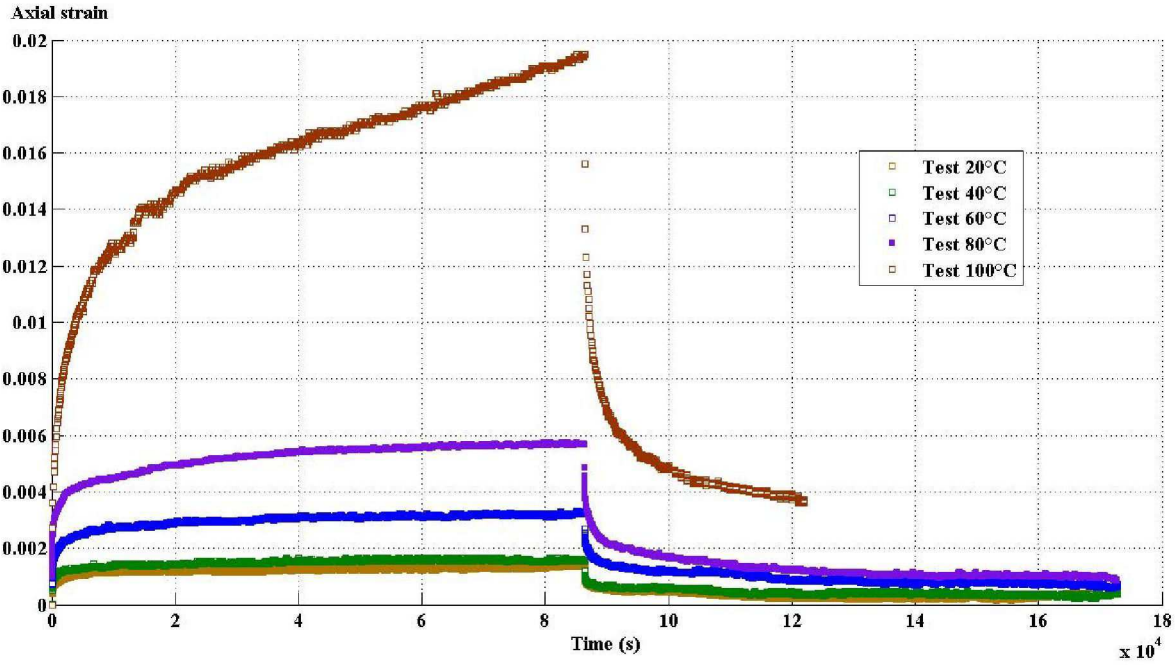

Fig. 4.15. Creep tensile test on DMA under low load (0.5 MPa) for different temperatures

The simple evolutions of the material parameters (E_{eff}, n_c, n_0) with respect to the temperature is assumed and the parameters of the models are estimated from an optimisation process (Tab. 4.1).

E_{eff} (MPa)	-12T+1420
ν_{eff}	0.32
A_{visc}	$5.402x10^{-6}T^4$-$1.106x10^{-3}T^3$+$8.188x10^{-2}T^2$-2.518T+30.268
n_c	$2.11x10^{-5}T^3$-$2.77x10^{-3}T^2$+$1.129x10^{-1}$T+2.184
n_0	$2.892x10^{-2}$T+2.953
n_b	5

Tab. 4.1. Parameters of the model

An example of results using the above parameters is shown in (Fig. 4.16). The model gives quite good results for temperatures between 25 and 80°C. A more complex evolution of the parameters with respect to temperature would improve the quality of the response for a larger range of temperatures.

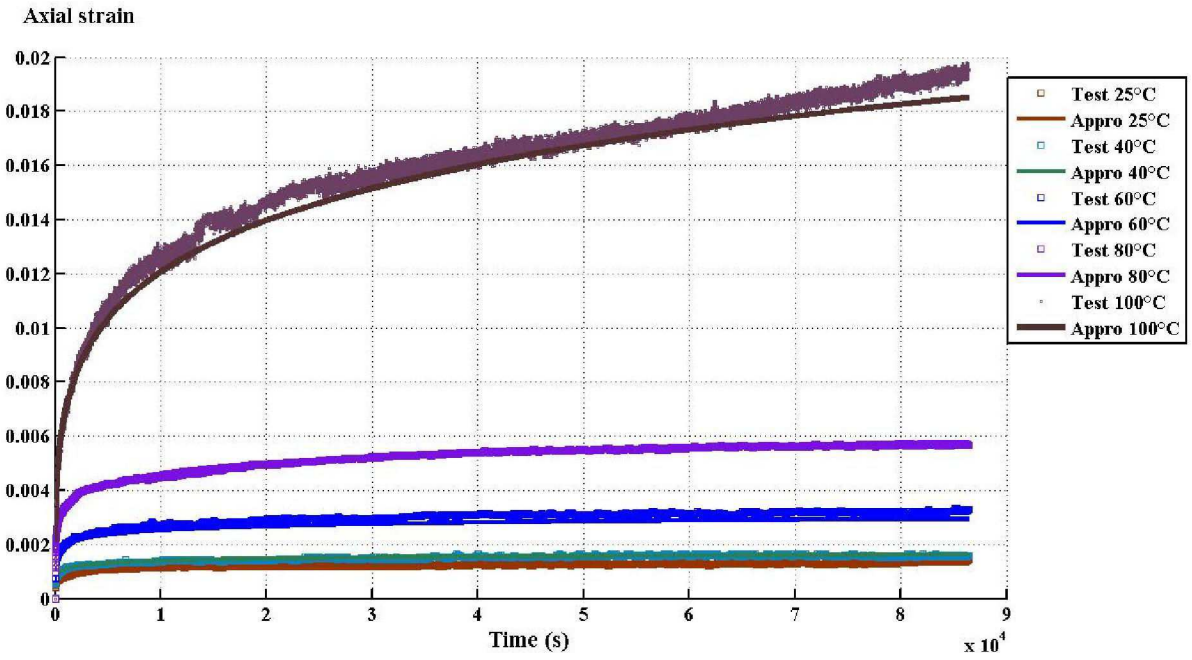

Fig 4.16. Comparison between the experimental and numerical responses for a large temperature range

- Consolidation effect

Considering the consolidation effect under hydrostatic pressure of GSPP (Chapter 3), its viscoelastic model is improved by adding the limit strain of phase 1 and the change of bulk modulus as the functions of temperature and the volumetric strain (Tab. 4.2).

Temperature (°C)	22.6	39.6	59.3	80.2
Limit pressure of phase 1 (MPa)	24.4	17.1	9.9	5.7
Limit strain of phase 1	0.026	0.021	0.017	0.013
Bulk modulus of phase 1 (MPa)	913.3	750.9	574.0	382.3
Bulk modulus of phase 2 (MPa)	4577.6	6350.0	7558.4	8334.7
Pressure at densification plateau (MPa)	48.6	44.2	38.7	37.7

Tab. 4.2. Different parameters of thermo mechanical behaviour under monotonic hydrostatic pressure

The limit strain of phase 1 (called ε_{change}) has a linear relation with temperature:

$$\begin{cases} \varepsilon_{change} = -2.1522.10^{-4}.T + 0.0302 \\ \varepsilon_{change} > 0 \end{cases}$$

Concerning the change of bulk modulus, based on the relation between bulk modulus, Young's modulus and Poisson's ratio of isotropic material, two changes are proposed.

The first one is the relation between the Young's modulus and the total volumetric strain, i.e. we considered that the viscous volumetric strain can lead to an increase of Young's modulus. From the fundamental mechanical equations, we have:

$$\underline{\underline{\sigma}} = K_{eff}.\left(\text{trace}\,\underline{\underline{\varepsilon^e}}\right)\underline{\underline{\delta}} + 2G_{eff}.\underline{\underline{\varepsilon^{eD}}}$$

$$\underline{\underline{\sigma}} = \frac{E_{eff}}{3\left(1-2v_{eff}\right)}.\left(\text{trace}\,\underline{\underline{\varepsilon^e}}\right)\underline{\underline{\delta}} + \frac{E_{eff}}{1+v_{eff}}.\underline{\underline{\varepsilon^{eD}}} \qquad \text{(Eq. 4.12)}$$

Where, $\underline{\underline{\varepsilon^{eD}}}$ is the deviator term of elastic strain tensor:

$$\underline{\underline{\varepsilon^{eD}}} = \underline{\underline{\varepsilon^e}} - \frac{1}{3}\left(\text{trace}\,\underline{\underline{\varepsilon^e}}\right)\underline{\underline{\delta}}$$

The new formula of Young's modulus replaces the last formula in the table 8:

$$E_{eff} = E_{eff}^0 + rm_1\left(\left|\left\langle \varepsilon_v \right\rangle_- \right| - \varepsilon_{change}\right).E_{eff}^0.rampE \qquad \text{(Eq. 4.13)}$$

Where

E_{eff}^0 is no more than the Young's modulus in table 8 which is calculated but does not take into account the volumetric strain's evolution. $E_{eff}^0 = -0.012T + 1.420\ \left(GPa\right)$

$\left\langle \varepsilon_v \right\rangle_-$ is a negative term of volumetric strain:

$$\langle \varepsilon_v \rangle_- = \langle \varepsilon_x^t + \varepsilon_y^t + \varepsilon_z^t \rangle_- = \begin{cases} \varepsilon_x^t + \varepsilon_y^t + \varepsilon_z^t \ \ if \ \ \varepsilon_x^t + \varepsilon_y^t + \varepsilon_z^t \le 0 \\ 0 \ \ if \ \ \varepsilon_x^t + \varepsilon_y^t + \varepsilon_z^t > 0 \end{cases}$$

$rm_1(x)$ is the function in COMSOL Multiphysics® used to avoid the singularity points [COMSOL]. It is equal to 0 when $x \le 0$ and have a linear relation with x when $x > 0$. In our case, if $x > 0$ then $rm_1 = 0.1x$.

$rampE$ is a dimensionless variable which represents the sensitivity of Young's modulus to temperature and the volumetric deformation. This variable is used to model the evolution of bulk modulus of phase 2 on temperature (Tab. 4.2). Its value is low at the low temperature and is supposed to reach to the maximal value at 80°C. Physically, this parameter is related to the rigidity of microspheres before collapse. The maximum values of $rampE$ correspond to the maximum rigidity of phase 2 (associated with the microspheres behaviour)

With regards to the second change of our model, the relation between the parameter B and the temperature is proposed to take into account the specific behaviour of GSPP when it is subjected to hydrostatic pressure (Chapter 3). It means that the Poisson's coefficient is not constant (in this case, it increases from 0.32 to over 0.4).

The same optimisation process with the Fminsearch function (Matlab®) is used. The test values come from the monotonic hydrostatic pressure at different temperatures of GSPP. Two variables needing to be determined are the variable B and the variable $rampE$. From the optimisation result, a simple relation between the parameters and the temperature are obtained:

$$B = 0.0028T^2 - 0.1861T + 7.3132 \qquad \text{(Eq. 4.14)}$$

The parameter C is calculated using an isotropy assumption for the material.

$$C = \frac{A.(1 + vB/A)}{1 + v}$$

The relation between $rampE$ and the temperature is presented in the figure (Fig. 4.17).

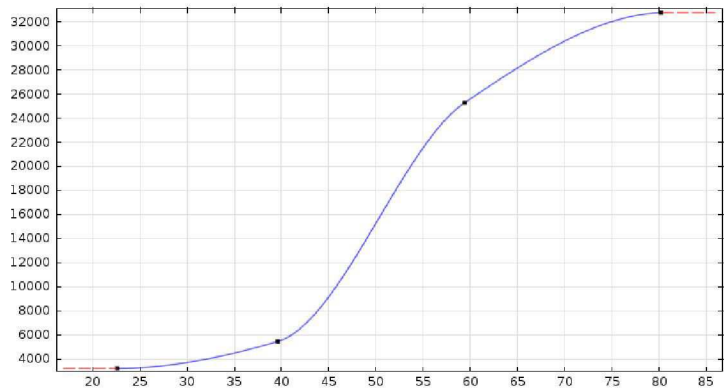

Fig 4.17. Relation between $rampE$ and the temperature

We have also plotted the evolution of Young's modulus with volumetric strain under hydrostatic pressure at different temperatures (Fig. 4.18). In the phase 1 (corresponding to the void compression, zone 1 on the Fig. 4.18), the volumetric strain is low, the Young's modulus decreases with temperature. In the phase 2 (corresponding to the microspheres compression, zone 3 on the Fig. 4.18), the Young's modulus increases with temperature. The limit strain of phase 1 (zone 2) decreases in a linear way with temperature.

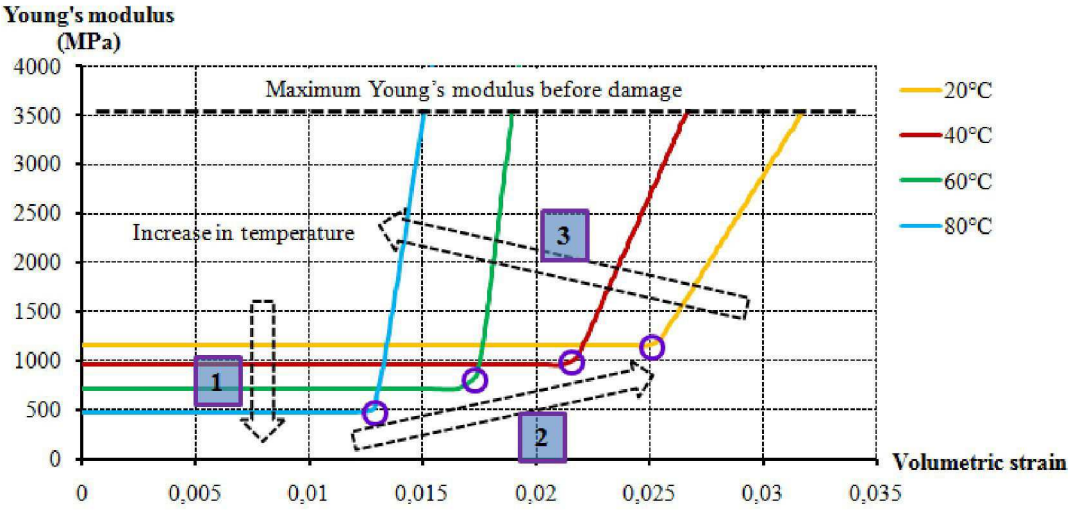

Fig. 4.18. Young's modulus evolution versus volumetric strain at different temperatures under hydrostatic pressure

The final result of this optimisation process is presented in the figure (Fig.4.19). We have a good correlation between the experimental data and the approximated data before the microspheres collapse.

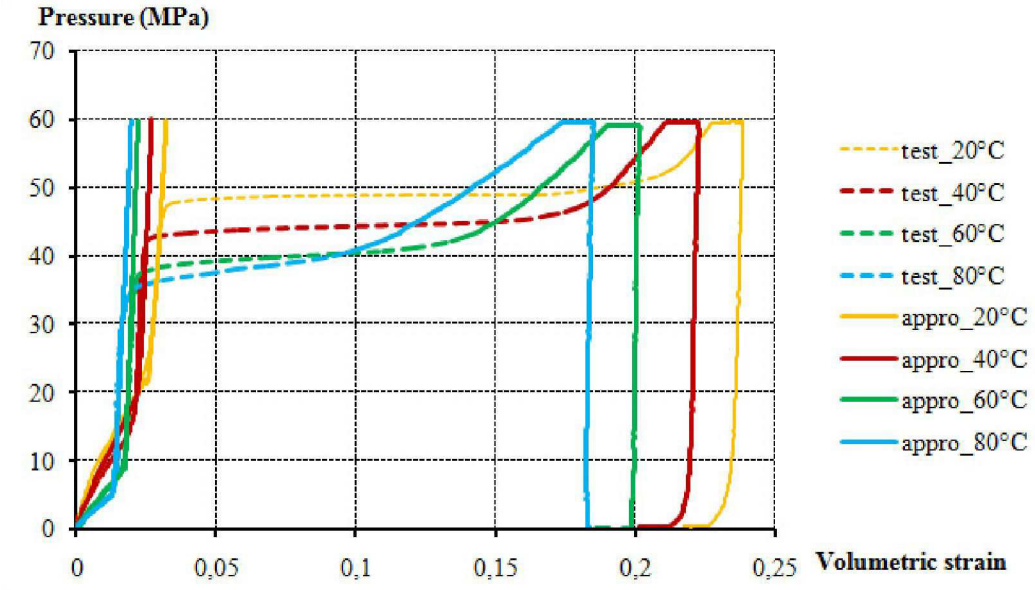

Fig. 4.19. Validation of monotonic hydrostatic pressure

In the next stage the model is further improved in order to simulate the behaviour of the material under cyclic hydrostatic pressure, an irreversible volumetric deformation p_{cul} is introduced.

The deformation associated with the initial porosity of the material depends on the temperature and remains low (at 60 ° C the maximum value is around 1%). The equation to describe the behaviour is such that:

$$\frac{\partial p_{cul}}{\partial t} + \frac{1}{9K}\left(\frac{\partial p}{\partial t}\right).H\left(-\frac{\partial p}{\partial t}\right) = 0 \qquad \text{(Eq. 4.15)}$$

$H(x)$ is the Heaviside function:

$$H(x) = 1\begin{cases} 0 & si\ x < 0 \\ 0 & si\ x \geq 0 \end{cases} \qquad \forall x \in R$$

and $p = -\frac{1}{3}(\sigma_x + \sigma_y + \sigma_z)$, hydrostatic pressure term.

The implementation of this variable means the irreversible volumetric deformation is simply the elastic volumetric deformation during loading (the material in hydrostatic compression, $\frac{\partial p}{\partial t} \geq 0$). In the case of unloading ($\frac{\partial p}{\partial t} < 0$), its value stays constant. The simple expression allows us to keep the elastic part of the volumetric strain during the unloading which is considered as a permanent deformation (chapter 3).

The total volumetric strain rate:

$$\dot{\varepsilon}_{volumique} = \dot{\varepsilon}_{tt} = \left(\dot{\varepsilon}_{tt} + \dot{\varepsilon}_{tt}^{e} + \dot{p}_{cul}\right) \qquad \text{(Eq.4.16)}$$

A differential equation is added to the model according to the calculation scheme (Fig. 4.20) which introduces consolidation and permanent deformation volume.

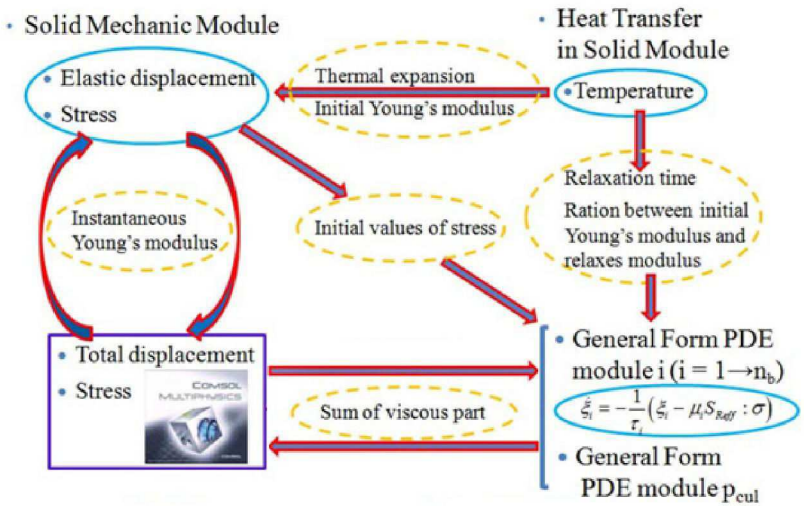

Fig. 4.20. Improving of the model

The result presented in (Fig. 4.21) reflects in a satisfactory manner the behaviour of the material before rupture of the microspheres.

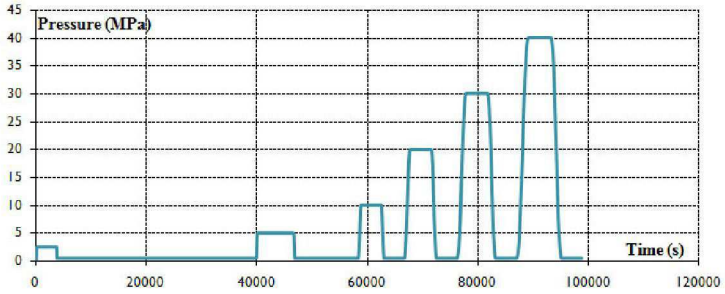

4.21.a. Loading profile

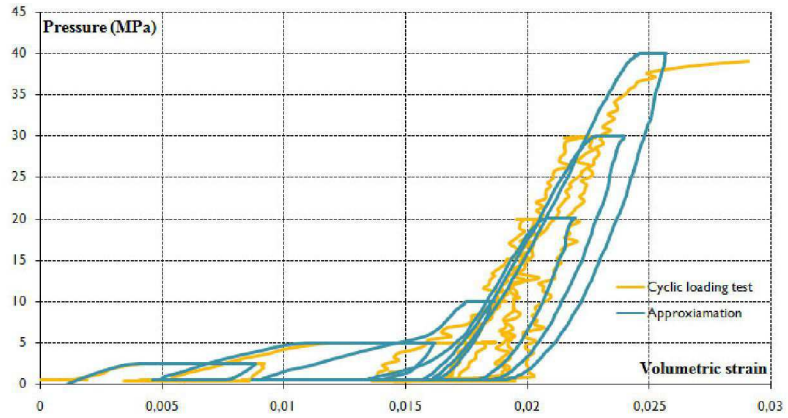

4.21.b. Hydrostatic pressure - volumetric strain diagram

Fig. 4.21. Validation of cyclic hydrostatic pressure at 60°C

However it can be noted that the viscous effect decreases at high loading level before collapse of microspheres. Therefore, the bulk modulus and the viscous effects depend on the porosity and will need additional improvement of the model. This phenomenon can be taken into account using a relationship between the constant A of the model and the porosity of material.

4.3 Viscoelastic model for solid polymer

4.3.1 Rheology model

To analyse the thermal mechanical behaviour of field joint material (Polypropylene), it is preferred to use the linear viscoelastic material. It is usually assumed that the viscous part of the deformation is incompressible, i.e. the volume change is purely elastic. In this case, a generalized Maxwell model is already proposed in COMSOL Multiphysics® (Fig.4.22) for the deviatoric stress components $\underline{\underline{\sigma}}^D$.

$$\underline{\underline{\sigma}} = -p\underline{\underline{\delta}} + \underline{\underline{\sigma}}^D$$

$p = -K\left[\text{trace}\,\underline{\underline{\varepsilon}} - 3\alpha\left(T - T_{ref}\right)\right]$, relation of the spherical components

The stress deviator is expressed by a hereditary integral of strain history:

$$\underline{\underline{\sigma}}^{D} = \int_0^t G(t-t')\frac{\partial \underline{\underline{\varepsilon}}^{D}}{\partial t'}dt'$$

Where,

$\underline{\underline{\varepsilon}}^{D} = \underline{\underline{\varepsilon}} - \frac{1}{3}\text{trace}\left(\underline{\underline{\varepsilon}}\right)\underline{\underline{\delta}}$, the deviator of strains tensor

$G(t)$, the relaxation shear modulus function:

The relaxation modulus function is often approximated by a Prony series [Chen, 2000]:

$$G(t) = G_0\left(\mu_0 + \sum_{m=1}^{M}\mu_m^{\frac{-t}{\lambda_m}}\right) \text{ with } \sum_{m=1}^{M}\mu_m = 1$$

Where:

μ_m is the m'th Prony constant (m =1, 2,...). Its physical signification is interpreted as the relative stiffness of the spring in the branch m of the model

λ_m is the time constant of the spring-dashpot pair in the same branch.

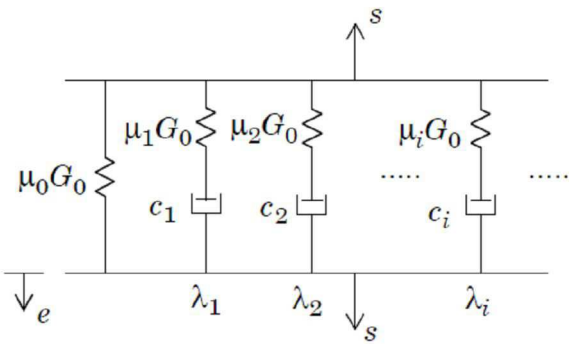

Fig. 4.22. Generalized Maxwell model

Mathematically, the viscous branch could be presented by the M differential equations with the variable $\underline{\underline{q_m}}$:

$$\dot{\underline{\underline{q_m}}} + \frac{1}{\lambda_m}\underline{\underline{q_m}} = \dot{\underline{\underline{\varepsilon}}}^{D}$$

$$\underline{\underline{\sigma}}^{D} = G_0\left(\mu_0\underline{\underline{\varepsilon}}^{D} + \sum_{m=1}^{M}\mu_m\underline{\underline{q_m}}\right)$$

The Prony series coefficient and relaxation times must be determined, a standard nonlinear method (the Marquardt-Levenberg Method) was proposed [Chen, 2000; Deheeger et al, 2011] with an error function χ^2:

$$\chi^2(\mathrm{a}) = \sum_{i=1}^{N}\left[\frac{y_i - y(x_i;\mathrm{a})}{\sigma_i}\right]^2$$

Where,

x_i and y_i are the experimental data,

$y(x_i;\mathrm{a})$ is the approximated function to be determined

σ_i is the standard deviation of measurement error of the i-th data point

4.3.2 Model implementation in a finite element analysis

To simplify the modelling, the same inverse identification method for GSPP has been used. The creep tensile tests at different temperatures (from 25°C to 120°C) were carried out to identify the parameters of this model (Fig.4.23).

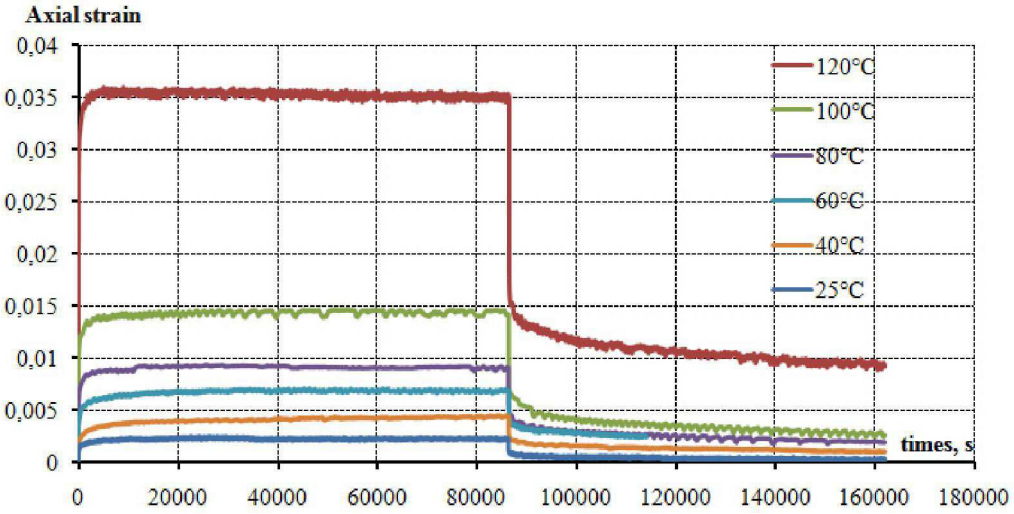

Fig. 4.23. Creep tensile test of solid PP in DMA under low load (1 MPa) for different temperatures

The relation between Young's modulus and the temperature proposed (Eq.4.17) and the use of only two viscous branches (Eq.4.18) gave a reasonable of modelling result when comparing to the test values (Fig.4.24).

$$E = -0.0018T^3 + 0.363T^2 - 39.921T + 1645.824 \qquad \text{(Eq.4.17)}$$

$$\mu_1 = 0.388 - 0.002T;$$
$$\lambda_1 = 6917 - 52.209T \ (s)$$
$$\mu_2 = 0.393 - 0.002T; \qquad \text{(Eq.4.18)}$$
$$\lambda_2 = 124 - 0.374T \ (s)$$
$$\mu_0 = 1 - \mu_1 - \mu_2$$

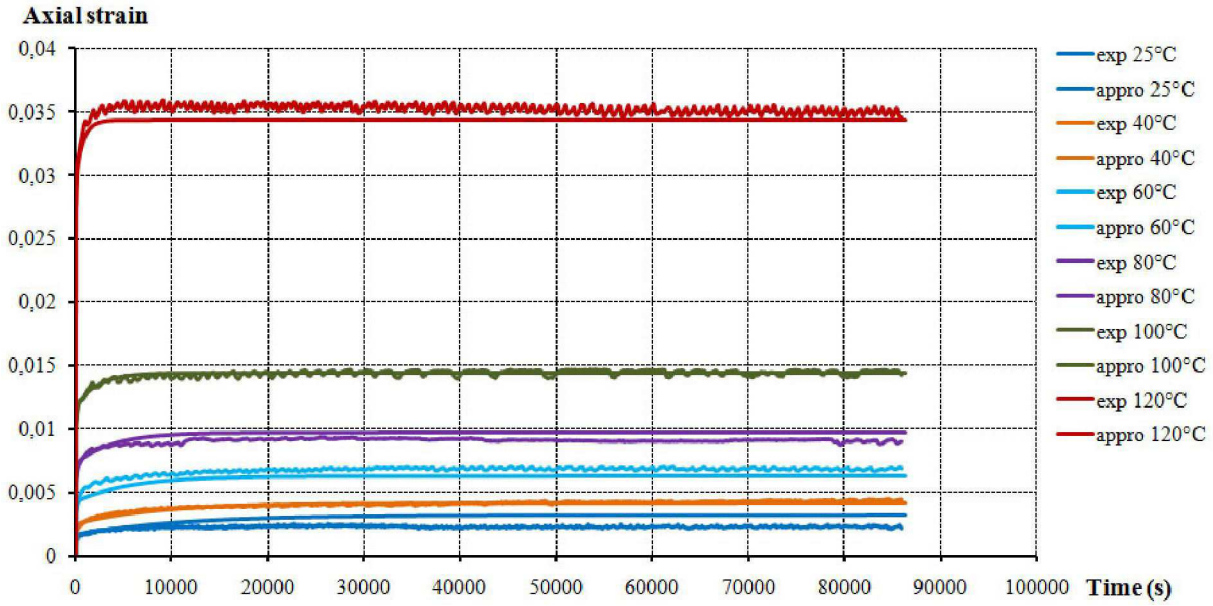

Fig 4.24. Comparison between the experimental and numerical responses of solid PP for a large range of temperatures

One of the main objectives is to estimate the stress evolution during the injection moulding of polypropylene. So, changing of Poisson's ratio must be considered. We propose the constant values of 0.38 and 0.45 for the solid phase and liquid phase respectively. During the phase transition, the COMSOL Multiphysic' built-in smoothed Heaviside step function flc2hs [COMSOL] is used to estimate the intermediate value of Poisson's ratio and to avoid the singularity points.

Chapter 5. Thermo viscoelastic analysis of a field joint under service conditions

Up until now, we have analysed the temperature evolution of the main thermo mechanical parameters of a GSPP and of a solid PP (heat capacity, thermal conductivity, coefficient of thermal expansion, Young's modulus, Poisson's ratio, and viscous parameters). In order to allow an optimisation of the industrial pipelines, a complete modelling of Five Layer Syntactic Polypropylene system using the injection moulded Polypropylene is presented. This modelling follows the simplified process of an industrial Field Joint coating and uses the J-lay installation type method for deep water applications. The model takes into account the influence of the manufacturing process and the influence of the service conditions (difference of external temperature and pressure). For each stage of the modelling, the evolutions of the thermomechanical state are analysed. The von Mises stress - hydrostatic pressure envelopes allow us to analyse the stress state. The stress at the interface GSPP - Field Joint coating material and also steel-Field Joint coating material which are known as the weakness parts of pipelines are presented. The proposed numerical tool allows an optimisation of the geometrical parameters of the Field Joint to be developed in order to reduce the stress state in the critical zones. Moreover a complementary experimental analysis has to be proposed in order to identify the behaviour and the strength of the interfaces.

5.1 Data for modelling

The complete modelling needs to use the representative thermo mechanical models of all the material layer of the pipeline. Concerning the solid PP, we assume that the solid PP layers in the main coating material have the same behaviour compared to the solid PP used to mould the Field Joint. About the GSPP, there is no damaged effect of microspheres. We only take into account the consolidation of the material under the hydrostatic pressure. The behaviour of steel is supposed to be temperature independent.

The simplified process of Field Joint coating Polypropylene used in this study, (Fig. 5.1), is such that:

- The surface of the steel and of the chamfer of the parent coating are heated by the heat flux in 2 minutes. The temperatures reached at the surfaces are about 150°C (Fig. 5.1.a).
- The injection of the Polypropylene is assumed to be instantaneous. The initial temperature of PP is 200°C.
- Cooling of Field Joint with external forced convection in the steel mould (Fig. 5.1.b).
- Cooling of Field Joint with natural convection in air without the steel mould (Fig. 5.1.c).
- Laying down of pipeline with the constant speed of 1m/min.
- Cooling in deep water and stabilization period before entering service conditions (the stabilization period is limited to 5 days; after such a period the mechanical state is nearly stable, in our case).
- In service condition of pipeline with inner temperature of 100°C (Fig. 5.1.d).

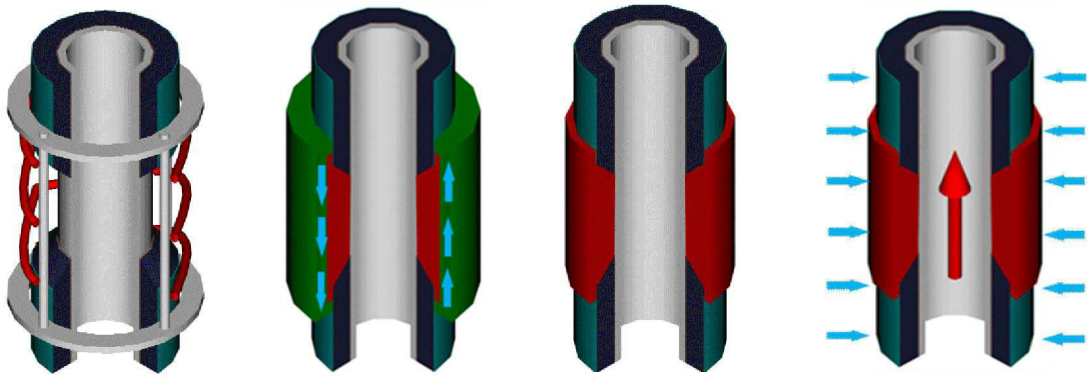

5.1.a 5.1.b 5.1.c 5.1.d

Fig. 5.1. Simplified process of the manufacturing Field Joint, of the installation and of the using condition

- Geometrical and thermo-mechanical data

The geometry used is presented in the figure 5.2. This industrial insulation system has the same dimensions as a real 5-layer insulation pipeline [Bouchnneau, 2010]. Because the geometry and the thermo-mechanical loads are assumed to be symmetric around the vertical axis and the pipeline is symmetric around the middle of Field Joint, a 2D axisymmetric model is used to model a half of the pipeline. In order to analyse correctly the various possible stress concentrations refined meshes are necessary in some zones. Details are provided in (Fig 5.2.b)

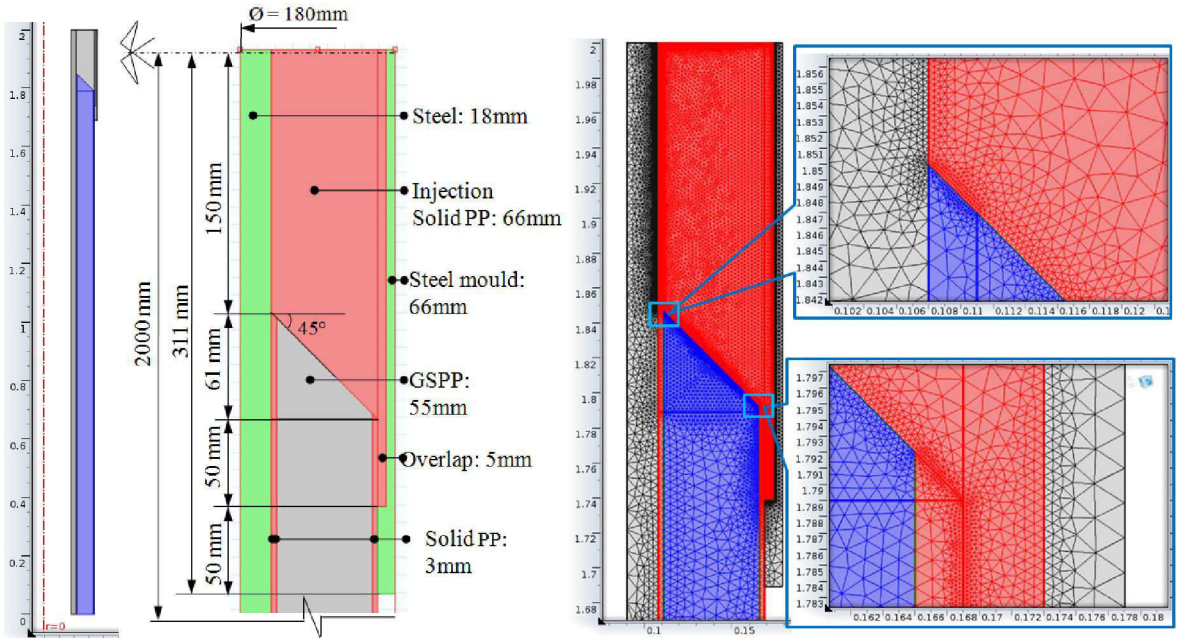

Fig. 5.2.a Fig. 5.2.b

Fig. 5.2. Geometry and mesh of pipeline

For the first step, two heat fluxes are applied on the Field Joint's area; the natural convection in air (with constant heat transfer coefficient) is used for other boundaries of inner and outer pipeline (Fig. 5.3.a). We assume that the length of pipeline is important. So the symmetry conditions can be used at the top and the bottom boundaries. The second and third steps are calculated using the previous stress and strain results with the corresponding boundary conditions (Fig. 5.3.b-c). During the laying down operation (step 4), the bottom pipeline is supposed to be open. So, the pressure and the temperature inside and outside the pipeline are the same (Fig. 5.3.d). The pipeline is laid down with the constant speed of 1m/min. Concerning the thermal effect, the temperature T(t) is assumed to be linear with the depth H (in meter), i.e. to be linear with time (in seconds). Starting from the ambiant temperature (20°C), its value is lowest (4°C) when the pipeline reaches the 3000m depth. The pressure P(t) has a relation with the depth by the following experimental formula:

$H = 1.t\ \ (m);\ \ t\ \ in\ \ \text{minute}$

$P(t) = P(H) = 0.01H + 0.05\times10^{-6}H^2\ (MPa)$ [Bouchonneau, 2007]

$P(H)$, the pressure (MPa)

H, immersion depth (m)

Step 5 represents the cooling in water and period before putting into service. In the service's step (step 6), the temperature associated with the hot oil reaches 100°C. All the thermal mechanical boundaries conditions are summarized in the Tab. 5.1.

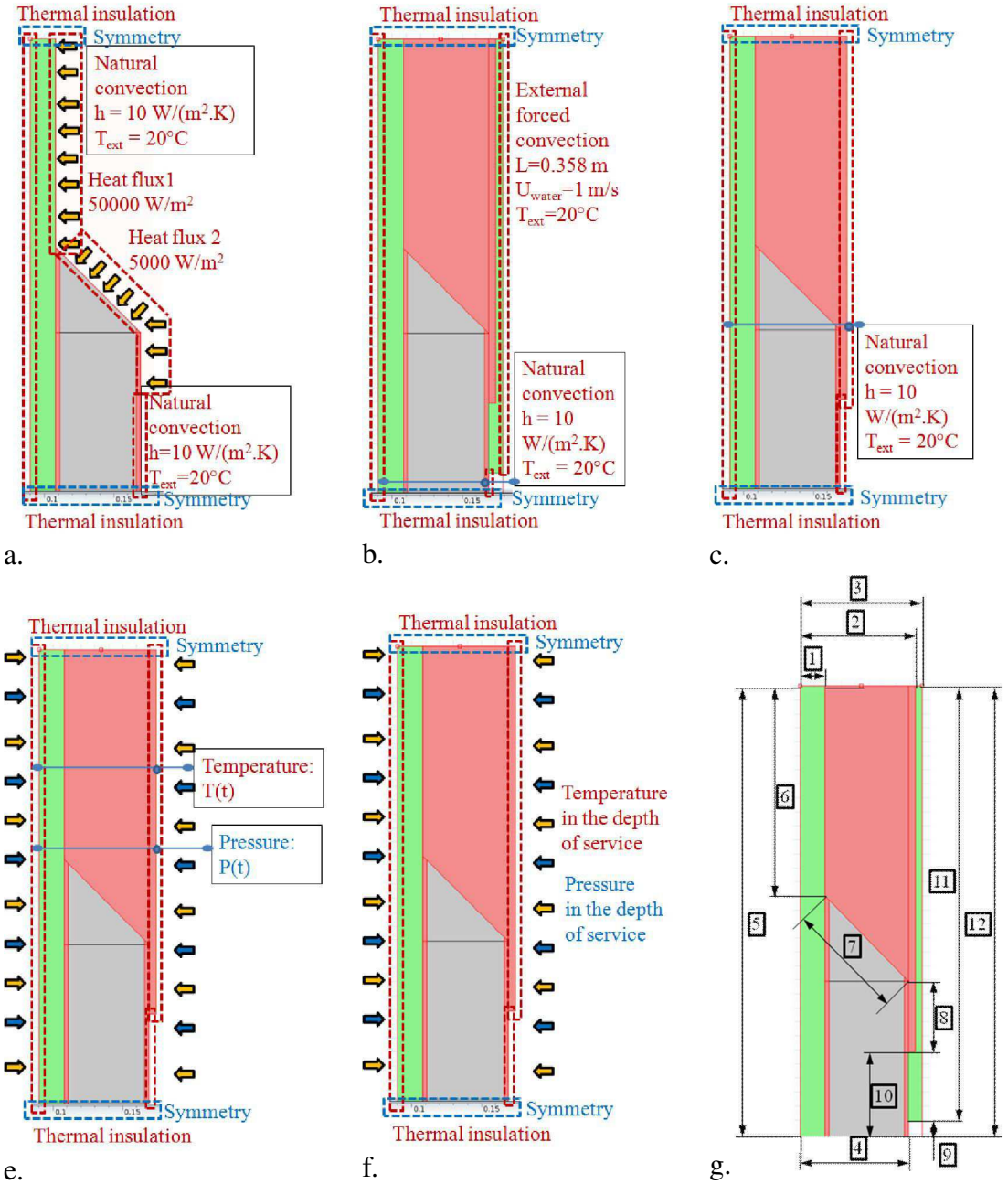

Fig. 5.3. Thermal mechanical boundary conditions during different phases of modelling

N0	Step 1	Step 2	Step 3	Step 4	Step 5	Step 6
1	- Thermal insulation Symmetry	- N/A	- N/A	- N/A	- N/A	- N/A
2	- No application	- N/A	- Thermal insulation Symmetry	- Thermal insulation Symmetry	- Thermal insulation Symmetry	- Thermal insulation Symmetry
3	- No application	- Thermal insulation - Symmetry	- N/A	- N/A	- N/A	- N/A
4	- Thermal insulation - Symmetry	- Thermal insulation - Symmetry	- Thermal insulation - Symmetry	- Thermal insulation - Symmetry	- Thermal insulation - Symmetry	- Thermal insulation - Symmetry
5	- Natural convection h = 10W/(m^2.K), 20°C - Free stress	- Natural convection h = 10W/(m^2.K) , 20°C - Free stress	- Natural convection h = 10W/(m^2.K) , 20°C - Free stress	-Temperature T(t) - Pressure P(t)	- Constant temperature - Constant pressure	-Temperature in service - Constant pressure
6	- Heat flux 50000 W/m^2	- N/A	- N/A	- N/A	- N/A	- N/A
7	- Heat flux 5000 W/m^2	- N/A	- N/A	- N/A	- N/A	- N/A
8	- Heat flux 5000 W/m^2	- N/A	- N/A	- N/A	- N/A	- N/A
9	- N/A	- Natural convection h = 10W/(m^2.K), 20°C - Free stress	- N/A	- N/A	- N/A	- N/A
10	- Natural convection h = 10W/(m^2.K), 20°C - Free stress	- N/A	- N/A	- N/A	- N/A	- N/A
11	- N/A	- External force convection - Free stress	- N/A	- N/A	- N/A	- N/A
12	- N/A	- N/A	- Natural convection h = 10W/(m^2.K), 20°C - Free stress	-Temperature T(t) - Pressure P(t)	- Constant temperature Constant pressure	-Temperature in service - Constant pressure

Tab. 5.1. Thermal mechanical boundary conditions

- Thermo-mechanical parameter evolution

The main thermo mechanical parameters used in the model come from the previous chapters 2 and 4. We gather them together in the following table.

GSPP	E_{eff} (MPa)	-12T+1420
	ν_{eff}	0.32 in solid state and 0.46 in liquid state
	A	$5.402\times10^{-6}T^4-1.106\times10^{-3}T^3+8.188\times10^{-2}T^2-2.518T+30.268$
	B	$0.0028T^2-0.1861T+7.3132$
	C	$\frac{A.(1+vB/A)}{1+v}$
	n_c	$2.11\times10^{-5}T^3-2.77\times10^{-3}T^2+1.129\times10^{-1}T+2.184$
	n_0	$2.892\times10^{-2}T+2.953$
	n_b	5
	ε_{change}	$-2.1522.10^{-4}.T+0.0302$
	$C_p^{gspp}(\mathrm{J/(kg.K)})$	$6.26T+1506.6$
	$\lambda^{gspp}(W/(m.\mathrm{K}))$	$10^{-4}T+0.165$
	$\rho^{gspp}(kg/m^3)$	640
Solid PP	$E(MPa)$	$-0.0018T^3+0.363T^2-39.921T+1645.824$
	ν	0.38 in solid state and 0.46 in liquid state
	μ_1	$0.388-0.002T$
	μ_2	$0.393-0.002T$
	μ_0	$1-\mu_1-\mu_2$
	$\lambda_1(s)$	$6917-52.209T$
	$\lambda_2(s)$	$124-0.374T$
	λ_{liquid}^{pp}	$-6.25\times10^{-5}T+0.189$
	λ_{solid}^{pp}	$-4.96\times10^{-4}T+0.31$
	λ^{pp}	$\lambda_{solid}^{pp}+(\lambda_{liquid}^{pp}-\lambda_{solid}^{pp})\,\mathrm{flc2hs}[(T-T_m),\Delta T]$
	$C_{pliquid}^{pp}$	$3.10T+2124$
	C_{psolid}^{pp}	$10.68T+1451$
	C_p^{pp}	$C_{psolid}^{pp}+(C_{pliquid}^{pp}-C_{psolid}^{pp})\,\mathrm{flc2hs}[(T-T_m),\Delta T]+\delta\Delta H$
	$T_m(°C)$	140
	$\Delta T(°K)$	15
	$\Delta H(kJ/kg)$	50
	$\rho^{solidpp}(kg/m^3)$	900

Tab. 5.2. Thermo mechanical parameters (T in °C)

The coefficients of thermal expansion have to be defined. For solid PP, we assume that its values in liquid phase and in solid phase do not change (simplified analysis). During the changing phase, the value can be estimated thanks to a smoothed Heaviside function (flc2hs function in Comsol)

(chapter 2). In the case of the GSPP, a linear relation between the coefficient of thermal expansion and the temperature is used [Bouchoneau, 2007] (Fig. 5.4).

$$\alpha^{pp} = 8.2\times10^{-5} + (2.16\times e^{-4}[1/K] - 8.2\times10^{-5})\, flc2hs((T - T_m), \Delta T)$$

$$\alpha^{gspp} = -3\times10^{-7} T + 7\times10^{-5}$$

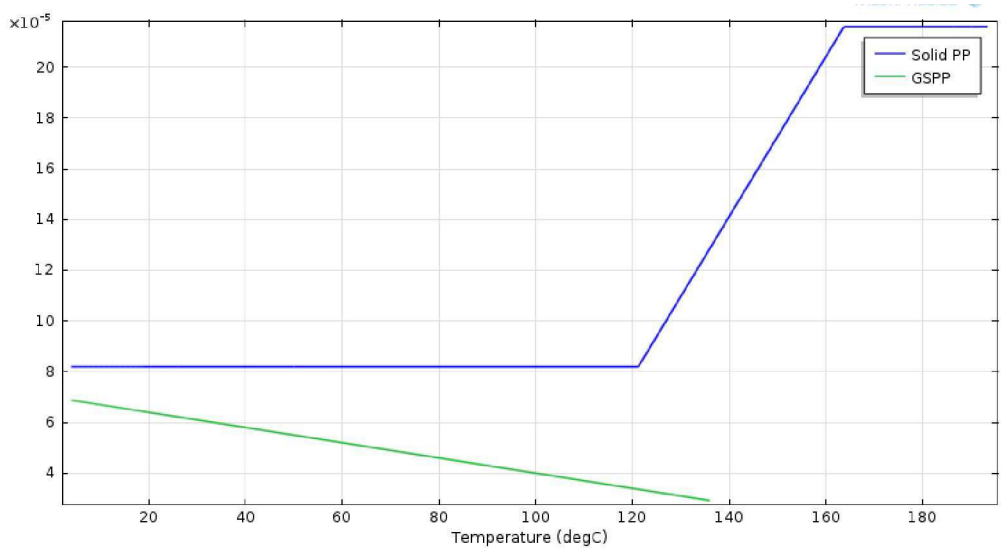

Fig. 5.4. Evolution of coefficient of thermal expansion with temperature

5.2 Thermo mechanical parameter evolution during the moulding

In the phase of the Field Joint moulding, the temperature plays an important role. Temperature, stress and strain in the different materials change significantly during this phase. In this model the material density evolution is not considered. In order to take into account the change of density during the phases, the strong coupling model would be needed. This would significantly increase the calculation time and increase also the risk of non convergence. It should be noted that the thermo mechanical properties (thermal conductivity, heat capacity, melting point, latent heat released, viscosity, Young's modulus and Poisson's ration) depend on the degree of crystallinity [Le Goff et al, 2005, 2011; Tardif et al, 2012; Bendada et al, 2004]. Assuming that the cooling rate is sufficiently slow, i.e. the degree of crystallinity reaches always 100%, the thermo mechanical parameters are also considered to only be functions of temperature. Concerning the liquid state of the material, Young's modulus is considered to be very small (10 MPa) and Poisson's ration is near to 0.5. There is no movement of material due to the temperature gradient, i.e., the material behaviour in liquid phase is considered as an incompressible solid material with low rigidity and low viscosity. The interface between injection material and GSPP is assumed to be perfect (continuity of displacement and normal component of stress). During the cooling phase the cooling rate of the material is mainly associated with an external forced convection. This forced convection is created by a fresh water flow inside the double layer steel mould which is replaced herein by a

simplified geometry. In the thermal part of the model, the forced convection applies directly to the steel layer of the mould but in the mechanical part, the steel layer is not modelled. The natural convection with the constant heat transfer coefficient is an optimal condition because in reality, the coefficient depends on the geometry and on the temperature of the material. However, the simplified conditions allow us to estimate quite good thermal mechanical effects.

5.2.1 Material properties and temperature evolution

After 600s of cooling with external forced convection and after 1200s with natural convection, from 600s to 1200s, the temperature distribution in the Field Joint is presented in figure 5.5.a. The first image allows us to demonstrate that the initial condition of cooling study of Field Joint (Fig 5.3.b) comes from the previous results. The index of liquid phase B (Fig 5.5.b) is equal to 1 if the material is liquid and is equal to zero if the material is totally solid. This simple parameter calculated directly from the temperature distribution represents an interesting index (Chapter 2). The reason is that the rigidity of the structure depends on the material thickness which has already solidified. From this data it is possible to estimate the deformations induced by manipulation (rolling of pipeline on the roller system of the stinger in S lay deployment, for example). So, the evolution of index of liquid phase could enable us to estimate when the Field Joint is ready to be layed down.

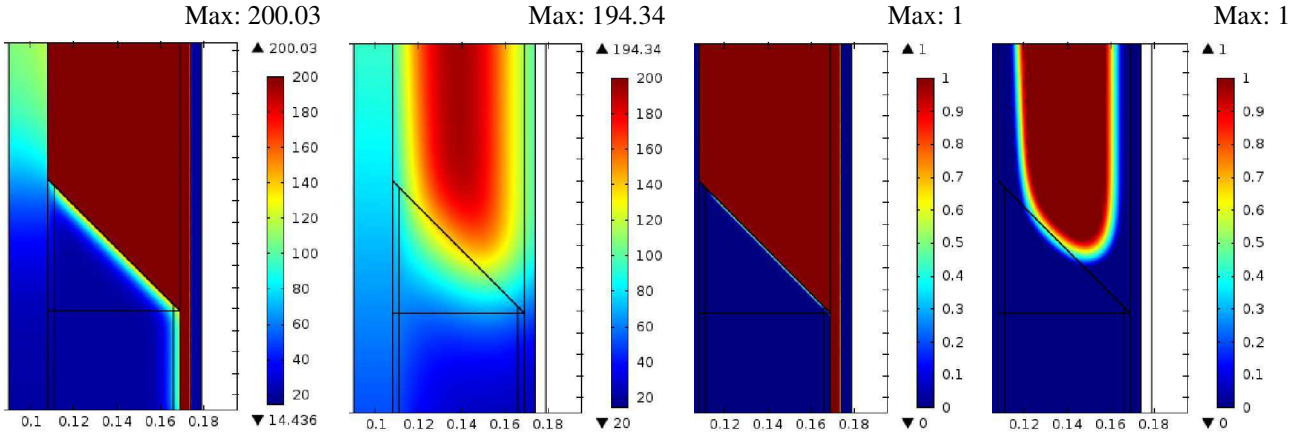

a. Temperature distribution (°C) (0, 1800s) b. Index of liquid phase (B) (0, 1800s)

Fig. 5.5. Temperature distribution (T°C) and index of liquid phase (B) during the moulding

With regard to the thermal parameters, in figure 5.6.a, the contribution of heat released during the phase change is illustrated in the heat capacity of material. The red zone corresponds to the liquid-solid zone transition. The evolution of thermal conductivity participates also in the cooling process (Fig 5.6.b).

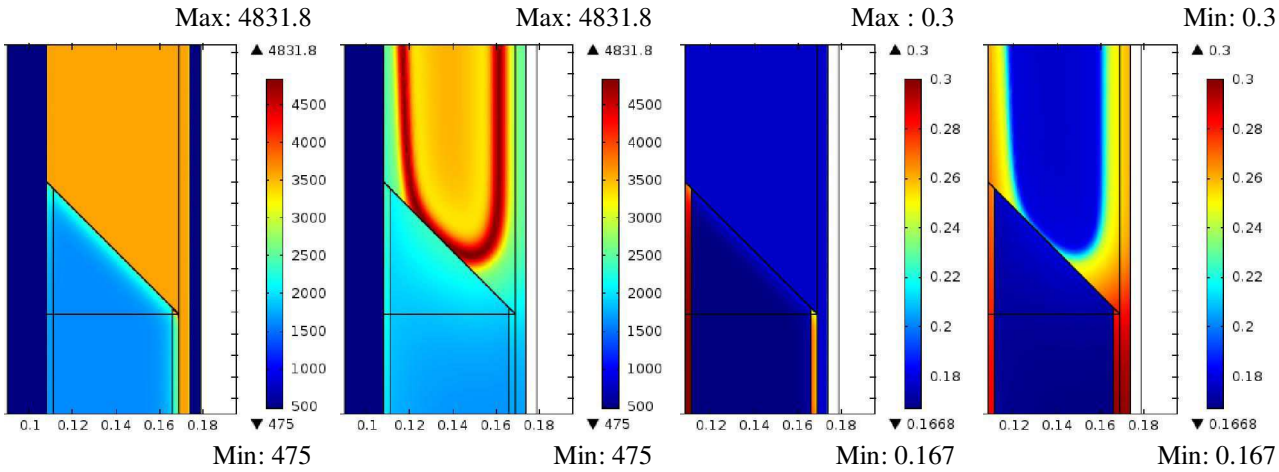

a. Heat capacity (J/kg.K) (0, 1800s) b. Thermal conductivity (W/(m.K) (0, 1800s)

Fig 5.6. Thermal parameter distribution during the moulding

Because of the singularity of modelling, we cannot put Young's modulus to a low value, Poisson's ratio to 0.5 but the values which are not far of the singularity ones to model the liquid material state could be used (Fig 5.7.a-b). However, because of the high coefficient of thermal expansion of polymer compared to the metal material (Fig 5.7.c), the low Young's modulus used (10 MPa) for the polypropylene and GSPP could cause certain unexpected stresses in the structure. The stress is hopefully small and decreases in time thanks to the viscous behaviour of the materials.

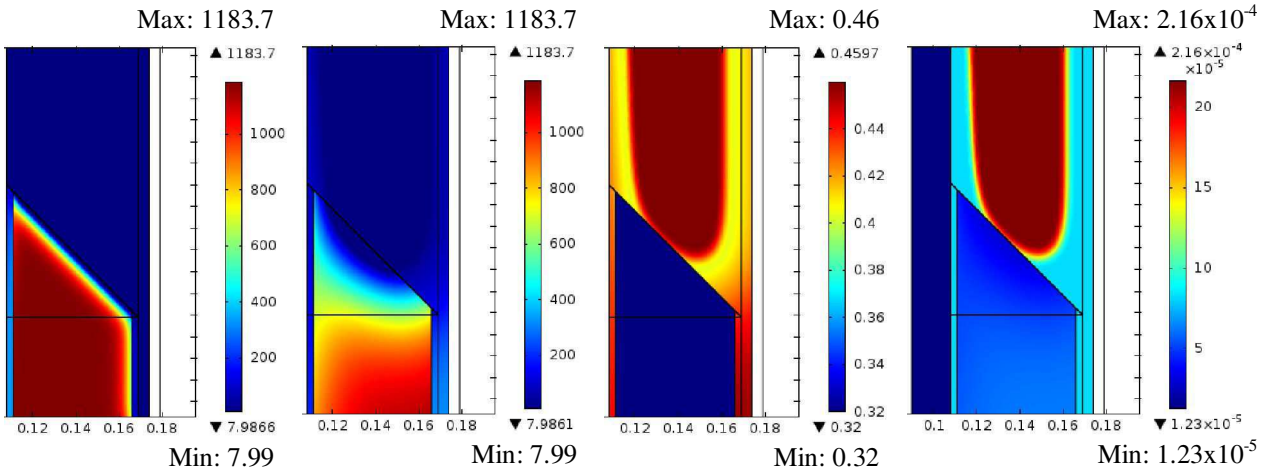

a. Young's modulus (MPa) (0,1800s) b. Poisson's ratio (1800s) c. Coefficient of thermal expansion (1/K) (1800s)

Fig 5.7. Mechanical parameter distribution during the moulding

5.2.2 Stress and strain during moulding process

One of the main disadvantages of the injection moulded polypropylene is the possible large shrinkage. Because of the high melting temperature and the coefficient of thermal expansion, the maximal displacement of Field Joint during the moulding process reaches about 1mm after 1800s of cooling (Fig. 5.8). This phenomenon which combines with the inhomogeneous cooling rate could lead to create defects in the material (Fig 5.9). Another phenomenon which is ignored in this model

is that there is not thermal resistance between some parts of the mould and the material in the case of large shrinkage. If it is taken into account, the cooling efficiency of forced convection will decrease with time.

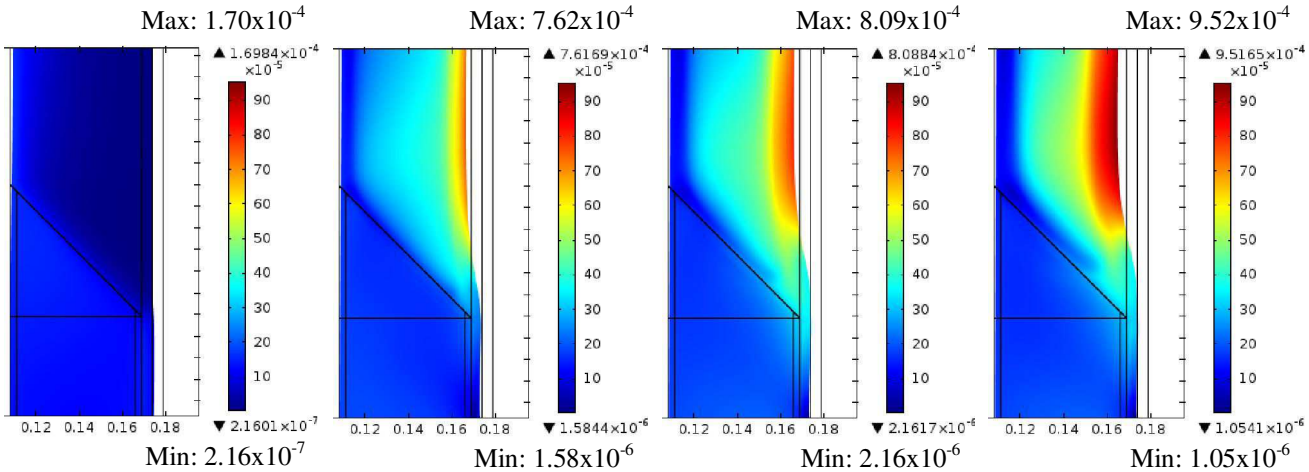

a. Initial condition b. After 600s cooling c. After 1200s cooling d. After 1800s cooling

Fig. 5.8. Total displacement (m) during the moulding (scale factor of 10)

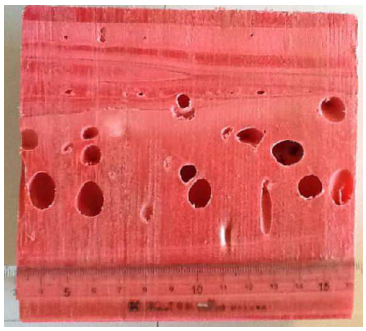

Fig. 5.9. Defects observed in the injected polypropylene

Regarding the stress distribution and its evolution in time (Fig. 5.10-13), there are low stresses at the initial state of the structure (about 2.5 MPa at the interface between the main coating material and the injection material) and this stress decreases. The external material layers support a quite large stress after 600s cooling. The maximal von Mises stress reaches about 15 MPa and the pressure component goes to -10 MPa (in tension). It should be noted that the pressure component p defined in COMSOL Multiphysics follows the equation (Eq. 5.1). The material is in compression if the pressure is positive and in tension if its value is negative. The stress distribution evolves in time because of two main coupling reasons. The first one is the shrinkage due to the thermal expansion. The second one is due to the viscous effects.

$$p = -\frac{\sigma_r + \sigma_\varphi + \sigma_z}{3} \qquad \text{(Eq. 5.1)}$$

To better understand the material loading in this phase, the figure 5.13 gives the stress state in the von Mises stress - hydrostatic pressure diagram for the injection PP and the GSPP with respect to

time. The diagram can be created by plotting the points in each material domain (Fig 5.12). The finer the grill of points, the more the results are precise. By increasing the number, the hot spot points will be strongly highlighted. A pattern of 25 (for radial points) by 500 (for z points) has been chosen to provide information on the stress gradient and its evolution during time. To distinguish the different material domains, the logic functions based on the geometry and the difference of density of materials are used. These functions give the value of 1 if they are true and the zero if they are false. Concerning the PP injection, the von Mises stress $\sigma_{solidPP}^{mises}$ and pressure $\sigma_{solidPP}^{pressure}$ are calculated in the area with green colour, and the von Mises stress σ_{GSPP}^{mises} and pressure $\sigma_{GSPP}^{pressure}$ come from the one with purple colour.

This information is useful to build the experimental tests which enable us to describe the real stress state in the structure. In the solid PP, the tensile stress plays an important role because of the shrinkage. However, there are the zones in GSPP where the material supports the compression stress (the hydrostatic pressure is positive).

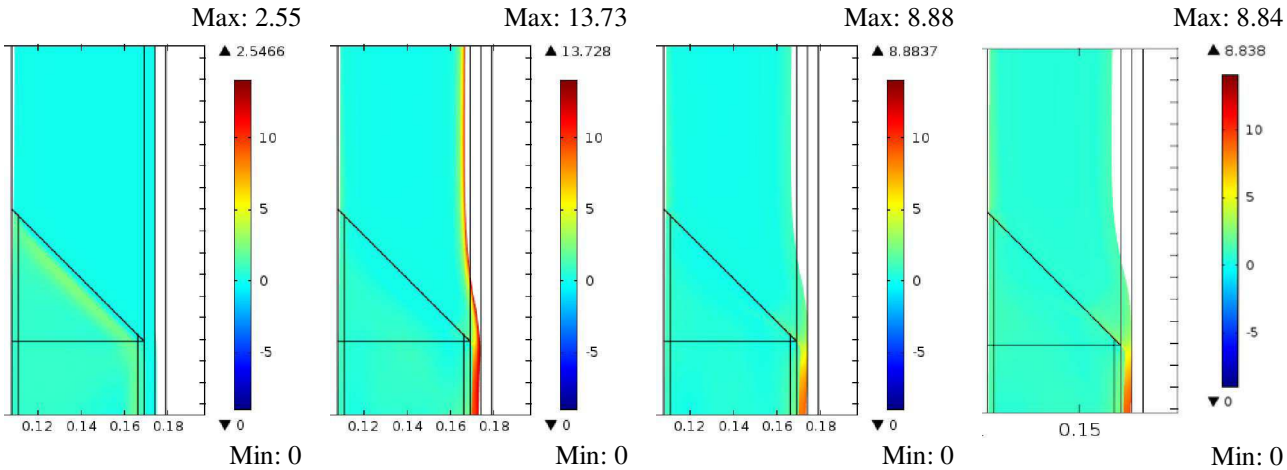

a. Initial condition b. After 600s cooling c. After 1200s cooling d. After 1800s cooling

Fig 5.10. Von Mises stress during the moulding (MPa)

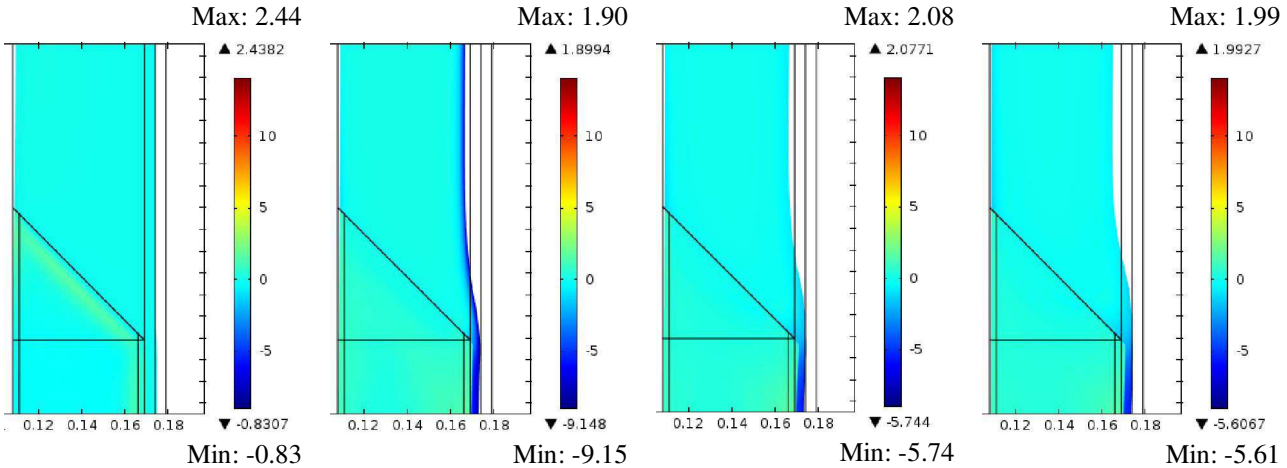

a. Initial condition b. After 600s cooling c. After 1200s cooling d. After 1800s cooling

Fig. 5.11. Hydrostatic pressure during the moulding (MPa)

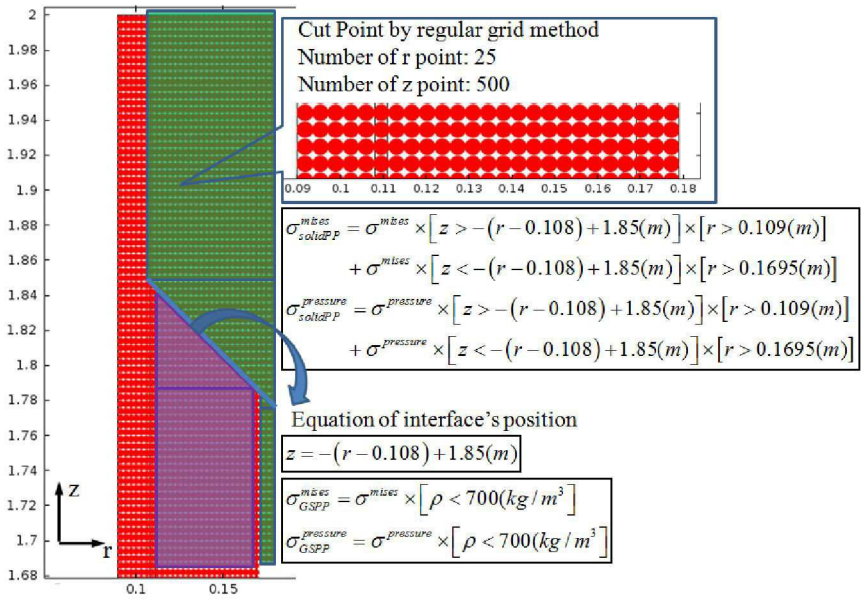

Fig. 5.12. Definition of material areas by the logic function

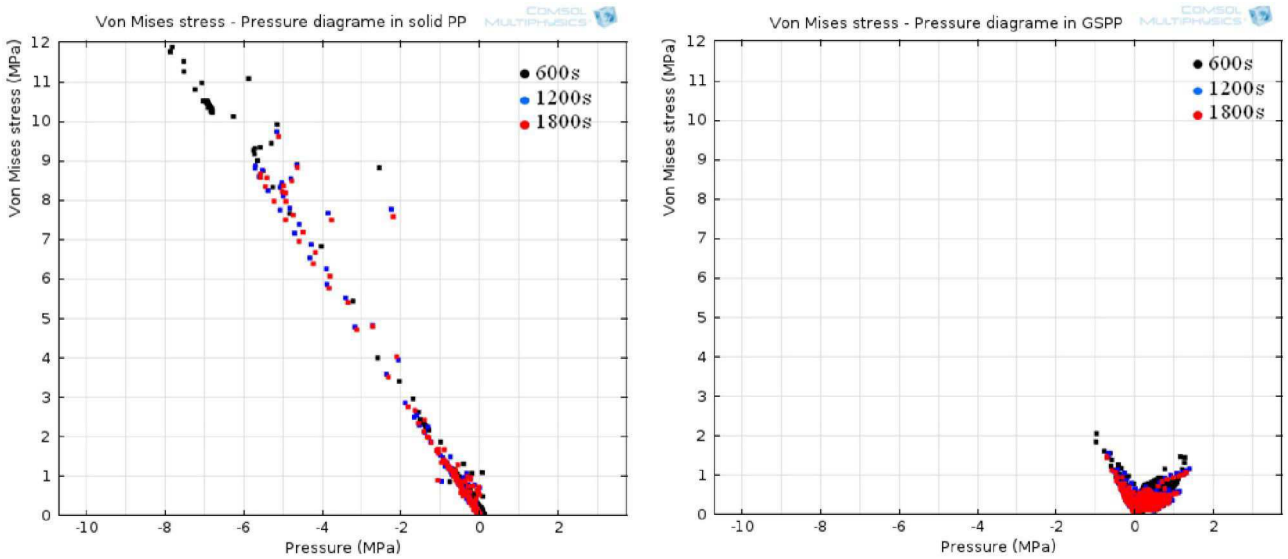

a. In the solid PP b. In the GSPP

Fig. 5.13. von Mises-hydrosatic Pressure diagram in the Field Joint

5.2.3 Stress evolution at the interfaces

It is important to analyse the stress state at the GSPP - Field Joint coating material and also steel-Field Joint coating material interfaces as these can be the weaknest parts of the pipeline.

The normal (σ_n) and shear (σ_τ) stresses on the plane could be calculated by the simple formula of resistance of materials' theory [Bazergui et al, 1987]. The interface between Field Joint-main coating material is an inclined plane which makes the angle of 45°C with the vertical axis.

$$\sigma_n = \frac{\sigma_r + \sigma_z}{2} + \tau_{rz}$$

$$\sigma_\tau = -\frac{\sigma_r - \sigma_z}{2}$$

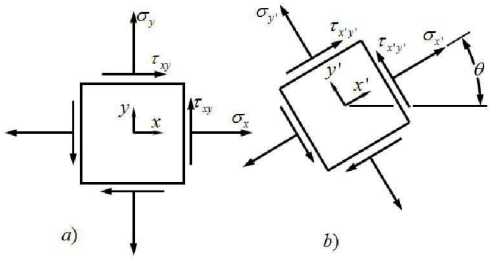

The figures 5.14 and 5.15 present the two main components of stress evolution following the interface's length with moulding time at the interface. The solid line corresponds to the section near the interface oriented to the injection PP and the dotted line is the result obtained on the section near the interface oriented to the GSPP. The components to note are the normal and shear components in the interfaces. As in the figures, the two components are continuous when they cross the interfaces.

The polymer near the steel pipe withstands tension; the exterior part supports the compression. After 600s of cooling, the zone in GSPP near the interface (black solid line) is under a light compression due to the thermal expansion. In time, the value comes down because the contact with hot injection material tends to melt the GSPP, its Young's modulus decreases.

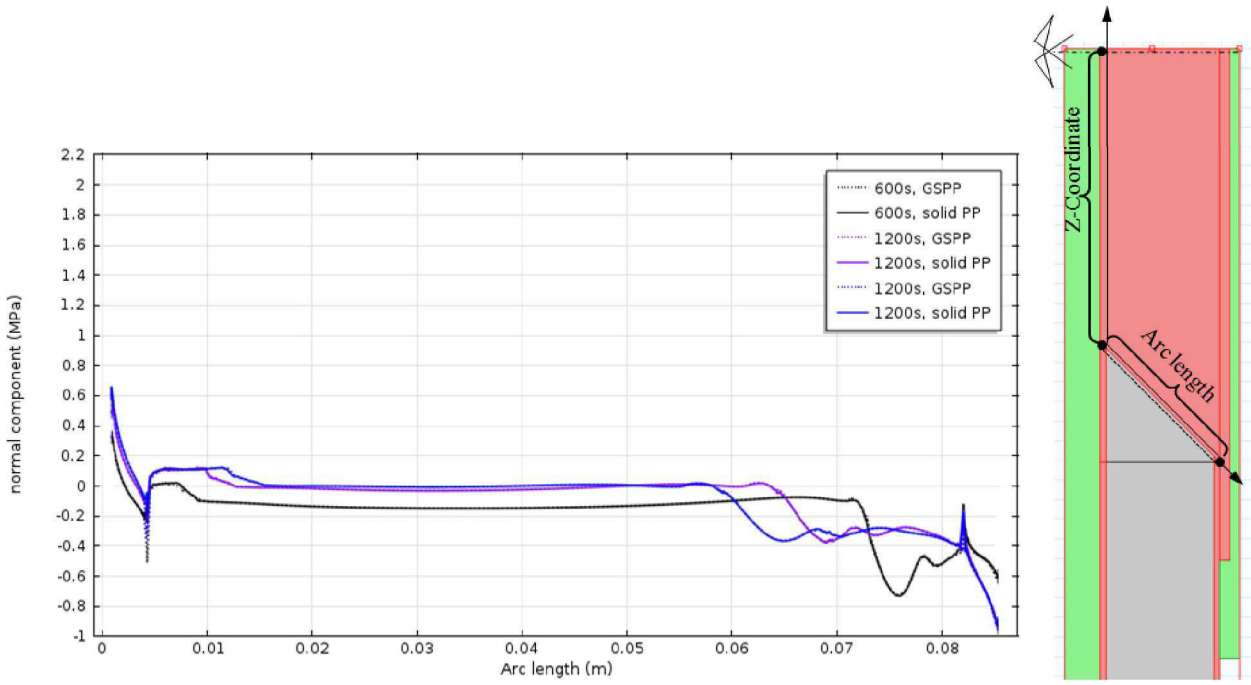

Fig. 5.14. Normal component at the interface Field joint - Main coating material during moulding

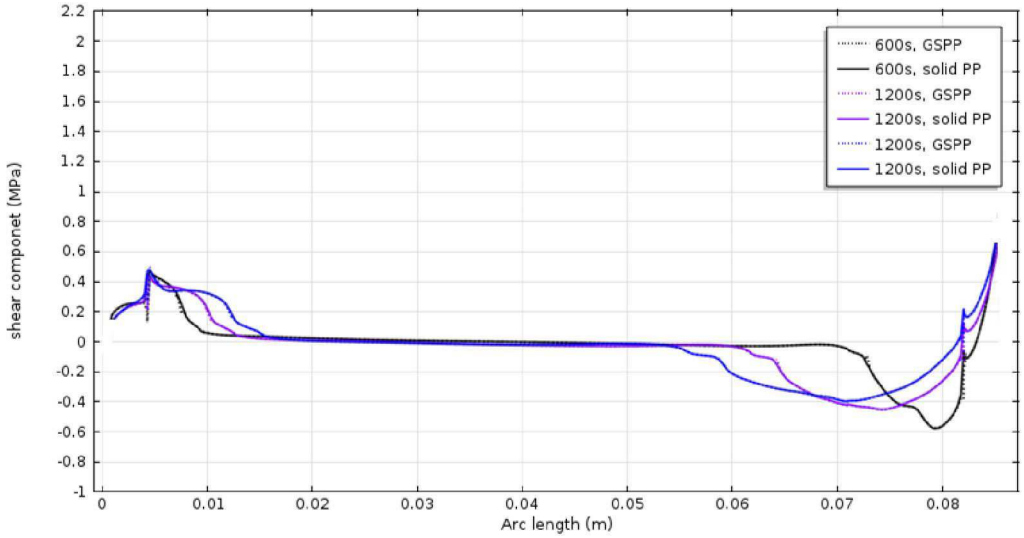

Fig. 5.15. Shear component at the Field joint - Main coating material interface during moulding

Due to the shrinkage of the hot PP material, the steel-injection PP interface supports the tensile load. The critical zone is near the leg of the Field Joint (Fig. 5.16-5.17).

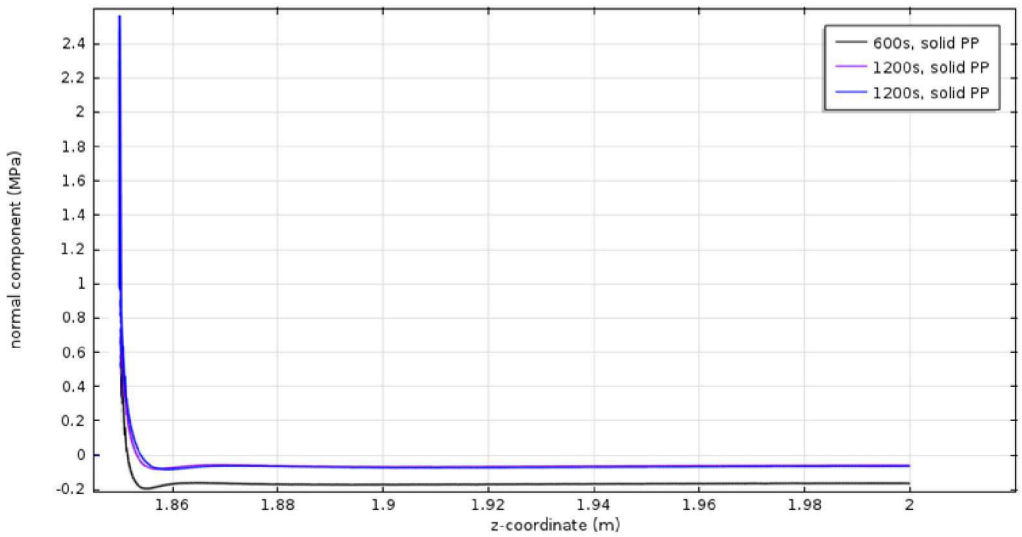

Fig. 5.16. Normal component at the steel-injection PP interface during moulding

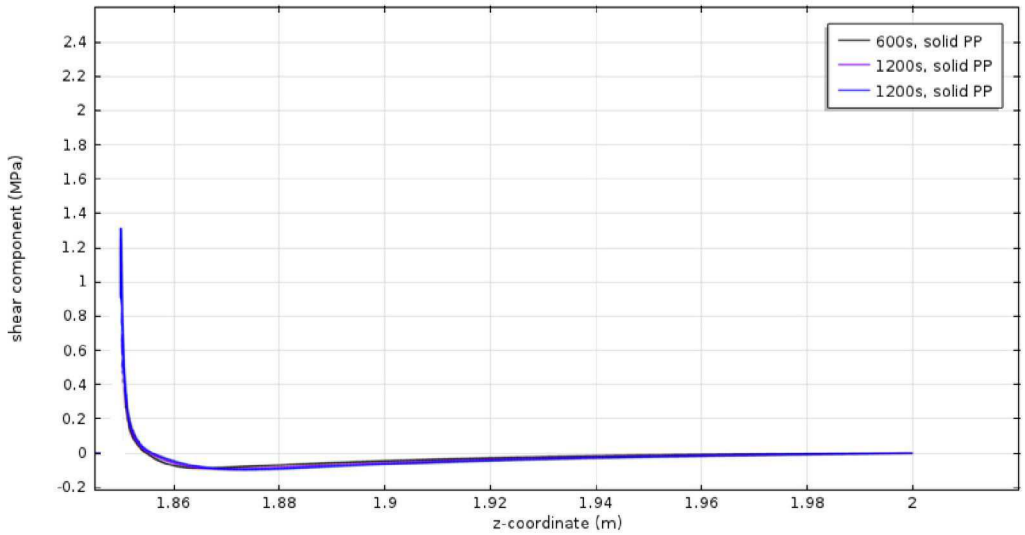

Fig. 5.17. Shear component at the steel-injection PP interface during moulding

5.3 Thermo-mechanical parameters' evolution during lay down phase

5.3.1 The thermal mechanical variables

When the pipeline is laid down, the temperature continues to decrease, the solidification of injection PP tends to finish, the hydrostatic pressure increases. The material behaviour is still influenced by the moulding temperature (Fig. 5.18). This is a moment when the consolidation of GSPP plays an important role (Fig. 5.20). The volumetric strain reaches the limit of phase change 1 of material (Tab. 3.4), the Young's modulus increases. This phenomenon may lead to stress redistribution in the structure. When the pipeline reaches the desired depth, the temperature is stabilized after 5 days, the exterior pressure stays constant. However, because of the viscous effect, the volumetric strain in GSPP still goes up and the Young's modulus changes too (Fig. 5.20, 5.21).

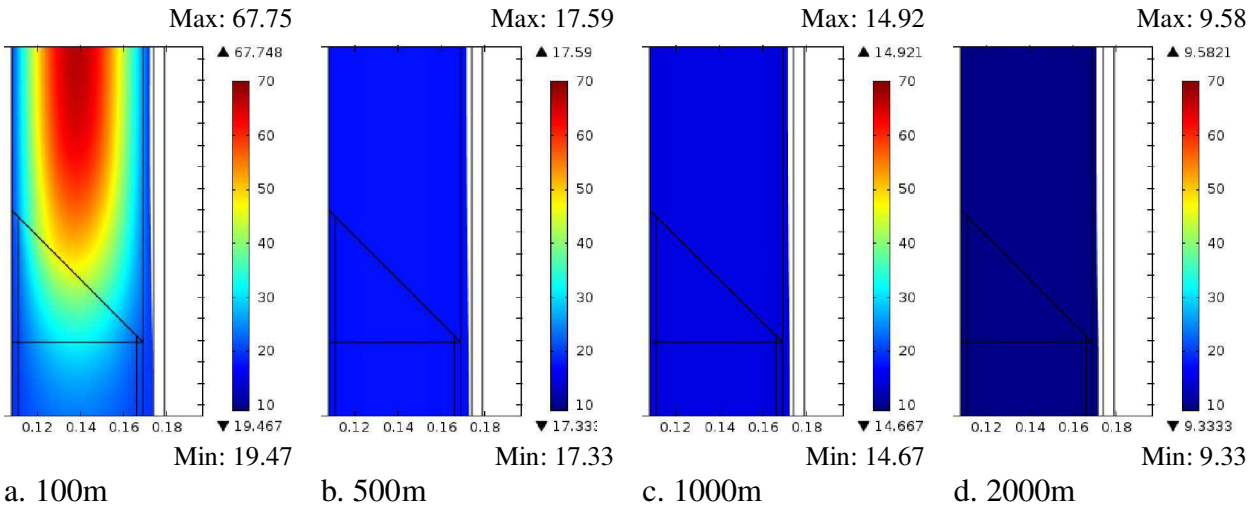

Fig. 5.18. Temperature distribution at different depths during laying down (°C)

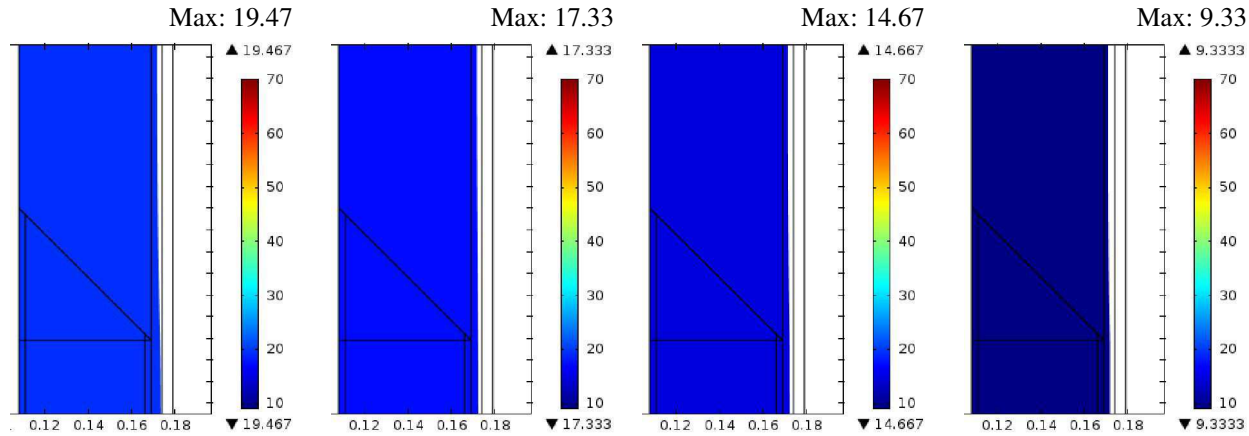

a. 100m b. 500m c. 1000m d. 2000m

Fig. 5.19. Temperature distribution at different depths after 5 days cooling (°C)

Concerning the stress state, the figures 5.22-5.25 represent the Von Mises stress and the pressure component of the structure. At lower depth, the critical zones are located near the steel - injection PP interface and near the overlap of the Field Joint. When the pipeline is placed in a high depth (1000m), because of the consolidation of GSPP, the Von Mises stress on the main coating near the steel pipe becomes important. It could lead to the collapse of microspheres and a brutal rigidity change of the structure.

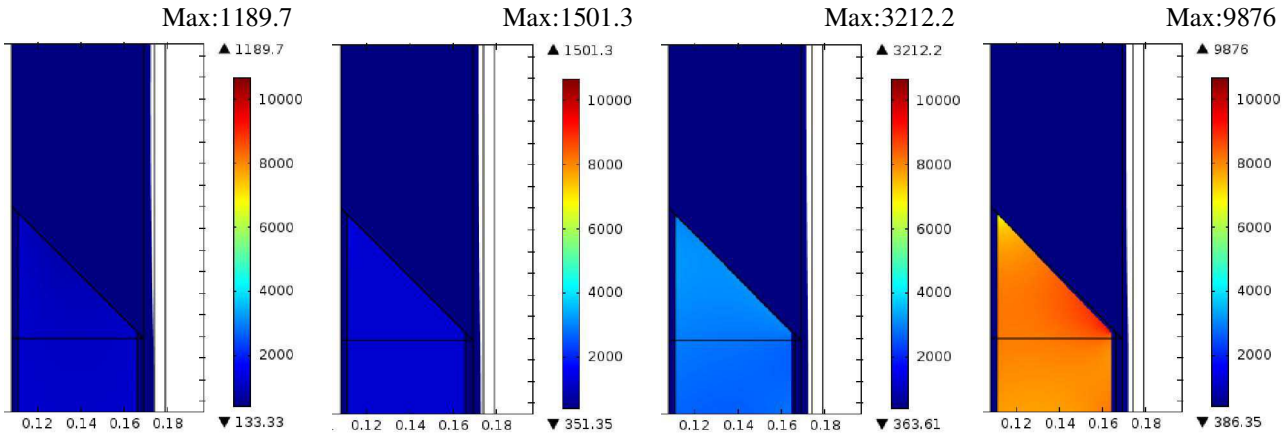

a. 100m b. 500m c. 1000m d. 2000m

Fig. 5.20. Young's modulus at different depths during laying down (MPa)

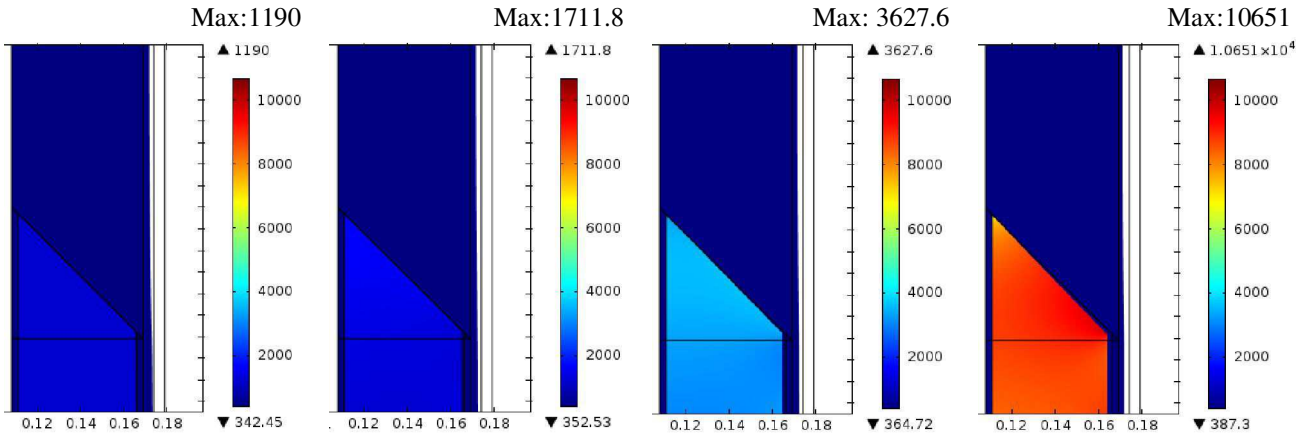

a. 100m b. 500m c. 1000m d. 2000m

Fig. 5.21. Young's modulus at different depths after 5 days cooling (MPa)

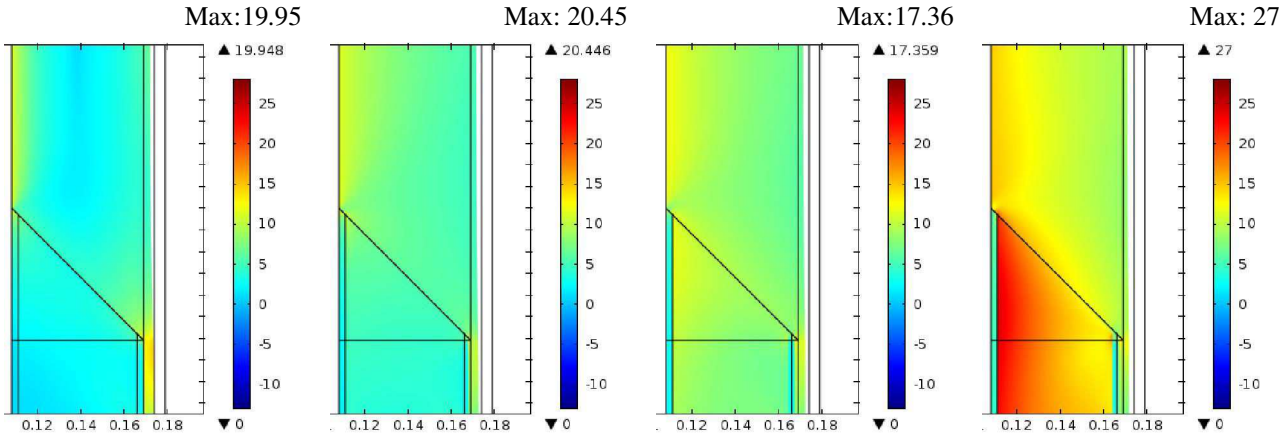

a. 100m b. 500m c. 1000m d. 2000m

Fig. 5.22. Von Mises stress at different depths during laying down (MPa)

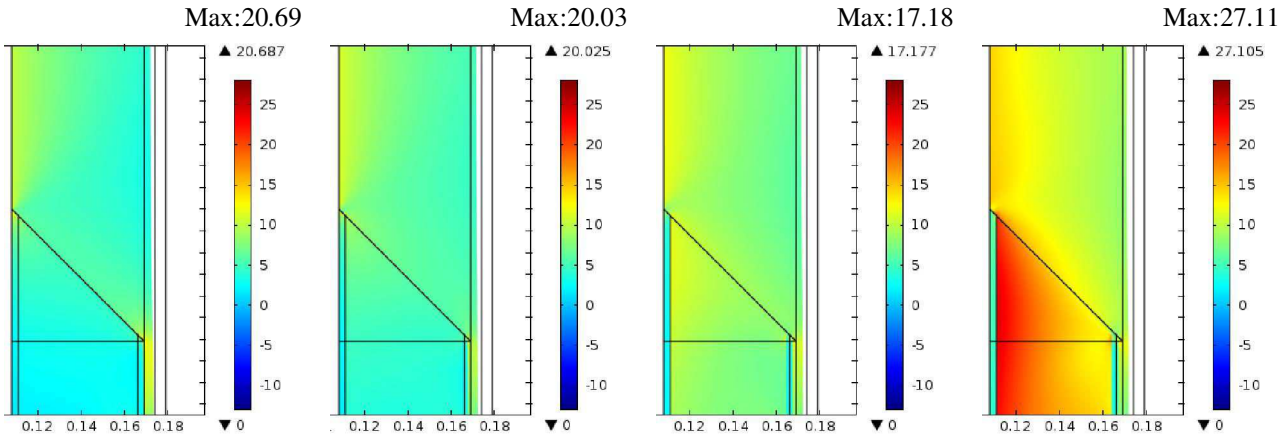

a. 100m b. 500m c. 1000m d. 2000m

Fig. 5.23. Von Mises stress at different depths after 5 days cooling (MPa)

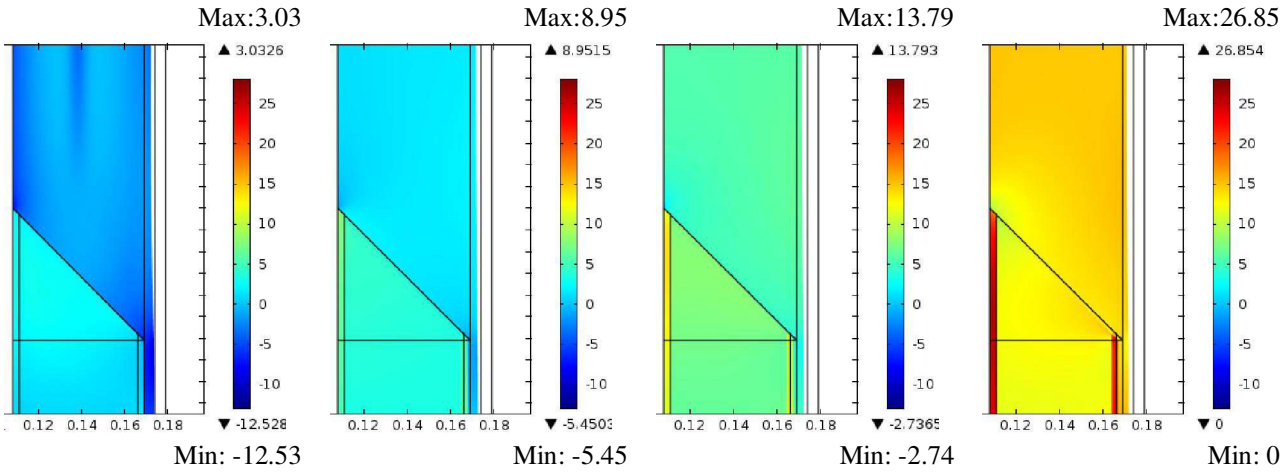

a. 100m b. 500m c. 1000m d. 2000m

Fig. 5.24. Pressure at different depths during laying down (MPa)

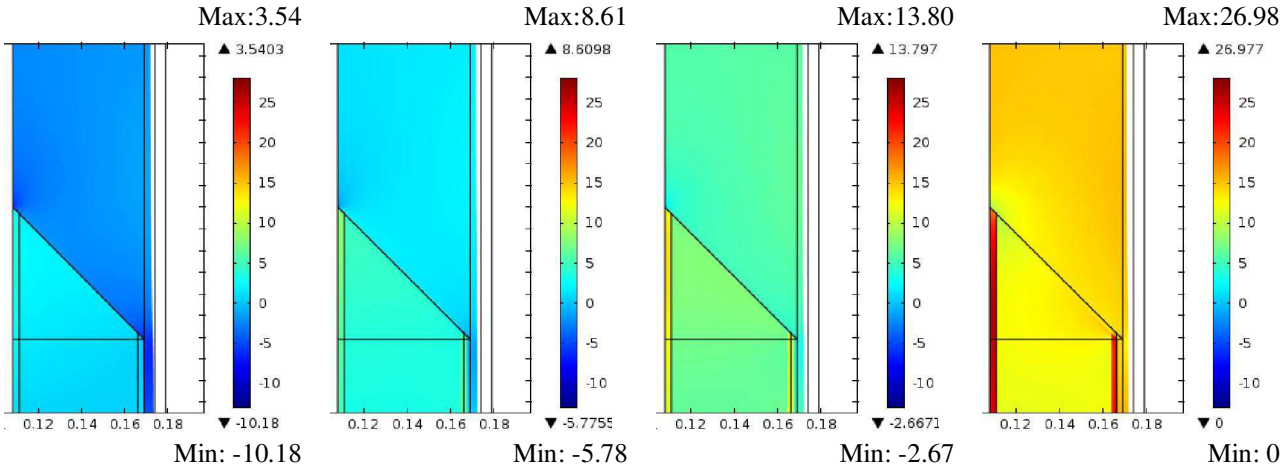

a. 100m b. 500m c. 1000m d. 2000m

Fig 5.25. Pressure at different depths after 5 days cooling (MPa)

To better understand the difference between the solid PP and GSPP's behaviour, the volumetric strain evolution graphs during laying down to 3000m have also been created (Fig. 5.26). The volumetric deformation of solid PP under the hydrostatic pressure is purely elastic, after having reached to 3000m, it does not change. But for the GSPP, the strain tends to increase due to the creep (Fig. 5.26.b).

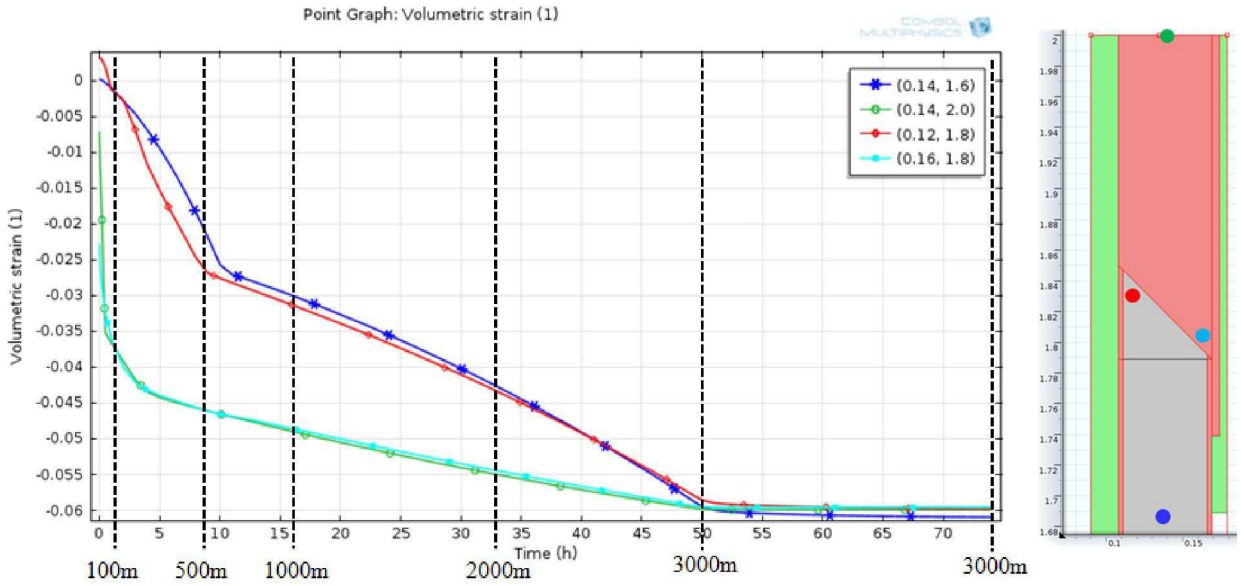

5.26.a. Evolution of volumetric strain when laying down (1m/min) and 24h at 3000m

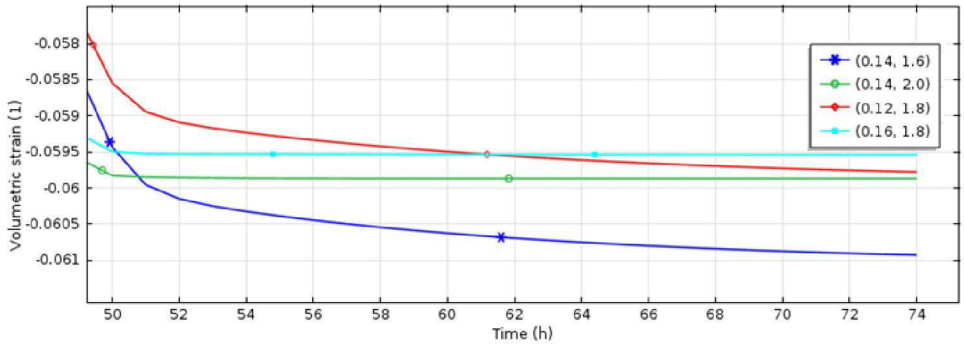

5.26.b. Evolution of volumetric strain at 3000m (creep volumetric strain of GSPP)

Fig. 5.26. Evolution of volumetric strain in injected PP and GSPP

The Von Mises stress - hydrostatic pressure envelopes allow us to analyse the stress behaviour of the systems. The maximal Von Mises stress reaches 20 MPa when the pipeline is laid down to 2000m of water depth (Fig. 5.27, 5.28). By observing the stress state at 100m depth, the stress redistribution in solid PP and GSPP is registered. It could be explained by the solidification of solid PP and the viscous effect of materials.

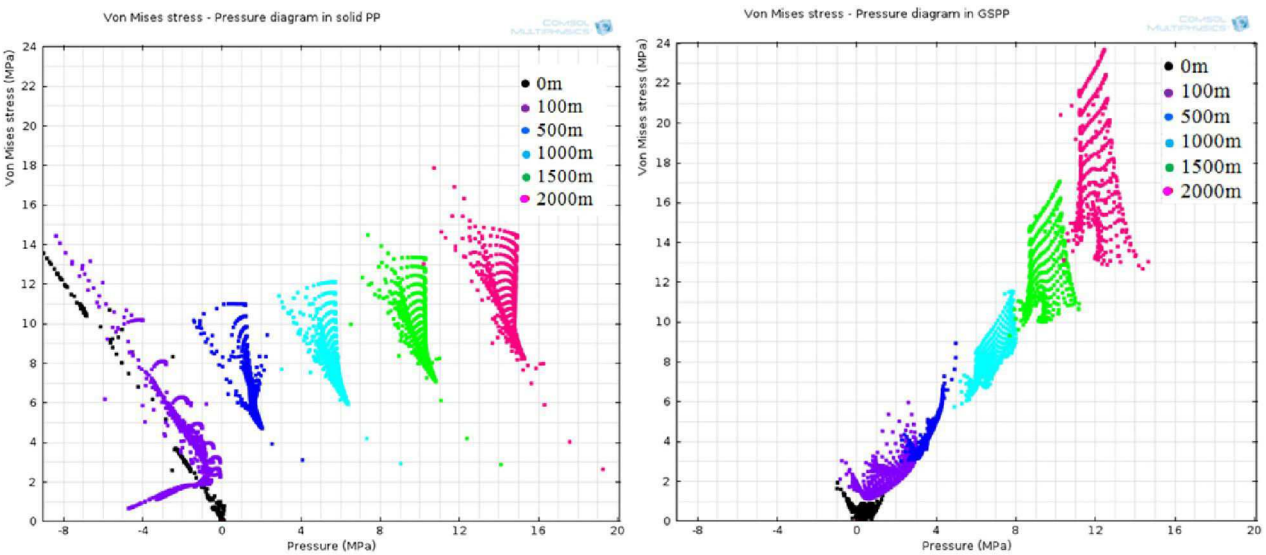

Fig. 5.27. Von Mises stress - pressure diagram at different depths during laying down

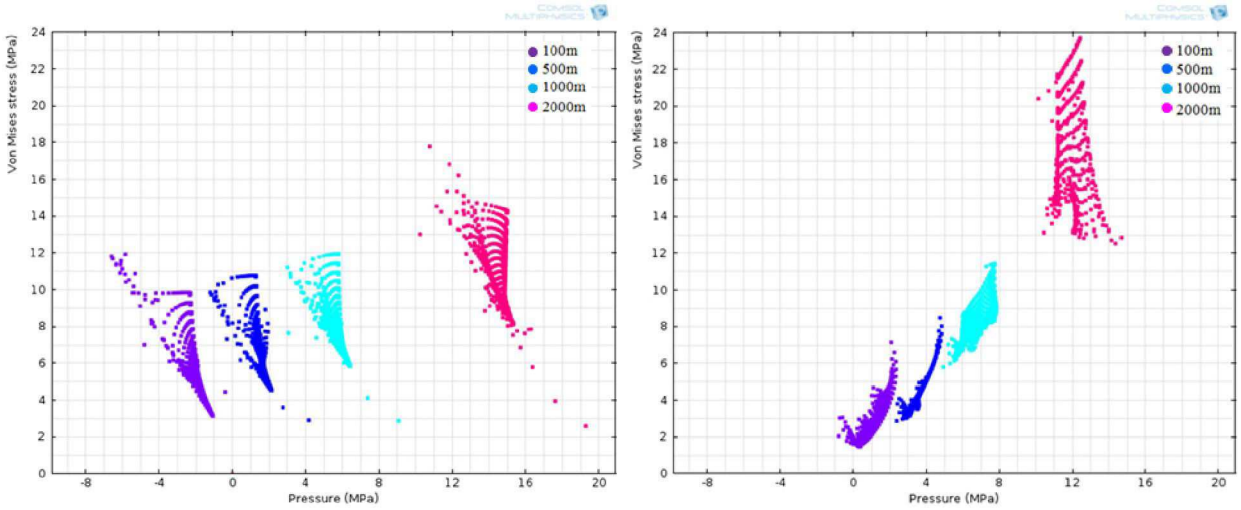

Fig. 5.28. Von Mises stress - pressure diagram at different depths after 5 days cooling

5.3.2 Stress evolution at the interface

With reference to the stress evolution at the interfaces, we return to the two main continuous components, normal and shear stress (Fig 5.29-5.36). The normal stress when the pipeline is at 100m depth is positive, i.e. the material is under the tension. For higher depth, this stress decreases and becomes negative because of the hydrostatic pressure. Comparing the stress distribution during laying down and after 5 days cooling, the viscous effect at this moment does not result in an important stress redistribution.

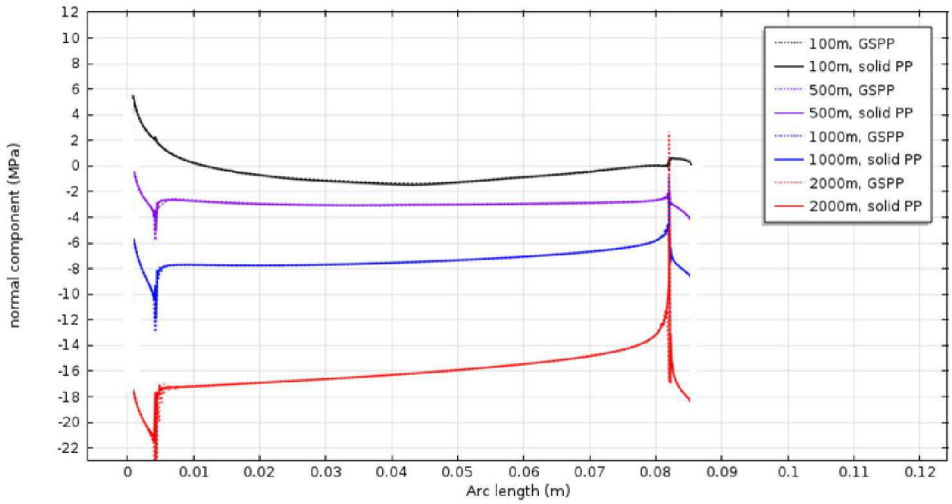

Fig. 5.29. Normal component at the interface Field joint - Main coating material during laying down

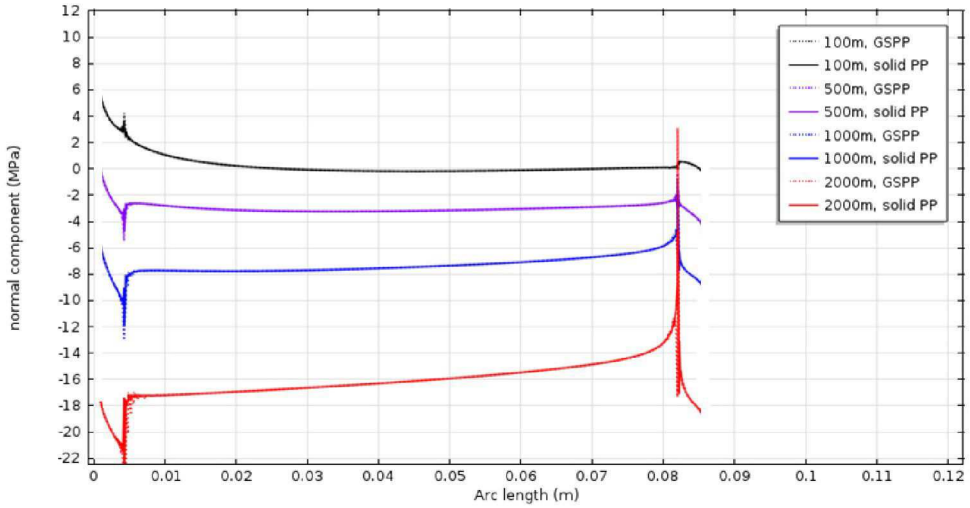

Fig. 5.30. Normal component at the Field joint - Main coating material interface after 5 days cooling

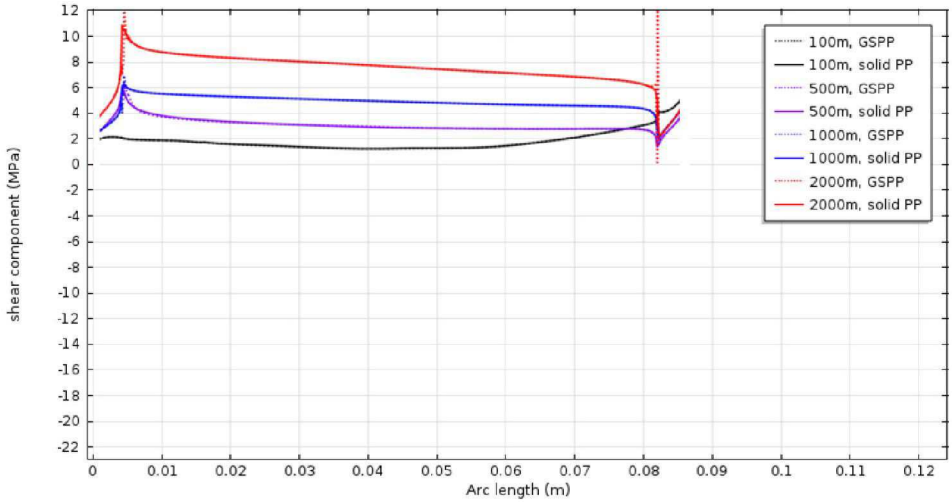

Fig. 5.31. Shear component at the interface Field joint - Main coating material during laying down

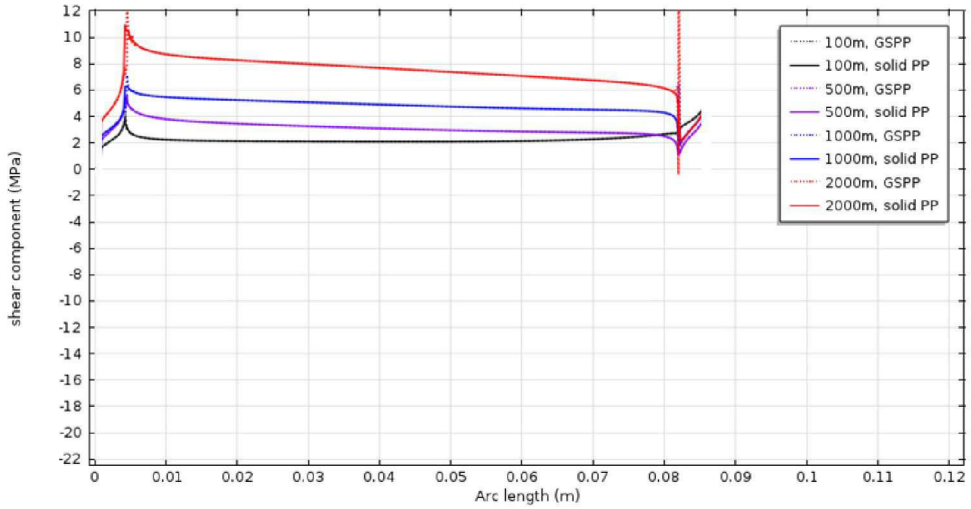

Fig. 5.32. Shear component at the Field joint - Main coating material interface after 5 days cooling

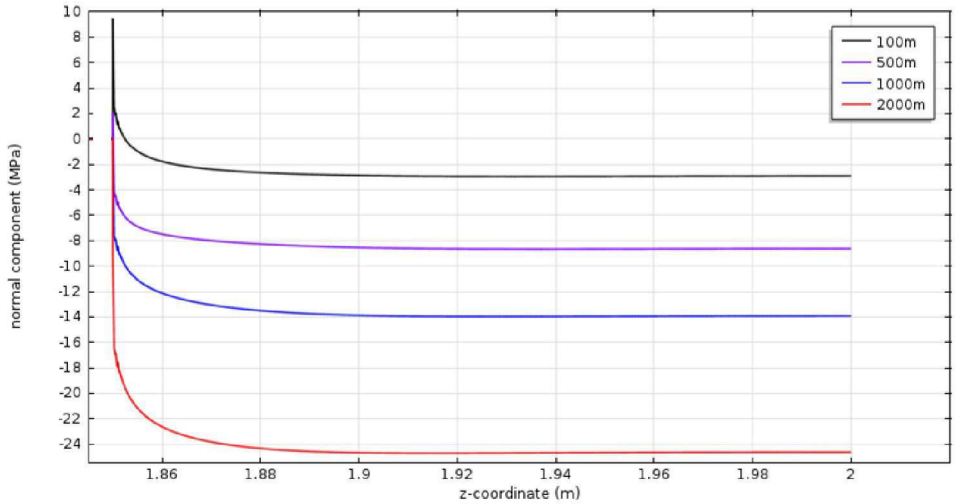

Fig. 5.33. Normal component at the steel - injection PP interface during laying down

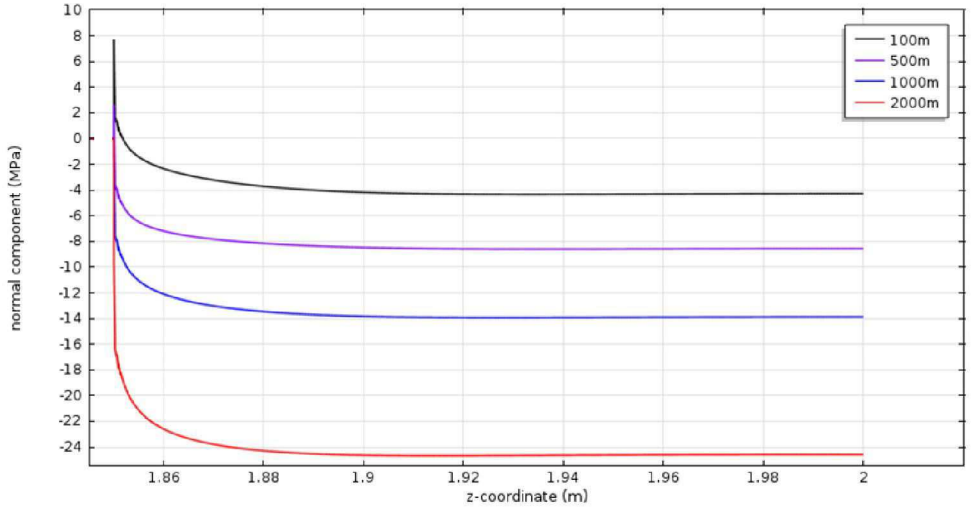

Fig. 5.34. Normal component at the steel - injection PP interface after 5 days cooling

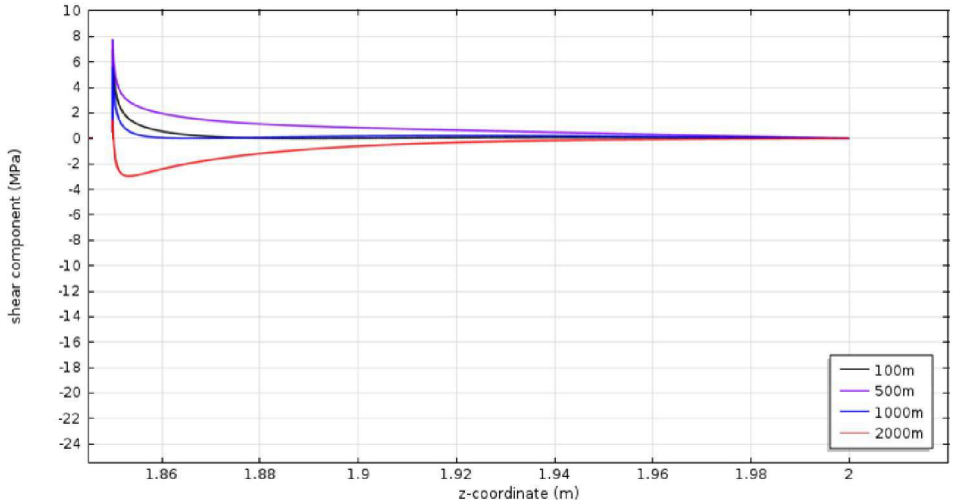

Fig. 5.35. Shear component at the steel - injection PP interface during laying down

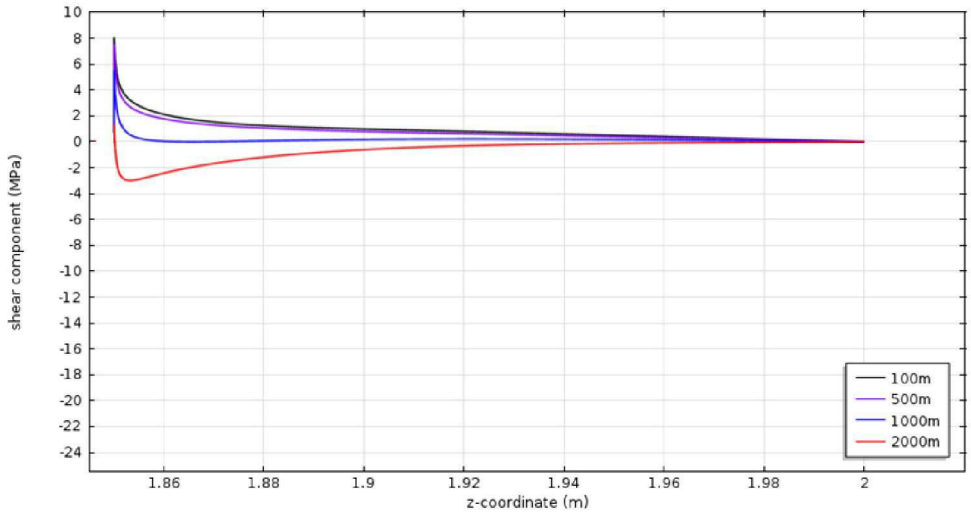

Fig 5.36. Shear component at the steel - injection PP interface after 5 days cooling

5.4 Thermo mechanical parameter evolution in service

To model the thermo mechanical behaviour of Field Joint in service and to simulate the internal oil flow, there are many solutions which are possible. It must be mentioned that the liquid circulating in the pipe is generally very complex and multiphase flow occurs which is very complex to simulate and which is not addressed in this study.

The first one is to use the fluid flow inside the pipeline (Chapter 2). This solution could give us not only the thermo mechanical variables' distribution but also the heat loss along the pipeline's length. However, because the fluid flow has one inlet and one outlet, i.e. the boundary conditions are not the same (differences of temperature, pressure and the velocity of fluid), our problem loses the symmetry through the middle of Field Joint.

The second solution is to use the internal convection coefficient corresponding to the nature of fluid inside the pipeline (Tab. 2.1). The symmetry is safeguarded but the estimation of this coefficient is not easy. It depends on the nature of fluid, the velocity and the geometry of the contact surface.

The simplest solution which is used here is applying directly the hot temperature at the inner surface of the pipeline. Taking into account the thermal contact resistance between the fluid and the steel at the interface and also easing the convergence of computing process, the temperature is supposed to take 1 hour to reach 100°C from the initial temperature. The initial temperature depends on the pipeline position in deep sea.

5.4.1 The thermo mechanical variables

The figure 5.37 represents the temperature's distribution as a function of the time. The temperature tends to stabilize after one day. From this moment, the only parameter affecting the evolution of the pipeline behaviour is the viscous response of the material. The Young's modulus of the materials is strongly influenced by the hot temperature (Fig. 5.38). In the solid PP, the Young's modulus decreases with temperature. But in the GSPP, considering the important volumetric strain in compression, its apparent modulus starts to increase at 500m.The consolidation of material changes the strain and stress distribution in GSPP (Fig. 5.39-5.41). The critical zones where the von Mises stress and the pressure component become important are localized near the steel part and also near the interface between the GSPP and solid PP (Fig. 5.39c,d & Fig. 5.40d).

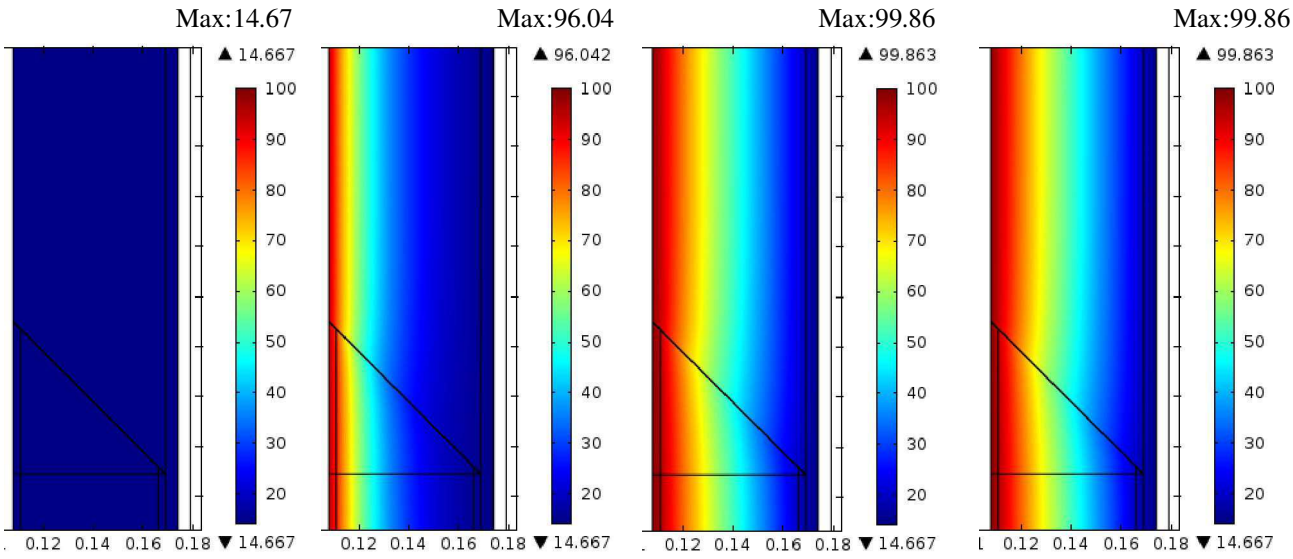

a. 0s b. 3600 c. 1day d. 7days

Fig 5.37. Temperature distribution during service (at 2000m) (°C)

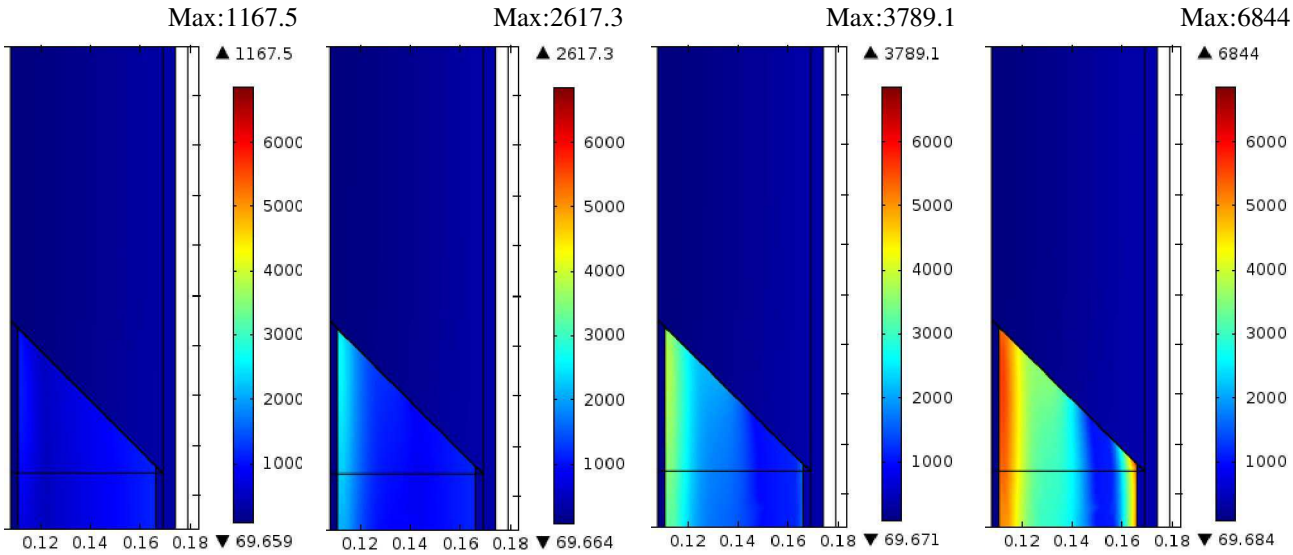

Fig. 5.38. Young's modulus at different depths in service after 7 days (MPa)

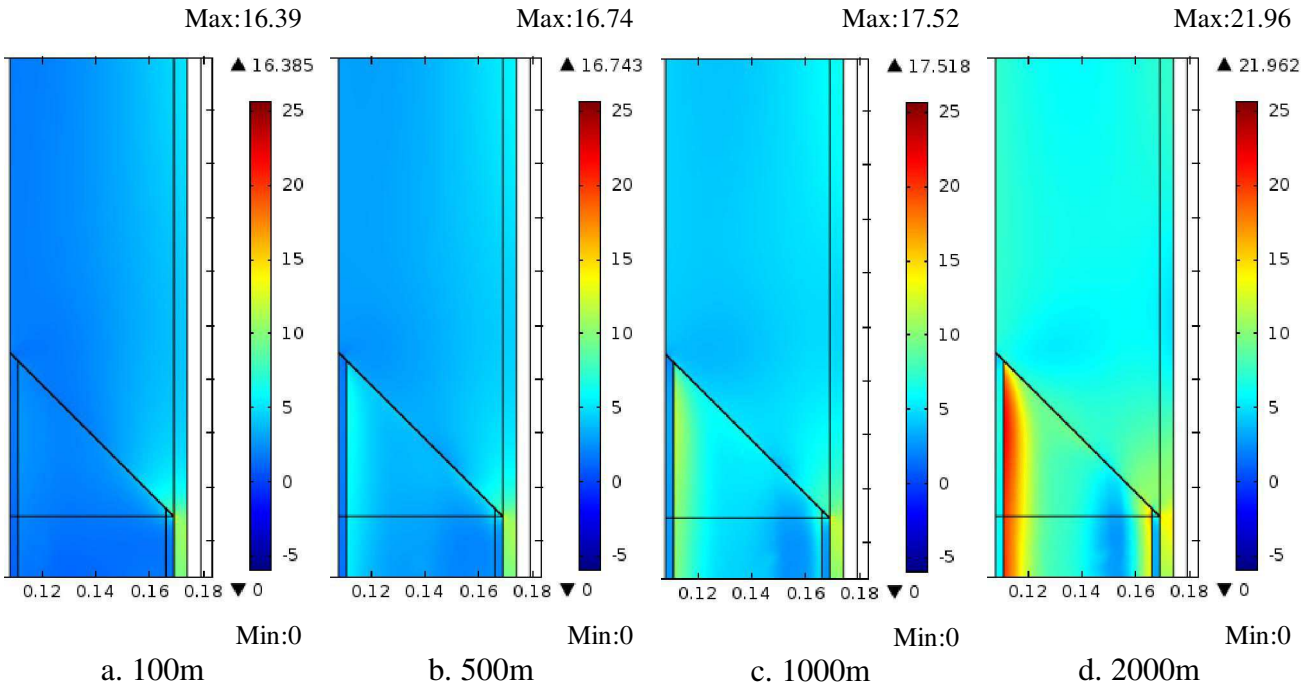

Fig. 5.39. Von Mises stress at different depths in service after 7 days (MPa)

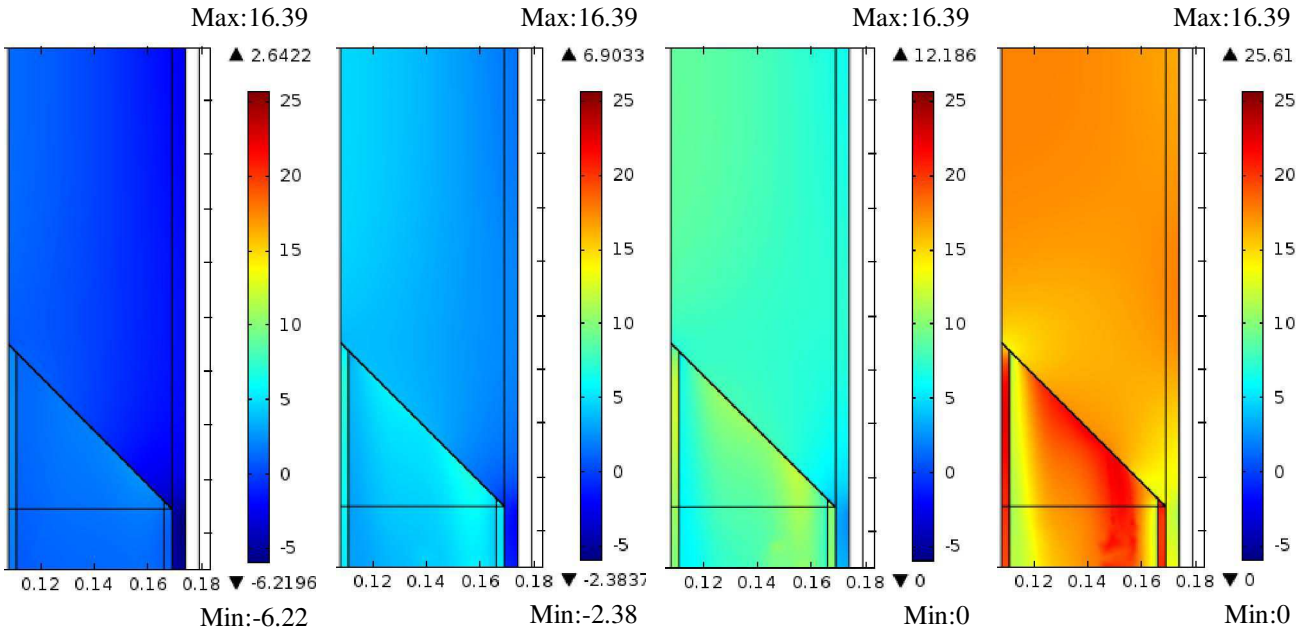

a. 100m b. 500m c. 1000m d. 2000m

Fig. 5.40. Pressure at different depths in service after 7 days (MPa)

The evolution of von Mises stress in the different materials is reported on figure 5.41. These curves reveal important stress gradients in particular in GSPP.

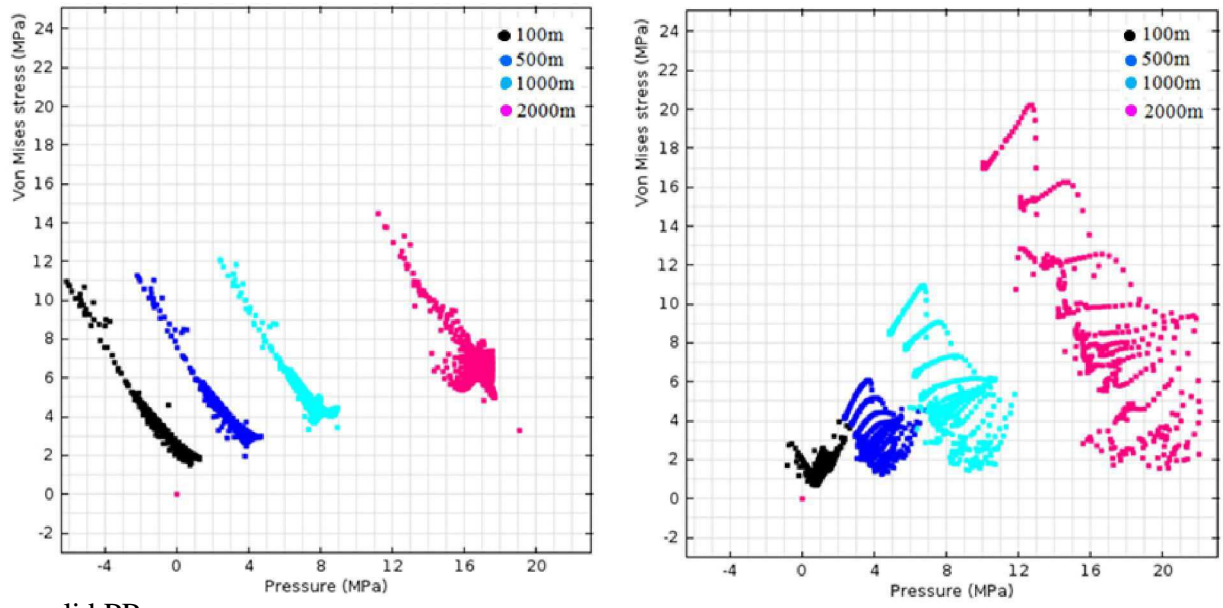

a. solid PP b. GSPP

Fig 5.41. Von Mises stress - pressure diagram in service at different depths after 7 day

5.4.2 Stress evolution at the interfaces

The stress evolutions at GSPP - solid PP and steel - solid PP interfaces are studied (Fig 5.42-5.45). It is clear that the normal component is negative which corresponds to the interface in compression. It is interesting to note that the stress distribution changed between the laying phase and cooling phase (Fig 5.29-5.36). In shallow water during the installation phase tensile stresses are noted near the steel which are not present in service. Because of the hot temperature inside the pipeline, the part supporting the tensile loads at 100m (Fig 5.29) decreases considerably. In deep water, in service it can be noted that there are important gradients in the stress distribution along the interface. However it must be mentioned that the critical stresses are mainly observed during the installation phase.

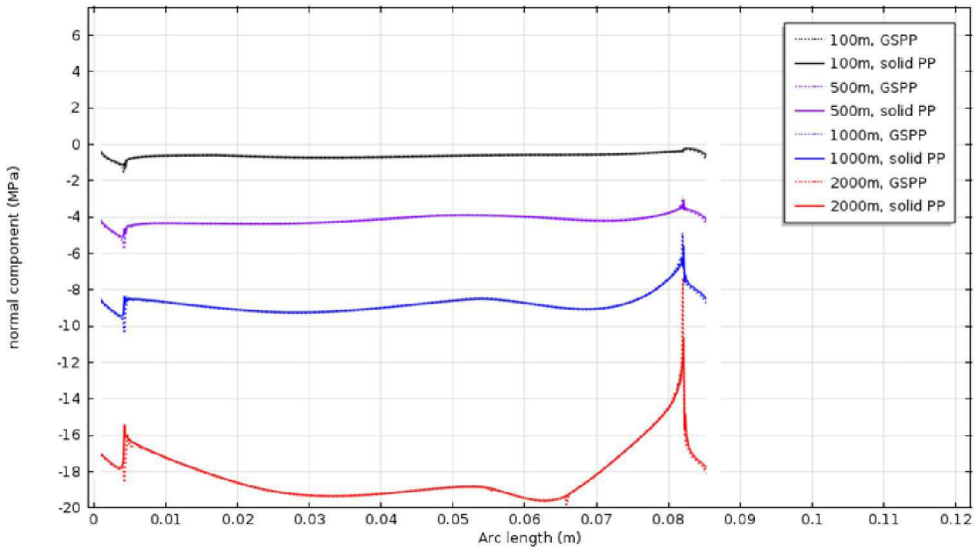

Fig. 5.42. Normal component at the Field joint - Main coating material interface in service after 7 days

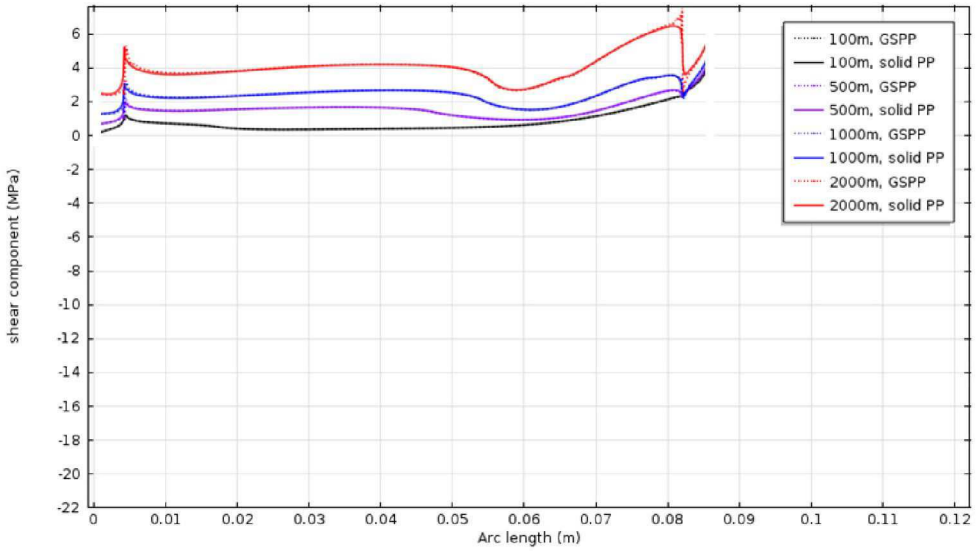

Fig. 5.43. Shear component at the Field joint - Main coating material interface in service after 7 days

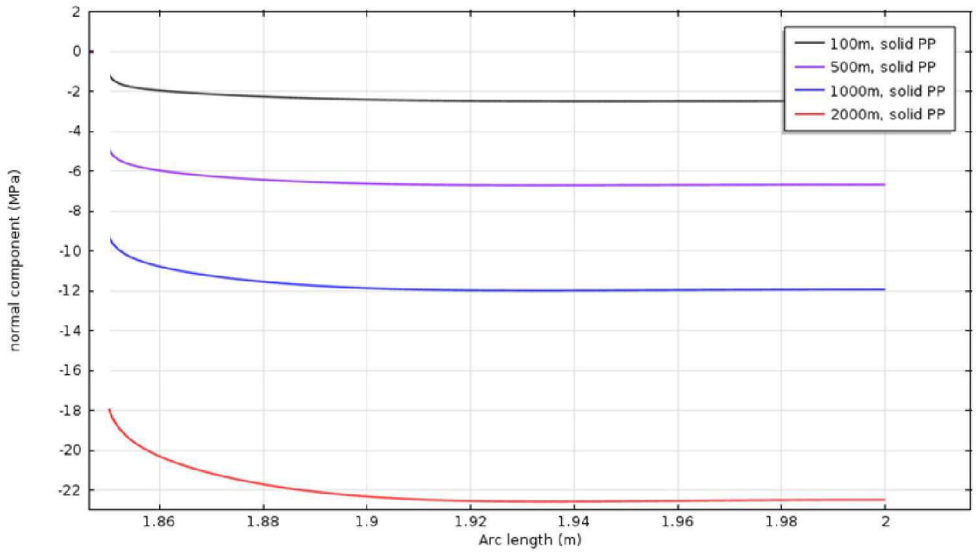

Fig. 5.44. Normal component at the steel - injection PP interface in service after 7days

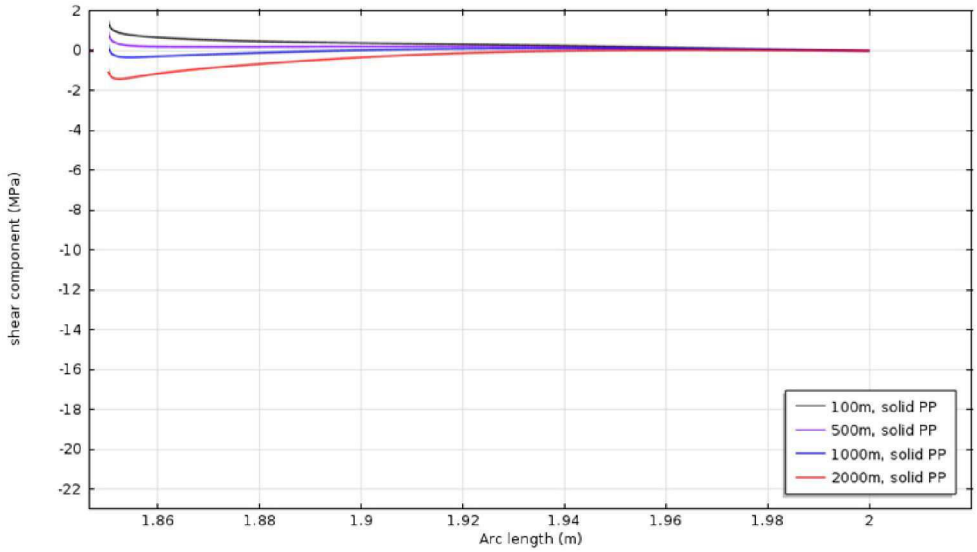

Fig. 5.45. Shear component at the steel - injection PP interface in service after 7days

5.5 Improvement of Field Joint form

To reduce the residual stress in Field Joints, a new shape is proposed (Fig 5.46).

The same moulding process is used and all the thermo mechanical parameters' evolution of classical Field Joint are followed as the previous study. The results presented in (Fig 5.47-5.51) are encouraging.

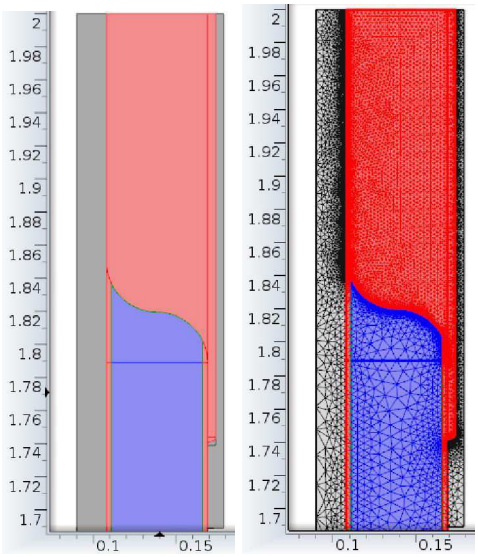

Fig. 5.46. New form of IMPP

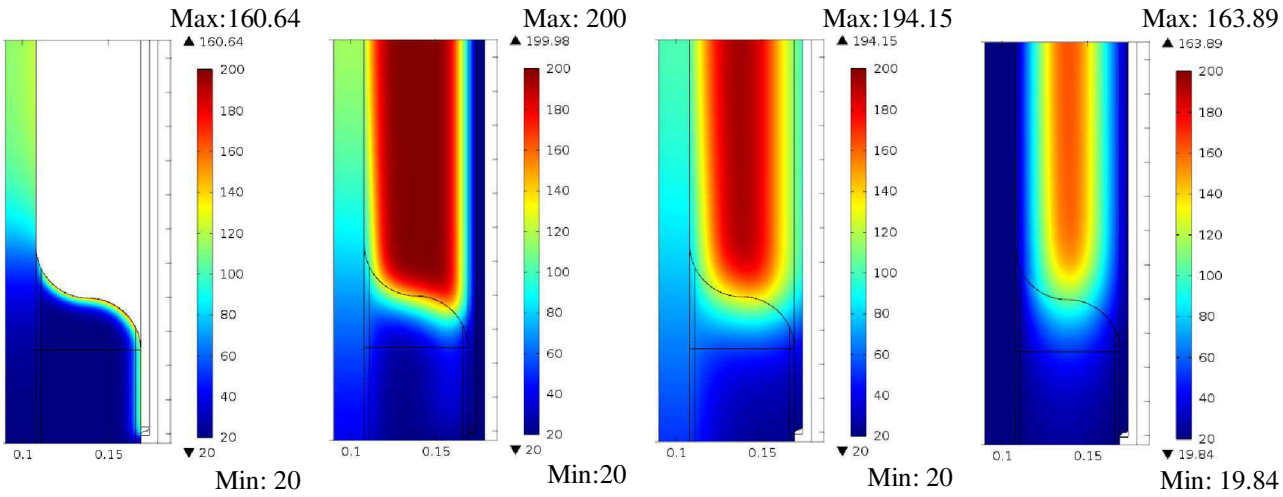

a. before moulding b. after 600s c. after 1800s d. after 3600s

Fig. 5.47. Temperature evolution during the Field joint's moulding (°C)

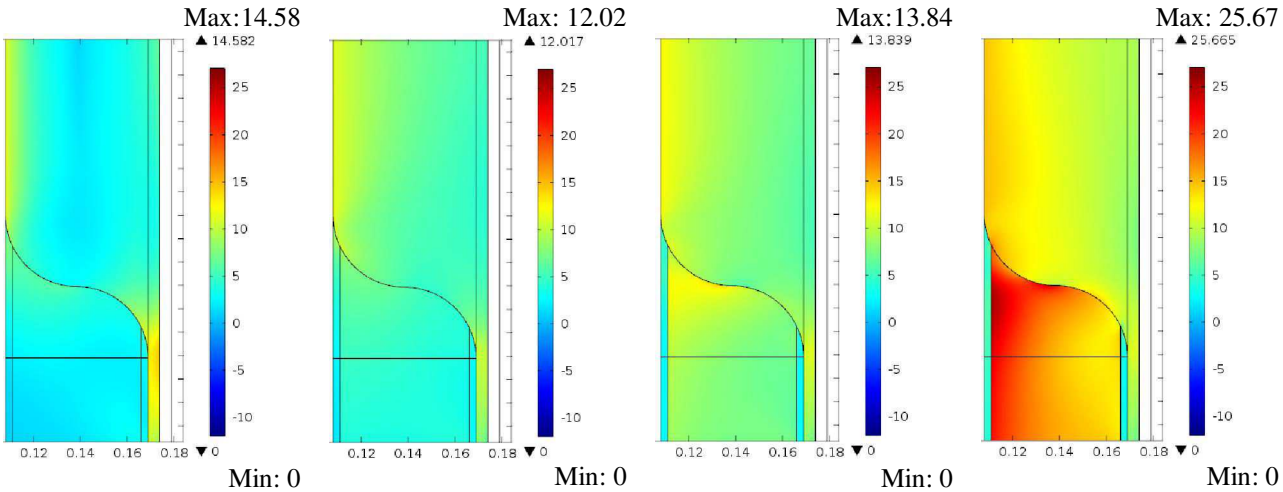

a. 100m b. 500m c. 1000m d. 2000m

Fig. 5.48. Von Mises stress at different depths during laying down (MPa)

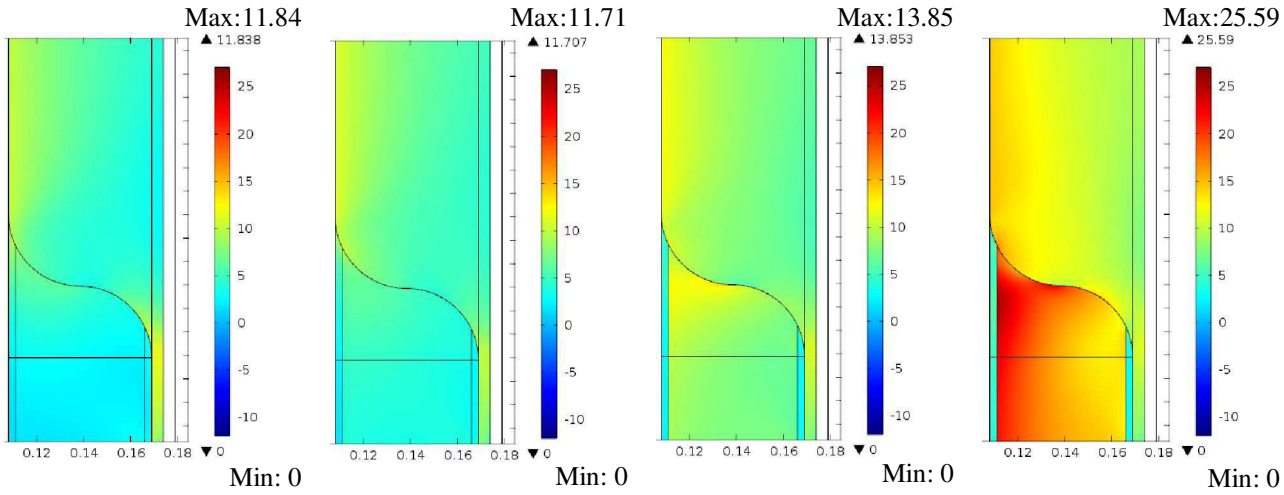

a. 100m b. 500m c. 1000m d. 2000m

Fig. 5.49. Von Mises stress at different depths after 5 days cooling (MPa)

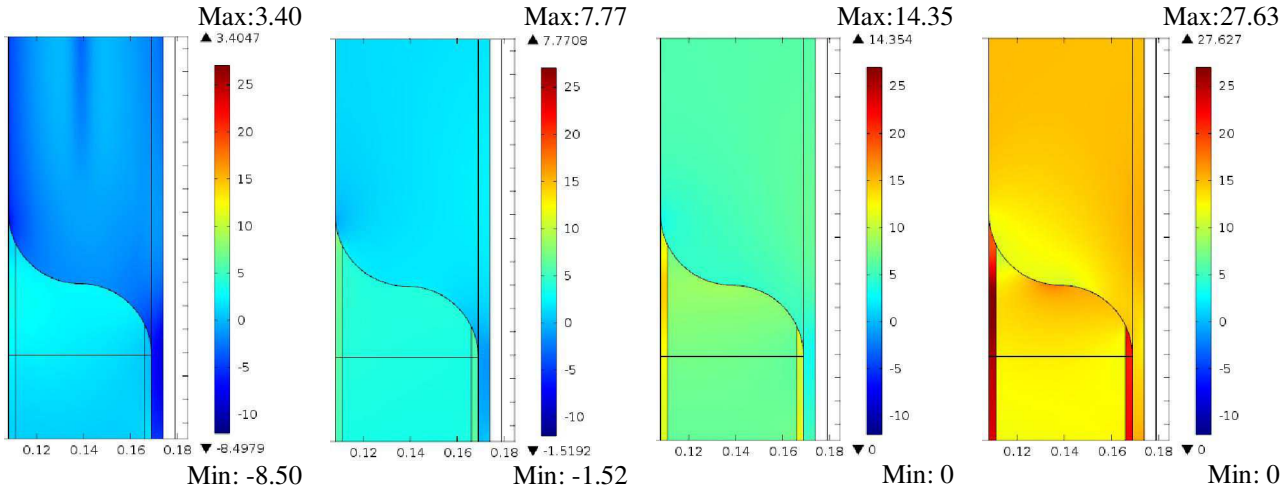

a. 100m b. 500m c. 1000m d. 2000m

Fig. 5.50. Pressure at different depths during laying down (MPa)

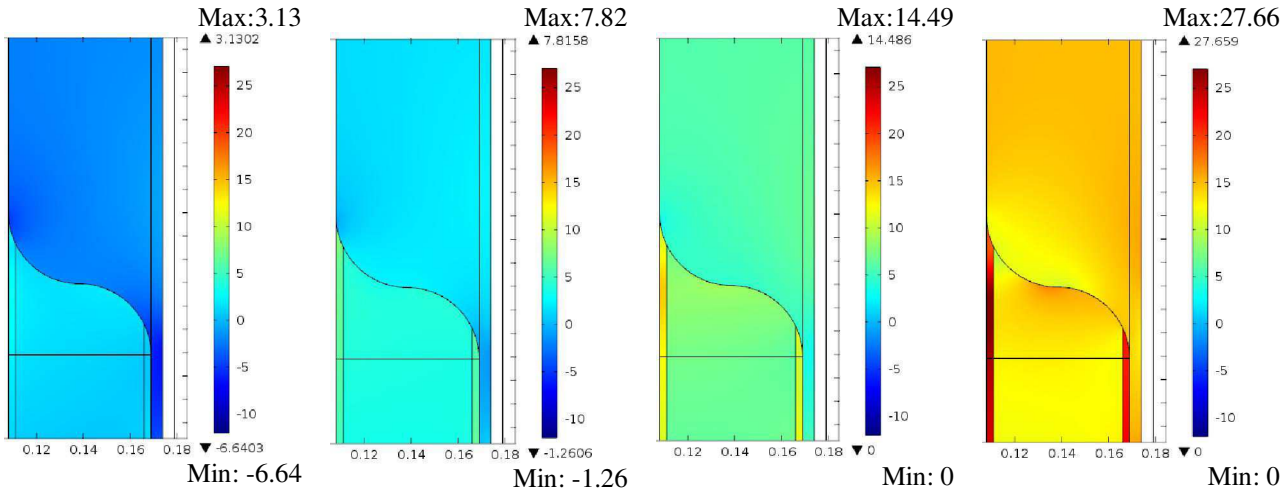

a. 100m b. 500m c. 1000m d. 2000m

Fig 5.51. Pressure at different depths after 5 days cooling (MPa)

5.6 Experimental study on the Arcan assembly

In Field Joint, the interfaces between the main coating material and the injecting material are one of the weakest links of the structure. Very few data are available on the experimental characterization of polymer-polymer or polymer-metal interfaces. In order to examine how such data might be obtained, it is proposed to use the experimental fixture called modified Arcan fixture to study the behaviour of the interfaces between two materials. This device enables us to combine the compression or tension with shear loads. Moreover, the sample's dimension must be representative compared to the real structure. Our ambition is to build the failure envelope of the interfaces which are useful for modelling the non-linear interface behaviour. The measure of deformation evolution is performed by image correlation. Using two cameras, the results give not only the deformation in plane but also the out-of-plane [Cognard et al, 2011, 2006].

The experimental procedure is adapted to the available equipment. Taking account of the difficulty to obtain at this stage, specimens with PP or GSPP material, a pre study has been performed on PVC-PU interfaces. This system has been retained considering the possibility to manufacture specimens in the lab and with properties of the materials close to the material properties of material used in Field Joint manufacturing (e.g. PU-PP interface).

This pre study must be considered as a first approach to characterise the polymer-polymer interface.

Considering significant differences in stiffness of PU and PVC material the double lap specimens have been designed with different bond line thickness (15mm and 5 mm) (Fig. 5.52). In order to limit the stress concentrations at the interface the specimens have been machined with local modification of the geometry (Tab. 5.3; Fig. 5.53). To take into account the viscous effects of materials, different loading profiles are proposed. The experimental results are provided in (Fig. 5.55).

	Bond line thickness	Loading rate (mm/min)
Test 1	5 mm	2.0
Test 2	5 mm	0.5
Test 3	15 mm	2.0

Tab. 5.3. Loading profiles for Arcan tests

FE analyses have been carried out to verify the pertinence of the use of the modified geometry (Fig. 5.56). The materials are assumed isotropic elastic. Young's modulus is 3GPa (for PVC) and 0.4 GPa (for PU); Poisson's ration is 0.4 for both materials. The stress obtained is shown in (Fig. 5.56) corresponding to transversal displacement of 1mm at the bolt hole.

This approach appears promising to determine the failure envelope under combined in-plane stress, further tests are underways.

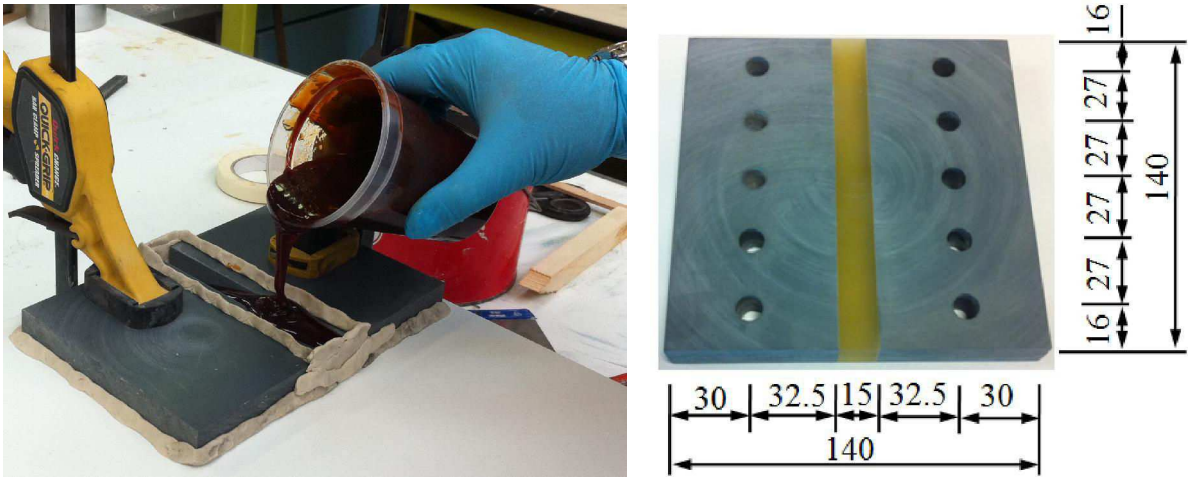

Fig. 5.52. Preparation of samples for tests on the Arcan assembly

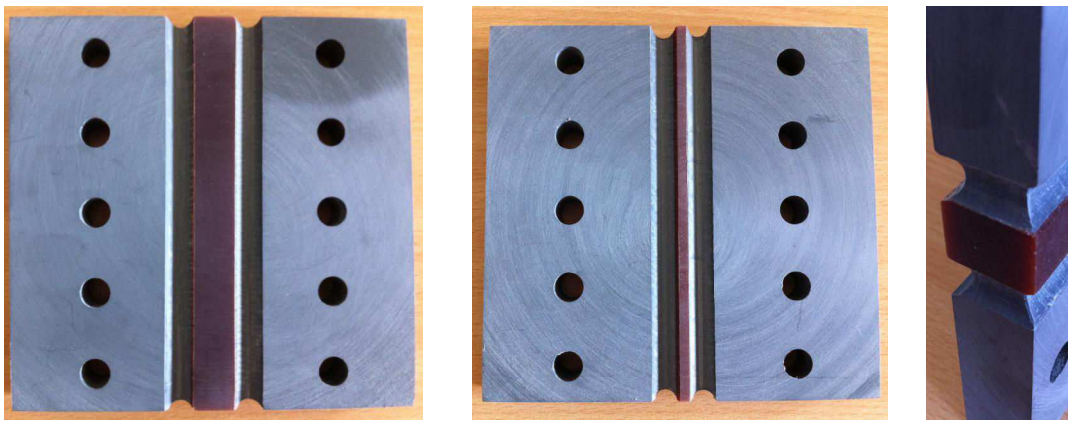

Fig. 5.53. Samples PVC-PU with beak

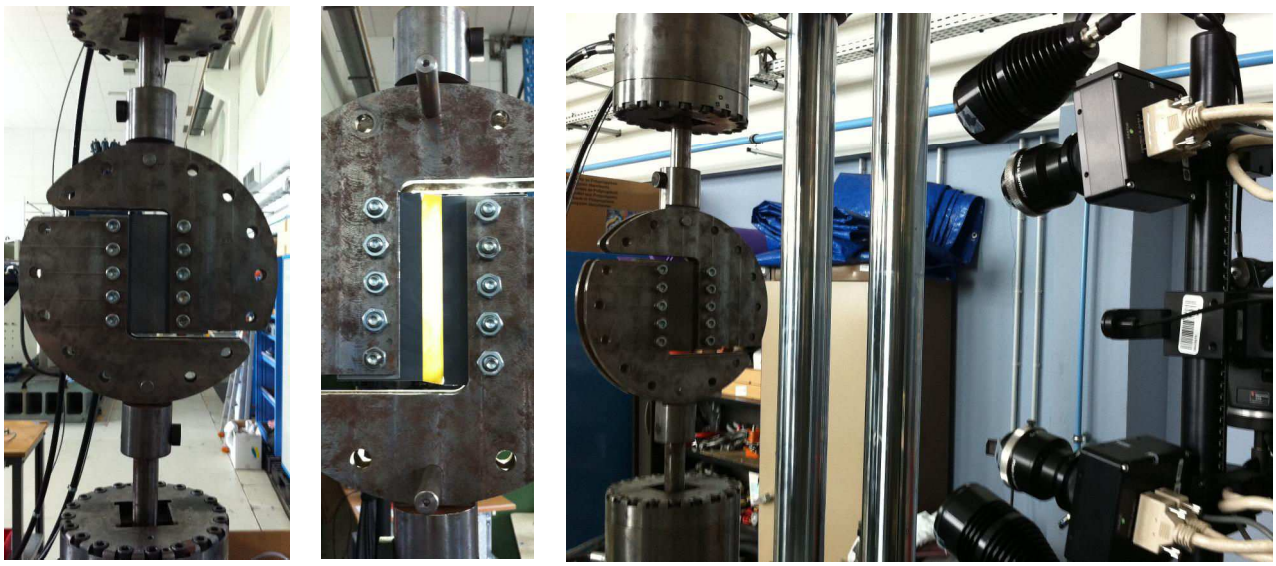

Fig. 5.54. Arcan assembly and measuring system

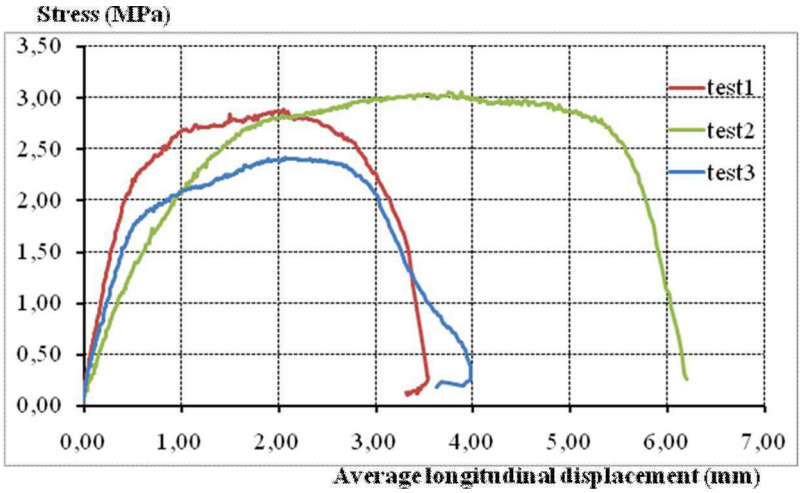

Fig. 5.55. Shear stress - Average longitudinal displacement diagram

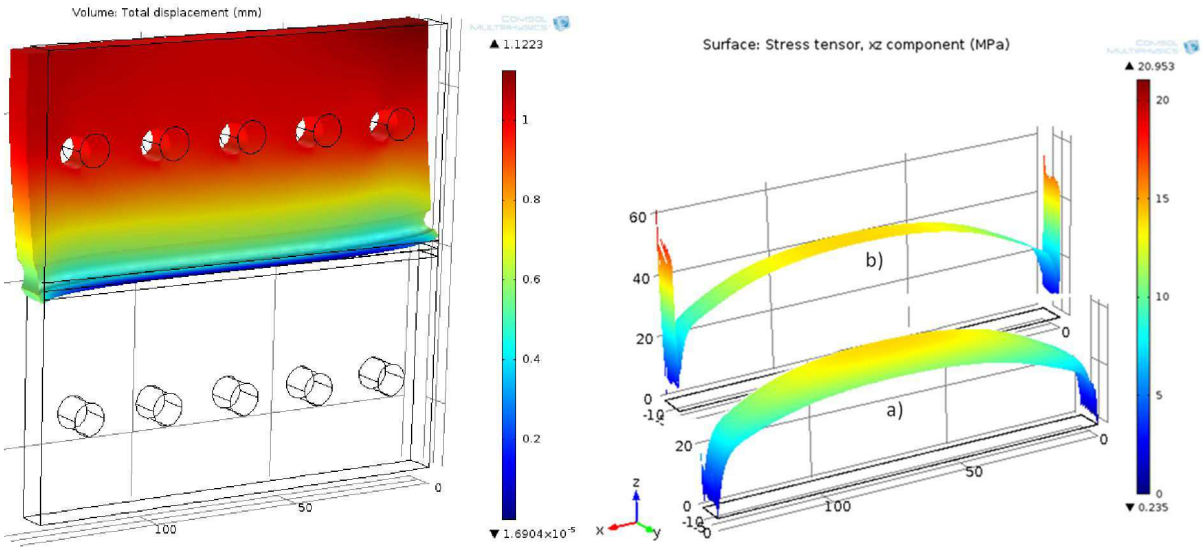

Fig. 5.56. Modelling of shear tests on Arcan's fixture with (a) and without beak (b)

Chapter 6. Conclusion and perspectives

Offshore oil exploitation in ultra deep water requires the use of efficient thermal protection systems. The mechanical behaviour of thermal insulation materials is quite complex and requires the use of time-dependent models due to the nature of the matrix. Moreover, some insulation materials use microspheres embedded in a polymer matrix. In order to analyse the long term behaviour of such materials two phenomena have been analysed: the influence of the hydrostatic pressure and of the temperature. Such thermo-mechanical loadings correspond to the industrial use of coating systems. The analysis of the time evolution of the volumetric strain, with respect to the temperature, under different time-evolutions of the applied hydrostatic pressure, using a hyperbaric chamber, gives interesting experimental data. Moreover, the mechanical response of the materials under uniaxial tensile creep tests has been examined using dynamic mechanical analysis tests. A thermo-mechanical model of GSPP is proposed to model the volumetric creep strain under hydrostatic pressure taking into account the properties of thermo-rheologically complex material. This model is also applicable to other syntactic foam materials (Glass/epoxy, Glass/polyurethane, and Glass/phenolic) which exhibit the same type of behaviour. Assuming the material behaviour is linear viscoelastic, its modelling requires the use of a relaxation time spectrum depending on the temperature. The first numerical results are encouraging. Concerning the field joint coating material (solid PP), the generalized Maxwell temperature-mechanical model with elastic volumetric deformation behaviour is useful.

Regarding the thermal effect, the use of boundary conditions in thermal modelling must be considered taking into account the position of pipeline and the nature of convective problem (due to the air, the water or the oil). The simple thermal modelling proposed in chapter 2 allows us to see the influence of the different thermal boundary conditions, follow the phase change of solid PP and also estimate the cooling time of a Field Joint. It must be noted that the addition of latent heat to the specific heat during the phase transition is valuable in the case of constant density.

Finally, a complete modelling of Five Layer Syntactic Polypropylene system using the injection moulded Polypropylene is presented. The model takes into account the influence of the manufacturing process and the influence of the service conditions (difference of external temperature and pressure). Such models are useful to analyse the stress distribution in an insulated pipeline under service conditions. However, the critical area of such assemblies is often the interface between the parent coating material and the field joint coating; therefore, the mechanical behaviour of this interface must also be accurately experimentally analysed and modelled. Thus, tests using a modified Arcan assembly [Cognard et al, 2006; Cognard, 2008; Cognard, 2011] are underway to analyse the influence of tension/compression-shear loadings on the mechanical behaviour of such polymer assemblies. This device can also be used to analyse the mechanical behaviour of the interface between the coating and the metallic pipe.

The perspectives of our study could be presented as follows:

In terms of modelling, the thermo-mechanical behaviour of materials could be improved by taking into account the different phenomena. Concerning the GSPP, the introduction of a damage variable is envisaged. One idea is to consider the damage variable as an integral function of microspheres' distribution. The evolution function of the variable is generally composed of two terms, one of Von Mises contribution and one of the pressure component [Perreux et al, 2008]. The introduction of the new variable transforms the model from small perturbations to a large deformation model where the transformation gradient must be considered in the stress calculation. The damage variable could play an important role in change of the porosity (percentage of void not embedded by microspheres), the viscous parameters and rigidity (Young's modulus and Poisson's ratio) of the material. In this case, the idea based on porous material theories [Moris & Tanaka, 1973 ; Martin, 2007] appears suitable. Anyway, the use of COMSOL Multiphysics is still adapted to the simulation by use of the other PDE module for damage variables and transforming from Piola-Kirchhoff stress (small perturbation assumption) to Cauchy stress (large deformation).

Considering the injected PP material, a new variable called degree of polymerisation [Le Goff et all, 2005; 2011] can be introduced. This parameter will be governed by the cooling rate of the material during the solidification phase and will affect the thermomechanical properties of the material as well as the temperature.

The main difficulty in improving the complex model is to take into account the interface's behaviour between the main coating material and the injected PP. Injection of melted PP at the interface with GSPP will affect the GSPP behaviour by local melting of the material. Additional tests have to be performed to verify the physical nature of this interface and then to take it into account in the global model of the structure. With the knowledge of the interface behaviour a 1D interface model can be used in addition to the global 3D model of the structure. However, at present the coupling between 1D and 3D models is not available in COMSOL multiphysics.

As shown with the S shape field joint geometry a reduction of stress can be obtained and by choosing the right objective function an ideal geometry can be reached.

In terms of an experimental plan, two tests can be proposed.

The first one is the improvement of the modified Arcan test for polymer-polymer assemblies. This will allow the determination of a failure envelope which could be applied to the proposed 1D interface model. By observing the stress distribution in modelling, the tests should enable us to follow the same type of loads as those seen in service of the structure.

The second test is the full scale test (like the bending test of a pipeline). This type of test is essential to give us a global image of the pipeline's behaviour.

In terms of materials, new materials are in development for Field Joint coating. These developments aim mainly to reduce the installation time and to increase the temperature of use. Therefore, in order to facilitate the development of such materials, the strategy developed in this study can be adapted to analyse the influence of new materials on the system response and limit expensive testing.

References

[3M®] 3M®. "multimedia.3m.com/mws/mediawebserver?mwsId=SSSSSu7zK1fslxtUOY_Zm82xev7qe17zHvTSevTSeSSSSSS--&fn=S38HS%20Prod%20Info%20DMR.pdf"

[Adrien et al, 2007] Adrien. J, Maire. E, Gimenez. N, Sauvant-Moynot. V, "Experimental study of the compression behaviour of syntactic foams by in situ X-ray tomography. Acta Materialia 55:1667-1679, 2007

[Antunes et al, 2011] Antunes. F.V, Ferreira. J.A.M, Capela. C "Numerical modelling of the Young's modulus of syntactic foams". Finite Elements in Analysis and Design 47:78-84, 2011

[Bai. Y, 2001] Bai. Y "Pipelines and risers". Elsevier, 2001

[Bai. Y & Bai. Q, 2005] Bai. Y, Bai. Q, "Subsea Pipelines and Risers". Elsevier, 2005

[Bardella and Genna, 2001] Bardella. L, Genna. F, "On the elastic behavior of syntactic foams". International Journal of Solid and Structure 38:7235-7260, 2001

[Bardenhagen et al, 1997] Bardenhagen. S.G, Stout. M.G, Gray. G.T, "Three-dimensional, finite deformation, viscoplastic constitutive models for polymeric materials" .Mechanics of Materials 25, 235-253, 1997

[Bardenhagen et al, 2005] Bardenhagen. S.G, Brydon. A.D, Guilkey. J.E, "Insight into the physics of foam densification via numerical simulation". Journal of the Mechanics and Physics of solids 53, 597–617, 2005

[Bazergui et al, 1987] Bazergui. A, Bui-Quoc. T, Biron. A, Mcintyre. G, Laberge. C, "Résistance des matériaux". Editions de l'école Polytechnique de Montréal. 1987

[Bejan & Kraus, 2003] Bejan. A, Kraus. A.D, "Heat transfer handbook". John Wiley & Sons Inc, 2003

[Bendada et al, 2004] Bendada. A, Derdouri. A, Lamontagne. M, Simard. Y, "Analysis of thermal contact resistance between polymer and mold in injection molding". Applied Thermal Engineering 24, 2029–2040, 2004

[Berti, 2004] Berti. E, "Syntactic polypropylene coating solution provides thermal insulation for Bonga risers", Offshore Magazine, 2004

[GBI, 2010] BGI Research “The Future of the Offshore Drilling Industry to 2015 – Market Analysis, Captial Expenditure and competitive Landscape”, GBIGE00026MR, 2010

[Borealisgroup] Borealisgroup, "www.borealisgroup.com/datasheets/10024028"

[Bouchonneau, 2007] Bouchonneau. N, "Etude du comportement des systèmes d'isolation thermique pour les grandes profondeurs d'eau". Thèse de l'Université de Franche-Comté, 2007

[Bouchonneau et al, 2010] Bouchonneau. N, Sauvant-Moynot. V, Choqueuse. D, Grosjean. F, Poncet. E, Perreux. D, "Experimental testing and modeling of an industrial insulated pipeline for deep sea application". Journal of Petroleum Science and Engineering, Volume 73, Issues 1-2:1-12, 2010

[Boutaous et al, 2010] Boutaous. M, Brahmia. N, Bourgin. P, "Parametric study of the crystallization kinetics of a semi-crystalline polymer during cooling". C. R. Mecanique 338, 78–84, 2010

[Brederoshaw] Brederoshaw, "Thermotite® Deep Foam (TDF) ". www.brederoshaw.com

[Buijvoets, 2011] Buijvoets. J, "Offshore O-lay pipe laying". 6th Pipeline Technology Conference, 2011

[Seymour & Carraher, 2003] Carraher. C.E, Seymour. R.B "Seymour/Carraher's Polymer Chemistry". Marcel Dekker, 2003

[Chen, 2000] Chen. t, "Determining a Prony series for a viscoelastic material from time varying strain data", NASA/TM-2000-210123 ARL-TR-2206, 2000

[Choquese et al, 2004] Choquese. D, Chomard. A, Chauchot. P, "How to Provide Relevant Data for the Prediction of Long Term Behavior of Insulation Materials Under Hot/Wet Condition?". Offshore Technology Conference, OTC 16503, 2004.

[Choqueuse et al, 2010] Choqueuse. D, Davies. P, Perreux. D, Sohier. L, Cognard. J.Y, "Mechanical behavior of syntactic foams for deep sea thermally insulated pipeline". Applied Mechanics and Materials 24-25:97-102, 2010

[Choqueuse et al, 2007] Choqueuse. D, Perreux. D, Sauvant-Moynot. V, "Modeling approach for damageable mechanical behavior of glass/polymer syntactic foams under hydrostatic pressure". Syntactic and Composite Foams II, 2007

[Cognard et al, Cognard. J.Y, Davies. P, Sohier. L, Créac'hcadec. R, "A study of the non-linear

2006] behaviour of adhesively-bonded composite assemblies". Composite Structures 76:34-46, 2006

[Cognard, 2008] Cognard. J.Y, "Numerical analysis of edge effects in adhesively-bonded assemblies application to the determination of the adhesive behaviour". Computers and Structures 86:1704-1717, 2008

[Cognard, 2011] Cognard. J.Y, Sohier. L, Davies. P, "A modified Arcan test to analyse the behavior of composites and their assemblies under out-of-plane loadings". Composites: Part A, 111-121, 2011

[COMSOL] COMSOL 4.2a, Buoyancy Flow in Free Fluids.

[COMSOL] COMSOL Multiphysics 4.2a, "Continuous Casting". COMSOL tutorial

[COMSOL] COMSOL Multiphysics User's Guide v4.2a. Specifying Discontinuous Functions.

[COMSOL] COMSOL Multiphysics User's Guide v4.2a. "Viscoelastic material"

[COMSOL] COMSOL V4.2a, "Heat Transfer Module Users Guide"

[Deheeger et al, 2011] Deheeger. A, Mathias. J.D, Grédiac. M, Verney. V, "Study the thermoviscoelastic response of the Redux 312 adhesive-Part 1: Experimental characterization". International Journal of Adhesion & Adhesives 31, 68-74, 2011

[Deheeger et al, 2011] Deheeger. A, Mathias. J.D, Grédiac. M, Verney. V, "Study the thermoviscoelastic response of the Redux 312 adhesive-Part 2: Modeling". International Journal of Adhesion & Adhesives 31, 57-67, 2011

[Dimier, 2003] Dimier. F, "Injection de systèmes réactifs: Détermination de lois cinétiques et rhéologiques et modélisation". Thèse de l'Ecole nationale supérieure des mines de Paris, 2003.

[Dixon & Jackson, 2003] Dixon. M, Jackson. D, "Deepwater Installation Techniques for Pipe-in-Pipe Systems - Incorporating Plastic Strains". Offshore Technology Conference, OTC 15373, 2003

[Edwin, 2005] Edwin. T.J.K, "Mechanical properties of solid polymers: constitutive modelling of long and short term behaviour". Technische Universiteit Eindhoven, 2005

[fminsearch] fminsearch, "http://www.mathworks.fr/help/toolbox/optim/ug/fminsearch.html"

[Genovese & Genovese. A, Shanks. R.A "Crystallization and melting of isotactic

Shanks, 2004] polypropylene in response to temperature modulation". Journal of Thermal Analsis and Calorimetry, vol. 75 233 - 248, 2004

[Gibson & Ashby, 1999] Gibson. L.J, Ashby. M.F, Cambridge University Press, 1999

[globalsecurity] globalsecurity,"http://www.globalsecurity.org/military/systems/ship/offshore-pipelaying.htm"

[Gueguen, 2005] Gueguen. M, "Couplage thermomécanique appliqué au procédé d'injection. Prise en compte de la cristallisation". Thesis in University of South Brittany, 2005

[Guidetti et al, 1996] Guidetti. G.P, Rigosi. G.L, Marzola. R, "The use of polypropylene in pipeline coatings". Progress in Organic Coating 27, 79-85, 1996

[Guo et al, 2005] Guo. B , Shanhong Song. S, Chacko. J, Ghalambor. A, "Offshore Pipelines". Elsevier, 2005

[Gupta et al, 2004] Gupta. N, Woldesenbet. E, Mensah. P, "Compression properties of syntactic foams: effect of cenosphere radius ratio and specimen aspect ratio". Composites: Part A 35:103-111, 2004

[Hammerschmidt, 1934] Hammerschmidt. E. G "Formation of Gas Hydrates in Natural Gas Transmission Lines". Industrial and Engineering Chemistry, 26 (8), pp 851-855, 1934

[Incropera et al, 2006] Incropera.F.P, DeWitt. D.P, Bergman. T.L, Lavine. A.S, "Fundamental of Heat and Mass Transfer". John Wiley & Sons Inc, 6th revised edition, 2006

[Islam and Kim, 2011] Md Mainul Islam, Ho Sung Kim, “Pre-mould processing technique for syntactic foams: Generalised modelling, theory and experiment”, Journal of Materials Processing Technology 211, 708–716, 2011

[Kim and Plubrai, 2004] Kim. H.S, Plubrai. P, "Manufacturing and failure mechanisms of syntactic foam under compression". Composites: Part A 35:1009-1015, 2004

[Kola ík & Pegoretti, 2006] Kola ík. J, Pegoretti. Q, "Non-linear tensile creep of polypropylene: Time-strain superposition and creep prediction", Polymer 47 346-356, 2006

[Kola ík & Pegoretti, 2008] Kola ík. J, Pegoretti. Q, "Proposal of the Boltzmann-like superposition principle for nonlinear tensile creep of thermoplastics", Polymer Testing 27 596-606, 2008

[Krevelen and Nijenhuis, 2009] Krevelen. D.W.V, Nijenhuis. K.T, "Properties of polymer: Their correlation with chemical structure; their numerical estimation and prediction from additive group contributions". Fourth, completely revised edition. Elsevier, 2009.

[Kyriakides & Corona, 2007] Kyriakides. S, Corona. E, "Mechanics of offshore pipelines, volume 1: buckling and collapse". Elsevier, 2007

[Lagarias et al, 1997] Lagarias. J.C, Reeds. J.A, Wright. M.H, Wright. P.E., "Convergence properties of the Nelder-Mead simplex method in low dimensions". SIAM J. OTIM. Vol 9. N0. 1, 112-147, 1997.

[Le Goff et al, 2011] Le Goff. R, Boyard. N, Sobotka. V, Lefèvre. N, Delaunay. D, "Inverse estimation of the crystallization kinetic function of semi-crystalline polymers and short fibre reinforced composites in moderate cooling conditions". Polymer Testing, 678-687, 2011

[Le Goff et al, 2005] Le Goff. R, Poutot. G, Delaunay. D, Fulchiron. R, Koscher. E, "Study and modeling of heat transfer during the solidification of semi-crystalline polymers". International Journal of Heat and Mass Transfer 48, 5417-5430, 2005

[Leblanc, 2003] Leblanc. J.L, "Propiétés mécaniques des polymères", editoo.com, 2003

[Lefebvre et al, 2009] Lefebvre. X, Sauvant-Moynot. V, Choqueuse. D, Chauchot. P, “The durability of syntactic foams for deep offshore insulation: Modelling of water uptake under representative ageing conditions in order to predict the evolution of buoyancy and thermal conductivity”. Oil & Gas Science and Technology, Vol. 64, No.2, 165-178, 2009

[Lemaitre & Chaboche, 2006] Lemaitre. J, Chaboche. J.L, "Mécanique des matériaux solides" 2e édition DUNOD, 2006

[Lienhard IV and V, 2001] Lienhard IV. J.H, Lienhard. J.H V, "A heat transfer textbook". http://web.mit.edu/lienhard/www/ahtt.html, 2001

[lsqcurvefit] lsqcurvefit, "http://www.mathworks.fr/help/toolbox/optim/ug/lsqcurvefit.html"

[Martin, 2007] Martin. B, Ayadi. Z, Nivoit. M, Galtier. A, Cunat. C, "Formulation DNLR intégrale des lois de comportement : généralisation du principle de superposition de Boltzman", C. R. Mecanique 332 907-913, 2004

[Marur, 2005] Marur. P.R, "Effective elastic moduli of syntactic foams". Materials Letters

59:1954-1957, 2005

[Marur, 2009] Marur. P.R, “Influence of imperfect interface on the elastic moduli of syntactic foams”. Computational Materials Science 46, 327–332, 2009

[Micromeritics] Micromeritics, "http://www.micromeritics.com/Product-Showcase/AccuPyc-II-1340.aspx"

[Moré, 1977] Moré. J, "the Levenberg-Marquardt algorithm: implementation and theory". Numerical analysis, ed. G.A Watson, Lecture notes in Mathematics 630, 106-116, 1977.

[Peacock, 2000] Peacock. J.A, "Handbook of polyethylene, Structure, Properties, and Application". Marcel Dekker, 2000

[Phan et al, 2012] Phan V.T, Choqueuse. D , Cognard. J.Y, Sohier. L, "Experimental analysis and modelling of the long term thermo-mechanical behaviour of glass/polypropylene syntactic used on thermally insulated offshore pipeline". Progress in Organic Coatings, in press.

[Moris & Tanaka, 1973] Mori. T, Tanaka. K, "Average stress in matrix and average elastic energy of materials with misfitting inclusions". Acta Metallurgica, Volume 21, Issue 5, P571-574, 1973

[Muliana & Khan, 2008] Muliana. A, Khan. K.A, "A time-integration algorithm for thermo rheologically complex polymers". Computational Materials Science 41:576-588, 2008

[Pampolini and Del Piero, 2008] Pampolini. G, Del Piero. G, "Strain localization in open-cell polyurethane foams: Experiments and Del Piero theoretical model". Journal of Mechanics of Materials and Structures 3: 969-981, 2008

[Perreux and Robinet, 2008] Perreux D, Robinet P, "Amélioration d’un modèle de comportement de mousse syntactique pour application d’isolation". Ifremer contrat 2008-2-20664127, 2008

[Privalko et al, 2005] Privalko. V.P, Dinzhos. R.V, Privalko. E.G, "Enthalpy relaxation in the cooling/heating cycles of polypropylene/organosilica nanocomposites, I: Non-isothermal crystallization". Thermochimica Acta 432, 76-82, 2005

[Rizzi et al, 2000] Rizzi. E, Papa. E, Corigliano. A, "Mechanical behavior of a syntactic foam: experiments and modeling". International Journal of Solids and Structures 37:5773-5794, 2000

[Roux et al, Roux. S, Hild. F, Viot. P, Bernard. D, "Three-dimensional image correlation

2008] from X-ray computed tomography of solid foam". Composites: Part A 39:1253-1265, 2008

[Salençon, 2009] Salençon. J, "Viscoélasticité pour le calcul des structures", Les presses des Ponts et Chaussées, édition de l'Ecole polytechnique, 2009

[Sanders and Gibson, 2003] Sanders. W. S, Gibson. L.J, “Mechanics of BCC and FCC hollow-sphere foams”. Materials Science and Engineering A352, 150 /161, 2003

[Sanders and Gibson, 2003] Sanders. W. S, Gibson. L.J, “Mechanics of hollow sphere foams”. Materials Science and Engineering A347, 70 /85, 2003

[Sauvant-Moynot et al, 2006] Sauvant-Moynot. V, Gimenez. N, Adrien. J, and Maire. E, "X-ray microtomography for a better understanding of syntactic foam performance and limits in ultra deep water" Oilfield Engineering with Polymers, 2006.

[Schwarz, 1986] Schwarz. G, "Thermal expansion of polymer from 4.2 K to room temperature". ICMC conference Non-Metallic Materials and Composites at Low temperature IV, Heidelberg, FRG, July 1986

[Shaw & MacKnight, 2005] Shaw. M.T, MacKnight. W.J, "Introduction to polymer viscoelasticity", John Wiley & Sons, 2005

[Singh et al, 2005] Singh. P, Haberer. S, Gritis. N, Worthingham. R, Cetiner. M, "New developments in high performance coatings", BHR Pipeline Protection, Paphos Cyprus, 2005

[Socotherm] Socotherm,"http://www.socotherm.com/en/products-a-services/pipe-coating/thermal insulation/polipropilene-sintattico-a-cinque-strati"

[Tailor et al, 2003] Tailor. D, Hodgins. W, Gritis. N, "Field joint developements and compatibility considerations", BHR 15th International Conference on Pipeline Protection, 2003

[Tardif et al, 2012] Tardif. X, Agazzi. A, Sobotka. V, Boyard. N, Jarny. Y, Delaunay. D, "A multifunctional device to determine specific volume, thermal conductivity and crystallization kinetics of semi-crystalline polymers". Polymer Testing, 819-827, 2012

[Treasurer, 2010] Treasurer. P, "Durability of tubular composite structures-fatigue and time-dependent damage modeling", thèse de l'Univsersité de Franche-Comté, 2010

[Ward Ward. I.M, Hadley. D.W, “An introduction to the mechanical properties of solid

&Hadley, 1993] polymer", John Wiley & Sons, 1993

[Watkins & Hershey, 2001] Watkins. L, Hershey. E, "Syntactic Foam Thermal Insulation for Ultra-Deepwater Oil and Gas Pipelines". Offshore Technology Conference, OTC 13134, 2001

[Williams et al 1955] Williams. M.L, Landel. R.F, Ferry. J.D, "The temperature dependence of relaxation mechanisms in amorphous polymers and other glass-forming liquids". University of Wisconsin, 1955

[Wouterson et al, 2005] Wouterson. E.M, Boey. F.Y.C, Hu. X, Shing-Chung. W, "Specific properties and fracture toughness of syntactic foam: Effect of foam microstructures". Composites Science and Technology 65:1840-1850, 2005

[Wysocki et al, 2005] Wysocki. M, Larsson. R, Toll. S, "Hydrostatic consolidation of commingled fibre composites". Composites Science and Technology 65, 1507–1519, 2005

[Young, 1981] Young. R.J "Introduction to polymers". Chapman and Hall, 1981